Editor's copy

SACLANTCEN Report
SR – 7

SACLANTCEN Report SR – 7

SACLANT ASW RESEARCH CENTRE REPORT

THE SEA SURFACE AS A RANDOM FILTER FOR UNDERWATER SOUND WAVES

by

LEONARD FORTUIN

15 JUNE 1974

NORTH ATLANTIC TREATY ORGANIZATION

VIALE SAN BARTOLOMEO 400
I – 19026 – LA SPEZIA, ITALY

This document is unclassified. The information it contains is published subject to the conditions of the legend printed on the inside cover. Short quotations from it may be made in other publications if credit is given to the author(s). Except for working copies for research purposes or for use in official NATO publications, reproduction requires the authorization of the Director of SACLANTCEN.

CLASSIFICATION REVIEWED
PCAC

This document is released to a NATO Government at the direction of the SACLANTCEN subject to the following conditions:

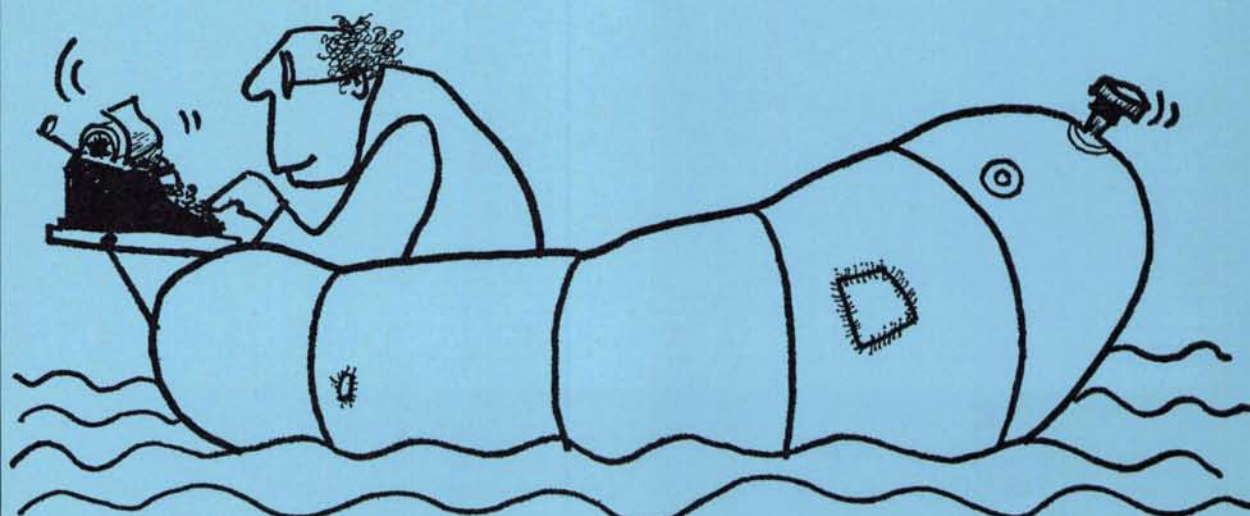
1. The recipient NATO Government agrees to use its best endeavours to ensure that the information herein disclosed, whether or not it bears a security classification, is not dealt with in any manner (a) contrary to the intent of the provisions of the Charter of the Centre, or (b) prejudicial to the rights of the owner thereof to obtain patent, copyright, or other like statutory protection therefor.

2. If the technical information was originally released to the Centre by a NATO Government subject to restrictions clearly marked on this document the recipient NATO Government agrees to use its best endeavours to abide by the terms of the restrictions so imposed by the releasing Government.



the sea surface as a random filter for underwater sound waves

leonard fortuin



THE SEA SURFACE AS A RANDOM FILTER FOR UNDERWATER SOUND WAVES

ISBN 90 212 4007 6

© 1973 by L. Fortuin, Eersel (N.B.) – The Netherlands

SACLANTCEN REPORT SR-7

NORTH ATLANTIC TREATY ORGANIZATION
SACLANT ASW Research Centre
Viale San Bartolomeo 400
I 19026 - La Spezia, Italy

THE SEA SURFACE AS A RANDOM FILTER FOR UNDERWATER SOUND WAVES

by

Leonard Fortuin

15 June 1974

APPROVED FOR DISTRIBUTION

J.G. RETALLACK
Director

Originally submitted by the author to the Technological University of Twente, The Netherlands (Technische Hogeschool Twente) in fulfilment of a degree of Doctor in Technical Sciences. (Doctor in de technische wetenschappen).

Printed by Uitgeverij Waltman, Delft, The Netherlands.

THE SEA SURFACE AS A RANDOM FILTER FOR UNDERWATER SOUND WAVES

PROEFSCHRIFT

ter verkrijging van de graad van doctor in de technische wetenschappen aan de Technische Hogeschool Twente, op gezag van de rector magnificus, prof. dr. ir. P. J. Zandbergen, volgens besluit van het College van Dekanen in het openbaar te verdedigen op donderdag 31 januari 1974 te 16.00 uur

door

LEONARD FORTUIN
elektrotechnisch ingenieur
geboren op 7 april 1937 te Meppel

UITGEVERIJ WALTMAN - DELFT - 1973

Dit proefschrift is goedgekeurd door de promotor.

Promotor: prof. ir. E. W. Gröneveld.
Co-referent: prof. dr. ir. P. J. Zandbergen.

Nessuna certezza delle scientie è, dove non si può applicare vna delle scientie matematiche e che non sono vnite con esse matematiche.

Leonardo da Vinci (1452–1519)

Cover and non-scientific drawings have been made by Wouter Stips, The Hague.

table of contents



TABLE OF CONTENTS

SUMMARY/SAMENVATTING 1

LIST OF SYMBOLS AND NOTATIONS 5

ASSUMPTIONS 11

CHAPTER 1 INTRODUCTION 15

1.1 Motivation of this study 17
1.2 Some remarks of a more detailed nature 19
1.3 Structure of the thesis 22

CHAPTER 2 LITERATURE ON PHYSICAL ASPECTS 25

2.1 Introduction 27
2.2 Literature up to the beginning of 1969 28
2.3 Literature up to the middle of 1973 48
2.4 Summary 52

CHAPTER 3 DESCRIPTION OF THE SEA SURFACE 57

3.1 Introduction 59
3.2 Surface wave spectrum theory 60
3.3 Correlation functions in time and space 61
3.4 The Pierson-Moskowitz spectrum 62
3.5 Numerical results derived from the Pierson-Moskowitz spectrum 63
3.6 Summary 67

CHAPTER 4 FILTER CONSIDERATIONS 69

4.1 Introduction 71
4.2 System functions for linear time-varying filters 72
4.3 Input-output relations 75
4.4 Statistical properties of the filter 77
4.5 Summary 80

CHAPTER 5 THE SEA SURFACE AS A RANDOM FILTER 81

5.1 Introduction 83
5.2 Derivation of a formula for the transfer function 84

5.3 Simplification of the formula for $H(\omega, t)$ 98
5.4 Behaviour of H for high frequencies 100
5.5 Justification of the use of the Helmholtz equation 104
5.6 Summary 109

CHAPTER 6 THE DETERMINISTIC PART OF THE FILTER 111
6.1 Introduction 113
6.2 Further simplification of H 113
6.3 Calculation of H_d 114
6.4 Absorption 116
6.5 Summary 118

CHAPTER 7 THE RANDOM PART OF THE FILTER 119
7.1 Introduction 121
7.2 Derivation of a formula for H_r 121
7.3 The variance of H_r 122
7.4 Numerical results 125
7.5 Approximation of H_r and H 126
7.6 Summary 127

CHAPTER 8 TIME AND FREQUENCY CORRELATION 129
8.1 Introduction 131
8.2 Correlation of the transfer function 132
8.3 The function $B_e(\omega, \omega, \Omega)$ 135
8.4 Correlation of the impulse response function 136
8.5 Summary 138

CHAPTER 9 SPACE CORRELATION 139
9.1 Introduction 141
9.2 Correlation on and across an average wave front 143
9.3 Correlation in cartesian coordinates 152
9.4 Wave front distortion 160
9.5 Summary 161

CHAPTER 10 STATISTICAL PROPERTIES OF OUTPUT SIGNALS . . 163
10.1 Introduction 165
10.2 Monochromatic input signals 165
10.3 Delta pulses at the input 172
10.4 Arbitrary input signals 173
10.5 Summary 174

CHAPTER 11 DISCUSSION OF THE RESULTS 177
11.1 Introduction 179
11.2 The validity of the specular point formula 180
11.3 Mean values of system functions 183
11.4 Examination of correlation functions 184
11.5 Various comments 186
11.6 Suggested experiments 187
11.7 Summary 187

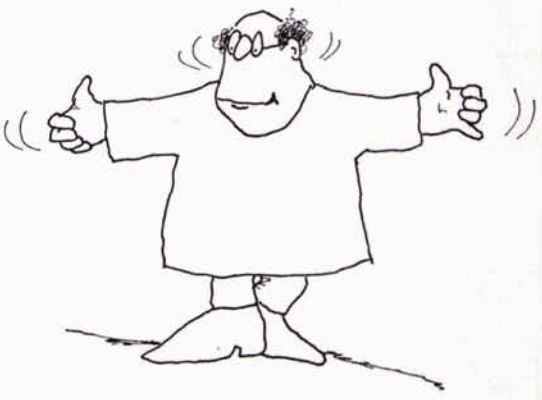
CHAPTER 12 CONCLUSIONS 189

ACKNOWLEDGEMENTS 193

CURRICULUM VITAE 197

APPENDICES 201

summary / samenvatting



SUMMARY

In this dissertation the phenomenon of scattering and reflection of underwater sound waves from the sea surface, is studied by considering the surface sound channel as a random, time-dependent filter. This filter can be best analyzed by means of its frequency transfer function, from which another important system function, the impulse response, can be derived as Fourier transform.

Starting from the wave equation for an iso-velocity medium with boundary condition of zero total pressure, a formula for the transfer function is found via the Helmholtz integral, by means of Meecham's perturbation technique. It is a six-fold integral that can be reduced to a converging series of surface integrals, when the specular angle of incidence is smaller than 84°. The convergence is then even so fast that the leading term is a good approximation for the whole series.

Next, the speed of the wind that generates the random sea surface is assumed to be at most 10 m/s, and the relative position of transmitter and receiver is chosen in such a way that the specular angle of incidence does not exceed 84°. Numerical analysis of first and second statistical moment of this term then shows that it can be replaced by a simple formula which is identical to the one that follows from the Kirchhoff-Eckart theory.

This Kirchhoff-Eckart formula is used for a statistical investigation of the random filter. First and second order moments are calculated under the assumption that the ocean surface is a stationary and homogeneous, but anisotropic, Gaussian process. Frequency, time, and space-correlation functions of the filter output, when delta pulses or harmonic signals are applied at the input, reflect in a simple way the statistical properties in frequency, time, and space of the sea surface, if the roughness parameter χ is less than one ($\chi = 2\,kh \cos\theta_s$). With increasing roughness, this property is gradually lost. These theoretical results are shown to be in agreement with experimental data found in the literature. Hence they can be used to predict the behaviour of the underwater communication channel via the surface, when the surface is characterized by its wave spectrum, or by its spatial and temporal correlation functions.

SAMENVATTING

In dit proefschrift worden de verstrooiing en weerkaatsing van geluidsgolven onder water door het zeeoppervlak bestudeerd door het geluidskanaal aan het oppervlak te beschouwen als een stochastisch, tijdsafhankelijk filter. Dit filter kan het beste worden geanalyseerd door middel van de frekwentieoverdrachtsfunktie, waarvan een andere belangrijke systeemfunktie, de impulsresponsie, kan worden afgeleid als Fourier-transformatie.

Uitgaande van de golfvergelijking voor een medium waarin de geluidsvoortplantingssnelheid konstant is, met als randvoorwaarde dat de totale druk op het oppervlak gelijk nul is, wordt een formule voor de overdrachtsfunktie gevonden via de Helmholtz-integraal, door middel van Meecham's perturbatiemethode. Het is een zesvoudige integraal die herleid kan worden tot een konvergerende reeks oppervlakte-integralen, als de speculaire hoek van inval minder dan 84° bedraagt. De konvergentie is dan zelfs zo groot, dat de eerste term een goede benadering voor de gehele reeks is.

Vervolgens wordt de snelheid van de wind welke het stochastische zeeoppervlak veroorzaakt verondersteld niet groter dan 10 m/s te zijn, en de onderlinge positie van zender en ontvanger wordt zodanig gekozen dat de speculaire invalshoek de 84° niet overschrijdt. Numerieke analyse van het eerste- en tweede-orde statistische moment van die eerste term toont dan aan dat deze vervangen kan worden door een eenvoudige formule, identiek aan die welke volgt uit de Kirchhoff-Eckart-theorie.

Deze Kirchhoff-Eckart-formule wordt gebruikt voor een statistisch onderzoek van het random filter. Eerste- en tweede-orde-momenten worden berekend onder de aanname dat het zeeoppervlak een stationair en homogeen, maar anisotroop, Gaussisch proces is. Korrelatiefunkties van het uitgangssignaal van het filter in de tijd, de ruimte, en in het frekwentiegebied, wanneer delta-impulsen of harmonische ingangssignalen worden aangewend, weerspiegelen op simpele wijze de statistische eigenschappen in tijd, ruimte en frekwentie van het zeeoppervlak, als de ruwheidsparameter χ kleiner is dan één ($\chi = 2\,kh \cos\theta_s$). Bij toenemende ruwheid gaat deze eigenschap geleidelijk verloren. Aangetoond wordt dat deze theoretische resultaten in overeenstemming zijn met experimentele waarnemingen welke in de literatuur worden aangetroffen. Zij kunnen daarom gebruikt worden om het gedrag te voorspellen van het onderwaterkommunikatiekanaal via het zeeoppervlak, wanneer het oppervlak beschreven is door het golfspectrum, of door de korrelatiefunkties in ruimte en tijd.

list of symbols and notations



LIST OF SYMBOLS AND NOTATIONS

Nota Bene

The parts of this thesis that are reprints of articles published in the Journal of the Acoustical Society of America, have their own list of symbols that differs on a few points from the following one.

Symbols

A	amplitude
A^2	surface wave variance spectrum
B_E	correlation function of E
B_e	idem, of e
B_H	idem, of H
B_h	idem, of h
b_s	constant depending on wind speed and geometry
b'_s	modified version of b_s
C	normalized correlation function; constant
C_a	absorption coefficient
c	correlation function
c_0	sound speed in ideal medium
D	path length from T to R via the surface
D_0	specular path length from T to R
d	distance from T to R
E	spreading function; expectation
e	bi-frequency function
F	spectral function; auxiliary function
f	time function; random function; probability density function
G_k	free space Green's function
g	gravity acceleration
H	frequency transfer function
H_a	absorption filter function
h	impulse response function; standard deviation of surface elevation
i	$(-1)^{\frac{1}{2}}$
J	Bessel function
$\mathscr{K}$	wave-number vector: $\mathscr{K} = (K_x, K_y, K_z)$
$\mathbf{K}$	wave-number vector: $\mathbf{K} = (K_x, K_y, 0)$
k	wave number of incident radiation
L	range; effective correlation distance; auxiliary function

$\mathscr{M}$	wave-number vector: $\mathscr{M} = (M_x, M_y, M_z)$
$\mathbf{M}$	wave-number vector: $\mathbf{M} = (M_x, M_y, 0)$
m	constant
n	integer
$\bar{p}$	pressure (time dependent)
p	pressure (with factor $\exp(-i\omega t)$ suppressed)
p_b	pressure, due to the boundary
p_0	pressure in unbound medium
$\mathscr{R}$	space vector: $\mathscr{R} = (x, y, z)$
$\mathbf{R}$	space vector: $\mathbf{R} = (x, y, 0)$
R	receiver
r	distance
T	transmitter; time
t	time
$\bar{U}$	velocity potential (time dependent)
U	velocity potential (with factor $\exp(-i\omega t)$ suppressed)
v	wind speed
W	distance to the average surface
w	distance to the random surface
X	horizontal distance; input spectrum
x	horizontal coordinate; input signal
Y	horizontal distance; output spectrum
y	horizontal coordinate; output signal
Z	vertical distance
z	vertical coordinate
α	angle with X-axis, in horizontal plane; constant
β	constant
γ	direction cosine; coherence function; constant
Δ	fraction
δ	Dirac delta function; constant
ζ	surface profile
η	difference in Y-coordinates
θ	angle with vertical, angle of incidence
κ	wave number of surface wave
ν	variance
ξ	difference in X-coordinates
$\boldsymbol{\varrho}$	correlation vector: $\boldsymbol{\varrho} = (\xi, \eta, 0)$
ϱ	correlation distance
ϱ_0	density
σ	standard deviation
τ	time difference
Φ	correlation function of surface elevation

φ	angle with horizontal, grazing angle
χ	roughness parameter ($\chi = 2\,hk \cos \theta_s$)
Ψ	auxiliary function
ψ	spectral function; phase
Ω	angular frequency
ω	angular frequency of incident wave
ω_s	surface wave frequency

Subscripts

cw	cross-wind
d	deterministic part
dw	down-wind
i	label
N	normalized
n	label
R	receiver
r	random part
s	specular point, stationary phase
T	transmitter
t	time derivative
WF	wave front
w	average wind
x	derivative with respect to X
y	derivative with respect to Y

Superscripts

s	on random surface

Notations

A number between () indicates an equation; example: (5.38) means "Equation 38 of Chapter 5".
A number between [] indicates a reference; example: [*2.52*] means "Reference 52 of Chapter 2".
The angular brackets $< >$ denote an ensemble average. *Re* and *Im* stand for "real part" and "imaginary part" of a complex quantity.

assumptions



ASSUMPTIONS

1. The sea surface is single-valued. There are no sub-surface bubbles.

2. The sea surface is a pressure release boundary; the Dirichlet boundary condition $p = 0$ is valid.

3. The sea surface elevation is a random process, in time as well as in space. It is stationary (in time) and homogeneous (in space).

4. The sea surface has Gaussian statistics.

5. The anisotropy of the sea surface can be expressed adequately by a $\cos^2(\alpha)$-law.

6. The Pierson-Moskowitz spectrum is the best starting point for a statistical description of a fully developed sea.

7. The medium is ideal: there are no inhomogeneities, and the sound speed is constant ($c_0 = 1500$ m/sec).

8. The bottom is so far away from the surface and from transmitter and receiver that bottom reflections and reflections from the surface are separated in time.

9. The source radiates equally in all directions, the receivers possess onmi-directional sensitivity.

10. The surface channel can be represented by a linear filter; the superposition principle is valid.

11. The depths of transmitter and receiver are much larger than the surface elevation: $Z_T \geqslant 100|\zeta|$, $Z_R \geqslant 100|\zeta|$.

12. The conclusion that mean value and variance of H can in practice be described sufficiently by the stationary phase approximation, may be extended to the correlation functions of H, in time, frequency and space.

1

introduction



CHAPTER 1

INTRODUCTION

1.1 Motivation of this study

Until modern times the oceans were of interest to man only as a source of food and as a medium that linked and separated the continents. The catching of fish, the transport of goods from one harbour to another, and the sea battles between warring nations, all these took place at the surface. Therefore little interest was shown in the ocean below the surface.

Recent times have seen both the development of submarines, giving the war at sea one more dimension, and the increasing need of food for a growing world population, which makes more efficient fishing necessary.

Connected with this development is a diversity of technical systems that operate with underwater sound waves and are used for detecting an enemy (active and passive sonar), distinguishing friend from foe (IFF systems), tracing schools of fish, or measuring depth (fathometry). There is at least one thing all these systems have in common: they can be considered as communication systems, since each one has a transmitter and a receiver, between which information is conveyed.

The medium that is used in these communication systems to carry the information from source to destination, i.e. the ocean, is certainly not perfect. In the first place there is the phenomenon of a sound speed changing with depth and, to a smaller extent, with range and time; it causes the formation of sound channels, caustics, shadow zones, etc. Next there is the so-called volume reverberation, introduced by inhomogeneities in the medium (e.g. fluctuations in temperature, salinity, pressure, and small particles), that influences the signals all along their propagation path and disturbs them in a random fashion. Finally, in many situations there is not only a direct path between transmitter and receiver, but also connection via the boundaries, especially at longer distances.

The signals that arrive at the receiver via these different paths may interfere or may be separated in time, depending on the geometry and the signal duration. If they interfere then one will probably try to build into the receiver a means of separating them; if they do not it is likely that the direct arrival will be given priority, as it carries the least disturbed information. Then the receiver will have to suppress the superfluous boundary-reflected signals, because their presence makes the system temporarily unusable for direct reception.

It is also possible to imagine a situation in which communication between transmitter and receiver can only take place via the bottom, or via the surface. This occurs when the receiver is placed in the shadow zone of the source.

From the foregoing observations it can be concluded that it is essential for the

designer of underwater communication systems to know how the propagation of sound is affected by the medium and its boundaries. A study of this effect can be split into three parts:

a. The surface,
b. The volume,
c. The bottom,

although in reality the occurring physical phenomena are not entirely independent. In this thesis we shall only be concerned with the surface effect. This means that the influence of the others will be neglected, or eliminated by proper choice of the parameters. At the SACLANT ASW Research Centre, scattering due to inhomogeneities in the medium has been analyzed by LAVAL *et al.* [*1.1*], and FORTUIN *et al.* [*1.2*]. Their work can be regarded as an extension to the broad-band case of the studies undertaken by CHERNOV [*1.3*] and TATARSKI [*1.4*] for a monochromatic wave that propagates through a random medium. As for the bottom reflection, at the SACLANT ASW Research Centre this phenomenon has been studied by HASTRUP (see for instance [*1.5*]).

The phenomenon of scattering and reflection of underwater sound waves from the rough surface of the sea can be studied in many ways. Ample illustration of this statement can be found in Chapter 2. Since we are interested in the underwater communication problem rather than in a detailed physical description of surface scattering, we consider the paths along which the sound waves travel from source to destination as a communication channel, or a filter. Two sections can then be distinguished immediately: the direct path, and the path via the surface (see Fig. 1.1). The surface effect can be studied by looking at the latter of these two.

Signals that travel via the surface path are subject to the influence of the sea surface.

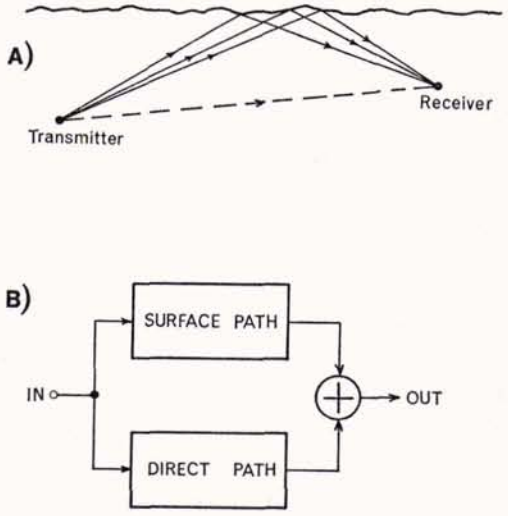


Fig. 1.1
Communication between transmitter and receiver, via the direct path and via the surface path; (A) ray diagram, (B) block diagram.

This boundary has a random character, both in space and time. Hence the scattered field is random too, and we arrive at our approach to the scattering phenomenon: we study *the sea surface as a random filter for underwater sound waves.* Once the statistical properties of this filter are known, and given an arbitrary input signal, the characteristics of the output can be predicted.

Basically, three steps have to be taken in order to reach the level of knowledge at which predictions are indeed feasable: First we have to find a suitable mathematical description of the physics that govern the scattering phenomenon; after that we have to apply filter theory to find an expression for one or more of the filter system functions; finally we need statistical techniques to derive quantities that are useful for the prediction of the output signals. *In this way we will have constructed a link between the statistics of the random sea surface and the statistics of the sound field scattered and reflected by a boundary. It may be regarded as the paramount purpose of the study here presented.*

With the insight thus obtained, we can return to the underwater communication problem. Questions like:

- What is the best frequency band in which to operate?
- What characteristics should the optimum receiver have?
- What is the best type of signal processing to reduce the effect of the signal distortion caused by the surface?

can then be answered. Also the inverse problem can be attacked:

- Given input and output signal, what are the statistical properties of the sea surface?

This problem is of interest to both underwater acousticians and oceanographers.

1.2 Some remarks of a more detailed nature

1.2.1 The sea surface

When wind is blowing over the surface, waves are generated, first small ones and later larger ones, until a state of equilibrium has been reached. If the wind speed increases, more energy is put into the surface waves. They can become so strong that rollers and breakers are formed. In that case the surface is not single-valued any more, and also sub-surface air bubbles appear. These bubbles can screen the surface to such an extent that the sound waves do not reach the surface any more. Volume scattering then takes over. As this is not the subject of the present study, we assume the wind speed low enough that the surface is still single-valued and free of sub-surface bubbles (*Assumption 1*).

The deformation of the sea surface due to the wind is not the only type of deformation that can occur: pressure waves in the water can also change the shape. A strong pressure wave, for instance one caused by an explosion not far below the surface, will even break this boundary. This is caused by the fact that the surface cannot support any pressure: it will yield when struck by a pressure wave. For this reason the upper boundary of the ocean is called a *pressure release surface.*

The pressure waves we are considering, however, are sound waves of such a small amplitude that the surface deformation caused by them is negligible when compared with the wind effect. The pressure release character of the surface is then merely present in the mathematical description of underwater sound propagation: it determines the boundary condition. In accordance with common usage, the Dirichlet condition[1] $p = 0$ is supposed to hold (*Assumption 2*).

The wind-generated sea surface is random in space and time; this random process is assumed to be homogeneous and stationary (*Assumption 3*). Its statistics are Gaussian with good approximation (*Assumption 4*). As a statistical description is needed, we have adopted the theory of the sea surface wave spectrum, which regards the sea surface as the combined effect of a large band of sinusoidal waves that travel over the upper boundary in all directions and each frequency having its own speed. The statistical properties in space are dependent on direction. This anisotropy can be represented by a $\cos^2(\alpha)$-law (*Assumption 5*). For the spectrum we assume the validity of the empirical formula suggested by PIERSON and MOSKOWITZ [*1.6*] for a fully developed sea (*Assumption 6*).

1.2.2 The medium

Propagation along straight lines occurs only in an iso-velocity medium. We require the bending of rays to be absent, hence we assume the sound speed to be constant (*Assumption 7*). In reality such is, with good approximation, the case during the spring time in the upper part of the ocean. Experimental data to check our theory have therefore to be collected in that time of the year and at not too great depths.

At long propagation distances, absorption in the medium can become important. It can be incorporated into our communication model by series connection of an absorption filter with the transfer function

$$H_a(\omega) = \exp(-C_a L \omega^2), \tag{1.1}$$

where $C_a = 4.5 \times 10^{-13}$ dB/m, at a temperature of about 20° C [*1.7, pp. 86–90*].

1.2.3 The bottom

The bottom effect can be eliminated by considering the sea to have infinite depth. In practice this means that the transmitter and receiver depths have to be small compared with the distance from surface to bottom (*Assumption 8*).

1.2.4 The sound source

One of the filter functions that we are interested in is the impulse response. This

[1] When electromagnetic waves are considered, the Dirichlet condition describes a perfectly conducting boundary.

presupposes, if it is to be determined experimentally, a broad-band source, preferably producing an impulse that – with good approximation – can be regarded as a delta function. At the SACLANT ASW Research Centre this ideal has been approximated by using explosive charges as sound sources, in connection with an equalizing filter on the receiver side that boosts the high frequencies in such a way that the spectrum of the explosive pulse approaches that of a delta pulse [*1.1*].

It is our intention to compare our theoretical results with data that are generated by means of this experimental technique. Hence we have to assume that our source radiates equally in all directions. Also the receivers have an omni-directional sensitivity (*Assumption 9*).

1.2.5 Geometry of transmitter and receiver

The positions of transmitter and receiver will be arbitrary. Both the monostatic (coinciding T and R) and the bi-static (separated T and R) case are hence covered. In principle the influence of any coordinate can be studied.

1.2.6 Physics

Our first step will be the construction of a model that describes the scattering and reflection. Physical considerations of a theoretical character indicate that the wave propagation is governed by a wave equation. This equation can be solved by standard techniques. In our case the solution is also determined by the boundary condition of zero total pressure.

Solutions of the wave equation with boundary condition can be found in the frequency domain via the Helmholtz integral [*1.8, p. 24*], or in the time domain by means of the Kirchhoff integral [*1.8, p. 37*]. Our study is begun in the frequency domain.

1.2.7 Linearity and filter theory

One of our basic assumptions is the linear character of the sea surface regarded as a filter. By this we mean that, if an input signal x_1 gives a reflected signal y_1, and if a signal x_2 results in an output signal y_2, then the result of a_1x_1 together with a_2x_2 equals $a_1y_1+a_2y_2$. In other words, the superposition principle is valid and the theory of linear time-dependent filters can be applied [*1.9*] (*Assumption 10*).

Another characteristic of our filter worth mentioning is its causality: the scattered or reflected signal cannot start before the input signal has begun.

Finally we remark that the formulae for the filter functions that will be derived eventually are not linear in ω. This indicates that "washboard" studies (i.e. scattering from a sinusoidal surface) have only limited importance for the problem of scattering by the random sea surface: as a deterministic exercise, and for the analysis of "swell".

1.2.8 Statistical properties

The fully-developed wind-generated sea surface is supposed to be a stationary and homogeneous random process (*Assumption 3*). As a possible random event or "experiment" we can take a description of $\zeta(x, y, t)$ for x and y belonging to a certain domain S_i and t being an element of a time-domain T_i. By assigning to i the values1, 2, 3, ..., n, we can generate a set of possible realizations of the random filter we are studying. Statistical properties such as mean value and variance of a system function can be constructed. Also correlation functions in time and frequency can be derived as ensemble averages. Phenomena like frequency spread (Doppler effect) and time spread can be analyzed. These properties describe the random channel formed by one transmitter, the surface, and one receiver. When more receivers are present, the *spatial* structure of the scattered field can be examined. This subject falls slightly outside the frequency and time analysis of the filter, but it is interesting and important enough in underwater communication to be included.

1.2.9 Coherence

A somewhat different way to look at the channel properties consists in an investigation of the coherence between input and output signal.

A channel that is free of dispersion may change the *amplitude* and *phase* of a transmitted signal but not the *shape*: all frequencies are treated in the same way, i.e. they are subject to the same attenuation and the same time shift. Such a channel processes the signal in a coherent way. This is what would happen if the sea surface were perfectly flat. The rough sea surface, however, does not treat all frequencies equally. Hence it changes the character of the input signal and causes a loss of coherence between input and output. The degree of this coherence loss increases with the surface roughness. In practice, it is often possible to distinguish in the output signal a coherent and an incoherent part. Usually the first one is called *reflection* and the second *scattering*.

1.3 Structure of the thesis

The structure of this thesis can be outlined as follows:

First we give some attention to the literature that is related to our subject. This is done in Chapter 2. We will see that only certain aspects of our problem are covered.

The description of the sea surface as a random process is the subject of Chapter 3. Numerical results that are needed later are collected there.

In Chapter 4 we recall some elements of the theory of linear, time-varying filters. Some statistical properties are included for later use.

Physical considerations that lead to a formula for the transfer function of the sea surface as a random filter can be found in Chapter 5. The result is a series of surface integrals of which the first term is a very good approximation.

The mean value of the transfer function is computed numerically in Chapter 6. It can be regarded as a representation of the deterministic part of the filter. If this deterministic part is set apart, the purely random portion (with zero mean value) is left. Its variance is calculated numerically in Chapter 7.

The results of Chapter 6 and 7 indicate that the filter can be described, with good approximation, by a simple formula. Starting with this formula, time and frequency correlation are studied in Chapter 8; the spatial correlation is discussed in Chapter 9.

With the results of Chapter 8, the properties of output signals can be described. In Chapter 10 this is done for monochromatic input signals, for delta pulses at the input, and (briefly) for arbitrary input signals.

Discussion of the results, and comparison with experimental and theoretical work found in the literature, is the subject of Chapter 11. There it is also indicated which results can be verified best by experiments. This applies to those results for which no comparable material is available.

Finally, in Chapter 12, the conclusions of this study are presented.

References

1.1 R. LAVAL et al., "Coherence Problems in Underwater Acoustic Propagation", SACLANT ASW Res. Centre, Tech. Rep. 102 (1967).

1.2 L. FORTUIN et al., "Wave Propagation in Random Media", SACLANT ASW Res. Centre, Tech. Rep. 221 (1973).

1.3 L. CHERNOV, *Wave Propagation in a Random Medium* (McGraw-Hill, New York, 1960).

1.4 V. I. TATARSKI, *Wave Propagation in a Turbulent Medium* (McGraw-Hill, New York, 1961).

1.5 O. F. HASTRUP, "Digital Analysis of Acoustic Reflectivity in het Tyrrhenian Abyssal Plain", J. Acoust. Soc. Amer. **47**, 181–190 (1970).

1.6 W. J. PIERSON, JR., and L. MOSKOWITZ, "A Proposed Spectral Form for Fully Developed Wind Seas Based on the Similarity Theory of S. A. Kitaigorodskii", J. Geophys. Res. **69**, 5181–5190 (1964).

1.7 R. J. URICK, *Principles of Underwater Sound for Engineers* (McGraw-Hill, New York, 1967).

1.8 B. B. BAKER and E. T. COPSON, *The Mathematical Theory of Huygens' Principle* (Clarendon Press, Oxford, 1953).

1.9 T. KAILATH, "Channel Characterization: Time-Variant Dispersive Channels", in *Lectures on Communication System Theory*, E. J. BAGHDADY, Ed. (McGraw-Hill, New York, 1961), Chapter 6.

2

literature on physical aspects



CHAPTER 2

LITERATURE ON PHYSICAL ASPECTS

2.1 Introduction

The phenomenon of scattering and reflection of waves at uneven surfaces has received much attention in the past 20–25 years. The literature that has resulted covers a wide variety of aspects: electromagnetic and sound waves, rigid boundaries, pressure release surfaces (in acoustics) and perfectly conducting surfaces (for electromagnetic studies), sinusoidal and random boundaries (in two and three dimensions), monochromatic and broadband sources, theoretical and experimental studies, etc. It is no wonder, therefore, that the number of papers and reports is rather impressive.

An excellent introduction to the subject has been provided by BECKMANN and SPIZZICHINO [*2.1*]. Although that book is mainly concerned with the case of electromagnetic waves, it contains enough material to be of interest to the acoustician too.

The literature explicitly dealing with diffraction of underwater sound waves from the sea surface and with the description of the surface is discussed in this chapter. The following system of classification has been used for this review:

1. General considerations,
2. Sinusoidal and other periodical boundaries,
3. Random boundaries,
4. Experimental results,
5. Special subjects.

This has proved to be a useful classification. Many papers, however, belong to more than one class.

Two journals stand out as the leading media for the communication of new results to the scientific world: first of all there is the *Journal of the Acoustical Society of America* with about 50% of the total number of publications, followed by *Soviet Physics-Acoustics* with 11%.

The publications up to the beginning of 1969 are discussed in Section 2.2. This part is a reprint of a paper I published in the *Journal of the Acoustical Society of America* [*2.2*]. More recent papers and articles (up to the middle of 1973), and also tendencies in the studies at present taking place, form the subject of Section 2.3.

The bibliography contained in Section 2.2 and the references at the end of this chapter, provide together a rather complete account of the available literature on scattering and reflection of underwater sound waves from the ocean surface, and related subjects.

2.2 Literature up to the beginning of 1969

This is the thirteenth in a series of review and tutorial papers on the various aspects of acoustics.

Received 9 July 1969

13.4, 13.6; 3.2

Survey of Literature on Reflection and Scattering of Sound Waves at the Sea Surface

LEONARD FORTUIN

SACLANT ASW Research Centre, La Spezia, Italy

The problem of diffraction of waves at uneven surfaces has received increasing attention in the past 15–20 years. This has resulted in a large number of reports and papers in the open literature. In this review article most of the publications dealing with sound waves and pressure release surfaces (both theoretical and experimental) that appeared up to the beginning of 1969 are mentioned as references. They are classified by subject, and the main currents in the literature (Rayleigh and Uretsky method for sinusoidal boundaries, Eckart theory with Kirchhoff approximation for random surfaces, experiments at sea) are analyzed and discussed. General trends, relations between studies, agreements, and contradictions are mentioned. It is found that nearly all of the publications cover only part of the problem: although the wave diffraction at rough surfaces is a function of three basic quantities simultaneously (i.e. time, frequency of incident wave, and geometry), most of the papers deal with only one or another of these three variables. Possible directions of future research are indicated.

LIST OF SYMBOLS

A, A_m, A_{max}, A_{min}	amplitude	J_n	Bessel function
a	effective correlation distance	j	integer
B_j	boundary coefficient	k	wavenumber if incident radiation $(2\pi/\lambda)$
b	constant		
C	constant	L	length of insonified area
c	sound speed	l	integer
c_0	sound speed in ideal medium	M	maximum number of scattering modes
D_x, D_y	wave parameter		
F	surface-wave spectrum	m	scattering mode number; integer
f	frequency of incident radiation (Hz)	n	surface normal; integer
		O	origin of coordinate system
G	generalized spectrum	P	directivity pattern
g	gravity acceleration	$p, p_0, p_1, p_T, p_r, p_s$	pressure
H	trough-to-crest surface wave height	q	probability function
$H_0^{(1)}$	Hankel function	R	receiver; shadowing function
h	amplitude of sinusoidal surface; standard deviation of surface elevation	r, r_{10}	distance
		S	surface; shadowing function
		s	surface profile
I_s, I_0	intensity	T	transmitter
J	autocovariance function of surface insonification	U	unit step function
		u	speed of surface wave

Copyright © 1970 by the Acoustical Society of America.

V	reflection coefficient
v	wind speed
x, x'	horizontal coordinate
y, y'	horizontal coordinate
z, z'	vertical coordinate
$\alpha, \alpha_T, \alpha_R$	direct cosine; angle with X axis
β, β_T, β_R	direction cosine
$\gamma, \gamma_T, \gamma_R$	direction cosine
Δ	layer thickness
ζ	(normalized) surface profile
ζ'	surface slope
η	difference in y coordinates; normalized y coordinate
$\theta, \theta_m, \theta_{in}, \theta_{out}$	angle with vertical
K, K_x, K_y	surface wavenumber $(2\pi/\Lambda)$
Λ	surface period
Λ_M	intensity of scattered waves
λ	incident wavelength
$\lambda, \lambda_0, \lambda_m$	direction cosine
μ, μ_0, μ_m	direction cosine
ν	direction cosine
ξ	difference in x coordinate; normalized x coordinate
ρ	correlation distance
σ	scattering coefficient
σ_B	backscattering strength
τ	time difference
Φ, Φ_1, Φ_2	surface correlation function
φ	grazing angle
χ	roughness parameter
Ψ	correlation function of pressure
ψ	phase angle
ω	radial frequency of incident wave
ω_D	frequency shift
ω_s	frequency of surface wave

INTRODUCTION

The problem of the diffraction of waves at uneven surfaces has received increasing attention in the past 15–20 years; "this is due to the growing application of acoustic waves and radio waves in the centimetre band" [*3, p.1*].

Mathematically, the problem is "marvelously complex" [*24, p. 1293*]. It consists of solving a wave equation for which certain boundary conditions have to be satisfied, whereas the shape of the boundary can be extremely complicated. For this reason, a general and exact treatment of the problem has not—so far—been published.

Nevertheless, a large number of publications in the open literature are devoted to the subject. But they cover only a part of the problem: all of them are restricted to a special case, and are based on certain assumptions—sometimes rather arbitrary—that make simplifications possible but at the same time cast doubt on their validity.

An excellent survey of the literature up to 1958 has been given by Lysanov [*3*]. Although this paper deals only with periodically uneven surfaces, it has a wider importance, because many techniques can be applied to both periodically and statistically uneven surfaces.

More recent work, up to the beginning of 1969, is discussed and analyzed in Ref. *2*. The present paper is a shortened version thereof.

Two types of waves can be found in the literature: sound waves and electromagnetic waves. Both types give rise to the same type of mathematics, when reflection and scattering at uneven surfaces is studied. There is an important difference, however: in the case of electromagnetic waves, the wavelength of the incident radiation is usually much smaller than the scale of roughness of the reflecting boundary. Ray theory and geometrical optics can then be applied. For sound waves that are scattered from the sea surface, incident wavelength and roughness scale can be of the same order of magnitude. A diffraction theory then applies.

Also two types of boundaries can be distinguished in practice, with some idealization:

(1) The free, elastic boundary (e.g., the sea surface) on which the wave potential vanishes is also called "pressure release" or "perfectly conducting."

(2) The rigid boundary (e.g., the rocky ocean floor) is that where the directional derivative of the wave potential becomes zero.

Except for the book by Beckmann and Spizzichino [*1*], this survey refers only to publications that deal with sound waves and with perfectly reflecting, free boundaries. The references at the end are grouped according to subject. But this is no strict division, as many papers belong to more than one group.

I. GENERAL CONSIDERATIONS

The phenomenon of scattering and reflection of sound waves at the sea surface is a random process, both in space and time. It depends basically on three parameters:

(*1*) *Frequency of incident wave:* For very high frequencies a behavior similar to "geometrical optics" is likely: shadowing of "valleys" by "peaks" may occur, whereas for low frequencies the waves will be diffracted and reach all surface points.

(*2*) *Time:* Even for fixed geometry and a monochromatic incident wave, the scattered field is not constant, because the boundary is continuously in movement, owing to winds and currents. A realistic description of the scattered field is hence impossible without involving the time variable.

(*3*) *Geometry of source and receiver:* The diffracted field depends strongly on the relative position of source and receiver with respect to the boundary. The shadow-

ing mentioned will become increasingly important when the grazing angle approaches zero. Volume scattering due to an inhomogeneous subsurface layer can also take place then.

A general statistical description of the diffracted field, complete up to second-order statistical moments, therefore requires both a realistic surface model that is valid for a broad range of incident frequencies and that takes into account the possibility of subsurface scattering, and observation of the field at an array of separately located receivers, at two frequencies, and at two instants of time. Only then can one obtain knowledge about the following subjects: impulse response of the surface, frequency spreading of signals due to the Doppler effect (coherence limits), and curvature of the wavefronts.

In view of the foregoing remarks, we can draw a general conclusion from the literature: most papers give a very incomplete description of the phenomenon of scattering and reflection of sound waves at the ocean surface, as they deal—roughly speaking—only with the following features:

(*1*) *Monochromatic waves* (In experimental work, explosives are sometimes used, but then the analysis is done via narrow-band filters, reducing the experiment to the monochromatic case again).

(*2*) *Time-independent surfaces* (The sinusoidal boundary is often encountered. This type of boundary is only a poor approximation of the true sea surface, but it offers the advantage of a rigorous treatment of the problem, without the need of statistical considerations. Most of the studies involve the (Rayleigh) expansion of the reflected field into an infinite set of plane waves. Details are given in Sec. II. The random surfaces are based on the assumption of a stationary Gaussian process, mainly for computational reasons. Analysis of the sea surface has shown that this assumption is not far from the truth. The spatial correlation function of the surface however, is often arbitrarily chosen, e.g., exponential or Gaussian, again with the excuse that it makes continuation of the calculations possible. In more recent publications, the Neumann–Pierson model of ocean wave spectra is receiving increasing attention.).

(*3*) *One receiver.*

(*4*) *Ideal subsurface layer.*

There is one important exception to this general conclusion: the quasiphenomenological approach of Middleton [*49, 50*]. A very short description of this approach can be found in Sec. III-C.

II. SINUSOIDAL BOUNDARIES

At the end of the 19th century, Lord Rayleigh studied the scattering of sound waves at periodically corrugated surfaces [*4*]. His method can be considered as the first attempt to solve the wave equation in combination with a boundary condition. It is an intuitive approach that has been used by many investigators, often with modifications, up to the present day.

The periodicity of the boundary prompted Rayleigh to expand the reflected field into a set of undamped plane waves. His assumption that this expansion is valid up to the boundary (which he made to use the boundary condition) has been questioned by many authors. The dispute about the Rayleigh method is condensed in Sec. II-B.

A. Rayleigh's Method for a Sinusoidal Surface

A simple and straightforward description of the Rayleigh method for a periodic boundary is given by Beckmann [*1, Chap. 4*], from which the following is a summary. A plane monochromatic sound wave with wavelength λ is incident on an infinitely long periodic boundary, with angle of incidence θ. In its most simple form, such a boundary can be described by:

$$z=\zeta(x)=\zeta(x+\Lambda) \quad (-\infty<x<\infty). \tag{1}$$

Because of the periodicity of the surface, the diffracted field is assumed to propagate in certain discrete modes, making angles θ_m with the vertical that are given by the grating formula:

$$\sin\theta_m=\sin\theta+m\lambda/\Lambda, \quad (m=0,\pm1,\pm2,\cdots),$$

or, in terms of the wavenumbers k and K,

$$\sin\theta_m=\sin\theta+m\mathrm{K}/k. \tag{2}$$

We remark that for $m=0$ the reflection is "specular."

According to Eq. 2, θ_m can only assume discrete values when λ and Λ are held constant. These are the directions of scattering. They have the property that in these directions the waves scattered from individual periods reinforce each other because their phase difference is an integral number of periods.

For a sinusoidal surface, namely for

$$\zeta(x)=h\cos(\mathrm{K}x), \quad (-\infty<x<\infty), \tag{3}$$

Rayleigh calculated the amplitudes $A_m(m=0,\pm1,\pm2,\cdots)$ of the scattered waves via the boundary condition $p=0$, where p is the total pressure field. His procedure for obtaining a solution of the wave equation, i.e., the coefficients A_m, is based on two assumptions:

(1) That the total field can be written as an infinite sum of plane waves:

$$p(x,z)=\exp[ik(x\sin\theta-z\cos\theta)] + \sum_{m=-\infty}^{\infty} A_m\exp[ik(x\sin\theta_m+z\cos\theta_m)] \tag{4}$$

(the first term on the right-hand side being the incident wave).

(2) That this equation holds everywhere above and on the boundary. This assumption is not at all obvious and has been seriously criticized (see Sec. II-B).

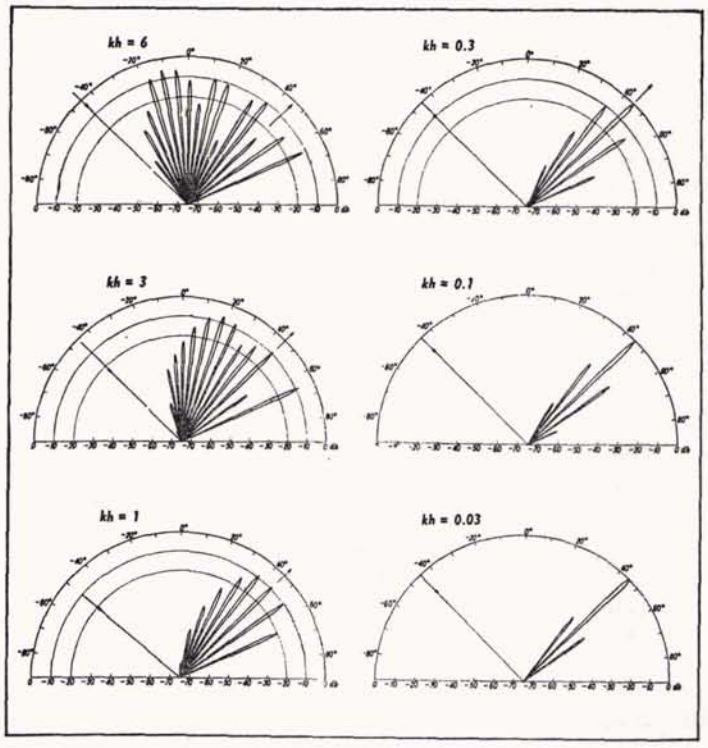


FIG. 1. Diffraction of a plane harmonic wave by a sinusoidal boundary of finite length; $\theta=45°$, $\Lambda=10\lambda$, and kh is a measure of the surface roughness. *From Beckmann and Spizzichino [1, pp. 50–53].*

With his two assumptions Rayleigh found, for a point (x,z) at the boundary, the equation

$$\exp[-ik\zeta(x)\cos\theta]$$

$$=-\sum_{m=-\infty}^{\infty} A_m \exp[imKx+ik\zeta(x)\cos\theta_m]. \quad (5)$$

"Both sides of this equation are now expanded in a Fourier series with respect to x (which will in general result in a double series on the right side) and the resulting Fourier coefficients are equated. This results in an infinite set of linear equations, each of which contains the unknown coefficient A_m. By progressive solution (or successive approximation) the coefficients A_m are then approximated" [*1, p. 43*]. Formulas for the first coefficients can be found in Appendix A.

The total number of possible modes as predicted by Eq. 2 is limited by the condition $|\sin\theta_m|\leq 1$. We call this maximum M. For $m>M$, the condition is violated. Then $\cos\theta_m$ becomes imaginary and we have (see Eq. 5) waves propagating along the surface (Rayleigh surface waves) that decay exponentially with depth.

The propagation in discrete modes described here is valid for "surfaces" that extend from $-\infty$ to $+\infty$. It is interesting to note what happens when the periodic surface is of finite length. Then the diffracted field—instead of being cancelled completely because of destructive interference between the directions given by the grating formula (Eq. 2)—decreases gradually and then increases again, when the observer is moved from the direction θ_m to θ_{m+1}. In this way, the so-called "lobes" are formed. Their width increases as the surface becomes shorter.

For several combinations of θ, Λ, and kh, Beckmann [*1*] gives figures that illustrate this formation of lobes. They show that with decreasing value of kh, the "roughness" becomes smaller so that fewer and fewer sidelobes appear and the lobe with $m=0$ (specular reflection) becomes more and more pronounced. With constant kh and Λ, the reflection becomes more specular as θ increases. Both facts agree with a definition of roughness of the form

$$\chi=Ckh\cos\theta. \quad (6)$$

Examples for $\theta=45°$ and $\Lambda=10\lambda$ are reproduced in Fig. 1.

B. The Dispute about the Rayleigh Method

Commenting upon Rayleigh's procedure for obtaining a solution for the wave equation in the presence of a sinusoidal boundary, Uretsky remarked that: "The crucial and unjustified step in this procedure is the assumption that Eq. 4 describes the solution everywhere above the bounding surface" [*25, p. 401*]. Referring to a lettter by Lippmann [*13*], he made it seem plausible that the assumption breaks down in the "valleys" between the "peaks," because there both up-

going and down-going waves should be expected. For this reason he carefully developed a solution to the problem, based on Green's theorem (Sec. II-C). Comparing his results with those of Rayleigh, one of his conclusions (based on numerical experimentation) is "that the Rayleigh equations are useful when the undulations of the bounding surface are gentle (small hK)" [*25, p. 421*].*

Meecham too [*17, 47*] remarked that the validity of Rayleigh's second assumption is doubtful. He developed a variational method, for the case of a periodic surface [*17*], which improves the Rayleigh method via an error-minimizing procedure, and a Fourier transform method for boundaries of arbitrary shape. This latter method, in which an approximation of the first derivative of the pressure at the boundary is obtained by placing a receiver at this boundary, is found to be "preferable to previous methods, notably those which can be classified as physical optics (such as Rayleigh's), since the error in the transform method is of second order in the surface slope, whereas the error in previous methods is of first order in the same quantity" [*47, p. 370—abstract*].

The question of the validity of Rayleigh's second assumption has been attacked from another side by Heaps. He presented "an investigation of the least possible value of the surface pressure consistent with the assumption that all the reflected radiation is in the form of undamped plane waves" [*10, p. 815*]. He arrived at the conclusion, after comparison of his results with experimental data "that if all reflected energy has the form of undamped plane waves then the surface is necessarily sound absorbing and of pressure significantly different from zero. Thus, in the neighborhood of a corrugated surface of zero pressure, it is necessary to take into account other forms of radiation and such forms play a significant part in satisfying the boundary condition" [*10, p. 818*].

As Marsh has generalized the Rayleigh method for random surfaces (Sec. III-A), he is arguing "In Defense of Rayleigh's Scattering from Corrugated Surfaces" [*16*]. His results (for simplicity he takes a sinusoidal surface) have been compared with those of Uretsky [*24, 25*] by Murphy and Lord. They showed "that Rayleigh's formulation is inadequate for the description of the scattered field" [*18, p. 1598—abstract*].

The results of the above mentioned papers lead us to the conclusion that the Rayleigh method is indeed incorrect in the way the boundary conditions are used. Nevertheless, for smooth surfaces (small hK), the method produces results that do not disagree more with experimental data than do other, more rigorous, solutions. It is therefore, useful to a limited extent. The method developed by Uretsky, on the other hand, is strict in a mathematical sense and therefore superior to the Rayleigh solution.

Finally we remark that Beckmann [*1*], surprisingly enough, does not touch upon the question of the validity of Rayleigh's assumptions.

C. Uretsky's Method for a Sinusoidal Surface

Uretsky devoted two publications to his method: a very short outline [*24*], which is no more than an introduction, and a very thorough and detailed treatment [*25*]. The latter one contains a complete description of the method with the necessary mathematical proofs, as well as valuable comments upon the Rayleigh method and the Kirchoff approximation. Application of the Uretsky procedure can be found in a study by Barnard *et al.* [*7*], who summarized the Uretsky approach, made numerical predictions, and compared these with experimental results from a pressure release cork surface in a model tank. Satisfactory agreement was obtained.

The method starts in the same way as the Rayleigh method. A plane monochromatic wave with direction cosines $\lambda_0(=\sin\theta)$ and $\mu_0(=\cos\theta)$ is incident on a sinusoidal pressure release surface as given by Eq. 3. Instead of assuming that the scattered field can be expanded into an infinite set of plane waves (as Rayleigh did), Uretsky proves that this is possible for observation points not too close to the boundary,

$$p_1(x,z)=\sum_{m=-\infty}^{\infty} A_m \exp[ik(x\sin\theta_m+z\cos\theta_m)] \qquad (z\geq h). \quad (7)$$

The difference from Rayleigh appears in the next step: the expansion of Eq. 7 is not valid for $z<h$, because there its terms fail to be solutions of the wave equation. The Helmholtz formula [*5a*] which expresses the scattered field p_1 as an integral over elementary sources induced on the boundary by the incident wave p_0, is invoked to avoid Rayleigh's second assumption. In terms of Green's functions,† the Helmholtz integral can be written for a two-dimensional case as

$$p_1(\mathbf{r})=\frac{i}{4}\int_{-\infty}^{\infty} dx' H_0^{(1)}(k|\mathbf{r}-\mathbf{r}'|)\nabla p(\mathbf{r}'), \qquad (8)$$

because the term in the original integrand containing the total pressure p vanishes on a free surface. "The crucial step in the present formulation of the problem is to recognize that $\nabla p(\mathbf{r}')$ admits a Fourier series representation" [*24, p. 1293*]; the proof is given in Ref. *25*. Hence, with $\lambda_j=\lambda_0+j\mathrm{K}/k$, Uretsky finds

$$p_1(x,z)=\frac{ik}{4}\sum_{j=-\infty}^{\infty}(i)^{-j}B_j\int_{-\infty}^{\infty} dx' H_0^{(1)}(k|\mathbf{r}-\mathbf{r}'|) \times\exp(ik\lambda_j x'). \quad (9)$$

In order to find the scattered field p_1, the boundary coefficients B_j have to be determined. This can be done via the boundary condition of zero total pressure, which gives

$$-p_1[x,\zeta(x)]=p_0[x,\zeta(x)] \equiv\exp\{ik[\lambda_0 x-\mu_0 h\cos(\mathrm{K}x)]\}. \quad (10)$$

At this point, the mathematics become rather involved. Details can be found in Refs. *24* and *25*, or in

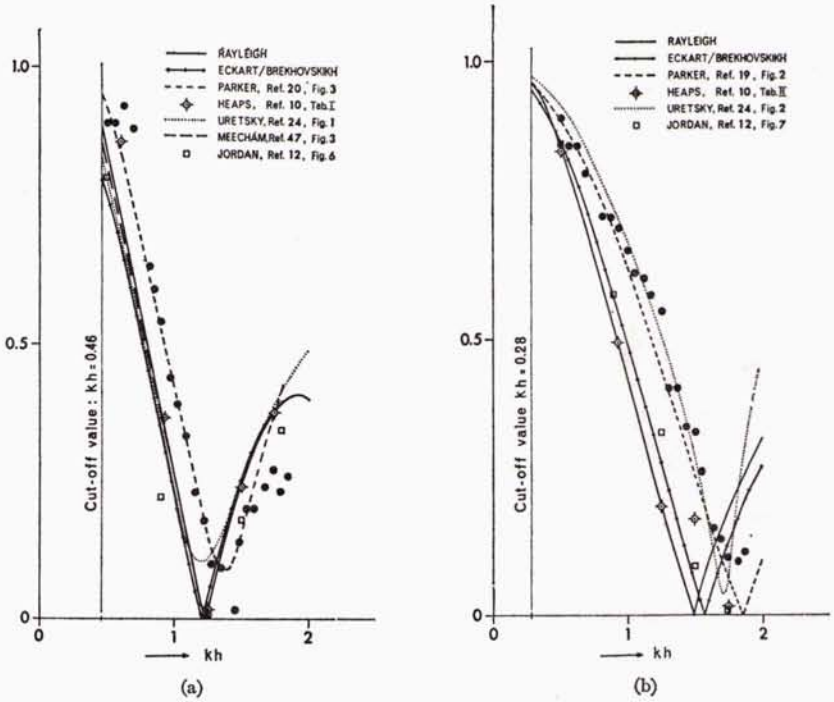


FIG. 2. The specularly reflected $|A_0|$ from a sinusoidal surface with roughness $h\mathrm{K}=0.46$; angle of incidence (a) $\theta=0^0$, (b) $\theta=40°$; black dots are experimental data from La Casce and Tamarkin [*69, Figs. 2C–3C*]. (Rayleigh and Eckart/Brekhovskikh values as shown in Appendix A.)

the summaries of Refs. *2* and *7*; here we indicate only the main steps. The exponential in Eq. 10 is expanded in a Fourier series, as in the Rayleigh method, after which an infinite set of algebraic equations for the B_j is derived:

$$\sum_{j=-\infty}^{\infty} M_{1j}B_j=(-1)^1J_1(hk\mu_0). \tag{11}$$

"The major complication of the problem (other than the usual difficulties associated with inverting infinite matrices) is in the calculation of the matrix elements M_{1j}" [*24, p. 1294*]. But the evaluation is possible, although the result is somewhat complicated.

Inversion of Eq. 11 yields the boundary coefficients B_j. A relation between A_m and B_j is then needed to calculate p_1 with Eq. 7. The required relation is proved to be

$$A_m=(-i)^{m+1}(2\mu_m)^{-1}\sum_j B_jJ_{m-j}(hk\mu_m). \tag{12}$$

The Uretsky method is far from simple, especially in comparison with the Rayleigh technique. But the results are obtained with a high degree of mathematical strictness and with a minimum of conditions on the validity. It may be noted that only the surface height h appears explicitly in the formulas; the surface wavenumber K is still present, though, as it should be, via μ_m and λ_m.

A generalization of the Uretsky method for random surfaces seems possible, by analogy to Marsh's extension of the Rayleigh method. The result could be interesting (although probably rather complicated), as it would be applicable to the ocean without too restrictive conditions for the roughness.

D. Comparison of Several Methods with Each Other and with Experimental Results

The experiments of La Casce and Tamarkin have provided the theoreticians with data that could serve as a check for their theories. These experimental data have been published in a study on the reflection of underwater sound from corrugated surfaces [*69*].

In addition to their experimental work, the authors have summarized the theories of Rayleigh, Eckart [*31*] and Brekhovskikh, and compared them with their data. Their formulae for the amplitude coefficients A_m are given in Appendix A.

Several authors have used the experimental results of Ref. *69* to check their own theories: Meecham [*47*] applied his Fourier transform method to a sinusoidal boundary, Parker [*19, 20*] extended the Rayleigh series of plane waves into an integral, Heaps derived from the Rayleigh method a recurrence relation for A_m [*9*] and (with the assumption that the reflected field contains only undamped plane waves) obtained values for A_m that minimize the mean square pressure at the boundary [*10*], Jordan [*12*] computed values for A_m via the coordinate transform

$$z'=z-h\cos(\mathrm{K}x), \tag{13}$$

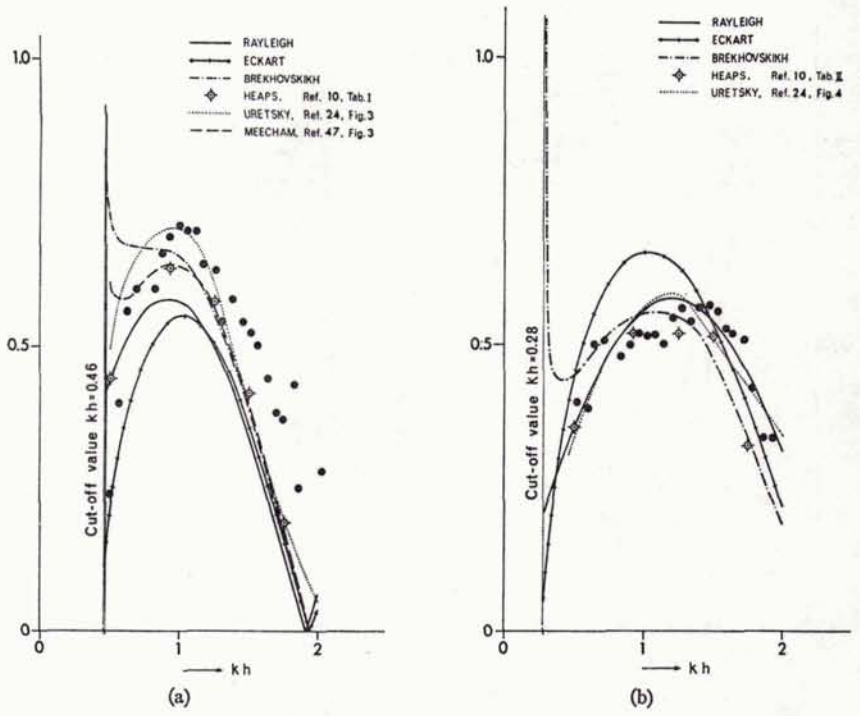


FIG. 3. The first-order backscattered amplitude $|A_{-1}|$ from a sinusoidal surface with roughness $h\mathrm{K}=0.46$; angle of incidence (a) $\theta=0°$, (b) $\theta=40°$; black dots are experimental data from La Casce and Tamarkin [*69, Figs. 6C–7C*]. (Rayleigh, Eckart, and Brekhovskikh values as shown in Appendix A.)

and Uretsky [*24*] avoided the mathematical defect of Rayleigh's procedure with a careful and rigorous solution. All these methods to describe the scattering from sinusoidal boundaries, though very different in formulation and final results, agree in predicting that the main directions of scattering are given by the grating formula (Eq. 2).

La Casce and Tamarkin obtained their results with pressure release cork surfaces of approximately sinusoidal form, floating on top of the water in a tank. Such a surface can be described by Eq. 3. For a concrete situation, values have to be assigned to the parameters θ, k, h, K, and m. La Casce and Tamarkin have experimented with three surfaces, for which $h\mathrm{K}$ equals 2.12, 0.75, and 0.46, respectively. They measured the scattered amplitude A_m for $m=0$, -1, -2, and $\theta=0°$, 20°, 40°, and 60°, as a function of kh, thus providing a rich source of data for comparison.

In order to facilitate the comparison of the available theories with each other and with experimental results, we have plotted in Figs. 2–4 some of the data of La Casce and Tamarkin together with theoretical curves and points. The ones according to Rayleigh, Eckart, and Brekhovskikh, we have computed with the formulas of Table I; the other data are copied from the discussed papers. The figures show the specularly reflected amplitude and the first- and second-order backscattered amplitudes for $\theta=0°$ and 40°, as functions of kh, for the third experimental surface ($h\mathrm{K}=0.46$), as this is the most sinusoidal one and because most of the theories presented are based on the assumption of small surface slopes.

Since the surface with $h\mathrm{K}=0.46$ is not very rough, the Rayleigh prediction is not significantly worse than other curves. The Uretsky curves, for which a small slope is not required, are satisfactory but do not appear superior to the others. More interesting, therefore, is the application of Uretsky's theory to rough surfaces. This has been done by Barnard *et al.* [*7*] in their model studies. Their surface can be characterized with: $h=1.5$ cm, $\mathrm{K}=1.4$ cm^{-1}, and hence $h\mathrm{K}=2.1$. The frequency of incident sound was 100 kHz (or $k=4.2$ cm^{-1}, making $hk=6.3$). They measured the backscattering as a function of grazing angle with fixed angle of incidence. "The agreement between the calculated and experimental curves (· · ·) is, in general excellent" [*7, p. 1168*].

III. RANDOM BOUNDARIES

A. The Marsh–Rayleigh Method

The method of Lord Rayleigh for a sinusoidal boundary (Sec. II-A) has been generalized by Marsh for the case of a random surface [*40*]. He published his generalization "in an heuristic form, in order to avoid presenting the exceedingly heavy analysis required for a rigorous treatment" [*p. 330*]. This omission of sufficient comments on the basic steps in his paper, together with a rather large number of misprints, makes his article somewhat hard to follow. Marsh's extension of the Rayleigh method is obtained via Wiener's concept of

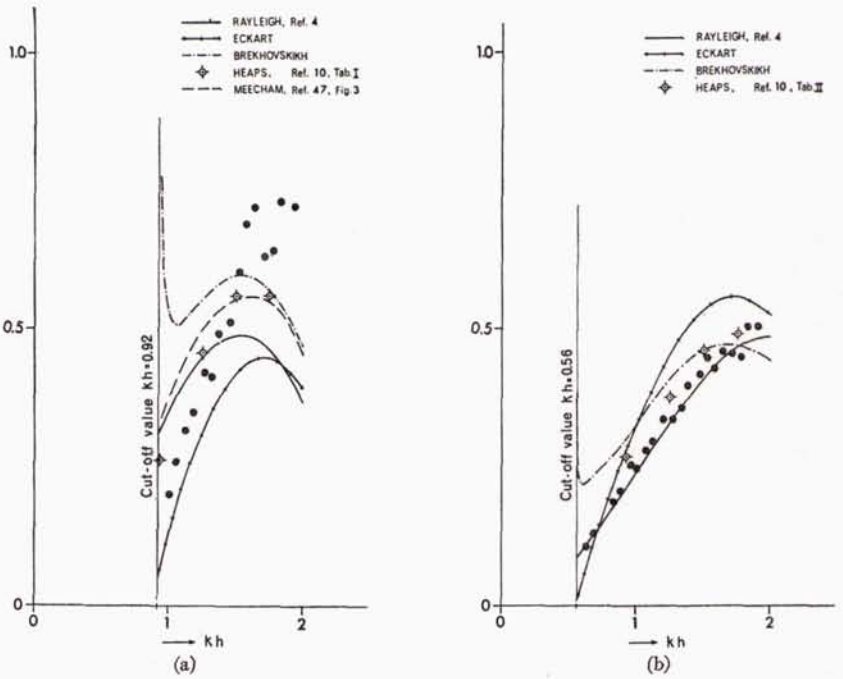


FIG. 4. The second-order backscattered amplitude $|A_{-2}|$ from a sinusoidal surface with roughness $h\mathrm{K}=0.46$; angle of incidence (a) $\theta=0°$, (b) $\theta=40°$; black dots are experimental data from La Casce and Tamarkin [*69, Figs. 8A–8B*]. (Eckart and Brekhovskikh values as shown in Appendix A.)

"Generalized Harmonic Analysis" [*56a*]. It produces an expression for the correlation function of the scattered field at two points in space in a horizontal plane below the rough surface upon which a plane monochromatic sound wave is incident, but "this solution is readily extended to include electromagnetic waves, general elastic waves, and non-planar, non-harmonic sources" [*p. 330—abstract*].

The "exact" solution for the problem of wave scattering by irregular surfaces can be summarized as follows. A monochromatic plane wave (direction cosines α, β, γ) is incident on a random pressure relief boundary $S[z=s(x,y)]$. For the diffracted field $p_1(x,y,z)$, a plane-wave representation is sought by writing

$$p_1(x,y,z)=\iint_{-\infty}^{+\infty}\exp[-ik(\lambda x+\mu y-\nu z)]dG(\lambda,\mu), \quad (14)$$

where $G(\lambda,\mu)$ is the generalized spectrum of $p_1(x,y,z)$ and λ, μ, ν are the direction cosines of the diffracted wave (hence: $\lambda^2+\mu^2+\nu^2=1$). The expansion in Eq. 14 is a straightforward generalization of the Rayleigh method for a periodic surface, in which $p_1(x,y,z)$ was decomposed into an infinite series of plane waves (see Eq. 4). Rayleigh's second assumption, that the expansion is valid up to the boundary, is also adopted by Marsh; the criticisms of Rayleigh's approach apply therefore equally to Marsh's (see Sec. II-B).

With the boundary condition of zero total pressure and after normalization of variables: $kx=\xi$, $ky=\eta$, $ks(x,y)=\sigma\zeta(\xi,\eta)$, $\sigma^2=k^2h^2$, $h^2=\langle(s-\langle s\rangle)^2\rangle$ and $\langle(\zeta-\langle\zeta\rangle)^2\rangle=1$, Marsh obtained

$$\exp[-i(\alpha\xi+\beta\eta+\gamma\sigma\zeta)]+\iint_{-\infty}^{+\infty}\exp[-i(\lambda\xi+\mu\eta-\nu\sigma\zeta)]dG(\lambda,\mu)=0. \quad (15)$$

After this, he expanded $G(\lambda,\mu)$ in a power series in σ:

$$G(\lambda,\mu)=\sum_{m=0}^{\infty}\sigma^m A_m(\lambda,\mu) \quad (16)$$

and the coefficients A_m are to be calculated. Substitution of Eq. 16 into Eq. 15 yields an infinite set of simultaneous linear equations for the determination of the $A_m(\lambda,\mu)$. By clever manipulation of these equations Marsh found a simple-looking expression for the scattered field at a point not on the boundary. Choosing the coordinate system in such a way that the point of observation lies in the plane $z=0$ (this includes: $\langle\zeta(x,y)\rangle\neq 0$, in contrast to most other theories), he obtained:

$$p(\xi,\eta,0)=-\exp[-i(\alpha\xi+\beta\eta+\gamma\sigma\zeta)]/(1+X), \quad (17)$$

where X is a complicated operator closely related to the basic expression in Wiener's work.

Marsh, Schulkin, and Kneale [*41*] have worked out the method in more detail, assuming σ so small that $G(\lambda,\mu)$ can be represented satisfactorily with three terms of the series in Eq. 16. The necessary condition for this approximation was not discussed. They calculated the correlation function

$$\Psi(\xi,\eta)=\langle p(\xi_1,\eta_1,0)p^*(\xi_1+\xi,\eta_1+\eta,0)\rangle \quad (18)$$

and found

$$\Psi(\xi,\eta)=\exp[-i(\alpha\xi+\beta\eta)]$$

$$\times\left[1+4\gamma^2\sigma^2\Phi(\xi,\eta)-4\gamma\sigma^2\int_{-\infty}^{+\infty}\int\nu F(\lambda-\alpha,\mu-\beta)d\lambda d\mu\right]. \quad (19)$$

In this formula, $F(\lambda,\mu)$ is the "power spectrum" of $\zeta(\xi,\eta)$, and $\Phi(\xi,\eta)$ the surface autocorrelation function; F and Φ are each other's Fourier transforms.

The Fourier transform of $\Psi(\xi,\eta)$, called $\Lambda_M(\lambda,\mu)$, has an important physical meaning: it "is proportional to the intensity of waves proceeding parallel to the line with direction cosines λ, μ." "In general, Λ_M will consist of both a discrete and a continuous portion. The discrete portion, where Λ_M is singular, represents plane scattered waves of finite amplitude (such as the specularly reflected wave). For such plane waves, the integral of Λ_M in the immediate vicinity of its singularity is equal to the square wave amplitude" [*40, p. 331*].

B. The Kirchhoff Approximation and Variations

When the scattered field at an observation point is expressed as an integral over elementary sources induced at the surface by the incident wave (this is the so-called Helmholtz integral [*25a*], an assumption has to be made for the first derivative of the scattered wave field at the free boundary. For a random surface, the exact value of this quantity is hard to obtain; approximation then takes the place of exactness. The assumption most frequently met is the "Kirchhoff approximation": the required directional derivative is put equal to the first derivative of the incident wave, which is a known quantity. The validity of this assumption is limited to the case of surfaces that are "locally flat"; this means that the radius of curvature of the surface has to be much larger than the incident wavelength.

A systematic derivation of the Kirchhoff approximation, which discusses its limits of validity and "shows the size of the errors incurred through its use," has been published by Meecham [*48*]. His formulas justify the foregoing qualitative statement.

The leading publication in the group of papers that adopted the Kirchhoff approximation is the paper by Eckart [*31*]. The interest of Eckart's work lies in the fact that he "obtained significant results with minimum mathematical complexity by relying on a highly developed physical insight into the problem," as has been remarked by Horton and Muir [*38, p. 627*].

Also the work of Brekhovskikh has to be mentioned here. His method of obtaining an estimate for the directional derivative of the scattered field at the boundary corresponds to the Kirchhoff approximation.

1. Eckart's Theory

The basic ideas of Eckart's theory can be summarized as follows. A transmitter T (monochromatic) and a receiver R are placed above a reflecting surface $S[z=\zeta(x,y)]$. The transmitter induces elementary sources at S; the scattered pressure field $p_1(R)$ can be obtained from these sources via the Helmholtz integral.

$$p_1(R)=\frac{1}{4\pi}\int\int dS\left[\frac{\partial p_1}{\partial n}\left(\frac{e^{ikr}}{r}\right)-p_1\frac{\partial}{\partial n}\left(\frac{e^{ikr}}{r}\right)\right], \quad (20)$$

in which r is the distance from dS to R, and $\mathbf{n}$ is the unit normal to dS directed away from R. For a pressure release surface, one has the boundary condition

$$p_0+p_1=0 \text{ on } S, \quad (21)$$

where p_0 is the incident pressure wave. The evaluation of the Helmholtz integral requires also the first directional derivative of p_1. As a second boundary condition, Eckart assumed the validity of the Kirchhoff approximation,

$$\partial p_1/\partial n=\partial p_0/\partial n \text{ on } S. \quad (22)$$

Mintzer [*51*] has criticized this assumption with good reasons: when p_1 is fixed on S, the quantity $\partial p_1/\partial n$ cannot be choosen independently [*25a, p. 27*]. He showed that the second assumption is at most a first approximation for smooth surfaces.

Eckart assumed that T is a directional source and so far away from S that for all points of the insonified area the distance to T is the same. A similar assumption is made for R. Indicating the positions of T and R with the direction cosines $(\alpha_T,\beta_T,\gamma_T)$ and $(\alpha_R,\beta_R,\gamma_R)$, putting $\alpha_T+\alpha_R\equiv\alpha$, etc., and replacing $\partial/\partial n$ by $\partial/\partial z$ (small surface slopes), he derived from Eq. 20:

$$4\pi p_1(R)=ik\gamma\frac{e^{ikr_{10}}}{r_{10}}\int_{-\infty}^{+\infty}\int dxdyP$$

$$\times\exp[-ik(\alpha x+\beta y+\gamma\zeta)], \quad (23)$$

where r_{10} is the distance from R to 0, the center of the insonified area, and P equals the incident pressure at 0. Equation 23 is the basic expression in Eckart's theory. It is used as the starting point for special cases.

Although the Eckart theory can be used for nonrandom-surface profiles, it is designed originally for a random surface $\zeta(x,y)$ that can be considered as a stationary two-dimensional process, in which case second-order moments of the scattered field are calculated. Two auxiliary functions, then, play a role:

$$\Phi(\xi,\eta)=\langle\zeta(x,y)\zeta(x+\xi,y+\eta)\rangle \quad (24)$$

and

$$J(\xi,\eta)=\int_{-\infty}^{+\infty}\int dxdyP(x,y)P^*(x+\xi,y+\eta). \quad (25)$$

Putting $\Phi(0,0)\equiv h^2$ and calling a the effective correlation distance of $\zeta(x,y)$ and L the effective size of the insonified area, the basic conditions of Eckart's theory

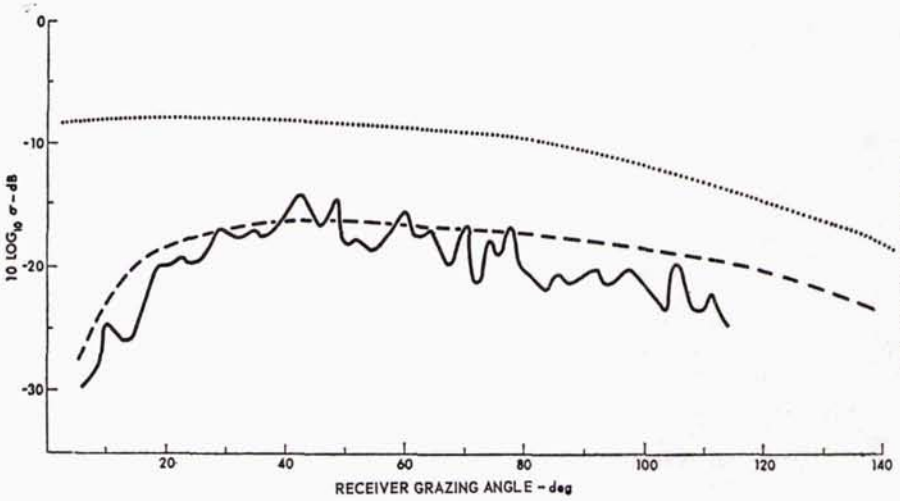


FIG. 5. Scattering from a rough surface with Gaussian correlation function. —— experimental; · · · Eckart theory with second boundary condition given by Eq. 22; – – – Eckart theory with second boundary condition given by Eq. 29; $f=100$ kHz, $h=9$ mm, $\theta=45°$. *From Horton, Mitchell, and Barnard [68].*

are

$$h \ll \lambda \ll a \ll L. \tag{26}$$

Eckart calculated the average scattered intensity $\langle I_s \rangle$, for the low-frequency and the high-frequency cases. For the low-frequency case, he found

$$\langle I_s \rangle = J(0,0)\sigma, \tag{27}$$

with

$$\sigma = (k^2\gamma^2/4\pi)^2 F(k\alpha, k\beta), \tag{28}$$

the function $F(K_x,K_y)$ being the surface wave spectrum. He refers to σ as "a dimensionless quantity that may be called the scattering coefficient, or more descriptively, the scattering cross section for unit solid angle per unit area of sea surface" [*31, p. 568*]. Equation 28 indicates an important result: "the low-frequency scattering is determined by the surface spectrum, and not by the height distribution" [*42, p. 197*].

In the high-frequency case, the calculation of σ is possible only if the characteristic function of the two-dimensional random variable $W \equiv [\zeta(x,y), \zeta(x',y')]$ is known. The hypothesis of a Gaussian probability density yields an expression for σ that is independent of frequency. This is a disappointing result for the "inverse problem" (see Sec. V-F) as it does not contain the function Φ but only the variances of the surface slopes.

2. *Variations of Eckart's Theory*

Horton and Muir [*38*] extended the low-frequency case by specifying $\Phi(\xi,\eta)$ [or $F(K_x,K_y)$, its Fourier transform] for isotropic cases. Among others they substituted an exponential and a Gaussian shape for Φ. They found in all considered cases that, if $a \gg h$, "the scattered energy is highly directional and is concentrated about the direction of specular reflection" [*38, p. 632*]. A companion paper by Horton, Mitchell, and Barnard [*68*] deals with experiments on a rough Gaussian surface in a model tank. The authors used the high-frequency formula for σ of Ref. *38* to check their experimental data. The agreement was not very satisfactory, until they changed the second boundary condition into

$$\partial p_1/\partial n = 0 \text{ on } S, \tag{29}$$

which is a compromise between Eq. 22 (valid for illuminated areas) and $\partial p_1/\partial n = -\partial p_0/\partial n$ (holding in the deep shadows). This modification can be interpreted as the introduction of a "shadowing function" (see Sec. V-E), with the value 0.5 over the whole surface. The remarkable effect of the new boundary condition can be observed in Fig. 5.

Although Eckart discussed only a low- and a high-frequency case, his theory is also valid in the intermediate range of frequencies. Proud, Beyer, and Tamarkin presented "a solution valid for all wavelengths" [*55, p. 544*] for a surface with Gaussian probability density (at least up to the second order), in which the Fourier integral plays an important part. There is a difference between their procedure and the one followed by Eckart, which may be important for practical purposes at low frequencies. "In the original Eckart theory, the scattering was described in terms of a scattered intensity proportional to the square of the magnitude of the difference in pressure reflected from the rough surface and that reflected from a plane surface replacing the rough one. This procedure dictates that one know both the amplitude and phase of these pressures in an experimental determination of the scattered intensity." The procedure adopted by Proud *et al.* "leads to the experimentally simpler operation of forming the difference between plane and rough surface reflected intensity. No consideration of phase is then necessary" [*55, p. 546*].

The authors investigated the dependence of the specular reflected intensity on the acoustic wavenumber, angle of incidence, and surface roughness. The experimental part of their investigations took place in a model

tank with surfaces that had approximately Gaussian characteristics. The quantity $kh\gamma$ ranged from 0.25 to 2.00 in the first case, i.e., from a smooth to a rough surface. The agreement between theory and experiment was good, notwithstanding the violation of the condition of small surface slope.

A comparison between theory and experiments at sea has been made by Clay [*30*]. Using the data of Brown and Ricard [*59*] [who placed a pulsed CW source (168 Hz, pulse length 89 msec) and a receiver at a depth of 1000 yd, varied their horizontal distance between 1000 and 5500 yd, and measured the fluctuations of the scattered field], he found from numerical calculation "a curve that had about the same dependence upon the source–receiver separation as the experimental data" [*30, p. 1551*]. Clay extended the Eckart theory to an omnidirectional source by subdivision of the surface into rectangles for which the original theory could be applied.

3. Brekhovskikh's Method

A detailed analysis of Brekhovskikh's work cannot be presented here, since translations of the original Russian papers are not available. But Lysanov [*3*] gave some qualitative statements about the method, and discussed the limits of validity, whereas La Casce and Tamarkin [*69*] provided some mathematical details.

It turns out that the method deals with periodic surfaces of zero total pressure. "The nature of the irregularities must be such that at each point of the irregular surface it is possible to draw a tangent plane in such a manner that the plane does not depart very far from the irregular surface at distances of the order of a wavelength" [*3, p. 3*].

The essence of the Brekhovskikh method lies in the assumption that the locally flat surface areas are only specularly reflecting. Introduction of a reflection coefficient V, "which in general depends, through a complex phase factor, on the surface coordinates, and which can also depend on the local angle of incidence" [*69, p. 142*], and use of the boundary condition Eq. 21 make it possible to obtain an expression for $\partial p_1/\partial n$. The total scattered field can then be computed via the Helmholtz integral. Application of this method to a sinusoidal boundary of limited size leads to Fig. 1, which has originally been published by Brekhovskikh. Comparison of his method with other techniques and with experimental results has been done in Sec. II-D.

C. The Quasiphenomenological Approach of Middleton

In contrast to the most widely employed "physical" methods, where the irregularity of the boundary is introduced via the boundary condition and where the solution of the wave equation has to satisfy this complex boundary condition, the quasiphenomenological approach of Middleton [*49, 50*] introduces the irregularities of the surface independent of the wave equation as a random distribution of point scatterers, each with its own impulse response function and directivity pattern. This makes the model very flexible from a theoretical point of view: time variation, frequency dependency of the scattering, broad-band signals, complex geometry, and directivity of transmitter and receiver, subsurface scatterers (and also bottom and volume scatterers) are easily incorporated into the model, and there is no limitation on the degree of surface roughness. For this reason, Middleton's is the most complete theoretical method. "The critical advantage of this approach are [sic] the elimination of impossibly complex boundary conditions, the inclusion of the essential geometry of the overall system, and the ability to handle general signals and aperture distributions. The principal, but not serious, limitation appears to lie in the ultimately empirical nature of the impulse response function of the scatterers, which must be quantified at some stage by experiment" [*49, p. 374*]. The problem of how these experiments should be performed is not discussed, unfortunately. For this reason, the practical significance of this elegant theory seems limited. The most promising application may be found in computer simulations of the scattering phenomenon, via a Monte Carlo method. On the other hand, the physical models, although very limited in their validity, seem to have a closer relation to experimental work.

IV. EXPERIMENTAL RESULTS

A. The Amplitude of the Scattered Waves

When a monochromatic sound wave is scattered from a wind-driven surface, the amplitude of the reflected wave shows fluctuations in time due to the time variation of the reflecting boundary. This effect has been measured by Liebermann [*70*] and Pollak [*73*] at sea, and by D'Antonio and Hill [*64*] with a model tank. Liebermann swept the frequency of his source from 27 to 33 kHz in 20 msec and observed the interference pattern between reflected and direct wave. He defined a reflection coefficient V as

$$V=(A_{\max}-A_{\min})/(A_{\max}+A_{\min}), \qquad (30)$$

where $A_{\max}$ and $A_{\min}$ are the first maximum and the first minimum of the signal envelope, and he found that (a) surface reflectivity is highly frequency dependent; (b) the median value of V is near to unity, but for approximately 10% of the time, $V>1$ because of focusing by the surface [*70, p. 498—abstract*]; and (c) no correlation exists between surface wave height and reflection coefficient [*70, p. 503*]. Pollak used a pulsed CW source of 100 kHz and analyzed the reflected amplitude statistically. His results indicate that the probability density function of the reflected amplitude follows approximately a Rayleigh curve. The same result has been obtained by D'Antonio and Hill with a wind driven surface in a model tank. They conclude that "(a) for CW transmission, the envelope of the received signal has a

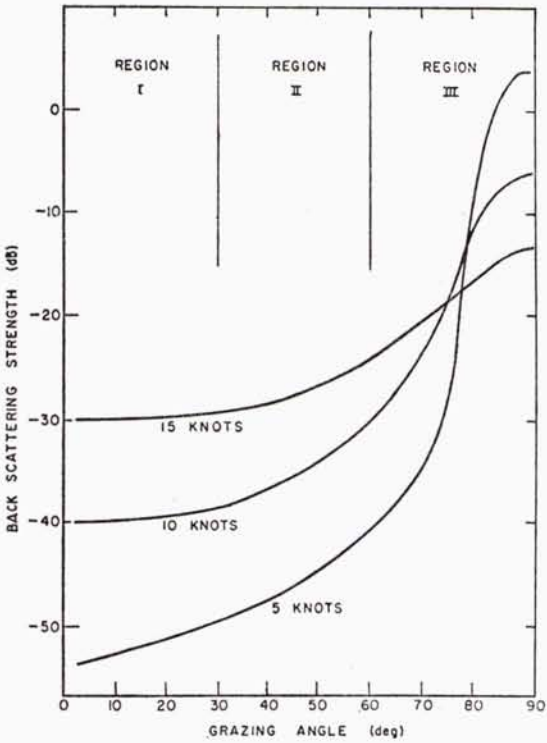


FIG. 6. Backscattering strength of the sea surface. In the three regions it is suggested that the scattering processes are different. From Urick [77].

bandwidth greater than the bandwidth of the surface amplitude; (b) crosscorrelations observed between envelopes of the received signals are low but finite; and (c) there is no correlation between the surface amplitude and the envelope of the received signal" [*64, p. 701—abstract*].

B. Intensity of the Backscattered Waves (Reverberation)

"The importance of surface reverberation in the applications of underwater acoustics can hardly be over-emphasized. As a result, measurements of the backscattering of sound from the region of the surface have occupied the attention of numerous observers. These efforts have been of considerable value in attempting to formulate a description of the phenomenon which is adequate for the designer of underwater sonic devices and to reach an understanding of the fundamental mechanisms of scattering at the air–water boundary defining the surface" [*65, p. 104*].

In experiments at sea, the scattered pressure or intensity is often recorded. For comparative purposes a logarithmic quantity seems more convenient. Hence, in most papers, a definition of surface backscattering strength (in decibels) appeared. And although these definitions differ from one author to another (sometimes attenuation and spreading loss are included [*65*], sometimes a simpler approach is followed [*77, 78*]), their true differences are small enough to make comparison possible, as is borne out by papers of a comparative character [*46, 65, 74, 75*]. As an example of such a definition, we mention the one presented by Urick [*77*] for plane waves, because of its simplicity. He defined the backscattering strength, which we call σ_B, as

$$\sigma_B = 10 \log(I_s/I_0), \tag{31}$$

where I_s/I_0 "is the ratio of the scattered intensity from the unit area, measured at unit distance, to the intensity of the incident sound beam. Following naval practice, these distances are expressed in yards" [*77, p. 136*].

Two types of sound sources are met: the directional transducer, mostly operated with pulsed CW [*22, 55, 59, 65–68, 72, 73*], and explosives [*43, 57, 58, 60–62, 74*]. In the latter case, the data processing is then carried out via narrow bandpass filters, making them an aggregate of simultaneous "monochromatic" sources.

All experiments considered here concentrate on the measurement of σ_B as a function of one or more of the parameters φ, v, and f. A typical result is shown in Fig. 6. The curves for σ_B as a function of φ prompted Urick to "divide the angular range from grazing to normal incidence into three regions, in each of which the dominant scattering process seems to be different" [*77, p. 140*]. These regions are indicated in Fig. 6. In Region I, the scattering by subsurface bubbles is predominant, at least when f is of the order of 60 kHz: "bubbles can be important at low grazing angles and high wind speeds, in the 60 kHz region, but definitely not at frequencies of a few kilocycles or below" [*43, p. 243*]. This scattering is not very dependent on φ for rough surfaces, indicated by a more or less horizontal curve. Increase of wind speed generates more air bubbles and hence increases σ_B. Clay and Medwin agree with this explanation [*63, p. 2134*], but Chapman and Harris doubt its validity, as they do not observe it at 30 kt. They believe "that the scatterers were in a layer of biological origin" [*61, p. 1596*] because a diurnal variation was observed.

"Turning next to Region III, near normal incidence, the slope of the curves in this region and their behavior with surface roughness suggests that sound is returned by reflection (rather than scattering), probably by small flat wave-facets oriented normal to the incident sound beam" [*77, p. 142*]. An increase of v now decreases σ_B because at the rougher surface, less wave-facets have a slope favorable for reflection. In Region II, Urick is tempted "to speculate that the slow rise of σ_B with angle in this region represents the effect of roughness scattering by surface irregularities that are much smaller than a wavelength" [*77, p. 145*].

"Except for the small angle region," Urick's theory is confirmed by Garrison *et al.* [*65, p. 111*]. Richter [*74*]

reported a σ_B decreasing with φ, and Patterson [54] derived a theoretical (phenomenological) model that produces curves similar to those of Fig. 6 in Regions II and III. His curves do not show a constant behavior in Region I, but this can be explained by the fact that Patterson only dealt with "facets having random distributions of size and slope" [54, p. 1150] and neglected bubbles.

Brown *et al.* [60] studied σ_B as a function of frequency. A proportionality of σ_B with f was found. This is in keeping with the results of Chapman *et al.* [61,62] and Richter [74]. On the other hand, in Marsh's theory of backscattering there appears to be an inverse dependence of σ_B on frequency [42, Figs. 11-1 and 11-2]. Also worth mentioning is that the results of Chapman and Harris are in qualitative agreement with Eckart's theory: at relatively low frequencies, σ_B decreases rapidly with decreasing f (see Eq. 28), whereas σ_B is independent of f when f is relatively high [61, p. 1594].

An interesting study has been made by Schulkin and Shaffer [75]. They reviewed experimental results on backscattering in their relation to the Rayleigh criterion of surface roughness ($h \sin\varphi < \lambda/8$). As most of the data are presented as a function of v rather than h, they employed the Neumann–Pierson surface wave spectrum for a fully risen sea in order to relate h and v:

$$2h = H = 0.0026v^{5/2}, \tag{32}$$

where H is measured in feet and v in knots. Then putting

$$\sigma_B = 10 \log(fH \sin\varphi/C)^b, \tag{33}$$

they calculated the constants C and b for a number of cases [61, 65, 78, plus data from an NDRC report] by drawing the best-fitting straight line through the data. As a result they found that b, the most significant parameter, varied between the values 1 and 2. They concluded that "there is no theory to date to relate all the backscattering-strength data satisfactorily [75, p. 1703].

The differences in the results of backscattering measurements are not only caused by differences in technique or in the definition of σ_B. A factor of great importance, which has not always been recognized by the interpretation of data, is the state of development of the sea surface, which strongly influences its scattering and reflection properties. More details can be found in Sec. V-G.

An operational model for sea surface roughness and acoustic reverberation, in which the theory of ocean wave spectra has been applied extensively, has been presented by Martin [46]. He distinguished scattering and reflection, more or less corresponding to Urick's regions II and III, and combined them into a "total reverberation coefficient." "The model, which has a physical basis over the whole range of incidence angles, is uncertain in its application mainly in present knowledge of the statistics of the surface elevation and of derivatives, yet correlates available experimental data as well as other attempts" [46, p. 706].

V. SPECIAL SUBJECTS

The subjects discussed in Secs. II–IV can be considered to be the main currents in the literature. There are, however, a number of studies that only touch these basic subjects in passing, or that concentrate on a very special aspect. These papers are considered briefly in this section. The last part (Sec. V-G) has an oceanographic rather than an acoustical character, in contrast to all the others, since it deals with the spectrum of the surface waves, and with their height and slopes. But these subjects play an important part in many papers: the height and slopes because they characterize the surface roughness, the wave spectrum because it provides the most realistic way to obtain an expression for the correlation function of the surface irregularity.

A. Amplitude and Phase Fluctuations

"The reflection of an acoustic signal from an uneven, time-variant surface leads to variation in the signal form. For a monochromatic wave, these variations appear as amplitude and phase fluctuations" [29, p. 88].

In previous sections, we have seen that for relatively smooth surfaces the total scattered field p_T can be separated into a specularly reflected wave p_r and a diffusely scattered wave p_s. Formulas for p_r and p_s can be obtained from Eq. 23, by taking the first two terms of the power series expansion of $\exp(-ik\gamma\zeta)$. The ratio p_s/p_r is hence a known quantity. Expressing the pressure p in amplitude and phase ($p = Ae^{i\psi}$) and following Chernov's almost classical work [7a] amplitude and phase fluctuations can be defined as

$$\delta A/A_r = \mathrm{Re}(p_s/p_r), \quad \delta\psi = \mathrm{Im}(P_s/P_r) \tag{34}$$

where it is supposed that $|p_s| \ll |p_r|$. This definition is employed by Gulin and Malyshev [8, 35, 36, 66, 67] for the surface diffraction. An important role in these papers, and also in the work of Smirnov and Tonakanov [76], is played by the Rayleigh roughness parameter χ:

$$\chi = 2kh \sin\varphi \tag{35}$$

(cf. Eq. 6).

Two different surface correlation functions appeared in the theory:

$$\Phi_1(\xi) = h^2 \exp(-\xi^2/a^2) \cos(\mathrm{K}\xi) \tag{36}$$

and

$$\Phi_2(\xi,\eta) = h^2 \exp[-(\xi^2+\eta^2)/a^2]; \tag{37}$$

Φ_1 is an approximation for a quasiharmonic surface ("swell"), Φ_2 for "sea." Together with these functions, the wave parameters D_x and D_y are used:

$$D_x = ka^2 \sin^2\varphi/R_0, \quad D_y = ka^2/R_0. \tag{38}$$

The transmitter and receiver are lying in the plane $y=0$, R_0 is half the distance between them via the specular path. Two regions of D_x are considered: either much smaller than unity, or much larger. The physical significance thereof is that a, the effective surface correlation distance, is either much smaller ($D_x \ll 1$) than the projection in X direction of the diameter of the first Fresnel zone along the propagation path [i.e., $(2\lambda R_0)^{\frac{1}{2}}(\sin\varphi)^{-1}$], or much larger ($D_x \gg 1$).

The probability density function for the amplitude, calculated from experimental data [66] (for "swell", $\chi > 1$, pulsed CW), confirmed the results of Pollak [73] and D'Antonio and Hill [64], who obtained approximately a Rayleigh curve. For $\chi < 1$, a Gaussian curve was found to be a good approximation.

Also the spatial autocorrelation of amplitude and phase fluctuations has been studied, both theoretically [36] and experimentally [67]. Small correlation distances in X, Y, and Z direction have been considered. It was found that the correlation in Z direction decreases much faster than in X direction (which is the direction from transmitter to receiver).

An important conclusion can be drawn from all these studies: both theory and experiment demonstrated the presence of a distinct correlation between the scattered field at one or more receivers and the state (period, roughness) of the diffracting surface. For the reflection coefficient, such a correlation has not been found (see Liebermann's third conclusion, Sec. IV-A).

B. Surfaces with Two Types of Roughness

At the surface of the ocean the roughness can very often be considered as a superposition of several types of roughness: "the typical sea surface is comprised of 'swell,' 'sea', and 'ripple' " [37, p. 599]. In three papers, a model with different types of roughness (large-scale plus small-scale) has been developed. Kur'yanov [39] and Beckmann [27] supposed them to be independent and demonstrated the relative importance of the small-scale irregularities.

Correlated roughnesses, with a normal distribution (four-dimensional), representing a statistically isotropic surface, have been analyzed by Hayre and Kaufmann [37]. They calculated the mean scattered power in an arbitrary direction when a plane monochromatic wave was incident. For a slightly rough surface, this scattered power contains two terms: a specular and a diffuse one, the latter containing the effect of both types of roughness plus their combined effect, in a rather complicated way. These effects are expressed in second-order quantities (variances and correlation coefficients). A moderately rough surface produces additional terms of a more complicated structure. The result of the last case, the "extremely" rough surface (but the Kirchhoff approximation is used and hence the surface cannot be too rough), can be interpreted as if the surface consisted of three independent processes: small-scale, large-scale, and a combined roughness.

C. Surfaces with a Sublayer

Below a wind-driven surface, air bubbles are often formed. Moreover, at sea sound speed can vary with depth and biological objects can also be present just below the surface. Consequently, the scattering of sound waves from the boundary can be accompanied by a subsurface scattering. In particular, Russian authors have tried to find out under what conditions this layer effect can become so important that it "screens" the surface scattering. In most cases, this is done via a modified Rayleigh approach. Glotov and Lysanov [33, 34] assumed a homogeneous layer of air bubbles whose diameters are small compared with the incident wavelength. Lysanov [14] characterized the inhomogeneous layer by the index of refraction $\mu(z)$ and also studied the effect of a layer for which the sound speed is a function of depth [15]:

$$c(z) = c_0[1 - b(z-\Delta)]^{-\frac{1}{2}} \quad (z \leq \Delta). \tag{39}$$

In this last case, the scattering possesses a resonance character: the reflection coefficient shows peaks "whenever the scattered wave turns out to be a natural vibrational mode for the given layer" [15, p. 70].

D. "Doppler" and Other Frequency Effects

Many papers deal with surfaces that are independent of time. But a simple observation at sea shows that a realistic description of its surface is not possible without introduction of the time variable. Because of the time dependency of the ocean surface, the transmission of a monochromatic wave results in a received signal that shows random fluctuations in amplitude and phase, when they are recorded as a function of time (see also Sec. IV-A). Since the phenomenon is due to movement of the surface elements, the terms "Doppler effect" or "frequency smear" are also used.

When a sinusoidal surface (wavenumber K) moving with constant speed u isconsidered, as has been done by Gulin [8], the scattered waves of order m are Doppler shifted over a frequency ω_D that is given by

$$\omega_D = m\mathrm{K}u. \tag{40}$$

It follows from this formula that the specularly reflected wave ($m=0$) is not influenced by the Doppler effect. This is correct, as the specular reflection comes from the "average" (flat) surface.

This case may seem somewhat theoretical since the ocean surface has a spectrum of sinusoidal waves rather than a single wavelength. But Liebermann stated that "monochromatic radiation will be preferentially scattered according to the familiar diffraction grating formula" [71, p. 932]: for a given geometry, the scattering of a monochromatic wave is mainly produced by the

surface wave of length Λ, where

$$\Lambda=\lambda(\sin\theta_{in}+\sin\theta_{out})^{-1}, \quad (41)$$

i.e., the scattering has a resonant character. This fact is also mentioned by Eckart (Eq. 28). Measurements made by Liebermann [*71*] have confirmed his statement, and formulas derived by Marsh also indicate that "the reverberation spectra will be narrow and centered at frequencies $\omega\pm\omega_D$" [*44, p. 1836*].

Parkins [*52*] studied the spectral density of the waves scattered from a Gaussian surface described by the Neumann–Pierson directional wave spectrum, for two cases: the slightly rough surface (low frequency or low sea state) and the very rough surface (high frequency or high sea state). This study has recently been extended to the coherence of acoustic signals that are reradiated by the sea surface. "The reradiation from a slightly rough surface is found to be principally a reflection: In the specular direction, there is a coherent, monochromatic reradiation, which becomes partially coherent as the direction of observation becomes off-specular and scattering becomes important. In the off-specular direction, the reradiation is still monochromatic, but there is a Doppler shifting away from the frequency of the incident radiation. When the sea surface becomes very rough and there is only diffuse scattering, there is no direction in which coherent radiation can be observed. In this case, the time variation is a sinusoid whose amplitude and phase change slowly at a rate determined by the wind velocity and the angles of incidence and observation" [*53, p. 123*].

E. Geometrical Shadowing

The phenomenon of "shadowing" of certain surface areas by other parts of the boundary, which can occur when the surface irregularities are large with respect to the wavelength of the incident radiation and at small grazing angles, has been treated separately. The papers devoted to this phenomenon are concerned with the calculation of a "shadowing function," based on the statistics of the surface, with which the scattering area has to be weighted. Two papers have been found in which the shadowing function is applied: in one explicitly [*27*], in the other implicitly [*68*]. The latter one is discussed in Sec. III-B-2.

The starting point in this area of investigation is the article by Beckmann [*79*]. His method, extended by others, can be explained with the aid of Fig. 7, in which a plane monochromatic wave is incident on a rough surface with incident angle θ. The shadowing function S is the probability that the point $\zeta(0)$ is illuminated. Beckmann found for this function the general formula

$$S(\theta)=\exp\left[-\int_0^\infty q(x)dx\right], \quad (42)$$

where $q(x)dx$ is the probability that $\zeta(0)$ is shaded by ζ in the interval $(x,x+dx)$, given it is not shaded by ζ in $(0,x)$. This probability is put approximately equal to the probabillty that ζ will interrupt the ray directed towards $\zeta(0)$ in $(x,x+dx)$ with slope greater than that of the ray, i.e., $\cot\theta$. Hence, the integrand in Eq. 42 contains two conditions: one on the surface elevation ζ in $(x,x+dx)$ and one on the slope ζ'. Although these quantities are correlated, Beckmann treated them as independent "so as not to complicate matters." The resulting error "turns out to be zero for symmetrical distributions" [*79, p. 385*]. For a surface with Gaussian correlation function, he obtained

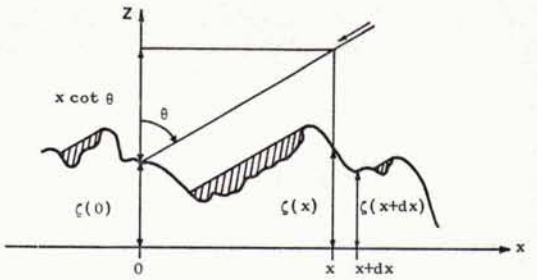


FIG. 7. Geometry for the shadowing of a random rough surface (two dimensional).

$$S(\theta)=\exp[-\tfrac{1}{4}\tan\theta\cdot\operatorname{erfc}(a\cot\theta/2h)]. \quad (43)$$

It is important to note that in Beckmann's calculation of $S(\theta)$ only the elevation $\zeta(0)$ of the surface observation point has been considered. But the slope $\zeta'(0)$ also plays a role: if its value is larger than $\cot\theta$ the point will certainly be shaded. This fact has been recognized by Wagner [*83*]. He calculated $S(\theta)$ for given $\zeta(0)$ and $\zeta'(0)$, using Beckmann's method. He found, instead of Eq. 42,

$$S[\theta|\zeta(0),\zeta'(0)]=\exp\left[-\int_0^\infty q(x)dx\right]U[\cot\theta-\zeta'(0)]. \quad (44)$$

To obtain $S(\theta)$, Eq. 44 has to be averaged over all possible values of height and slope. Wagner performed this operation while maintaining the correlation between these quantities.

A simplified method for the evaluation of the integral in Eq. 44 has been published by Smith [*82*]. He neglected the correlation between height and slope, but obtained for Gaussian Φ results that do not differ significantly from the more complete solution of Wagner (see Fig. 8).

Shadowing in the case of backscattering has been simulated on a digital computer by Brockelman and Hagfors [*80*]. Their shadowing function $R(\theta)$ puts special emphasis on those surface elements that are perpendicular to the line of sight of the observer. This different concept of shadowing, which is based on reflecting facets, caused serious disagreement with Beckmann [*80, p. 626: Discussion*].

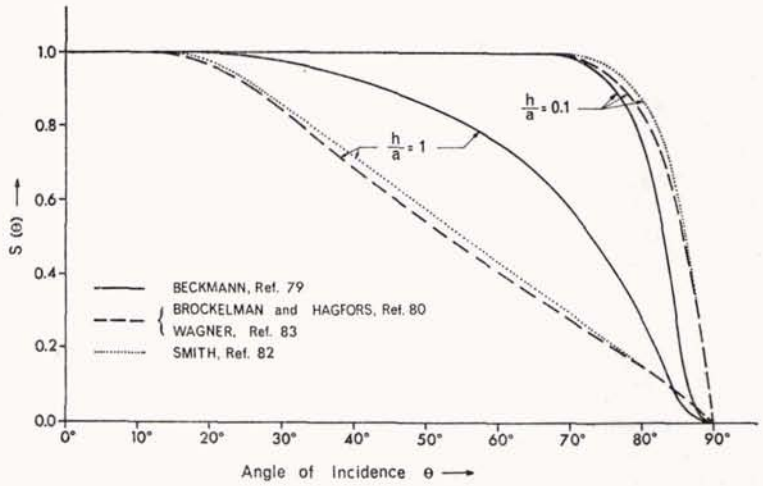


FIG. 8. The shadowing function $S(\theta)$ for a surface with Gaussian correlation function; $S(\theta)$ is the probability that an arbitrary surface point is illuminated by a plane wave with angle of incidence θ.

In Fig. 8, we have combined some results of the papers mentioned. The disagreement between Beckmann's theory and the computer "experiment" is especially large for the rougher surface ($h/a=1$). It is also clear that Wagner is in excellent agreement and that the simplified approach of Smith is very useful.

F. The Inverse Problem

The present section deals with the problem of how the surface correlation function $\Phi(\xi,\eta)$ and related parameters can be derived from the properties of the scattered field. Eckart [*31*] was the first to touch upon this "inverse problem." He observed that the surface wave spectrum F (the Fourier transform of Φ) could in theory be measured for low frequencies via σ (see Eq. 28). "Unfortunately, it is necessary to vary the directional parameters α and β as well as the frequency of the incident radiation. This may be difficult in practice" [*31, p. 568*]. Even more disappointing is the result for high frequencies: in that case σ does not contain the function Φ but only the variances of the slopes.

Proud, Beyer, and Tamarkin [*55*], who have slightly modified the Eckart theory, expressed $\Phi(\xi)$ as the ratio of two empirical functions: one is related to the scattered intensity as a function of frequency; the other describes the source radiation pattern. The formula holds for a smooth surface: $|k\zeta_{\max}\cos\theta|\ll 1$. The authors showed "that in theory one can form an estimate of the reflecting surface correlation function from acoustic measurements alone. It was shown, furthermore, that all the information about the surface is contained in the backscattering" [*55, p. 552*].

A very simple experiment to perform a spectral analysis of a rough surface has been described by Liebermann [*71*]. He used the fact that the scattering of a monochromatic wave from a rough surface is resonant: for a given geometry and incident wavelength, it is mainly a narrow band of surface waves that produces the scattering. Hence, "a 'spectrum' analysis of surface roughness can be obtained by slowly varying the frequency of the incident monochromatic radiation and observing the magnitude of the scattered radiation" [*71, p. 932*]. Marsh [*44*] provided the corresponding formulas for the two-dimensional case and showed how the reverberation spectrum and the surface wave spectrum are related.

Medwin [*72*] analyzed the specular reflection from a wind-driven surface at normal incidence and for several values of the roughness parameter χ, as defined by Eq. 6. He found that measurement of the specularly reflected intensity makes it possible to predict the rms wave height if $\chi^2\leq 0.1$, and the rms surface slope if $\chi^2\geq 10$.

G. Surface of the Ocean

1. Surface Height and Slopes

In all studies that deal with a random surface, it is assumed that the surface elevation and slopes can be considered as Gaussian processes, stationary (in time) and homogeneous (in space). It has become clear from measurements that this assumption, although made mainly for computational reasons, is fortunately not too far from reality. Kinsman [*85*] recorded wave height with a capacitance pole and computed the probability density function of the surface displacements. The surface slopes have been studied by Cox and Munk [*84*]. Their method consisted "in photographing from a plane the sun's glitter pattern on the sea surface, and translating the statistics of the glitter into the statistics of the slope distribution" [*84, p. 838*].

2. Surface Correlation Function and Wave Spectrum

As for the correlation function of the surface roughness, mainly two types have been applied, namely the

ones given in Eqs. 36 and 37. They have been chosen for their relative simplicity in the evaluation of integrals. Moreover, the first one is not too bad for "swell," a narrow band type of waves. More realistic, however, seems the introduction of the theory of a surface wave spectrum, which is very well explained by Kinsman [*85*], among others. In this theory the surface roughness is considered as the combined effect of a band of surface waves that travel in all directions over the surface, each of them having its own wavelength. For the deep ocean the waves are gravity waves; their wavenumber K is related to the frequency ω_s via

$$\mathrm{K}=\omega_s^2/g. \tag{45}$$

The surface correlation function $\Phi(\varrho)$ for an anisotropic surface can be described in terms of the energy spectrum function $A^2(\omega_s,\alpha)$, where α represents the direction of travel of the waves with frequency ω_s. These functions reduce to $\Phi(\rho)$ and $A^2(\omega_s)$ when the surface is isotropic. The relation between $A^2(\omega_s)$ and $\Phi(\rho)$ can easily be found. A plane wave with frequency ω_s and direction α arrives at two observation points, situated on the X axis at distance ρ, at times that differ by an amount τ, such that

$$\tau=\rho\cos\alpha/u. \tag{46}$$

Here u is the frequency-dependent wave velocity,

$$u=g/\omega_s, \tag{47}$$

which follows from Eq. 45. The contribution of this wave to $\Phi(\rho)$ equals $\exp(-i\omega_s\tau)$; this has to be averaged over all possible directions and weighted with the energy spectrum $A^2(\omega_s)$. The final result is

$$\Phi(\rho)=\frac{1}{2}\int_0^\infty d\omega_s A^2(\omega_s)J_0\left(\frac{\omega_s^2\rho}{g}\right), \tag{48}$$

a formula applied by Marsh [*41, 42, 43*].

There is some disagreement in the literature about the explicit form of the function $A^2(\omega_s)$. At least part of the discrepancies can be explained by realizing that the measurements on which the empirical formulas for $A^2(\omega_s)$ are based have not all been made in seas with the same state of development. We have already observed that this fact also plays a role in the different outcomes for backscattering measurements (see Sec. IV-B). When a constant wind starts creating waves on the sea surface, the stationary situation (that is, a "fully aroused sea") is not reached immediately but after a certain lapse of time. Before that moment, the sea is partially developed and has a wave spectrum that is different from that of the completely developed sea. When the wind stops, or when the waves travel outside the "fetch" where they have been generated, their spectrum changes from broad-band ("sea") to a narrow-band and low-frequency spectrum ("swell"), because the low frequencies outrun the high ones (cf. Eq. 47). An excellent account of the generation and propagation of ocean waves is given by Kinsman [*85*].

Marsh [*41, 42*] applied the Neumann–Pierson model for $A^2(\omega_s)$, in which the wind speed v appears as a parameter:

$$A^2(\omega_s)=C\omega_s^{-6}\exp(-2g^2/\omega_s^2v^2); \tag{49}$$

v is expressed in centimeters/second and $C=4.8\times10^4$ cm^2/s^5. Parkins [*52, 53*] used the anisotropic version

$$A^2(\omega_s,\alpha)=C\omega_s^{-6}\exp(-2g^2/\omega_s^2v^2)\cos^2\alpha \times(-\tfrac{1}{2}\pi\leq\alpha\leq\tfrac{1}{2}\pi), \tag{50}$$

and $C=3.05$ m^2/s^5. In Ref. *43* [*p. 240*] Marsh stated: "Arguments have been presented that a more satisfactory form of the equation is

$$A^2(\omega_s)=Cg^2\omega_s^{-5}, \tag{51}$$

where $C=7.4\times10^{-3}$, an absolute, dimensionless constant." This formula "contains no dependence on wind speed‡ and is intended to apply to the fully developed sea." Still another spectral form is proposed by Pierson and Moskowitz [*87*]:

$$A^2(\omega_s)=Cg^2\omega_s^{-5}\exp(-0.74g^4/\omega_s^4v^4), \tag{52}$$

with $C=8.10\times10^{-3}$.

The meaning of "fully developed sea" or "fully aroused sea" can be understood with the function $A^2(\omega_s)$. It is a sea whose spectrum, for a given wind speed, contains components of all frequencies $0\leq\omega_s<\infty$, each with the maximum energy of which it is capable under the given wind. The total energy in a fully aroused "Neumann sea" can be found by integration of Eq. 51 over ω_s from 0 to ∞ [*85, p. 390*]. With Eq. 48, it can be seen that this integral equals $2\Phi(0)$, or $2h^2$.

VI. SUMMARY

(1) Scattering and reflection of sound waves by the sea surface is dependent on time, on frequency of incident waves, and on the geometry of transmitter and receiver. No theoretical models have been found in which these three basic variables are considered simultaneously, except the quasiphenomenological model (Middleton). This latter model, however, has a serious disadvantage: it is based on quantities that have to be found by experiment.

(2) Almost all scattering theories are only valid for smooth surfaces (small slopes). Of these theories, the Eckart approach has been applied most frequently, because of its relative simplicity. The Rayleigh procedure, and its generalization for random boundaries (Marsh), is based on a seriously criticized assumption. For very smooth surfaces, however, its results are comparable with those of other theories.

(3) The Uretsky theory not only covers the scattering at smooth boundaries, but also gives a fairly good prediction for rough boundaries. Unfortunately it has been developed only for a sinusoidal surface.

(4) The surface elevation and slopes are generally assumed to be stationary Gaussian processes. Measurements at sea have indeed shown the validity (with limitations) of this assumption.

(5) The most realistic way to incorporate the correlation functions of surface height and slopes is via the theory of the surface wave spectrum (Neumann–Pierson).

(6) The scattering of a monochromatic wave at a random surface is resonant: the scattering is mainly produced by a small band of surface waves that fit the incident radiation (Liebermann).

(7) The backscattering contains all statistical information about the surface. An acoustical determination of the surface statistics is therefore possible, in theory.

(8) A large quantity of experimental data has been collected at sea and by using model tanks. The influence of several parameters has been studied: wind velocity, frequency of incident radiation, grazing angle, etc. The data indicate three mechanisms: reflection by wave facets near normal incidence, scattering by small air bubbles below the surface at small grazing angles, and scattering by irregularities that are small compared with the incident wavelength in the intermediate region (Urick).

(9) No correlation has been found between the height of a random surface and the reflection coefficient. The second-order statistical moments of the diffracted field (spatial correlation functions, intensity, etc.), however, show good correlation with the surface irregularities.

ACKNOWLEDGMENTS

The author is grateful to Dr. J. L. Uretsky and Dr. M. Briscoe for their encouragement to publish this survey. The study of the papers by Marsh *et al.* [*40–43*] has been facilitated by the assistance of G. Wittek, from the Max-Planck-Institut für Strömungsforschung, Göttingen, W. Germany, who worked at Saclantcen during the summer of 1968.

* Millar (National Research Council, Canada), stated in a private communication, that "it is possible to show that the Rayleigh assumption is valid if $hK<0.448$ and invalid (à la Petit and Cadilhac) if $hK>0.448$." See also [*17a*].

† A Green's function $G_k(\mathbf{r}/\mathbf{r}')$ expresses the field at $\mathbf{r}$ due to a monochromatic unit point source at $\mathbf{r}'$.

‡ But it has a lower limit that depends on v [Neumann spectrum].

Appendix A: Amplitude Coefficients for a Sinusoidal Boundary (Absolute Values)

$c=\cos\theta$, $s=\sin\theta$, $c_m=\cos\theta_m$, $s_m=\sin\theta_m$ (from La Casce and Tamarkin—Ref. *69*).

Rayleigh

$$A_0=J_0(2hkc)+\tfrac{1}{2}(c-c_{-1})hkJ_1(2hkc),$$
$$A_{-1}=J_1(2hkc).$$

Eckart

$$A_0=J_0(2hkc),$$
$$A_m=\frac{c+c_m}{2c}J_m[(c+c_m)hk].$$

Brekhovskikh

$$A_0=J_0(2hkc),$$
$$A_m=\frac{(c+c_m)^2+(s-s_m)^2}{2c_m(c+c_m)}J_m[(c+c_m)hk].$$

Bibliography

General

1. **P. Beckmann and A. Spizzichino,** *The Scattering of Electromagnetic Waves from Rough Surfaces* (Macmillan, New York, 1963).
2. **L. Fortuin,** "A Survey of Literature on Reflection and Scattering of Sound Waves at the Sea Surface," Saclant ASW Research Centre, Tech. Rep. 138 (1969).
3. **Yu. P. Lysanov,** "Theory of the Scattering of Waves at Periodically Uneven Surfaces," Sov. Phys.—Acoust. **4**, 1–10 (1958).
4. **J. W. Strutt, Lord Rayleigh,** *Theory of Sound* (Dover, New York, 1945).

Theoretical Studies

Sinusoidal and other periodical boundaries

5. **I. Abubakar,** "Scattering of Plane Elastic Waves at Rough Surfaces," Proc. Cambridge Phil. Soc. **58**, 136–157 (1962).

5a. **B. B. Baker and E. T. Copson,** *The Mathematical Theory of Huygen's Principle* (Clarendon Press, Oxford, 1953), Chap. 1.

6. **R. G. Barantsev,** "Plane Wave Scattering by a Double Periodic Surface of Arbitrary Shape," Sov. Phys.—Acoust. **7**, 123–126 (1961).
7. **G. R. Barnard, C. W. Horton, M. K. Miller, and F. R. Spitznogle,** "Underwater-Sound Reflection from a Pressure-Release Sinusoidal Surface," J. Acoust. Soc. Amer. **39**, 1162–1169 (1966).

7a. **L. A. Chernov,** *Wave Propagation in a Random Medium* (McGraw-Hill, New York, 1960).

8. **É. P. Gulin,** "Amplitude and Phase Fluctuations of a Sound Wave Reflected from a Sinusoidal Surface," Sov. Phys.—Acoust. **8**, 223–227 (1963).
9. **H. S. Heaps,** "Non-Specular Reflection of Sound from a Sinusoidal Surface," J. Acoust. Soc. Amer. **27**, 698–705 (1955).
10. ——, "Reflection of Plane Waves of Sound from a Sinusoidal Surface," J. Appl. Phys. **28**, 815–818 (1957).
11. ——, "Propagation Theory," Proc. NATO Adv. Study Inst. Signal Processing with Emphasis on Underwater Acoust., Enschede, The Netherlands (August 1968).

12. **R. J. Jordan,** "Reflection of a Plane Sound Wave by a Sinusoidal, Pressure-Release Surface," Master of Engineering thesis, Nova Scotia Technical College, Halifax, Canada (1967).
13. **B. A. Lippmann,** "Note on the Theory of Gratings," J. Opt. Soc. Amer. **43**, 408 (L) (1953).
14. **Yu. P. Lysanov,** "Diffraction of a Plane Wave, Transmitted through an Inhomogeneous Layer, by a Periodically Uneven Surface of Arbitrary Configuration," Sov. Phys.—Acoust. **12**, 52–54 (1966).
15. ——, "Influence of Inhomogeneity of the Medium on Wave Scattering by an Uneven Surface," Sov. Phys.—Acoust. **13**, 66–70 (1967).
16. **H. W. Marsh,** "In Defense of Rayleigh's Scattering from Corrugated Surfaces," J. Acoust. Soc. Amer. **35**, 1835–1836 (L) (1963).
17. **W. C. Meecham,** "Variational Method for the Calculation of the Distribution of Energy Reflected from a Periodic Surface," J. Appl. Phys. **27**, 361–367 (1956).
17a. **R. F. Millar,** "On the Rayleigh Assumption in Scattering by a Periodic Surface," Proc. Cambridge Phil. Soc. **65**, 773–791 (1969).
18. **S. R. Murphy and G. E. Lord,** "Scattering from a Sinusoidal Surface—A Direct Comparison of the Results of Marsh and Uretsky," J. Acoust. Soc. Amer. **36**, 1598–1599 (L) (1964).
19. **J. G. Parker,** "Reflection of Plane Sound Waves from an Irregular Surface," J. Acoust. Soc. Amer. **28**, 672–680 (1956).
20. ——, "Reflection of Plane Sound Waves from a Sinusoidal Surface," J. Acoust. Soc. Amer. **29**, 377–380 (1957).
21. **R. Petit and M. Cadilhac,** "Sur la diffraction d'une onde plane par un reseau infiniment conducteur," Compt. Rend. Acad. Sci. Paris **262B**, 468–471 (1966).
22. **J. M. Proud, P. Tamarkin, and W. C. Meecham,** "Reflection of Sound from a Surface of Saw-Tooth Profile," J. Appl. Phys. **28**, 1298–1301 (1957).
23. **R. F. Salant,** "Acoustic-Wave Propagation Past a Sinusoidal Surface," J. Acoust. Soc. Amer. **44**, 38–40 (1968).
24. **J. L. Uretsky,** "Reflection of a Plane Sound Wave from a Sinusoidal Surface," J. Acoust. Soc. Amer. **35**, 1293–1294 (L) (1963).
25. ——, "The Scattering of Plane Waves from Periodic Surfaces," Ann. Phys. (N. Y.) **33**, 400–427 (1965).

Random boundaries

26. **AVCO,** "Sound Reflection and Scattering by the Ocean Boundaries," AVCO Marine Electron. Office (1963).
27. **P. Beckmann,** "Scattering by Composite Rough Surfaces," Proc. IEEE **53**, 1012–1015 (1965).
28. **A. Berman,** "Effect of Rough Surfaces on the Resolution of Acoustic Rays in the Ocean," J. Acoust. Soc. Amer. **34**, 298–304 (1962).
29. **S. D. Chuprov,** "Correlation of a Narrowband Acoustic Signal Scattered by a Statistically Rough Surface," Sov. Phys.—Acoust. **13**, 88–92 (1967).
30. **C. S. Clay,** "Fluctuations of Sound Reflected from the Sea Surface," J. Acoust. Soc. Amer. **32**, 1547–1551 (1960).
31. **C. Eckart,** "The Scattering of Sound from the Sea Surface," J. Acoust. Soc. Amer. **25**, 566–570 (1953).
32. **R. L. Fante,** "Discussion of a Model for Rough Surface Scattering," Trans. IEEE Antennas Propagation **13**, 652–653 (L) (1965).
33. **V. P. Glotov and Yu. P. Lysanov,** "Coherent Reflection of Sound from an Ocean Surface Layer Containing Resonance Scatterers," Sov. Phys.—Acoust. **10**, 360–364 (1965).
34. —— **and** ——, "Relative Contribution of Surface Air Bubbles and Waves to the Formation of Sea Reverberation," Sov. Phys.—Acoust. **14**, 311–314 (1969).
35. **É. P. Gulin,** "Amplitude and Phase Fluctuations of a Sound Wave Reflected from a Statistically Uneven Surface," Sov. Phys.—Acoust. **8**, 135–140 (1962).
36. ——, "The Correlation of Amplitude and Phase Fluctuations in Sound Waves Reflected from a Statistically Rough Surface," Sov. Phys.—Acoust. **8**, 335–339 (1963).
37. **H. S. Hayre and D. E. Kaufman,** "Plane-Wave Scattering from a Rough Surface with Correlated Large- and Small-Scale Orders of Roughness," J. Acoust. Soc. Amer. **38**, 599–603 (1965).
38. **C. W. Horton and T. G. Muir,** "Theoretical Studies on the Scattering of Acoustic Waves from a Rough Surface," J. Acoust. Soc. Amer. **41**, 627–634 (1967).
39. **B. F. Kur'yanov,** "The Scattering of Sound at a Rough Surface with Two Types of Irregularity," Sov. Phys.—Acoust. **8**, 252–257 (1963).
39a. **Y. W. Lee,** *Statistical Theory of Communication* (Wiley, New York, 1960), Chap. 2.
40. **H. W. Marsh,** "Exact Solution of Wave Scattering by Irregular Surfaces," J. Acoust. Soc. Amer. **33**, 330–333 (1961).
41. ——, **M. Schulkin, and S. G. Kneale,** "Scattering of Underwater Sound by the Sea Surface," J. Acoust. Soc. Amer. **33**, 334–340 (1961).
42. ——, "Non-Specular Scattering of Underwater Sound by the Sea Surface," in *Underwater Acoustics*, V. M. Albers, Ed. (Plenum, New York, 1962), Lecture 11, pp. 193–197.
43. ——, "Sound Reflection and Scattering from the Sea Surface," J. Acoust. Soc. Amer. **35**, 240–244 (1963).
44. ——, " 'Doppler' of Boundary Reverberation," J. Acoust. Soc. Amer. **35**, 1836(L) (1963).
45. —— and E. Y. T. Kuo, "Further Results on Sound Scattering by the Sea Surface," AVCO Marine Electron. Office (1965).
46. **J. J. Martin,** "Sea-Surface Roughness and Acoustic Reverberation—An Operational Model," J. Acoust. Soc. Amer. **40**, 697–710 (1966).
47. **W. C. Meecham,** "Fourier Transform Method for the Treatment of the Problem of the Reflection of Radiation from Irregular Surfaces," J. Acoust. Soc. Amer. **28**, 370–377 (1956).
48. ——, "On the Use of the Kirchhoff Approximation for the Solution of Reflection Problems," J. Rational Mech. Anal. **5**, 323–333 (1956).
49. **D. Middleton,** "A Statistical Theory of Reverberation and Similar First-Order Scattered Fields—Part I: Waveforms and the General Process," Trans. IEEE Information Theory **13**, 372–392 (1967).
50. ——, "A Statistical Theory of Reverberation and Similar First-Order Scattered Fields—Part II: Moments, Spectra, and Special Distributions," Trans. IEEE Information Theory **13**, 393–414 (1967).
51. **D. Mintzer,** "Discussion of the Paper by C. Eckart on Sea Surface Scattering," J. Acoust. Soc. Amer. **25**, 1015 (L) (1953).
52. **B. E. Parkins,** "Scattering from the Time-Varying Surface of the Ocean," J. Acoust. Soc. Amer. **42**, 1262–1267 (1967).
53. ——, "Coherence of Acoustic Signals Reradiated from the Time-Varying Surface of the Ocean," J. Acoust. Soc. Amer. **45**, 119–123 (1969).
54. **R. B. Patterson,** "Model of a Rough Boundary as a Backscatterer of Wave Radiation," J. Acoust. Soc. Amer. **36**, 1150–1153 (1964).
55. **J. M. Proud, R. T. Beyer, and P. Tamarkin,** "Reflection of Sound from Randomly Rough Surfaces," J. Appl. Phys. **31**, 543–552 (1960).
56. **R. R. Rojas,** "Coherency Limits of the Ocean Due to Random Surface Motion," General Atronics Corp. Rep. 907-223-33 (1961).

56a. **N. Wiener,** *Extrapolation, Interpolation and Smoothing of Stationary Time Series* (Wiley, New York, 1960).

Experimental Work

57. **R. H. Adlington,** "Acoustic-Reflection Losses at the Sea Surface, Measured with Explosive Sources," J. Acoust. Soc. Amer. **35**, 1834–1835 (L) (1963).
58. **I. B. Andreeva and E. G. Kharat'yan,** "Sound Scattering by the Surface of the Ocean and by Surface Scattering Layers," Sov. Phys.—Acoust. **12**, 350–354 (1967).
59. **M. V. Brown and J. Ricard,** "Fluctuations in Surface-Reflected Pulsed CW Arrivals," J. Acoust. Soc. Amer. **32**, 1551–1554 (1960).
60. **J. R. Brown, J. A. Scrimger, and R. G. Turner,** "Reverberation from the Ocean Surface," Pacific Naval Lab., T.M. 66-8 (1966).
61. **R. P. Chapman and J. H. Harris,** "Surface Backscattering Strengths Measured with Explosive Sound Sources," J. Acoust. Soc. Amer. **34**, 1592–1597 (1962).
62. —— **and H. D. Scott,** "Surface Backscattering Strengths Measured over an Extended Range of Frequencies and Grazing Angles," J. Acoust. Soc. Amer. **36**, 1735–1737 (L) (1964).
63. **C. S. Clay and H. Medwin,** "High-Frequency Acoustical Reverberation from a Rough-Sea Surface," J. Acoust. Soc. Amer. **36**, 2131–2134 (1964).
64. **R. A. D'Antonio and R. F. Hill,** "Distortion of Underwater Acoustic Signals Reflected from a Time and Space Random Surface," J. Acoust. Soc. Amer. **38**, 701–706 (1965).
65. **G. R. Garrison, S. R. Murphy, and D. S. Potter,** "Measurements of the Backscattering of Underwater Sound from the Sea Surface," J. Acoust. Soc. Amer. **32**, 104–111 (1960).
66. **É. P. Gulin and K. I. Malyshev,** "Statistical Characteristics of Sound Signals Reflected from the Undulating Sea Surface," Sov. Phys.—Acoust. **8**, 228–234 (1963).
67. —— **and** ——, "Experiments in the Spatial Correlation of the Amplitude and Phase Fluctuations of Acoustic Signals Reflected from a Rough Ocean Surface," Sov. Phys.—Acoust. **10**, 365–368 (1965).
68. **C. W. Horton, S. K. Mitchell, and G. R. Barnard,** "Model Studies on the Scattering of Acoustic Waves from a Rough Surface," J. Acoust. Soc. Amer. **41**, 635–643 (1967).
69. **E. O. La Casce and P. Tamarkin,** "Underwater Sound Reflection from a Corrugated Surface," J. Appl. Phys. **27**, 138–148 (1956).
70. **L. N. Liebermann,** "Reflection of Underwater Sound from the Sea Surface," J. Acoust. Soc. Amer. **20**, 498–503 (1948).
71. ——, "Analysis of Rough Surfaces by Scattering," J. Acoust. Soc. Amer. **35**, 932 (L) (1963).
72. **H. Medwin,** "Specular Scattering of Underwater Sound from a Wind-Driven Surface," J. Acoust. Soc. Amer. **41**, 1485–1495 (1967).
73. **M. J. Pollak,** "Surface Reflection of Sound at 100 Kc," J. Acoust. Soc. Amer. **30**, 343–347 (1958).
74. **R. M. Richter,** "Measurements of Backscattering from the Sea Surface," J. Acoust. Soc. Amer. **36**, 864–869 (1964).
75. **M. Schulkin and R. Shaffer,** "Backscattering of Sound from the Sea Surface," J. Acoust. Soc. Amer. **36**, 1699–1703 (1964).
76. **G. E. Smirnov and O. S. Tonakanov,** "Fluctuations in Hydroacoustic Pulse Signals on Reflection from a Water Surface on which Waves are Present," Sov. Phys.—Acoust. **6**, 480–487 (1961).
77. **R. J. Urick,** "The Processes of Sound Scattering at the Ocean Surface and Bottom," J. Marine Res. **15**, 134–148 (1956).
78. —— **and R. M. Hoover,** "Backscattering of Sound from the Sea Surface: Its Measurement, Causes, and Application to the Prediction of Reverberation Levels," J. Acoust. Soc. Amer. **28**, 1038–1042 (1956).

Shadowing

79. **P. Beckmann,** "Shadowing of Random Rough Surfaces," Trans. IEEE Antennas Propagation **13**, 384–388 (1965).
80. **R. A. Brockelman and T. Hagfors,** "Note on the Effect of Shadowing on the Backscattering of Waves from a Random Rough Surface," Trans. IEEE Antennas Propagation **14**, 621–629 (1966).
81. **L. Shaw,** "Comments on 'Shadowing of Random Rough Surfaces,'" Trans. IEEE Antennas Propagation **14**, 253 (L) (1966).
82. **B. G. Smith,** "Geometrical Shadowing of a Random Rough Surface," Trans. IEEE Antennas Propagation **15**, 668–671 (1967).
83. **R. J. Wagner,** "Shadowing of Randomly Rough Surfaces," J. Acoust. Soc. Amer. **41**, 138–147 (1967).

Sea Surface Description

84. **C. Cox and W. Munk,** "Measurement of the Roughness of the Sea Surface from Photographs of the Sun's Glitter," J. Opt. Soc. Amer. **44**, 838–850 (1954).
85. **B. Kinsman,** Wind Waves, Their Generation and Propagation on the Ocean Surface (Prentice Hall, Englewood Cliffs, N. J., 1965).
86. **G. E. Latta and J. A. Bailie,** "On the Autocorrelation Functions of Wind Generated Ocean Waves," Z. Angew. Math. Phys. **19**, 575–586 (1968).
87. **W. J. Pierson and L. Moskowitz,** "A Proposed Spectral Form for Fully Developed Wind Seas, Based on the Similarity Theory of S. A. Kitaigorodskii," J. Geophys. Res. **69**, 5181–5190 (1964).

2.3 Literature up to the middle of 1973

2.3.1 General considerations

During the four years that have elapsed since the preparation of [*2.2*], the interest in the subject has maintained its high level. The general conclusion that "most papers give a very incomplete description of the phenomenon of scattering and reflection of sound waves at the ocean surface" [2.2, *p. 121*] is still valid, but there is a strong tendency towards a more complete, and also a more realistic approach to the problem. This is evidenced by the following facts:

1. Deterministic models (sinusoidal or other periodical boundaries) are almost entirely replaced by models in which the sea surface is a random process.
2. Point sources, both omni-directional and with a certain beam pattern, have taken the place of the plane wave sources.
3. In many theoretical models the time variation of the sea surface is taken into account. The broadband case is covered by treating the surface as a random, linear, time-varying filter.
4. The statistical properties of the ocean surface are more and more expressed in terms of the surface wave "energy" spectra.
5. Theoretical models and experimental studies are no longer restricted to the determination of amplitude and phase fluctuation, scattered intensity or scattering strength, but also deal with subjects like Doppler effect, time correlation of the scattered field, and spatial correlation. Sometimes, in experimental work, the statistics of the sea surface are measured concurrently with the acoustical quantities.
6. Shadowing and multiple scattering are incorporated in some of the theoretical studies.

One article has to be named explicitly in this sub-section: the review paper by HORTON [*2.3*]. This article does not contain more information than the survey I made [*2.2*], although it is slightly more up-to-date. Its interest lies in the fact that it considers the literature in a wider context, from a point of view aimed more at application, and guided by a large experience in the field.

2.3.2 Sinusoidal and other periodical boundaries

Theoreticians are still intrigued by the possibility of solving, once and for ever, the diffraction problem for a periodical boundary. HOLFORD [*2.5*] obtained "An Exact Solution" by differentiation of the Helmholtz equation. This differentiation allowed him to employ the work of URUSOVSKII, who studied surfaces that are *not* of the pressure release type. His analysis also leans heavily on the work of URETSKY (Section 2.2, [*24*, *25*]), which he criticizes in passing because of its process of truncation and matrix inversion.

The discussion on the Rayleigh assumption is continued by MILLAR [*2.6*].

It may also be noted that in two articles the sea surface is explicitly considered to consist of a set of sinusoidals [*2.35*, *2.48*].

2.3.3 *Random boundaries*

An often encountered assumption, namely that the Fraunhofer approximation can be used when source and receiver are distant enough from the surface (because then they are in the "far field"), is discussed in a paper by MELTON and HORTON [*2.23*]. They show that in practical cases the far-field condition is often not satisfied, so that the Fresnel approximation is superior. Comparison with experimental data [*2.40*] confirms this. The implications of the Fresnel correction are investigated by MCDONALD and SPINDEL [*2.21*].

As the Fraunhofer approximation leads to simpler formulae than the Fresnel approach, application of the former is very tempting, notwithstanding its limitations [*2.12*]. One method to overcome its drawback has been suggested by CLAY, as was already pointed out in Section 2.2 (p. 1219). It consists of subdivision of the scattering area into surface units for which the Fraunhofer formula can be used. In this way the Eckart theory, still attractive for its relative simplicity, is again applicable [*2.10*, *2.33*]. The Eckart model is also still in use without division of the surface [*2.30*, *2.48*].

As for the sound source, most theoretical papers deal (for simplicity) with incident plane waves, or sometimes with an omni-directional point source. But point sources of arbitrary directivity can be handled in a relatively simple way by expansion of their sound field in an angular plane wave spectrum. This is demonstrated by CLARKE [*2.9*], in a study of the coherent part of the reflected field.

A new aspect in the literature on random boundaries is the application of filter theory to the surface scattering phenomenon. In this view the sea surface is considered as a linear, random, time-dependent filter [*2.12*, *2.21*, *2.28*, and *2.49*]. Its impulse-response function, its frequency-transfer function, or any other system function, can then be used to describe the scattering, of course in a statistical sense. With this concept, subjects like Doppler spread and time smear of the surface channel are investigated.

The quasi-phenomenological model of MIDDLETON (see Section 2.2 – Part III.C) has been extended to include "the often critical effects of absorption in the medium, multiple specular reflections, and nonzero velocity gradients" [*2.24, p. 35 – abstract*]. My criticism on this approach, expressed in Section 2.2 (pp. 1219 and 1225) and regarding its practical limitations, are commented in [*2.25, p. 86*]. It is claimed that "in the light of the recent works (...), earlier comments on this practical limitation to the usefulness of our theory (...) seem no longer in force". One of these "recent works" can be found in the open literature, namely [*2.27*] together with [*2.28*].

It is admitted [*2.25, p. 87*] that the model applies better to volume reverberation than to surface scattering. Hence I maintain my doubts about the usefulness of the quasi-phenomenological approach, as far as surface reverberation is considered.

Two more phenomenological approaches have been published [*2.14 and 2.29*]. Especially ROEBUCK's paper [*2.29*] is interesting, because it is one of the rare studies that use the Kirchhoff formula (time domain) instead of the usual Helmholtz integral (frequency domain).

2.3.4 *Experimental results*

The collection of data at sea seems unlimited, as so many parameters (e.g. wind speed, wind direction, sea state, grazing angle, type of sound source, transmitted frequency) can be varied. In general there is good agreement between new data and existing results, and between the theoretical predictions and experimental outcomes [*2.34, 2.36, 2.37, 2.39, 2.43, 2.47, 2.48, and 2.51*]. In particular the work of ANDREYEVA [*2.34*] should be mentioned, because it compares the data of many authors.

Experiments in model tanks are also described [*2.38, 2.40, 2.42, 2.45, 2.48, 2.49, 2.51, 2.53*]. They have the advantage that the parameters are easier to control.

Although the measurement of backscattering strength [*2.34, 2.35, 2.37, 2.38, 2.39 2.40, 2.47, 2.49*] and forward scattered intensity [*2.36, 2.42, 2.45*] is still receiving much attention, we can discover the tendency towards the experimental verification of theories for more complex quantities like correlation functions in time and space [*2.43, 2.45, 2.48, 2.51, 2.52*].

The theoretical models that are used in comparison with the data for scattered intensity are mainly based on Eckart's work (Kirchhoff approximation) or on the derivations of BECKMANN and SPIZZICHINO [*2,40, 2.42, 2.48*]. FUNG and LEOVARIS [*2.40*] describe an *improved* Kirchhoff theory that fits the data better than the ordinary Kirchhoff model.

When explicit formulae for the sea surface correlation functions are needed, the exponential and Gaussian attenuated cosine functions are still encountered [*2.45*]. There is an increasing awareness, however, of the necessity to describe the sea surface by its wave spectrum. Consequently, the (concurrent) measurement of such spectra becomes part of the experiments [*2.37, 2,47, 2.48, 2.49, 2.51*]. The directional wave-number spectrum is gaining the interest of experimentalists. DUNN [*2.39*] describes a new buoy for its measurement.

A new type of "experiment" is introduced by BOURIANOFF and HORTON [*2.35*]. It consists of a computer simulation of backscattering from a two-dimensional "sea". The conclusions are not very satisfactory, but continuation and improvement of this type of work seems promising.

Azimuthal dependence of backscattering is measured by REEVES *et al.* [*2.47*]. They used a three-axis gyrostabilized transducer with a very narrow beam, and found no azimuthal dependence for wind speeds above 9 knots. An explanation is sought in the formation of sub-surface bubbles.

The idea of treating the surface scattering phenomenon from a communication standpoint is also gaining popularity among experimental workers. Thus the impulse response of the wind-driven surface appears as the subject of measurements [*2.51*].

2.3.5 *Special subjects*

A. Amplitude and phase fluctuations

The mean value and variance of $\Delta A/A_0$ and $\Delta\psi$, random quantities defined accord-

ing to CHERNOV [*2.2, p. 1221*], are calculated by MELTON and HORTON [*2.23*], with the Fraunhofer as well as with the Fresnel approximation. They showed that the Fresnel approximation is superior to the Fraunhofer approach only for the prediction of amplitude fluctuations.

B. Surfaces with two types of roughness

A paper by HUANG [*2.18*] deals with this subject. Its main improvement over older work lies in the implication of the surface slope distribution. It is found that surface slope, incident angle, and acoustic wavelength play a dominant role, the latter being most important. "The effect of the small irregularities on the surface is to broaden the angular distribution of the scattered acoustic wave at high frequency" [*2.18, p. 1608*].

C. Surfaces with a sub-layer

A model study by BUDDRUSS [*2.38*] confirms the results of GLOTOV and LYSANOV [*2.2, p. 1222*] that after a certain concentration of air bubbles is reached, the surface is completely screened.

D. "Doppler" and other spreading effects

An interesting article has been published by RODERICK and CRON [*2.48*]. They investigated the frequency spectra of forwardscattered sound from the ocean surface in three ways:

1. a theoretical study;
2. a model-tank experiment;
3. an ocean experiment.

Their theory for a travelling sinusoidal, based on Eckart's scattering integral, is confirmed by the model-tank experiment. Their ocean trials agree with the conclusion of PARKINS [*2.2, p. 1223*] that the important parameter for frequency spread is the power spectral density of the ocean waves.

Transmitting CW-pulses of 750 and 1500 Hz simultaneously, they found that:

> "(1) Both amplitude and phase modulation are present. (2) The frequency spectrum consists of a carrier equal to the original transmitted frequency, with sideband frequencies related to the ocean spectrum and peaked at the frequency of maximum energy on the surface. (3) For all conditions for the ocean experiment, the frequency spread is less than 1 Hz, and under low sea state conditions, the spread is about 0.2 Hz" [*2.48, p. 765*].

These results are further supported by the latest work of PARKINS [*2.26*], and by that of FORTUIN [*2.12*].

Other spreading effects, such as the time smear in the channel, are observed by SPINDEL and SCHULTHEISS [*2.51*].

E. Geometrical shadowing

Two papers, one by LYNCH [*2.19*] and one by LYNCH and WAGNER [*2.20*], deal with geometrical shadowing and multiple scattering. Their shadow-corrected theories hold for high frequencies, retain curvature effect, show that "the neglect of multiple scattering effects in the theory of high-frequency scatter from random rough surfaces is manifested as a nonphysical energy loss or gain" [*2.20a, p. 816*], and satisfy the law of energy conservation for near grazing incidence.

The shadowing function, earlier derived only for incident *plane* waves, has been calculated by HARDIN [*2.54*] for a random surface that is illuminated by a *point* source. He analyses the effect of source height and surface variability, and shows that WAGNER's expression for the shadowing function (see Section 2.2, p. 1223) can be obtained as a limit of his analysis.

The statistics of specular points on a Gaussian surface, important when very high frequencies are transmitted, have been studied by SELTZER [*2.55*], for a corrugated, a composite and an isotropically rough surface. His digital simulation indicates that SMITH's shadowing formula (Section 2.2, [*82*]), provides the best approximation.

F. The inverse problem

No papers have been found that throw new light on the inverse problem.

G. Surface of the ocean

There is a growing interest in the proper statistical characterization of the sea surface. For acoustical purposes not only the wave-frequency spectrum, but also the directional wave-number spectrum is important. More and more effort is put in the measurement of the latter [*2.60, 2.61, 2.64*], but a satisfactory method has yet to be found.

For a fully developed sea, surface correlation functions in time or space can be obtained by integration of an empirically established surface wave spectrum. This is done by FORTUIN and DE BOER [*2.59*] for the Pierson-Moskowitz spectrum and the Neumann-Pierson spectrum. They find little differences in the correlation functions.

In most work on the characterization of the sea surface it is assumed that the surface statistics are bivariate Gaussian. Measurements made by SPINDEL and SCHULTHEISS [*2.63*] seem to indicate that this may not always be realistic.

2.4 Summary

The literature on reflection and scattering of underwater sound waves from the ocean surface (and on related subjects) that appeared before the middle of 1973, has been analyzed in this chapter. It is found that the phenomenon is still considered as an important and interesting problem. As a complete description is yet missing, work is going on in this field, theoretical as well as experimental. The theoretical models for the prediction of the scattering are becoming more sophisticated and more realistic, the data collection more complete and refined.

References [2]

General

2.1 P. Beckmann and A. Spizzichino, *The Scattering of Electromagnetic Waves from Rough Surfaces* (Macmillan, New York, 1963).

2.2 L. Fortuin, "Survey of Literature on Reflection and Scattering of Sound Waves at the Sea Surface", J. Acoust. Soc. Amer. **47**, 1209–1228 (1970).

2.3 C. W. Horton, Sr., "A Review of Reverberation, Scattering and Echo Structure", J. Acoust. Soc. Amer. **51**, 1049–1061 (1972).

2.4* T. V. Stephens, "The Reflection of Underwater Sound from a Wind-Driven Surface", Master of Engineering Thesis, Nova Scotia Technical College, Halifax, Canada (1966).

Theoretical Studies

Sinusoidal and other periodical boundaries

2.5 R. L. Holford, "Scattering of Sound Waves at a Periodic, Pressure Release Surface: An Exact Solution", Bell Telephone Laboratories, Whippany, N. J. (1971).

2.6 R. F. Millar, "On the Rayleigh Assumption in Scattering by a Periodic Surface", II, Proc. Cambridge Phil. Soc. **69**, 217–226 (1971).

2.7 W. R. Scott, "The Synthesis of Green's Functions for Acoustic Boundary Value Problems Using an Integral Equation Method", Master of Science Thesis, Nova Scotia Technical College, Halifax, Canada (1970).

Random boundaries

2.8 D. S. Bugnolo, "On the Effects of Stochastic Boundary Perturbations on Acoustic Wave Propagation – The Theory", J. Acoust. Soc. Amer. **45**, 1560–1562 (1969).

2.9 R. H. Clarke, "Coherent Reflection by the Rough Sea Surface of the Acoustic Field from a Source of Arbitrary Directivity", J. Acoust. Soc. Amer. **52**, 287–293 (1972).

2.10 C. S. Clay and H. Medwin, "Dependence of Spatial and Temporal Correlation of Forward-Scattered Underwater Sound on the Surface Statistics. I. Theory", J. Acoust. Soc. Amer. **47**, 1412–1418 (1970).

2.11* P. A. Crowther, "Basic Theory of Acoustic Scattering from the Sea Surface in Terms of Ascertained Surface Statistics", Elliott Brothers, Naval Division, Tech. Rep. ND(F) 121 (1968).

2.12 L. Fortuin, "The Sea Surface as a Random Filter for Underwater Sound Waves", J. Acoust. Soc. Amer. **52**, 302–315 (1972).

2.13* A. K. Fung and R. K. Moore, "The Correlation Function in Kirchhoff's Method of Solution of Scattering of Waves from Statistically Rough Surfaces", J. Geophys. Res. **71**, 2939–2943 (1966).

2.14 N. G. Gatkin, V. A. Geranin, M. I. Karnovskii, L. G. Krasnyi and V. G. Lozovik, "Sea Reverberation for a Spaced Transmitter and Receiver", Sov. Phys.-Acoust. **15**, 309–310 (1970).

2.15 É. P. Gulin, "Correlation of Noisy Radiation Reflected from a Statistically Uneven Surface", Sov. Phys.-Acoust. **18**, 183–189 (1972).

2.16 T. Hagfors, "Comment on Paper by A. K. Fung and R. K. Moore, 'The Correlation Function in Kirchhoff's Method of Solution of Scattering of Waves from Statistically Rough Surfaces'", J. Geophys. Res. **71**, 6150–6151 (1966).

2.17 R. L. Holford, "Scattering of Sound Waves at the Ocean Surface: A Diffraction Theory", Bell Telephone Laboratories, Whippany, N. J. (1971).

2.18 J. C. Huang, "Analysis of Acoustic Wave Scattering by a Composite Rough Surface", J. Acoust. Soc. Amer. **49**, 1600–1608 (1971).

2.19 P. J. Lynch, "Curvature Corrections to Rough-Surface Scattering at High Frequencies", J. Acoust. Soc. Amer. **47**, 804–815 (1970).

2.20a P. J. Lynch and R. J. Wagner, "Energy Conservation for Rough-Surface Scattering", J. Acoust. Soc. Amer. **47**, 816–821 (1970).

---

[2] Some papers and reports published before 1969 have escaped my attention during the preparation of [*2.2*], either because they appeared in less current journals or because they do not belong to the open literature. They are included here for completeness, and marked with an asterisk.

2.20b _____, "Rough-Surface Scattering: Shadowing, Multiple Scatter, and Energy Conservation", J. Math. Phys. **11**, 3032–3042 (1970).
2.21 J. F. McDonald and R. C. Spindel, "Implications of Fresnel Corrections in a Non-Gaussian Surface Scatter Channel", J. Acoust. Soc. Amer. **50**, 746–757 (1971).
2.22 J. V. McNicholas, "Spectrum Broadening Due to Ocean-Wave Interference", J. Acoust. Soc. Amer. **45**, 1053–1054 (1969) (L).
2.23 D. R. Melton and C. W. Horton, Sr., "Importance of the Fresnel Correction in Scattering from a Rough Surface. I. Phase and Amplitude Fluctuations", J. Acoust. Soc. Amer. **47**, 290–298 (1970).
2.24 D. Middleton, "A Statistical Theory of Reverberation and Similar First-Order Scattered Fields – Part III. Waveforms and Fields", Trans. IEEE Information Theory **18**, 35–67 (1972).
2.25 _____, "A Statistical Theory of Reverberation and Similar First-Order Scattered Fields – Part IV. Statistical Models", Trans. IEEE Information Theory **18**, 68–90 (1972).
2.26 B. E. Parkins, "Reflection and Scattering from a Time-Varying Rough Surface – the Nearly Complete Lloyd's Mirror Effect", J. Acoust. Soc. Amer. **49**, 1484–1490 (1971).
2.27 T. D. Plemons, J. A. Shooter and D. Middleton, "Underwater Acoustic Scattering from Lake Surfaces. I. Theory, Experiment, and Validation of the Data", J. Acoust. Soc. Amer. **52**, 1487–1502 (1972).
2.28 _____, "Underwater Acoustic Scattering from Lake Surfaces. II. Covariance Functions and Related Statistics", J. Acoust. Soc. Amer. **52**, 1503–1515 (1972).
2.29 I. Roebuck, "Scattering of Short Acoustic Pulses from a Rough Surface", J. Sound Vibration **12**, 383–386 (1970) (L).
2.30 A. N. Venetsanopoulos and F. B. Tuteur, "Stochastic Filter Modeling for the Sea-Surface Scattering Channel", J. Acoust. Soc. Amer. **49**, 1100–1107 (1971).
2.31* G. Wade, "Plane-Wave Approach to Fresnel and Fraunhofer Diffraction", Trans. IEEE Sonics Ultrasonics **15**, 51–52 (1968) (L).
2.32* A. G. D. Watson, "Scattering of a Plane Sound Wave from a Rough Surface – Formal Solution", Admiralty Res. Lab., Tech. Rep. N 58 (1961).
2.33 Yu. Yu. Zhitkovskiy and Yu. P. Lysanov, "On Certain Features of the Fresnel Diffraction of Sound on the Agitated Surface and on the Bottom of the Ocean", Izv. Atm. Oceanic Phys. **5**, 566–568 (1969).

Experimental Work

2.34 I. B. Andreyeva, "Experimental Data on the Backscattering of Sound by the Ocean Surface", Izv. Atm. Oceanic Phys. **5**, 431–434 (1969).
2.35 G. I. Bourianoff and C. W. Horton, Sr., "Ensemble and Time Averages of Reverberation from a Sea Surface: A Computer Study", J. Acoust. Soc. Amer. **49**, 237–245 (1971).
2.36 M. V. Brown, "Intensity Fluctuations in Reflections from the Ocean Surface", J. Acoust. Soc. Amer. **46**, 196–204 (1969).
2.37 M. V. Brown and R. A. Saenger, "Bistatic Backscattering of Low-Frequency Underwater Sound from the Ocean Surface", J. Acoust. Soc. Amer. **52**, 944–960 (1972).
2.38 C. P. Buddruss, "Model Studies of Scattering of Underwater Sound by the Sea Surface Caused by Waves and Air Bubbles Screens in the Upper Layers", Acoustica (Internat.) **22**, 1–22 (1969).
2.39 D. J. Dunn, "Reverberation as a Factor in Sonar Performance", British Acoust. Soc., Symposium on Underwater Acoustic Propagation (1969).
2.40 A. K. Fung and A. Leovaris, "Experimental Verification of the Proper Kirchhoff Theory of Wave Scattering from Known Randomly Rough Surfaces", J. Acoust. Soc. Amer. **46**, 1057–1061 (1969).
2.41* R. R. Hartley, "Temporal Coherence of Surface-Scattered Signals", J. Acoust. Soc. Amer. **37**, 1147–1149 (1965) (L).
2.42 C. W. Horton, Sr., and D. R. Melton, "Importance of the Fresnel Correction in Scattering from a Rough Surface. II. Scattering Coefficient", J. Acoust. Soc. Amer. **47**, 299–303 (1970).
2.43 Y. Igarashi and R. Stern, "Observation of Wind-Wave-Generated Doppler Shifts in Surface Reverberation", J. Acoust. Soc. Amer. **49**, 802–809 (1971).

2.44* E. O. La Casce, Jr., "Note on the Backscattering of Sound from the Sea Surface", J. Acoust. Soc. Amer. **30**, 578–580 (1958).
2.45 H. Medwin and C. S. Clay, "Dependence of Spatial and Temporal Correlation of Forward-Scattered Underwater Sound on the Surface Statistics. II. Experiment", J. Acoust. Soc. Amer. **47**, 1419–1429 (1970).
2.46* R. H. Mellen, "Doppler Shift of Sonar Backscatter from the Sea Surface", J. Acoust. Soc. Amer. **36**, 1395–1396 (1964) (L).
2.47 J. Reeves, Y. Igarashi and L. Beck, "Azimuthal Dependence of Sound Backscattered from the Sea Surface", J. Acoust. Soc. Amer. **46**, 1284–1288 (1969).
2.48 W. I. Roderick and B. F. Cron, "Frequency Spectra of Forward-Scattered Sound from the Ocean Surface", J. Acoust. Soc. Amer. **48**, 759–766 (1970).
2.49 J. W. Rouse, Jr., and R. K. Moore, "Measured Surface Spectrum Dependence of Backscattering from Rough Surface", Trans. IEEE Antennas Propagation **20**, 211–214 (1972) (L).
2.50* R. L. Shaffer, "Masking of Surface Reverberation by Volume Reverberation", J. Acoust. Soc. Amer. **39**, 408–411 (1966) (L).
2.51 R. C. Spindel and P. M. Schultheiss, "Acoustic Surface-Reflection Channel Characterization through Impulse Response Measurements", J. Acoust. Soc. Amer. **51**, 1812–1824 (1972).
2.52 R. L. Swarts, "Doppler Shift of Surface Backscatter", J. Acoust. Soc. Amer. **52**, 457–461 (1972) (L).
2.53 P. J. Welton, H. G. Frey, and P. Moore, "Experimental Measurements of the Scattering of Acoustic Waves by Rough Surfaces", J. Acoust. Soc. Amer. **52**, 1553–1563 (1972).

Shadowing

2.54 J. C. Hardin, "Theoretical Analysis of Rough-Surface Shadowing from Point-Source Radiation", J. Acoust. Soc. Amer. **52**, 227–233 (1972).
2.55 J. E. Seltzer, "Spatial Densities for Specular Points on a Gaussian Surface", Trans. IEEE Antennas Propagation **20**, 723–731 (1972).

Sea Surface Description

2.56* D. E. Cartwright, "Modern Studies of Wind-Generated Ocean Waves", Contemporary Phys. (GB) **8**, 171–183 (1967).
2.57* P. A. Crowther, "Description, Prediction and Measurement of Sea-Surface Waves Responsible for the Scattering of Underwater Sound", Elliott Brothers, Naval Division, Tech. Rep. ND (F) 92 (1967).
2.58* J. R. Ford, R. C. Trimme and A. Trampus, "A New Method for Obtaining the Directional Spectrum of Ocean Surface Waves", Trans. IEEE Geosci. Electronics **6**, 190–197 (1968).
2.59 L. Fortuin and J. G. de Boer, "Spatial and Temporal Correlation of the Sea Surface", J. Acoust. Soc. Amer. **49**, 1677–1679 (1971) (L).
2.60 G. V. Matushevskiy, "The Relation Between the True and Mean Slopes of the Disturbed Sea Surface", Izv. Atm. Oceanic Phys. **5**, 224–229 (1969).
2.61 H. Medwin, C. S. Clay, J. M. Berkson and D. L. Jaggard, "Traveling Correlation Function of the Heights of Wind-Blown Water Waves", J. Geophys. Res. **75**, 4519–4524 (1970).
2.62* R. J. Schwartz and J. M. Marchello, "Onset of Wind-Driven Waves", J. Geophys. Res. **73**, 5133–5143 (1968).
2.63 R. C. Spindel and P. M. Schultheiss, "Two-Dimensional Probability Structure of Wind-Driven Waves", J. Acoust. Soc. Amer. **52**, 1065–1068 (1972) (L).
2.64 D. Stillwell, Jr., "Directional Energy Spectra of the Sea from Photographs", J. Geophys. Res. **74**, 1974–1986 (1969).

Additional References (not discussed in the text)

F. J. Kingsbury, "An Experimental Model Study of Underwater Acoustic Scattering from a Wind-Driven Surface", Naval Underwater Systems Centre, Rep. No. NL-3021 (1970).
W. Bachmann, "Generalisation and Application of Rayleigh's Theory of Scattering of Sound", Acustica, **28**, 223–228 (1973).
M. L. Boyd and R. L. Deavenport, "Forward and specular scattering from a rough surface: theory and experiment", J. Acoust. Soc. Amer. **53**, 791–801 (1973).

R. R. GARDNER, "Acoustic backscattering from a rough surface at extremely low grazing angles", J. Acoust. Soc. Amer. **53**, 848–857 (1973).
J. C. NOVARINI and J. W. CARUTHERS, "Numerical modeling of acoustic-wave scattering from randomly rough surfaces: an image model", J. Acoust. Soc. Amer. **53**, 876–884 (1973).
R. G. WILLIAMS, "Estimating ocean wind wave spectra by means of underwater sound", J. Acoust. Soc. Amer. **53**, 910–920 (1973).
R. H. CLARKE, "Surface Reverberation Spectrum of Underwater Sound", J. Sound Vibration, **27**, 1–15 (1973).
C. S. CLAY, H. MEDWIN and W. M. WRIGHT, "Specularly scattered sound and the probability density function of a rough surface", J. Acoust. Soc. Amer. **53**, 1677–1682 (1973).
L. FORTUIN, "The wave equation in a medium with a time-dependent boundary", J. Acoust. Soc. Amer. **53**, 1683–1685 (1973).

3

description of the sea surface



CHAPTER 3

DESCRIPTION OF THE SEA SURFACE

3.1 Introduction

When wind is blowing over the surface of the sea, a complicated mechanism of interaction between air and water causes the formation of surface waves. Many studies have been made to investigate this phenomenon, and many models have been proposed to describe it, but a description that covers all aspects is not yet available.

Attempts have been made to characterize the sea surface with only one parameter, especially the wind speed. But the time during which a certain constant wind has been blowing (the "duration") and the size of the area over which it has been blowing (the "fetch") also play an important role. This has lead to the concept of a "fully-developed sea", over which the wind speed and direction have been constant long enough for the wave system to contain the maximum amount of energy it can possibly have: an equilibrium has been reached. Clearly, this is mainly a theoretical construction: winds of constant speed and direction do not last very long, certainly not in large areas. Nevertheless, the idea of a "fully-aroused sea" has produced useful results.

A very good introduction to the subject is given by KINSMAN [*3.1*]. More recent insights are presented by PHILLIPS [*3.2*]. Both authors point out that the sea surface is a random process, in space as well as time. This process, $z = \zeta(\mathbf{R}, t)$, is not Gaussian (there is a certain skewness of the waves, and waves of infinite height have zero probability), but in many respects it may be assumed to be Gaussian (*Assumption 4*), as measurements have indicated (see Section 2.2–V.G.). This is an important result, because it signifies that the surface can be described statistically by only two quantities, namely mean value and correlation function.

The process ζ is homogeneous and stationary (*Assumption 3*). From this it follows that the mean value can arbitrarily be set at zero:

$$< \zeta(\mathbf{R}, t) > = 0, \tag{3.1}$$

and that the correlation function depends not on the actual observation positions and times, but only on their differences:

$$\begin{aligned} < \zeta(\mathbf{R}_1, t_1)\zeta(\mathbf{R}_2, t_2) > &= h^2 \Phi(\mathbf{R}_1 - \mathbf{R}_2, |t_1 - t_2|), \\ &= h^2 \Phi(\xi, \eta, \tau). \end{aligned} \tag{3.2}$$

The normalizing constant h^2 (so that $\Phi(0, 0, 0) = 1$) is the variance of the surface elevation. The spatial argument of Φ has two components, because the surface is anisotropic.

In the following not only the surface elevation ζ will be encountered, but also the slopes ζ_x and ζ_y, the time derivatives ζ_t and ζ_{tt}, and the second order space derivatives ζ_{xx}, ζ_{xy} and ζ_{yy}. As ζ is Gaussian (*Assumption 4*), it can be shown [*3.3, pp. 145–147*] that these derivatives have Gaussian statistics too. Their mean values equal zero when the elevation has zero expectation, i.e. when (3.1) is valid.

Once the correlation function of ζ is known, those of ζ_x, ζ_y, ζ_t, ζ_{xx}, ζ_{xy}, ζ_{yy}, ζ_{tt} can be found by differentiation. Indicating the combination $(\mathbf{R}_1, t_1)$ by the subscript 1 and $(\mathbf{R}_2, t_2)$ by 2 (c.f. (3.2)), we have:

$$\begin{aligned} <\zeta_{x1}\zeta_{x2}> &= -h^2\partial^2\Phi/\partial\xi^2 \\ <\zeta_{x1}\zeta_{y2}> &= -h^2\partial^2\Phi/\partial\xi\partial\eta \\ <\zeta_{y1}\zeta_{y2}> &= -h^2\partial^2\Phi/\partial\eta^2, \end{aligned} \tag{3.3}$$

$$\begin{aligned} <\zeta_{xx1}\zeta_{xx2}> &= h^2\partial^4\Phi/\partial\xi^4 \\ <\zeta_{xx1}\zeta_{yy2}> &= h^2\partial^4\Phi/\partial\xi^2\partial\eta^2 \\ <\zeta_{yy1}\zeta_{yy2}> &= h^2\partial^4\Phi/\partial\eta^4, \end{aligned} \tag{3.4}$$

$$\begin{aligned} <\zeta_{t1}\zeta_{t2}> &= -h^2\partial^2\Phi/\partial\tau^2, \\ <\zeta_{tt1}\zeta_{tt2}> &= h^2\partial^4\Phi/\partial\tau^4. \end{aligned} \tag{3.5}$$

In these formulae Φ stands for $\Phi(\xi, \eta, \tau)$. The variances follow from these equations by letting $(\mathbf{R}_1, t_1)$ and $(\mathbf{R}_2, t_2)$ coincide after the differentiation.

The actual shape of the function Φ depends on the duration of the wind that generates the waves, on its speed, and on the fetch. The determination of Φ is the subject of many oceanographic studies, as can be seen from [*3.1*] and [*3.2*], and as is also indicated in Chapter 2.

Of the many proposed models to describe the surface statistically, one using the "surface wave spectrum" seems the most realistic approach. This theory considers the surface "as the combined effect of a large band of sinusoidal waves that travel over the surface in very many directions, each having its own speed and hence its own wave number. In this way the idea of a surface wave energy spectrum has been formed" [*3.4, p. 6*]. A brief outline of this theory is given in Section 3.2.

The correlation functions in time and space can be expressed as integrals over the wave spectrum. This is shown in Section 3.3. The Pierson-Moskowitz spectrum, at present the best spectral function (*Assumption 6*), is discussed in Section 3.4. Numerical results that are obtained from it, are collected in Section 3.5, for later use.

3.2 Surface wave spectrum theory

The theory assumes that the surface can be characterized by a spectral function ψ that depends on wave number, wave frequency and wave direction. But for small-amplitude deep-water waves, the dispersion relation

$$\kappa = \omega_s^2/g \tag{3.6}$$

reduces the spectrum to $\psi(\omega_s, \alpha)$. A problem is caused by the anisotropy of the surface. There is evidence that a directionality law of the type $\cos^s(\alpha/2)$ has to be used, where s is frequency-dependent and ranges from 1 to 5. Nevertheless, for simplicity, a $\cos^2(\alpha)$-law is often assumed (*Assumption 5*), in which case[3] [*3.1, pp. 389, 399*]

$$\psi(\omega_s, \alpha) \equiv \frac{2}{\pi} A^2(\omega_s) \cos^2(\alpha) \qquad \left(-\frac{\pi}{2} \leqslant \alpha \leqslant \frac{\pi}{2}\right) \qquad (\omega_s \geqslant 0), \tag{3.7}$$

and Φ follows from [*3.1, p. 378*]

$$\Phi(\xi, \eta, \tau) = (\pi h^2)^{-1} \int_0^\infty \mathrm{d}\omega_s A^2(\omega_s) \int_{-\pi/2}^{\pi/2} \mathrm{d}\alpha \cos^2(\alpha) \times$$
$$\times \cos\left[\frac{\omega_s^2}{g}\{\xi \cos(\alpha) + \eta \sin(\alpha)\} - \omega_s \tau\right]. \tag{3.8}$$

The space-correlation function (two different points observed at the same time) and the time-correlation function (one observation position at different times) follow from (3.8) as special cases.

3.3 Correlation functions in time and space

3.3.1 The time-correlation function

When the two observation points coincide, we find readily from (3.8) that the time-correlation function is proportional to the Fourier cosine transform of the wave spectrum:

$$\Phi(0, 0, \tau) = (2h^2)^{-1} \int_0^\infty \mathrm{d}\omega_s A^2(\omega_s) \cos(\omega_s \tau). \tag{3.9}$$

In Section 3.5 we will use this relation together with an empirical formula for $A^2(\omega_s)$ to compute $\Phi(0, 0, \tau)$. But the inverse of (3.9) is also interesting: when the temporal correlation of the sea surface elevation at one position is measured (and this measurement is not too difficult in practice – see for instance [*3.5*]), the wave spectrum can then be obtained via the formula

---

[3] The spectral function $A^2(\omega_s)$ is frequently called "energy spectrum", a name derived from communications engineering and obtained by considering the process ζ as an electrical signal. The proper name, however, is *variance spectrum*.

$$A^2(\omega_s) = 2\int_0^\infty d\tau < \zeta(\mathbf{R}, t)\zeta(\mathbf{R}, t+\tau) > \cos(\omega_s \tau), \tag{3.10}$$

as follows from (3.2).

Another property of (3.9) worth mentioning regards the variance h^2. Apparently, this quantity can be obtained by integration of the variance spectrum:

$$h^2 = \tfrac{1}{2}\int_0^\infty d\omega_s A^2(\omega_s). \tag{3.11}$$

This follows from (3.9) by putting $\tau = 0$.

3.3.2 The space-correlation function

If the observation times coincide the results become more complicated, as we are now dealing with a two-dimensional function. But it turns out that this function can be expressed in terms of two one-dimensional functions, which reduces the computational work considerably.

Putting $\tau = 0$ in (3.8) and integrating over α, we get

$$\Phi(\xi, \eta, 0) = [\xi^2 l_1(\varrho) + (\eta^2 - \xi^2) l_2(\varrho)]\varrho^{-2}. \tag{3.12}$$

The functions l_1 and l_2 are to be found by a weighted integration of $A^2(\omega_s)$:

$$l_1(\varrho) = h^{-2}\int_0^\infty d\omega_s A^2(\omega_s) J_0\left(\varrho\frac{\omega_s^2}{g}\right), \tag{3.13}$$

$$l_2(\varrho) = h^{-2}\int_0^\infty d\omega_s A^2(\omega_s) \frac{J_1\left(\varrho\frac{\omega_s^2}{g}\right)}{\left(\varrho\frac{\omega_s^2}{g}\right)}. \tag{3.14}$$

3.4 The Pierson-Moskowitz spectrum

For a fully developed sea the Pierson-Moskowitz spectrum [*3.6*]:

$$A^2(\omega_s) = Cg^2\omega_s^{-5}\exp(-0.74g^4/\omega_s^4 v^4), \tag{3.15}$$

where $C = 8.10 \times 10^{-3}$ and $v > 0$, is the best empirical formula available at present (*Assumption 6*). With this function, for which a curve is shown in Fig. 3.1, DE BOER[4]

[4] Ir. J. G. DE BOER worked as a *Summer Research Assistant* under my supervision at the Saclant ASW Research Centre during the summer of 1969.

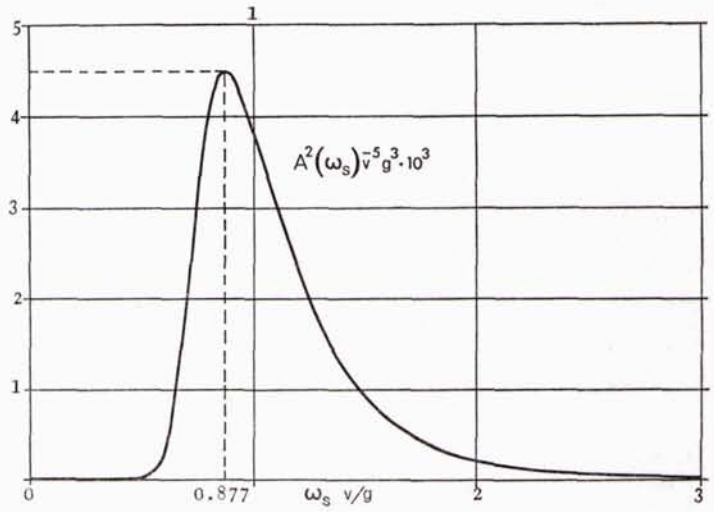


Fig. 3.1. The surface wave frequency spectrum as proposed by PIERSON and MOSKOWITZ [*3.6*] for a fully developed sea.

[*3.4*] has calculated the time-correlation function $\Phi(0, 0, \tau)$ and the space-correlation function $\Phi(\xi, \eta, 0)$, by solving numerically the integrals (3.9), (3.13) and (3.14). His results have been published in a condensed form [*3.7*]. The parts that we need in this study are summarized in the next section.

3.5 Numerical results derived from the Pierson-Moskowitz spectrum

3.5.1 The variance of the sea surface elevation

The variance h^2 is the most elementary quantity to characterize the surface. Its value can be found by integration of the surface wave spectrum. Combination of (3.11) and (3.15) yields:

$$h^2 = 1.35 \times 10^{-5} v^4 \qquad (\mathrm{m}^2). \tag{3.16}$$

3.5.2 The time-correlation function

As was suggested by PIERSON and MOSKOWITZ [*3.6*], it turns out to be convenient to normalize the time difference τ with respect to the wind speed via the relation

$$\tau_N = g\tau/v. \tag{3.17}$$

This is a dimensionless quantity. Sample values for the correlation function[5]

[5] Strictly speaking, $\Phi(0,0,\tau_N)$ and $\Phi(0,0,\tau)$ are different functions. But since there is no chance for confusion, we use the same symbol for both. A similar argument holds for the space-correlation function.

Table 3.1 The time-correlation function $\Phi(0,0,\tau_N)$, derived from the Pierson-Moskowitz spectrum, for $\tau_N = 0(0.5)30$ (see Fig. 3.2).

τ_N	$\Phi(0,0,\tau_N)$	τ_N	$\Phi(0,0,\tau_N)$	τ_N	$\Phi(0,0,\tau_N)$
0.0	1.000000				
0.5	0.831970	10.5	−0.130653	20.5	−0.021439
1.0	0.435359	11.0	−0.131462	21.0	−0.017792
1.5	−0.013626	11.5	−0.115366	21.5	−0.014609
2.0	−0.381110	12.0	−0.088852	22.0	−0.009173
2.5	−0.597637	12.5	−0.055724	22.5	−0.004494
3.0	−0.650945	13.0	−0.023009	23.0	−0.000685
3.5	−0.568268	13.5	0.007122	23.5	0.004313
4.0	−0.397249	14.0	0.030089	24.0	0.005633
4.5	−0.189753	14.5	0.046436	24.5	0.007958
5.0	0.009200	15.0	0.053584	25.0	0.009160
5.5	0.167687	15.5	0.054395	25.5	0.007376
6.0	0.268584	16.0	0.048173	26.0	0.006404
6.5	0.308504	16.5	0.039010	26.5	0.005432
7.0	0.294782	17.0	0.025777	27.0	0.003859
7.5	0.240843	17.5	0.013967	27.5	0.003124
8.0	0.162847	18.0	0.001141	28.0	−0.000010
8.5	0.077346	18.5	−0.008255	28.5	−0.001131
9.0	−0.002095	19.0	−0.015968	29.0	−0.000928
9.5	−0.066518	19.5	−0.020423	29.5	−0.004203
10.0	−0.109608	20.0	−0.021577	30.0	−0.002692

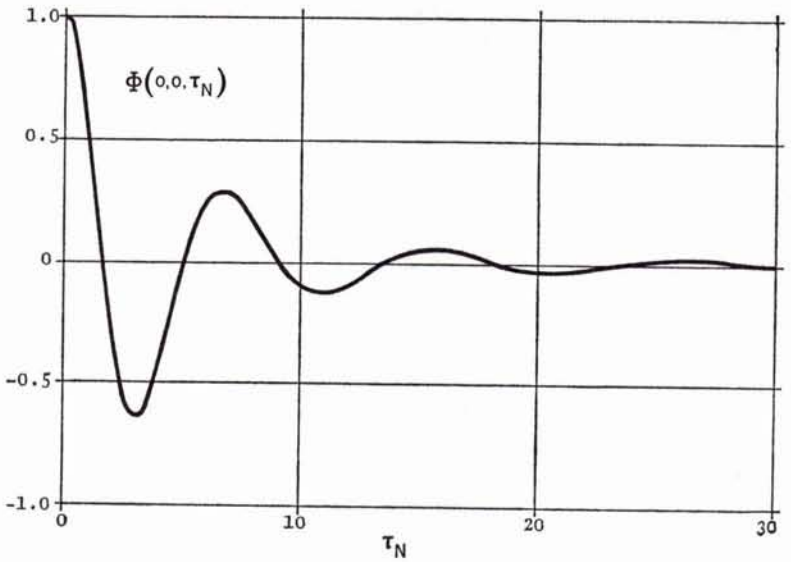


Fig. 3.2. The time-correlation function of the sea surface, derived from the Pierson-Moskowitz spectrum. The normalized time difference τ_N equals the actual time difference τ multiplied by g/v (from [3.4]).

$\Phi(0, 0, \tau_N)$, derived from (3.9) and (3.15), can be found in Table 3.1; a curve is plotted in Fig. 3.2.

The variances of the time derivatives ζ_t and ζ_{tt} follow readily by differentiating (3.9) and solving the new integrals, as is indicated by (3.5). The result is (see Appendix A)

$$\begin{aligned} &<\zeta_t^2> = 0.002v^2 \qquad (\mathrm{m^2 s^{-2}}), \\ &<\zeta_{tt}^2> = 0.4 \qquad\quad (\mathrm{m^2 s^{-4}}). \end{aligned} \tag{3.18}$$

3.5.3 The space-correlation function

Normalization of the distances with respect to the wind speed is also convenient here. Following again PIERSON and MOSKOWITZ [*3.6*] we put

$$\varrho_N = 2g\varrho/v^2 \qquad (v \neq 0), \tag{3.19}$$

so that (3.12) reduces to (see footnote on page 63)

$$\Phi(\xi_N, \eta_N, 0) = \{\xi_N^2 L_1(\varrho_N) + (\eta_N^2 - \xi_N^2) L_2(\varrho_N)\} \varrho_N^{-2}. \tag{3.20}$$

We note that the normalized distances are dimensionless. The functions L_1 and L_2, proportional to l_1 and l_2, and calculated with (3.13), (3.14), and (3.15), are presented numerically and graphically, in Table 3.2 and Fig. 3.3, respectively. An impression

Table 3.2 The auxiliary functions $L_1(x)$ and $L_2(x)$, derived from the Pierson-Moskowitz spectrum, for $x = 0(1)40$ (see Fig. 3.3).

x	$L_1(x)$	$L_2(x)$	x	$L_1(x)$	$L_2(x)$
0	2.000000	1.000000			
1	1.685109	0.910138	21	0.031476	−0.007071
2	1.207823	0.760491	22	0.031200	−0.005058
3	0.765871	0.606300	23	0.029420	−0.003309
4	0.410755	0.466145	24	0.027955	−0.001871
5	0.150207	0.346600	25	0.023396	−0.000733
6	−0.025481	0.248841	26	0.019119	0.000152
7	−0.132343	0.171491	27	0.016490	0.000777
8	−0.186940	0.112086	28	0.010976	0.001198
9	−0.203925	0.067769	29	0.008360	0.001459
10	−0.195557	0.035761	30	0.004846	0.001557
11	−0.172261	0.013510	31	0.001924	0.001578
12	−0.141542	−0.001208	32	0.000640	0.001495
13	−0.108166	−0.010259	33	−0.002759	0.001378
14	−0.075907	−0.015168	34	−0.002500	0.001215
15	−0.046841	−0.017151	35	−0.003234	0.001042
16	−0.022416	−0.017162	36	−0.003968	0.000861
17	−0.002859	−0.015920	37	−0.003838	0.000684
18	0.011061	−0.013957	38	−0.003708	0.000518
19	0.020852	−0.011660	39	−0.003743	0.000369
20	0.028004	−0.009303	40	−0.003778	0.000237

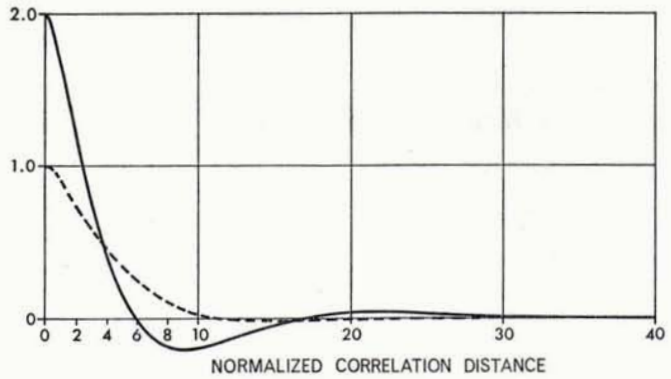


Fig. 3.3.
The auxiliary functions $L_1(x)$ and $L_2(x)$, for the Pierson-Moskowitz spectrum (Table 3.2); ——— $L_1(x)$, – – – $L_2(x)$.

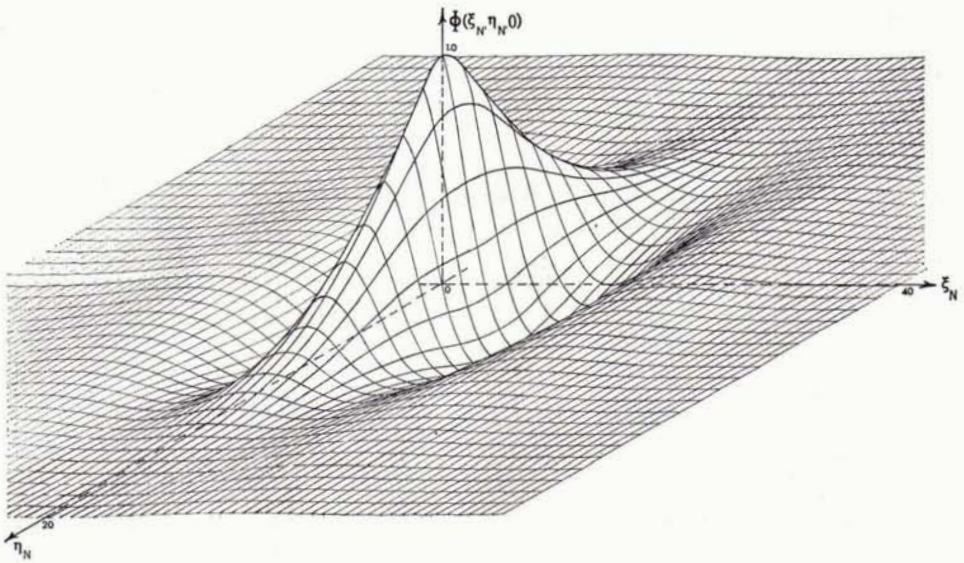


Fig. 3.4. The space-correlation function of the sea surface, derived from the Pierson-Moskowitz spectrum. The normalized correlation distances are $2g/v^2$ times the actual distances; ξ_N is the down-wind, η_N the cross-wind direction [*3.4*, *3.7*].

of the complete correlation function is given in Fig. 3.4. From this last figure, the spatial correlation can only be studied qualitatively, because it depicts a three-dimensional surface in a two-dimensional plane. It is therefore worth considering the cross-sections in the down-wind and the cross-wind directions (Fig. 3.5). Obviously, the cross-wind correlation is stronger than the down-wind correlation.

From the curves in Fig. 3.5 we can derive estimates for L_{dw} and L_{cw}, the "effective correlation distances" in down-wind and cross-wind directions. To this end we define the effective correlation distance as the distance at which the normalized correlation function has dropped to the value e^{-1}. With this criterium we find

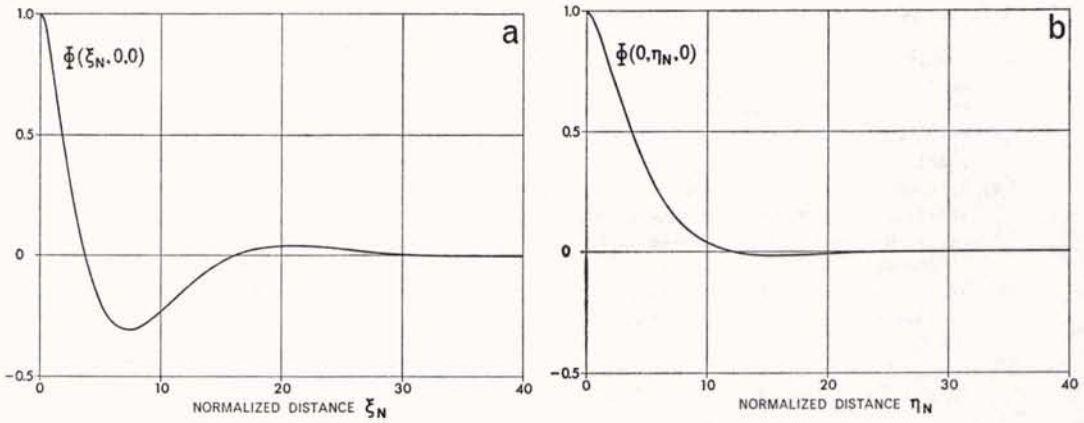


Fig. 3.5. The space-correlation functions in (a) down-wind and (b) cross-wind direction, derived from the Pierson-Moskowitz spectrum [*3.4*, *3.7*]; the normalized distances are $2g/v^2$ times the actual distances.

$$L_{dw} = 0.125v^2 \quad \text{(m)}, \tag{3.21}$$

$$L_{cw} = 0.250v^2 \quad \text{(m)}. \tag{3.22}$$

The variances of the spatial derivatives can be obtained in the way given by (3.3) and (3.4). The following results are found (see Appendix A for details):

$$\begin{aligned} &<\zeta_x^2> = 0.003 \\ &<\zeta_y^2> = 0.001, \end{aligned} \tag{3.23}$$

and

$$\begin{aligned} &<\zeta_{xx}^2> = 5v^{-4} \quad (\text{m}^{-2}) \\ &<\zeta_{yy}^2> = \ v^{-4} \quad (\text{m}^{-2}), \end{aligned} \tag{3.24}$$

in which the X-axis coincides with the down-wind direction and the Y-axis with the cross-wind direction. The restriction $v \neq 0$ is important for (3.24) and is originated by the fact that $\Phi(\xi, \eta, 0)$ is not defined for $v = 0$. This behaviour for $v \to 0$ is a serious defect of the Pierson-Moskowitz formula. On physical grounds, of course, we know that all derivatives vanish for $v = 0$, because the surface reduces then to a flat plane for which $z = 0$.

3.6 Summary

This chapter deals with the statistical properties of the sea surface. Correlation functions in time and space are described, tabulated and plotted; they are derived from the Pierson-Moskowitz spectrum. Related quantities, required later on, are also computed.

References

3.1 B. KINSMAN, *Wind Waves, their Generation and Propagation on the Ocean Surface* (Prentice-Hall, Englewood Cliffs, N.J., 1965).

3.2 O. M. PHILLIPS, *The Dynamics of the Upper Ocean* (University Press, Cambridge, 1966).

3.3 P. BECKMANN, *Elements of Applied Probability Theory* (Harcourt, Brace & World, New York, 1968).

3.4 J. G. DE BOER, "On the Correlation Functions in Time and Space of Wind-Generated Ocean Waves", SACLANT ASW Research Centre, Tech. Rep. 160 (1969).

3.5 M. G. BRISCOE and E. GOUDRIAAN, "Research Use of the Waverider Buoy in Deep Water", Underwater J. **4**, 142–148 (1972).

3.6 W. J. PIERSON, Jr. and L. MOSKOWITZ, "A Proposed Spectral Form for Fully Developed Wind Seas Based on the Similarity Theory of S. A. Kitaigorodskii", J. Geophys. Res. **69**, 5181–5190 (1964).

3.7 L. FORTUIN and J. G. DE BOER, "Spatial and Temporal Correlation of the Sea Surface", J. Acoust. Soc. Amer. **49**, 1677–1679 (1971) (L).

4

filter considerations



CHAPTER 4

FILTER CONSIDERATIONS

4.1 Introduction

The active element in the communication channel from transmitter to receiver is formed by the upper boundary of the ocean. In Chapter 3 we assumed that the sea surface is a random, time-dependent process (*Assumption 3*). Hence, the filter is random and time-variant too.

When certain average filter characteristics are known, it becomes possible to compute the average output behaviour of the channel for any known input signal. The determination of those filter characteristics is consequently an important object.

As the filter is time-variant, the system functions depend on two variables, e.g. time and frequency.[6] The filter system functions, which enable us to express the output signal $y(t)$, or its spectrum, in terms of the input signal $x(t)$, or its spectrum, are consequently two-dimensional. This represents an important difference with the time-invariant filter, where one independent variable is sufficient.

Two effects are, generally speaking, present in the output signal of a time-variant filter as compared with the input: time spread (also called delay spread or dispersion) and frequency spread (or Doppler spread). Time spread is *not* a consequence of the filter's time-dependency: it also occurs with time-independent filters. It becomes noticeable when short pulses (i.e. signals with a broadband character) are transmitted: different frequencies are delayed differently so that the pulses are stretched or smeared out in time. Frequency spread, on the other hand, is indeed caused by the time-dependency of the filter. This effect can be observed when the input signal is a pure tone (i.e. a signal with a very narrow spectrum): the amplitude and phase are subject to fluctuations so that new frequency components are generated, both slightly higher and lower than the input frequency.

The two cases mentioned above are extremes: one deals with a signal short in time and long in frequency, the other with just the opposite. An arbitrary signal will therefore be spread both in time and frequency.

Time and frequency spread are important for the behaviour of the communication channel. They can be analyzed by means of the system functions. The most common ones are discussed in Section 4.2, after which they are used to describe the input-output relations (Section 4.3). In both sections we have assumed that all system functions have Fourier transforms with respect to both variables. Later on we will see

---

[6] A third variable can be distinguished in our case, namely the geometry of transmitter and receiver. But the character of this variable differs so strongly from time and frequency that its significance will be discussed separately in Chapter 9.

that for the sea surface sound channel this is not true, so that certain system functions lose their meaning.

For a random filter, time and frequency spread are stochastic phenomena, which can only be described statistically. Thus a statistical characterization of the system functions is required. The most complete description in this respect would be given by their probability density functions, but there is little hope of finding these. We will therefore content ourselves with the first and second statistical moment, i.e. with mean values and correlation functions. Some details are presented in Section 4.4.

Finally, we remark that the random time-variant filter is assumed to be linear (*Assumption 10*). This means that the superposition principle is valid: all signals may be decomposed into their frequency components, the effect of the filter on each of them may be evaluated, after which the total effect can be found by summation. The Fourier transform and its inverse will thereby play an important role, as will the two-dimensional versions, when correlation functions are analyzed. For later reference we give here the definitions we have adopted:

a. Simple Fourier Transform

$$F(\omega) = \int_{-\infty}^{\infty} \mathrm{d}t f(t) \exp(i\omega t), \tag{4.1}$$

$$f(t) = \frac{1}{2\pi} \int_{-\infty}^{\infty} \mathrm{d}\omega F(\omega) \exp(-i\omega t); \tag{4.2}$$

$F(\omega)$ is the Fourier transform of $f(t)$, the inverse transform of $F(\omega)$ is $f(t)$.

b. Double Fourier Transform

$$F(\omega_1, \omega_2) = \int_{-\infty}^{\infty} \mathrm{d}t_1 \int_{-\infty}^{\infty} \mathrm{d}t_2 f(t_1, t_2) \exp[i(\omega_1 t_1 - \omega_2 t_2)], \tag{4.3}$$

$$f(t_1, t_2) = \frac{1}{4\pi^2} \int_{-\infty}^{\infty} \mathrm{d}\omega_1 \int_{-\infty}^{\infty} \mathrm{d}\omega_2 F(\omega_1, \omega_2) \exp[-i(\omega_1 t_1 - \omega_2 t_2)], \tag{4.4}$$

$F(\omega_1, \omega_2)$ is the double Fourier transform of $f(t_1, t_2)$, the inverse of $F(\omega_1, \omega_2)$ is $f(t_1, t_2)$.

4.2 System functions for linear time-varying filters

4.2.1 The impulse response

There are several ways to describe the impulse response of a time-varying filter [*4.1, 4.2*]. In this study we have adopted the definition that $h(\tau, t)$ is the response

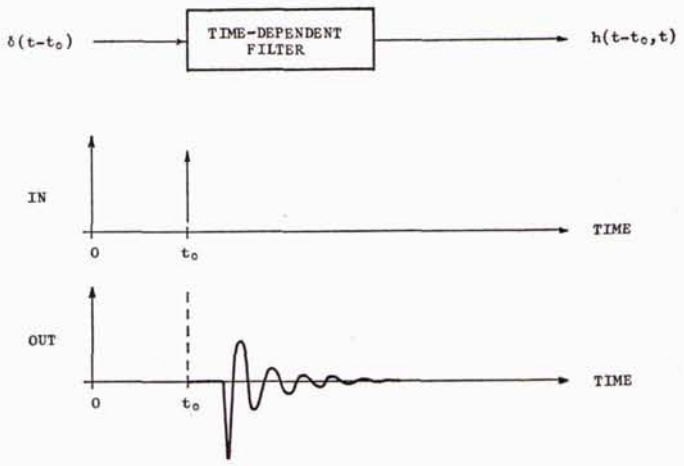


Fig. 4.1.
The response of a time-dependent filter to a unit delta pulse; $h(t-t_0,t) \equiv 0$ for $t < t_0$ because of causality.

measured at time t to a unit impulse applied at time $t-\tau$, where $\tau \geqslant 0$. Physically, this means that when a unit delta-pulse is applied at the input at time $t = t_0$, i.e. $x(t) = \delta(t-t_0)$, the output is given by $y(t) = h(t-t_0, t)$. This time spread is illustrated in Fig. 4.1.

In general, for an arbitrary input signal, the impulse response can be interpreted as a weighting function by which the signal inputs in the past must be multiplied to determine their contributions to the present output [*4.1, p. 101*]. The total output is then obtained by summation:

$$y(t) = \int_0^\infty \mathrm{d}\tau h(\tau, t)x(t-\tau). \tag{4.5}$$

Only the past of $x(t)$ gives a contribution ($\tau \geqslant 0$). This reflects the fact that the filter cannot weight portions of the input signal that have yet to occur.

4.2.2 The transfer function

The filter can also be described by the transfer function $H(\omega, t)$, which is the Fourier transform (with respect to τ) of the impulse response:

$$H(\omega, t) = \int_{-\infty}^\infty \mathrm{d}\tau h(\tau, t)\exp(i\omega\tau), \tag{4.6}$$

$$h(\tau, t) = \frac{1}{2\pi}\int_{-\infty}^\infty \mathrm{d}\omega H(\omega, t)\exp(-i\omega\tau). \tag{4.7}$$

If in (4.5) the input signal is harmonic, i.e. $x(t) = \exp(-i\omega t)$, then

$$y(t) = H(\omega, t)\exp(-i\omega t) \tag{4.8}$$

follows by using (4.6). This indicates an important property of the transfer function:

$$H(\omega, t) = \frac{\text{response of the filter to } \exp(-i\omega t), \text{ at time } t}{\exp(-i\omega t)}; \tag{4.9}$$

it permits the application of monochromatic sources (with variable frequency), in accordance with the mathematical formulation of the scattering phenomenon, which is most conveniently performed in the frequency domain, via the Helmholtz integral (Chapter 5).

4.2.3 The spreading function

A more unconventional system function is obtained by taking the Fourier transform of $h(\tau, t)$ with respect to t [*4.3, p. 25–5*]:

$$E(\tau, \Omega) = \int_{-\infty}^{\infty} \mathrm{d}t h(\tau, t) \exp(i\Omega t). \tag{4.10}$$

This is the spreading function. It gives the spectrum, with Ω as frequency variable, of the time variations of the impulse response.

4.2.4 The bi-frequency function

Also $H(\omega, t)$ can be transformed with respect to t. In this way the bi-frequency function $e(\omega, \Omega)$ is found:

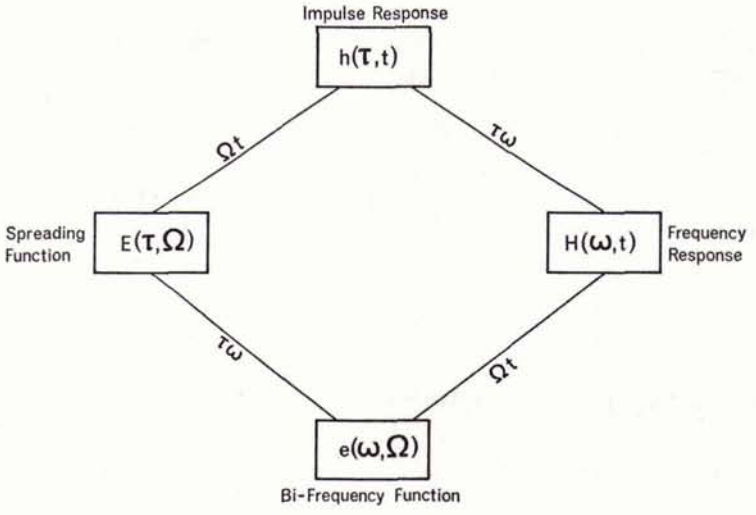


Fig. 4.2. Relations between system functions.

$$e(\omega, \Omega) = \int_{-\infty}^{\infty} \mathrm{d}t H(\omega,t) \exp(i\Omega t). \tag{4.11}$$

Its significance will become clearer, when input-output relations are discussed (Section 4.3). The same result is obtained by Fourier transformation of the spreading function, with respect to τ.

4.2.5 Relations between system functions

The four system functions mentioned in the preceding sub-sections are interrelated via Fourier transforms. This is illustrated in Fig. 4.2, by means of a general diagram. We emphasize that in the derivation we have assumed that the various Fourier transforms indeed exist. In practice it may happen that this assumption is not correct. The system function under consideration is then not defined.

4.3 Input-output relations

The most elementary relation has been encountered in (4.8): an harmonic input signal of the type $x(t) = \exp(-i\omega t)$ yields an output signal $y(t) = H(\omega, t) \exp(-i\omega t)$. An arbitrary input signal $x(t)$ can be decomposed into its spectral components, according to (4.2):

$$x(t) = \frac{1}{2\pi} \int_{-\infty}^{\infty} \mathrm{d}\omega X(\omega) \exp(-i\omega t); \tag{4.12}$$

the spectrum $X(\omega)$ may be regarded as a weighting function. As each component $\exp(-i\omega t)$ causes at the output of the filter a signal $H(\omega, t) \exp(-i\omega t)$ and since linearity is assumed (*Assumption 10*), we can add the response of all components, with their proper weight. So we get

$$y(t) = \frac{1}{2\pi} \int_{-\infty}^{\infty} \mathrm{d}\omega X(\omega) H(\omega, t) \exp(-i\omega t). \tag{4.13}$$

It may be noted that this is not the inverse Fourier transform of $X(\omega)H(\omega, t)$, because that product is not independent of time.

Equation (4.13) relates the output signal to the input spectrum. This can be illustrated by returning to the example of Sub-Section 4.2.1, where the input signal was a unit delta pulse at time $t = t_0$. Such a signal, $x(t) = \delta(t - t_0)$, has the spectrum $X(\omega) = \exp(i\omega t_0)$, as results from (4.1). Substitution into (4.13) yields then, together with (4.7), the output $y(t) = h(t - t_0, t)$.

A relation between input and output signal has been mentioned already in (4.5), the convolution integral for time-variant filters:

$$y(t) = \int_{-\infty}^{\infty} d\tau h(\tau, t) x(t-\tau). \tag{4.14}$$

Again, when $x(t) = \delta(t-t_0)$, we find $y(t) = h(t-t_0, t)$.

The inverse of (4.10) can be put into (4.14); it gives

$$y(t) = \int_{-\infty}^{\infty} d\tau \int_{-\infty}^{\infty} d\Omega x(t-\tau) \exp(-i\Omega t) E(\tau, \Omega). \tag{4.15}$$

The quantity $x(t-\tau) \exp(-i\Omega t)$ may be considered as a time and frequency shifted version of $x(t)$. The output signal $y(t)$ is formed as a sum of such components, weighted with $E(\tau, \Omega)$. Apparently, $E(\tau, \Omega)$ determines the spread in time and frequency the signal will suffer in the channel. For this reason it is called "spreading function".

The spectrum of $y(t)$ can be expressed in terms of the input spectrum and the bi-frequency function:

$$Y(\omega) = \frac{1}{2\pi} \int_{-\infty}^{\infty} d\Omega X(\omega-\Omega) e(\omega-\Omega, \Omega). \tag{4.16}$$

This formula has been obtained by Fourier transformation of $y(t)$ with (4.1), followed by substitution of (4.13) and the inverse of (4.11). It indicates that the output at frequency ω is not determined merely by the input at that frequency, but by components in a frequency band around ω. The width of that band and the weight of each component are given by the bi-frequency function.

The simplest way to illustrate the foregoing statement is to take a purely harmonic input signal: $x(t) = \exp(-i\omega_0 t)$, or $X(\omega) = 2\pi\delta(\omega-\omega_0)$. Putting this into (4.16) gives $Y(\omega) = e(\omega_0, \omega-\omega_0)$, which clearly shows the described frequency spread. A schematic form of this can be found in Fig. 4.3.

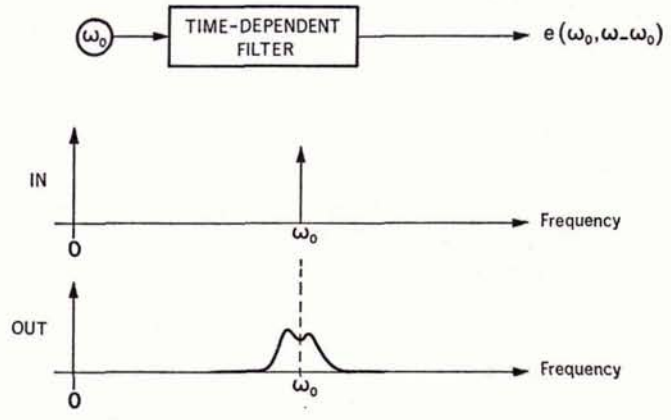


Fig. 4.3.
The response of a time-dependent filter to a harmonic input signal of radial frequency ω_0.

For later reference it is useful to summarize the input-output relations for the two special cases that we have discussed:

A. A unit delta pulse at the input,
B. A purely harmonic input signal.

This summary is given in Table 4.1.

Table 4.1 Input-output relations for a time-dependent filter.

	input	output
A	Unit Delta-Pulse $x(t) = \delta(t-t_0)$ $X(\omega) = \exp(i\omega t_0)$	$y(t) = h(t-t_0,t)$
B	Harmonic Input $x(t) = \exp(-i\omega_0 t)$ $X(\omega) = 2\pi\delta(\omega-\omega_0)$	$y(t) = H(\omega_0,t)\exp(-i\omega_0 t)$ $Y(\omega) = e(\omega_0,\omega-\omega_0)$

4.4 Statistical properties of the filter

4.4.1 General

It has already been remarked that the filter we are studying has a random character. Consequently, the system functions have to be regarded as random functions of two variables. Their description has to be limited to statistical properties, of which only mean value and correlation function are simple enough to find.

In general, the mean value of the system functions is non-zero. But in many statistical analyses it is convenient to deal with processes or functions that do have zero mean value. This applies to our filter for the first part of the investigation. Hence, we temporarily split the filter into two parts: a *deterministic* part (equal to the mean value) and a *random* part (which is obtained from the true random filter by singling the

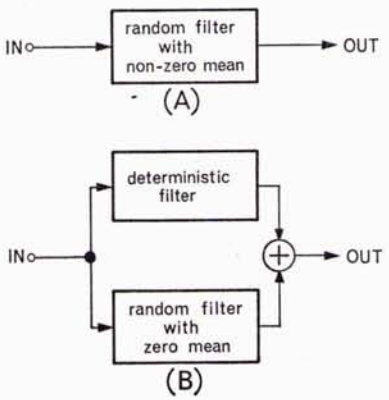


Fig. 4.4.
Decomposition of (A) a random filter with non-zero mean value into (B) a deterministic filter and a random filter with zero mean value.

deterministic part out). These two filter pieces, if considered as separate "black boxes", have to be connected in parallel, as is sketched in Fig. 4.4. In formula, with the frequency response as an example, we have then

$$H(\omega, t) = H_d(\omega, t) + H_r(\omega, t), \tag{4.17}$$

where the subscripts d and r indicate respectively "deterministic part" and "random part".

Similar decomposition relations hold for all the other system functions. This is due to two facts: (1) they are all related via Fourier transforms, and (2) the Fourier transform is a linear operator. An interesting result therefore follows immediately: Fig. 4.2 and all the input-output relations remain formally valid when the system functions are given either the subscripts d or r. This signifies that the deterministic part and the random part may be treated separately.

A possible statistical approach to an arbitrary random filter can now be outlined as follows: first, one considers the mean value of any system function and deals with it as a fixed part; second, one subtracts the mean value and studies the properties of the remaining random part. Nevertheless, it should be remembered that the filter is not really divided in two parts. For the analysis of correlation functions it is often better to consider the filter as a whole.

4.4.2 The stationary filter

In Chapter 6 and following chapters we will see that the random filter we are studying is stationary in time. This has an important consequence: Fourier transformation of $h(\tau, t)$ and $H(\omega, t)$ with respect to t is impossible, and the scheme of Fig. 4.2 degenerates into an elementary relation:

$$h(\tau, t) \leftrightarrow H(\omega, t). \tag{4.18}$$

Spreading function and bi-frequency function have thus lost their significance. Formally, (4.18) is also correct when h and H carry the subscript d or r.

4.4.3 Mean values

Due to the stationarity of the filter, the time-dependency will disappear when mean values are computed in (4.18). Hence this relation reduces to

$$h_d(\tau) \leftrightarrow H_d(\omega). \tag{4.19}$$

4.4.4 Filter correlation functions

The system functions are functions of two independent variables. So the correlation functions depend in general on four, because they are defined as an average (conjugate)

product. For the impulse response, for instance, we have the following definition:

$$B_h(\tau_1, \tau_2, t_1, t_2) \equiv < h(\tau_1, t_1) h^*(\tau_2, t_2) >, \tag{4.20}$$

while the other possible correlation functions, that is B_H, B_e and B_E, are defined in a similar way. They are interconnected by double Fourier transforms (see (4.3) and (4.4)), a property that can – for the general case – be derived from Fig. 4.2. The corresponding diagram is shown in Fig. 4.5.

Modifications occur again, when the stationarity of the filter is taken into account: B_E and B_e are no longer defined, and $B_h(\tau_1, \tau_2, t_1, t_2)$ and $B_H(\omega_1, \omega_2, t_1, t_2)$ reduce

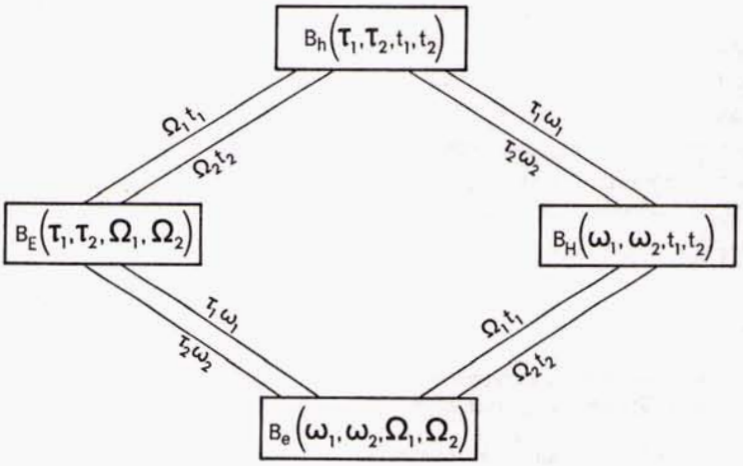


Fig. 4.5. Relations between system correlation functions, in general.

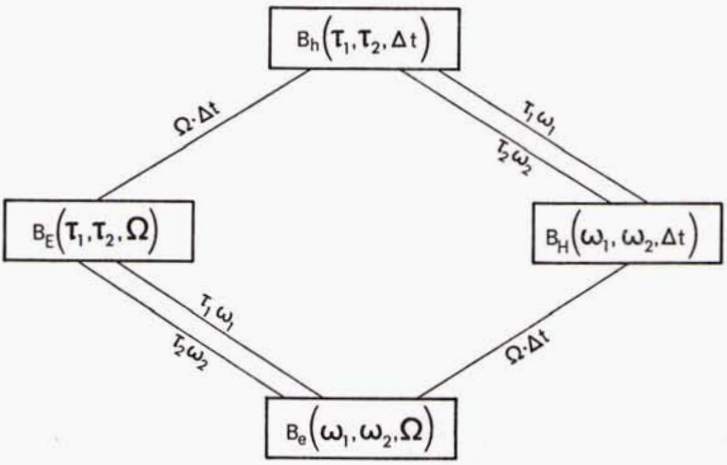


Fig. 4.6. Relations between system correlation functions, when $H(\omega,t)$ is stationary in time.

to $B'_h(\tau_1, \tau_2, \Delta t)$ and $B'_H(\omega_1, \omega_2, \Delta t)$, where $\Delta t = t_1 - t_2$. Fourier transformation of B'_h and B'_H with respect to Δt will turn out to be possible (see Chapter 8). This leads to the functions $B'_E(\tau_1, \tau_2, \Omega)$ and $B'_e(\omega_1, \omega_2, \Omega)$. B'_H is the double Fourier transform of B'_h with respect to ω_1 and ω_2, and vice versa. It can easily be shown that a similar relationship exists between B'_E and B'_e. In this way the primed functions are related according to the diagram of Fig. 4.6. For simplicity we have dropped the primes, bearing in mind that B_E and B_e are *not* the correlation functions of E and e, because these functions are not defined.

4.5 Summary

The basic properties of time-variant linear filters are described in this chapter. Input-output relations are derived and discussed. Since the filter is random, the mean values and the correlation functions of the system functions are also considered.

The mean values are non-zero. Therefore the filter is divided into a deterministic part and a purely random part, connected in parallel.

Also the consequences of stationarity in time are analyzed. It is found that various relationships simplify or disappear, because spreading function and bi-frequency function are no longer defined.

References

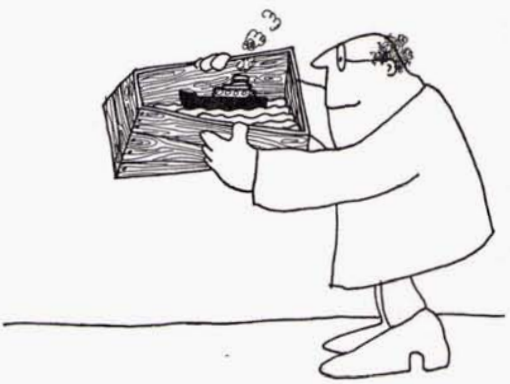
4.1 T. KAILATH, "Channel Characterization: Time-Variant Dispersive Channels", in *Lectures on Communication System Theory*, E. J. BAGHDADY, Ed. (McGraw-Hill, New York, 1961), Chapter 6.

4.2 P. A. BELLO, "Characterization of Randomly Time-Variant Linear Channels", Trans. IEEE Communication Systems **11**, 360–393 (1963).

4.3 K. A. SØSTRAND, "Mathematics of the Time-Varying Channel", Lecture at the Nato Advanced Study Institute on Signal Processing (Enschede – The Netherlands, 1968).

5

the sea surface as a random filter



CHAPTER 5

THE SEA SURFACE AS A RANDOM FILTER

5.1 Introduction

In this chapter we are faced with the task of finding an expression for one of the system functions of the underwater communication channel from transmitter to receiver via the surface. The most convenient system function to deal with appears to be the transfer function $H(\omega, t)$, because the problem can then be formulated in the frequency domain[7] (by means of the Helmholtz integral), and monochromatic sources can be used (see (4.9)).

Physically, the derivation of a formula for $H(\omega, t)$ consists in solving the wave equation (Helmholtz equation)

$$(\nabla^2 + k^2)p = 0, \tag{5.1}$$

with the boundary condition $p = 0$, since the sea surface is a pressure release surface on which the sound pressure has to vanish (*Assumption 2*). This is done in Section 5.2, which is a reprint of a paper that I published in the *Journal of the Acoustical Society of America* [*5.2*]. It also contains some preliminary results of a statistical analysis; a more complete treatment can be found in the Chapters 6–10.

The result of Section 5.2 is rather complicated: $H(\omega, t)$ is expressed there as a six-fold integral which renders the analysis of this system function somewhat problematic. In Section 5.3 a simplification is applied in such a way that $H(\omega, t)$ can be written as a series of surface integrals. In addition to the fact that these double integrals are more suitable for a detailed analysis, they allow a simple physical interpretation.

When ω is sufficiently large, the surface integrals can be solved approximately by application of the method of *stationary phase*. Section 5.4 is devoted to this subject. It also contains a comparison of the first few terms, and derives the conditions for which the whole series can be represented by the term of zero order. These results, here produced as a side-issue, will turn out to be useful later on in this study.

The wave equation (5.1) is, strictly speaking, only valid when the boundary is time-independent. Its use in combination with a time-varying surface such as the upper boundary of the ocean has hence to be justified. For this justification we refer to Section 5.5. Part of this section is a reprint of a paper that I published in the *Journal of the Acoustical Society of America* [*5.3*].

---

[7] A formulation in the time domain via the impulse response function is possible (Kirchhoff's formula [*5.1, p. 36*]), but will not be used here.

13.2, 13.6

Received 2 March 1971

The Sea Surface as a Random Filter for Underwater Sound Waves

LEONARD FORTUIN

SACLANT ASW Research Centre, La Spezia, Italy

When underwater sound waves propagate from a transmitter to a receiver, part of the energy reaches the receiver after reflection and scattering from the sea surface. This boundary effect can be called the *impulse response* of the sea surface if the incident sound field is caused by a delta pulse. In this paper the Helmholtz diffraction integral is used together with a perturbation technique for the derivation of a formula for the corresponding transfer function. The result is a random function that depends on the frequency of the incident wave, on time, and on the source–receiver configuration. Its validity is limited by three assumptions: (1) the medium is ideal (constant velocity, no subsurface layer), (2) source and receiver depth are many times larger than the surface elevation, and (3) the bottom is infinitely far away. For very high frequencies the formula indicates specular reflection from each surface "highlight." In the Fraunhofer domain, the transfer function reduces to specular reflection with phase fluctuations. Some results of a statistical analysis are included for that frequency domain.

LIST OF SYMBOLS

B	correlation function
c_0	sound speed in ideal medium
D_0	specular path length from T to R
D	path length from T to R via the surface
f	frequency of incident radiation
G_k	free space Green's function
g	gravity acceleration
H	transfer function
h	impulse response function; standard deviation of surface elevation
i	$(-1)^{\frac{1}{2}}$
$\mathbf{K}$	wavenumber vector in the plane $K_z=0$: $\mathbf{K}=(K_x,K_y,0)$
k	wavenumber of incident radiation
L	integral operator
m	integer
$\mathbf{n}$	outward surface normal
n	integer, order of Fresnel ellipse
P	perturbation
$\tilde{p}$	pressure (time dependent)
p	pressure (time independent)
p_b	pressure, due to the boundary
p_0	pressure in unbound medium
$\mathfrak{R}$	vector in three-dimensional space: $\mathfrak{R}=(x,y,z)$
$\mathbf{R}$	vector in the plane $z=0$: $\mathbf{R}=(x,y,0)$
R	receiver
r, r_0	distance
S	surface; spectral density function
T	transmitter
t	time
V	volume
v	wind speed
W	distance to the average surface
w	distance to the random surface
X, Y	horizontal distance
Z	vertical distance
α	semimajor axis of Fresnel ellipse
Δ	fraction
δ	Dirac delta function
ϵ, ϵ_0	constant
ζ	surface profile
η	difference in Y coordinate
θ	angle with vertical, angle of incidence
ξ	difference in X coordinate
ρ	source distribution; correlation distance
τ	time difference
Φ	correlation function of surface elevation
φ	angle with horizontal, grazing angle
χ	roughness parameter
Ψ	auxiliary function; proportional with the normal derivative of the total field at the boundary
ψ	phase

ω angular frequency of incident wave
ω_s frequency of surface wave

Subscripts

D Doppler
F frequency correlation
N normalized
n order of Fresnel ellipse
R receiver
S spatial correlation
s point of stationary phase, specular point
T transmitter; time correlation
z Z direction

Superscript

s on random surface

INTRODUCTION

In studies of reflection and scattering of underwater sound waves from the sea surface, two assumptions are often encountered that make the phenomenon describable in terms of plane waves: (1) transmitter and receiver have a narrow beam, and (2) they are far away from the surface. Another useful simplification, the Kirchhoff approximation, is possible when a monochromatic sound source of sufficiently high frequency is considered. A detailed survey of these approaches can be found in Refs. 1 and 2, together with an analysis of other currents in the existing literature.

Although these simplifications are useful to gain insight into the phenomenon, their drawback is evident when the path from transmitter to receiver via the surface is considered as a communication channel, or a filter. A broad-band source is then required, and, as this is often an explosive charge, the plane-wave assumption also becomes invalid.

The broad-band source should possibly have a flat frequency spectrum, so that impulse response and transfer function of the sea surface can be investigated. An experimental procedure has therefore been developed at SACLANT ASW Research Centre that consists of firing explosive charges and recording the surface-reflected signals after passing them through a filter that boosts the high frequencies in such a way that the spectrum of the explosive pulse approaches that of a delta pulse.[3]

The theoretical counterpart of this experimental technique is formed by a description of the scattered field, in which the characteristics of the sea surface and the relative position of source and receiver are parameters (see Fig. 1 for the geometry). Such a description is the subject of this paper. It is derived with the Helmholtz integral as a starting point, and Meecham's method[4] is applied to obtain an estimate for the normal derivative of the sound field at the surface. The result is a formula that connects the scattered field at an arbitrary point below the surface with the random process that describes the surface elevation in time and space. Consequently, it presents the scattered field as a random process. Useful information can hence only be obtained by means of statistical operations (e.g., mean value, correlation function—both in time and in space). This will be the subject of a subsequent study. Nevertheless, some preliminary results are included here.

Although we are eventually interested in the impulse response $h(\tau,t)$ of the random sea surface (i.e., the response measured at time t to a unit impulse applied at time $t-\tau$), we prefer to formulate the problem in the frequency domain and study the transfer function $H(\omega,t)$ first. The functions h and H are each other's Fourier transform[5]:

$$H(\omega,t)=\int_{-\infty}^{\infty} d\tau h(\tau,t)\exp(i\omega\tau),$$
$$h(\tau,t)=\frac{1}{2\pi}\int_{-\infty}^{\infty} d\omega H(\omega,t)\exp(-i\omega\tau). \tag{1}$$

An important advantage of the use of $H(\omega,t)$ is that it enables us to apply a monochromatic source (with

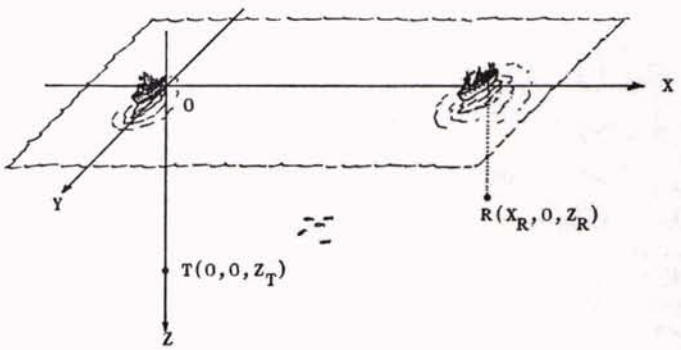


FIG. 1. Positioning of transmitter and receiver. The transmitter (T) and the receiver (R) are placed in the plane $y=0$, but this causes no loss of generality if the wind direction can make an arbitrary angle with the X axis.

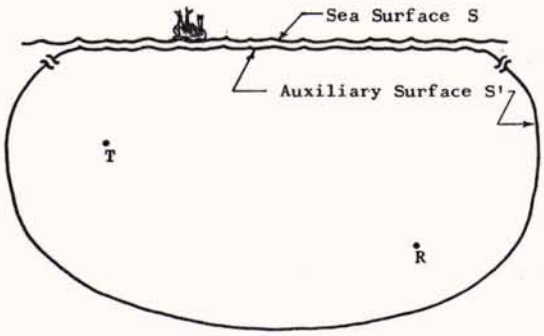


FIG. 2. The sea surface S and the auxiliary surface S'. S' can be thought to consist of two parts: a part S'' just below S, and a part S''', infinitely far away, that makes S' a closed surface.

variable frequency) of the type $\tilde{p}=p\exp(-i\omega t)$, since[5]

$$H(\omega,t)=\frac{\text{response of the filter to } \exp(-i\omega t)}{\exp(-i\omega t)}. \quad (2)$$

I. THE SCATTERED FIELD

A. Solution of the Wave Equation

Since we are only interested in the surface effect, we assume the medium to be ideal. We require a solution of the wave equation [suppressing the time dependency $\exp(-i\omega t)$]

$$(\nabla^2+k^2)p=0, \quad (3)$$

with the boundary condition $p=0$ (pressure release surface). The field at the receiver can be thought of as the sum of p_0, the field that would exist in the absence of boundaries, and p_b, the boundary effect:

$$p=p_0+p_b. \quad (4)$$

It is the second term that we are interested in.

A generalized version of the Helmholtz integral can be derived from Ref. 6 by application of Green's theorem[7]:

$$\frac{1}{4\pi}\oint dS'\left[G_k(\mathfrak{R},\mathfrak{R}_0{}^{s'})\frac{\partial}{\partial\mathbf{n}}p(\mathfrak{R}_0{}^{s'})-p(\mathfrak{R}_0{}^{s'})\frac{\partial}{\partial\mathbf{n}}G_k(\mathfrak{R},\mathfrak{R}_0{}^{s'})\right]$$

$$+\int\int\int dV_0 G_k(\mathfrak{R},\mathfrak{R}_0)\rho(\mathfrak{R}_0)$$

$$=p(\mathfrak{R}) \quad \text{if } \mathfrak{R} \text{ is on or inside the closed surface } S',$$
$$=0 \quad \text{if } \mathfrak{R} \text{ is outside } S'. \quad (5)$$

As is shown in Fig. 2, the closed surface S' can be thought to consist of the parts S'' and S'''. The latter does not contribute to the surface integral (Sommerfeld's radiation condition) and S'' approaches the sea surface S, on which the total pressure vanishes. Moreover, we have $\rho(\mathfrak{R}_0)=\delta(\mathfrak{R}_0-\mathfrak{R}_T)$, so that Eq. 5 yields

$$p(\mathfrak{R}_R)=\frac{1}{4\pi}\int\int dSG_k(\mathfrak{R}_R,\mathfrak{R}_0{}^s)\frac{\partial}{\partial\mathbf{n}}p(\mathfrak{R}_0{}^s)$$
$$+G_k(\mathfrak{R}_R,\mathfrak{R}_T). \quad (6)$$

The second term is recognized as the undisturbed wave $p_0(\mathfrak{R}_R)$. Hence by combination of Eqs. 4 and 6, we arrive at an expression for the scattered field:

$$p_b(\mathfrak{R}_R)=\frac{1}{4\pi}\int\int dSG_k(\mathfrak{R}_R,\mathfrak{R}_0{}^s)\frac{\partial}{\partial\mathbf{n}}p(\mathfrak{R}_0{}^s). \quad (7)$$

This formula has an interesting physical meaning. It shows that one can imagine that the transmitter induces elementary sources on S, and that these radiate omnidirectionally. The effect at the receiver of one of them, that is $G_k(\mathfrak{R}_R,\mathfrak{R}_0{}^s)$, has to be weighted with $\partial p(\mathfrak{R}_0{}^s)/\partial\mathbf{n}$, the normal derivative of the total field at the boundary. This derivative depends on the position of the unit source relative to the transmitter and on the slope of the surface at that position. The total effect p_b is obviously obtained by summation over all sources.

B. Derivative of the Field at the Boundary

Before Eq. 7 can be used for the calculation of the scattered field, the normal derivative of the total field at the boundary has to be known. It is here that difficulties arise for a surface that is not perfectly flat,[8] because then $\partial p/\partial\mathbf{n}$ is unknown. However, an integral equation for the desired function can be found if we consider an observation point on the boundary; here also the diffraction integral (Eq. 7) holds. If we then use the boundary condition of zero total pressure, a Fredholm equation of the first kind is found for the derivative:

$$-p_0(\mathfrak{R}_1{}^s)=\frac{1}{4\pi}\int\int dSG_k(\mathfrak{R}_1{}^s,\mathfrak{R}_0{}^s)\frac{\partial}{\partial\mathbf{n}}p(\mathfrak{R}_0{}^s). \quad (8)$$

The surface element dS can be written as

$$dS(\mathfrak{R}_0{}^s)=\frac{dx_0dy_0}{\cos\theta(x_0,y_0)}=\frac{d\mathbf{R}_0}{\cos\theta(\mathbf{R}_0)}, \quad (9)$$

where θ is the angle between the vertical axis and the surface normal $\mathbf{n}$ at $\mathbf{R}_0(x_0,y_0)$. For convenience we define a function Ψ:

$$\Psi(\mathbf{R})=\frac{\partial}{\partial\mathbf{n}}p(\mathfrak{R}^s)\Big/4\pi\cos\theta(\mathbf{R}). \quad (10)$$

The scattered field is then determined by the following

pair of equations:

$$p_b(\mathfrak{R}_R)=\int_{-\infty}^{\infty}\int d\mathbf{R}_0 G_k(\mathfrak{R}_R,\mathfrak{R}_0^s)\Psi(\mathbf{R}_0), \quad (11a)$$

$$-p_0(\mathfrak{R}_1^s)=\int_{-\infty}^{\infty}\int d\mathbf{R}_0 G_k(\mathfrak{R}_1^s,\mathfrak{R}_0^s)\Psi(\mathbf{R}_0). \quad (11b)$$

The random function Ψ has to be solved from Eq. 11b and substituted into Eq. 11a. Examination of Eq. 11b shows that this integral equation has a somewhat peculiar kernel: It depends not only on $\mathbf{R}_0$ and $\mathbf{R}_1$, as it would in a regular case, but also on the surface elevation at the positions $\mathbf{R}_0$ and $\mathbf{R}_1$. To illustrate this statement, we write out the kernel in full:

$$G_k(\mathfrak{R}_1^s,\mathfrak{R}_0^s)=\exp(ikr)/r, \quad (12)$$

where

$$r=\{(x_1-x_0)^2+(y_1-y_0)^2+[\zeta(x_1,y_1)-\zeta(x_0,y_0)]^2\}^{\frac{1}{2}}. \quad (13)$$

The dependence of G_k on ζ_1 and ζ_0 has an important consequence: An exact solution for Ψ cannot be found. However, its approximation is possible by means of a perturbation method.

C. Perturbation Method

Equation 11b can be solved exactly when $\zeta=0$ (perfectly plane surface), because then the kernel becomes a regular one. This fact leads us to consider the irregular kernel $G_k(\mathfrak{R}_1^s,\mathfrak{R}_0^s)$ as a disturbed version of $G_k(\mathbf{R}_1,\mathbf{R}_0)$. If the disturbance is small, a perturbation technique can be applied to approach the exact solution.

The perturbation method starts by substitution into Eq. 11b of

$$G_k(\mathfrak{R}_1^s,\mathfrak{R}_0^s)=G_k(\mathbf{R}_1,\mathbf{R}_0)+P(\mathbf{R}_1,\mathbf{R}_0), \quad (14)$$

where P represents the disturbance:

$$P(\mathbf{R}_1,\mathbf{R}_0)\equiv G_k(\mathfrak{R}_1^s,\mathfrak{R}_0^s)-G_k(\mathbf{R}_1,\mathbf{R}_0). \quad (15)$$

If the condition $P\ll G_k(\mathbf{R}_1,\mathbf{R}_0)$ is satisfied, we may apply Meecham's perturbation method,[4] so we put $P=\epsilon P$, with $\epsilon\rightarrow 1$, and try to find a solution of the form[9]

$$\Psi=\sum_{m=0}^{\infty}\epsilon^m\Psi_m, \quad (\epsilon\rightarrow 1). \quad (16)$$

Substituting this expansion into Eq. 11b, together with Eq. 14, and equating equal powers of ϵ, gives a set of equations for the Ψ_m:

$$\int\int d\mathbf{R}_0 G_k(\mathbf{R}_1,\mathbf{R}_0)\Psi_0(\mathbf{R}_0)=-p_0(\mathfrak{R}_1^s), \quad (17a)$$

$$\int\int d\mathbf{R}_0 G_k(\mathbf{R}_1,\mathbf{R}_0)\Psi_{m+1}(\mathbf{R}_0)$$

$$=\int\int d\mathbf{R}_0 P(\mathbf{R}_1,\mathbf{R}_0)\Psi_m(\mathbf{R}_0) \quad \text{if } m\geq 0. \quad (17b)$$

Equation 17a can be solved easily (see Sec. I-D). Its solution, substituted into Eq. 17b with $m=0$, yields a similar equation for Ψ_1. Solving this and using the result in Eq. 17b with $m=1$, we find an equation for Ψ_2, and so on. In this way the terms Ψ_m of Eq. 16 can be calculated successively.

D. Inversion of the Integral Equations

The integral equations for the functions Ψ_m are Fredholm equations of the first kind. As their kernel is a Green's function, we expand it in eigenfunctions[10,11]:

$$G_k(\mathbf{R}_1,\mathbf{R}_0)=\frac{i}{2\pi}\int\int\frac{d\mathbf{K}}{K_z}\exp[i\mathbf{K}\cdot(\mathbf{R}_1-\mathbf{R}_0)], \quad (18)$$

where $K_z=(k^2-K^2)^{\frac{1}{2}}$. Substitution of this expansion into Eq. 17a and exchange of the order of integration yields

$$-p_0(\mathfrak{R}_1^s)=\int\int d\mathbf{K}\exp(i\mathbf{K}\cdot\mathbf{R}_1)$$

$$\times\frac{i}{2\pi K_z}\int\int d\mathbf{R}_0\exp(-i\mathbf{K}\cdot\mathbf{R}_0)\Psi_0(\mathbf{R}_0). \quad (19)$$

Both the integral over $\mathbf{K}$ and the one over $\mathbf{R}_0$ can be considered as two-dimensional Fourier integrals. The desired function Ψ_0 can hence be obtained in three steps: (a) transformation of $-p_0$, (b) multiplication of the result by $-i2\pi K_z$, and (c) inverse Fourier transformation. In this way we find

$$\Psi_0(\mathbf{R}_0)=\frac{i}{8\pi^3}\int\int d\mathbf{K}K_z\int\int d\mathbf{R}_1$$

$$\times\exp[i\mathbf{K}\cdot(\mathbf{R}_0-\mathbf{R}_1)]p_0(\mathfrak{R}_1^s). \quad (20)$$

This is the solution of Eq. 17a. The terms $\Psi_{m+1}(m\geq 0)$ are obtained if p_0 is replaced by the right-hand side of Eq. 17b.

It may be useful to remark that Ψ_0 can also be derived from Eq. 17a without the expansion of $G_k(\mathbf{R}_1,\mathbf{R}_0)$. This function namely depends on the difference $\mathbf{R}_1-\mathbf{R}_0$, so that Eq. 17a can be considered as a convolution integral. Application of the Fourier transform and its inverse then yield an expression identical to Eq. 20. This is the method used by Meecham.[4]

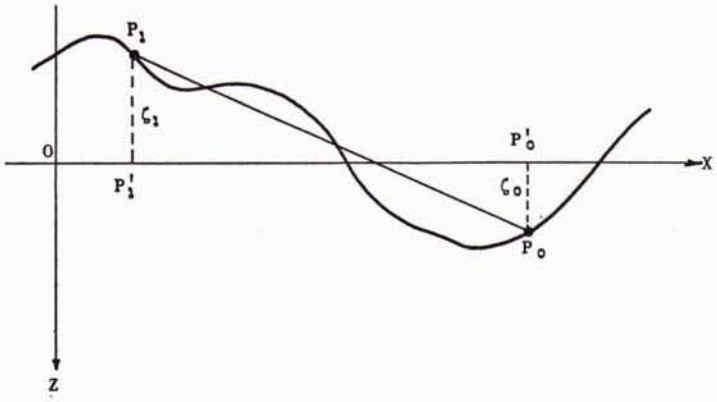


FIG. 3. Two points at the surface: P_1 and P_0 are arbitrary points with position vectors $\mathcal{R}_1^s$ and $\mathcal{R}_0^s$; $P_1P_0=|\mathcal{R}_1^s-\mathcal{R}_0^s|=r$, $P_1'P_0'=|\mathbf{R}_1-\mathbf{R}_0|=r_0$.

E. Conditions for the Perturbation Method

Figure 3 indicates the surface area that contains the points $\mathcal{R}_1^s$ and $\mathcal{R}_0^s$. For simplicity, a cross section in the plane $y=0$ is shown, but the points may have arbitrary positions.

First we consider the distance r between the points. A formula is given in Eq. 13. If we put

$$r_0=|\mathbf{R}_1-\mathbf{R}_0|=[(x_1-x_0)^2+(y_1-y_0)^2]^{\frac{1}{2}}, \quad (21)$$

then we can write

$$r=r_0+\Delta r_0. \quad (22)$$

An expression for Δr_0 can be found by series expansion of r:

$$\Delta r_0=(\zeta_1-\zeta_0)^2/2r_0 \quad \text{if} \quad \Delta r_0/r_0\ll 1. \quad (23)$$

For large r_0 the condition $\Delta r_0\ll r_0$ is always satisfied. However, if $r_0\to 0$, it can only be met if Δr_0 goes to zero faster than r_0. The square of the surface slope is then approached, and we arrive at the condition[4]

$$(\partial\zeta/\partial x)^2\ll 1, \quad (\partial\zeta/\partial y)^2\ll 1. \quad (24)$$

According to Kinsman,[12] the slope of the sea-surface waves cannot exceed the value 2/7, so that the condition on the slope quadrature is easily satisfied.

Next we examine the perturbation P. Using Eqs. 12 and 22 in Eq. 15, we get

$$P(\mathbf{R}_1,\mathbf{R}_0)\approx ik\Delta r_0 G_k(\mathbf{R}_1,\mathbf{R}_0), \quad (25)$$

because $\Delta r_0\ll r_0$. The condition $P\ll G_k(\mathbf{R}_1,\mathbf{R}_0)$, to which the perturbation method is subject, is hence satisfied if the phase difference between the paths P_1P_0 and $P_1'P_0'$ in Fig. 3 is much less than 1 rad: $k\Delta r_0\ll 1$. Following Meecham,[4] we investigate this inequality by distinguishing three regions for kr_0, the phase difference between P_1' and P_0':

(1) $kr_0\ll 1$, (2) $kr_0\gg 1$, (3) $0.1\leq kr_0\leq 10$.

Region 1. The condition $k\Delta r_0\ll 1$ is rewritten as $(kr_0)(\Delta r_0/r_0)\ll 1$. This is satisfied, because both factors are small compared to unity.

Region 2. For $kr_0\gg 1$ the situation is more complicated. With Eq. 23 the condition $k\Delta r_0\ll 1$ leads to

$$\tfrac{1}{2}k^2(\zeta_1-\zeta_0)^2\lesssim 1. \quad (26)$$

This inequality is hard to examine, as ζ_1 and ζ_0 are random quantities. We replace it therefore by its mean value, and find the condition

$$kh\lesssim[1-\Phi(\mathbf{r}_0)]^{-\frac{1}{2}}. \quad (27)$$

The spatial correlation function of the surface, $\Phi(\mathbf{r}_0)$, can be calculated when the sea-surface spectrum is known. For the Pierson–Moskowitz spectrum[13] this calculation has been done by De Boer.[14,15] His results are used in Fig. 4 to draw a cross-wind and a down-wind curve for $(1-\Phi)^{-\frac{1}{2}}$. The condition expressed in Eq. 27 means that kh can only assume values below or very close to these curves. Obviously the down-wind case is in this respect more critical than the cross-wind case. In principle, the condition implies a frequency limitation depending on the horizontal distance between the two surface points under consideration. However, in practice there is the fact that integration over the whole XY plane can be replaced by integration over a limited area—the effective scattering domain—the size of which decreases with the incident wavelength. This signifies that in Fig. 4, for a certain value of kh, the distance r_0 does not have to assume all values between zero and infinity (in which case the "forbidden" area above the curves would be entered when $kh>1$), but only those between zero and the maximum size of the effective scattering area, say, $2\alpha_n$, the length of the Fresnel ellipse of order n.

To investigate the importance of the frequency limitation in practical cases, we have plotted in Fig. 5 the normalized values of $2\alpha_n$ for which $kh>1$ as a function of kh, together with the curves for $(1-\Phi)^{-\frac{1}{2}}$. The parameter values $n=1$, 2, 3, $Z_T=50$ m, $X_R=0$, 50, 100, 150, and 200 m, $k=6$, 60, and 600 (i.e., $f=1.5$, 15, and 150 kHz), and $v=1$, 2, 5 and 10 m/sec are used. Values for v are required to calculate h. Many of the $2\alpha_n$ points lie below these curves, but not all of them.

Especially for $n>2$ and $X_R>150$ m we find points in the prohibited zone. However, the condition on kh (Eq. 27) is not very strong: if kr_0 is large enough, kh may even be greater than $(1-\Phi)^{-\frac{1}{2}}$. We conclude hence that in region 2 the condition $k\Delta r_0 \ll 1$ is satisfied in practice.

Region 3. When kr_0 is neither much smaller nor much larger than 1 ($0.1 \leq kr_0 \leq 10$), we apply the same reasoning as in region 1 and find

$$10(\Delta r_0/r_0) \ll 1. \quad \cdots\cdots (28)$$

This inequality emphasizes the importance of Eq. 24.

Collecting the results of the foregoing investigations, we conclude that the perturbation method used here is subject to only one important condition, the one on the slope quadrature.

F. Convergence of the Perturbation Series

Defining an integral operator L that acts on a function of $\mathbf{R}_1$:

$$L\{f(\mathbf{R}_1)\} \equiv \frac{i}{8\pi^3} \int\int d\mathbf{K} K_z \int\int d\mathbf{R}_1 \times \exp[i\mathbf{K}\cdot(\mathbf{R}_0-\mathbf{R}_1)] f(\mathbf{R}_1), \quad (29)$$

the terms of the series expansion of Ψ can be written as

$$\Psi_m(\mathbf{R}_0) = L\{p_0(\mathcal{R}_1^a)\} \quad (m=0)$$

$$= L\left\{-i\int\int d\mathbf{R}_0 (k\Delta r_0) G_k(\mathbf{R}_1,\mathbf{R}_0)\Psi_{m-1}(\mathbf{R}_0)\right\} \quad (m>0). \quad (30)$$

The inverse operator L^{-1} follows readily from Eq. 17a:

$$L^{-1}\{g(\mathbf{R}_0)\} \equiv \int\int d\mathbf{R}_0 G_k(\mathbf{R}_1,\mathbf{R}_0) g(\mathbf{R}_0). \quad (31)$$

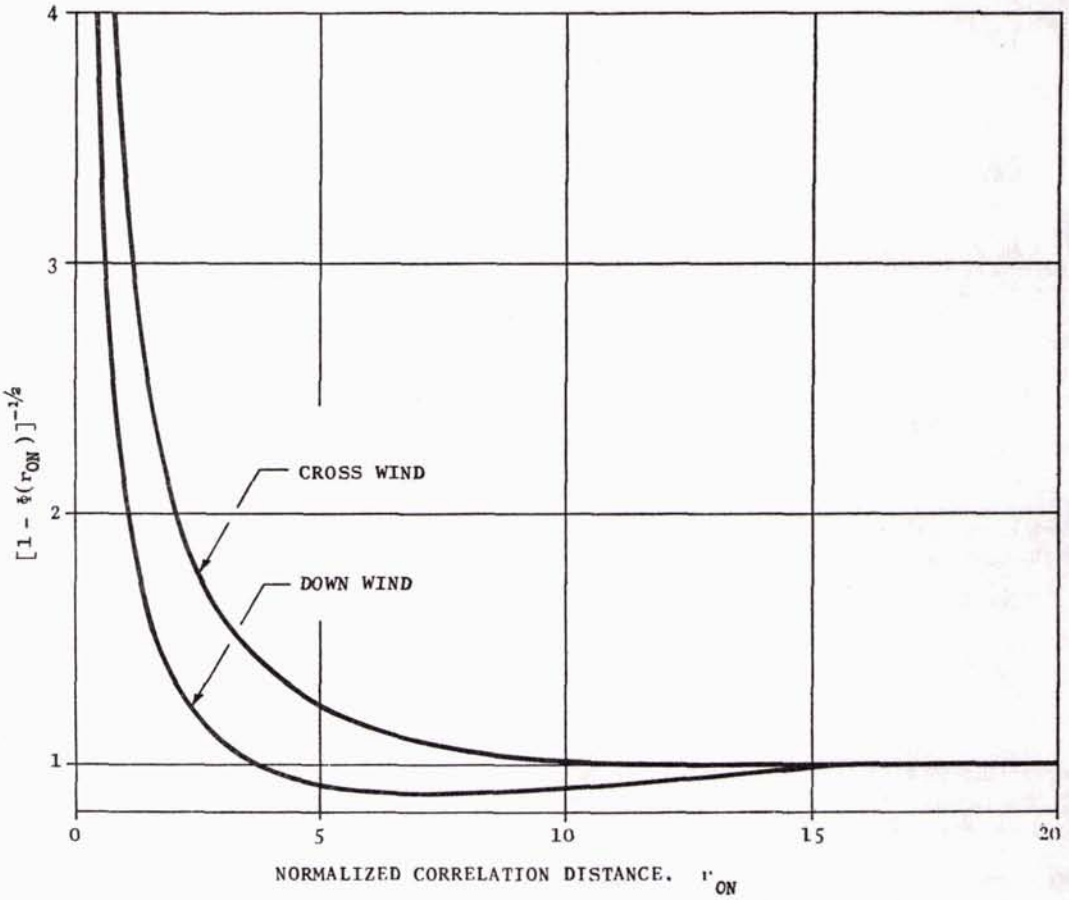


FIG. 4. The upper limit for kh. The cross-wind and down-wind curves of $[1-\Phi(r_0)]^{-\frac{1}{2}}$ are calculated for the Pierson–Moskowitz sea-surface frequency spectrum, with data from Ref. 14. The horizontal scale is normalized with respect to the wind speed: $r_{0N} = 2gr_0/v^2$.

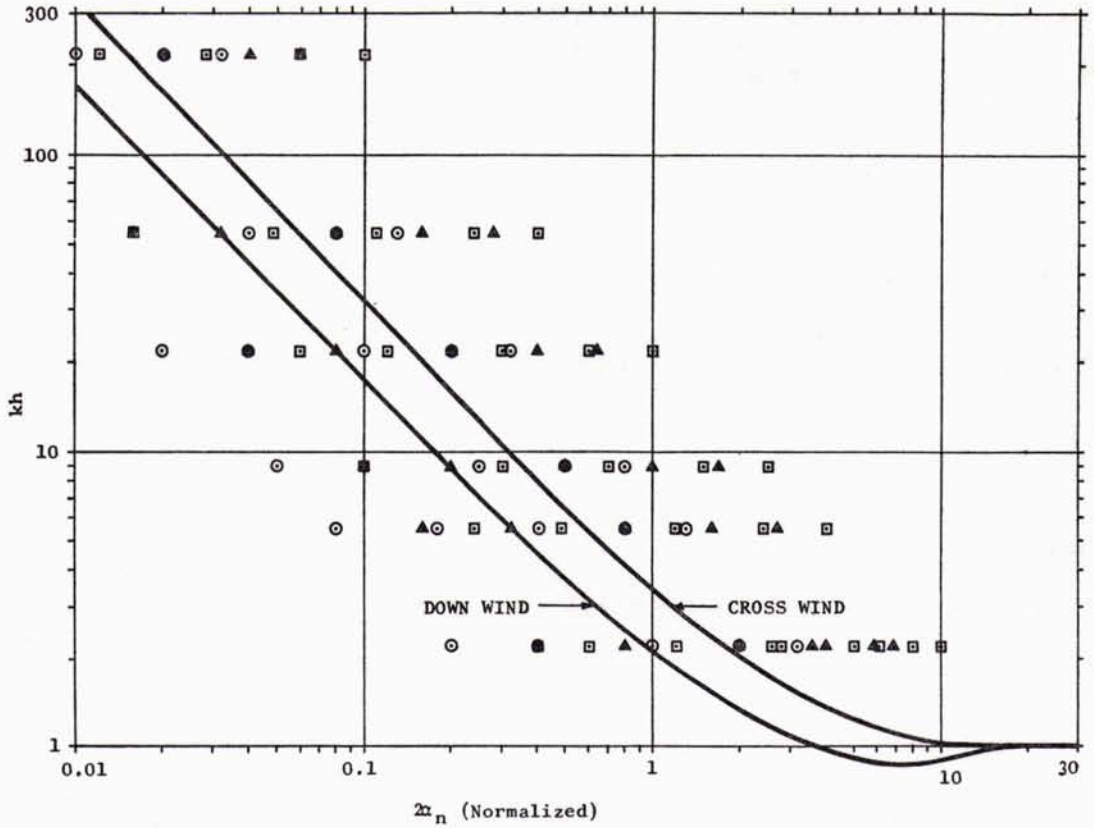


FIG. 5. Normalized values of $2\alpha_n$, the length of the Fresnel ellipse of order n, vs kh. The plotted points are calculated with Eq. 52a of Ref. 17, for $Z_T=50$ m, $X_R=0$, 50, 100, 150, and 200 m, $k=6$, 60, and 600, and $v=1$, 2, 5, and 10 m/sec. The curves show the function $[1-\Phi(r_{0N})]^{-\frac{1}{2}}$. $\odot: n=1$; $\triangle: n=2$; $\square: n=3$.

About the quantity $k\Delta r_0$ we can remark that (a) it is never negative if $k\geq 0$, (b) it equals zero for $\mathbf{R}_1=\mathbf{R}_0$, and (c) it tends to zero when $|\mathbf{R}_1-\mathbf{R}_0|\to\infty$. We know also that $k\Delta r_0\ll 1$, so there must exist a positive constant ϵ_0 such that

$$k\Delta r_0<\epsilon_0\ll 1. \tag{32}$$

In view of this inequality we can derive from Eq. 30, with the definition of L^{-1}, an important relation:

$$\Psi_m(\mathbf{R}_0)<-i\epsilon_0\Psi_{m-1}(\mathbf{R}_0) \quad \text{for} \quad m>0. \tag{33}$$

If this were an equality, the perturbation series would be a geometric one, convergent as $\epsilon_0<1$, with sum $\Psi_0(1+i\epsilon_0)^{-1}$. Each of the terms of the true series is smaller than the corresponding term in this geometric series. Therefore, the perturbation series converges even more rapidly, to a value that is about Ψ_0, because $\epsilon_0\ll 1$, when $k\Delta r_0\ll 1$. Consequently, if the condition for the applicability of the perturbation method is satisfied, the convergence of the series is guaranteed at the same time. The convergence is even so fast that the first term of the series is a very good approximation of the exact solution of the integral equation. Hence, from now on, we can take

$$\Psi(\mathbf{R}_0)\approx\Psi_0(\mathbf{R}_0)=L\{p_0(\mathcal{R}_1')\}. \tag{34}$$

G. Transfer Function of the Sea Surface

We are now ready to write the final formula for the scattered field, by substitution of Eqs. 34 and 20 into Eq. 11a. The result is rather complicated:

$$p_b(\mathcal{R}_R)=\frac{i}{8\pi^3}\int\int d\mathbf{R}_0\int\int d\mathbf{K}K_z\int\int d\mathbf{R}_1$$
$$\times\exp[i\mathbf{K}\cdot(\mathbf{R}_0-\mathbf{R}_1)]G_k(\mathcal{R}_1',\mathcal{R}_T)G_k(\mathcal{R}_R,\mathcal{R}_0'). \tag{35}$$

Some simplification is possible, as for the Green's functions. They depend on the distances w_T and w_R from T and R, respectively, to the random boundary (see Fig. 6). However, as Z_T and Z_R are much larger than the surface elevation, these distances are about equal to W_T and W_R, their values for $\zeta=0$. Therefore, we expand w_T and w_R, and have

$$\begin{aligned} w_T&\approx W_T-(Z_T/W_T)\zeta(\mathbf{R}_1),\\ w_R&\approx W_R-(Z_R/W_R)\zeta(\mathbf{R}_0). \end{aligned} \tag{36}$$

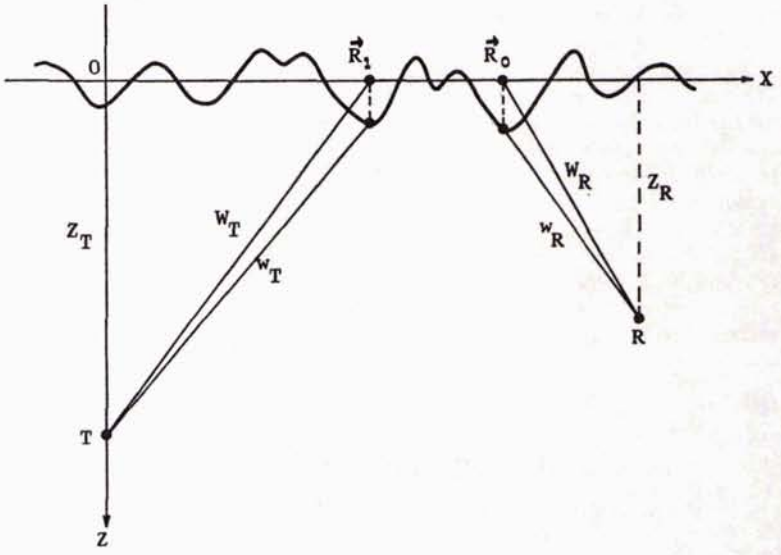


FIG. 6. The distance from T and R to the surface. If Z_T and Z_R are much larger than ζ, w_T and w_R are approximately equal to W_T and W_R.

The random term in these expressions is important for the phase of G_k, but not for the amplitude. Equation 35 can therefore be changed into

$$p_b(\mathfrak{R}_R)=\frac{i}{8\pi^3}\int\int d\mathbf{R}_0\int\int d\mathbf{K}K_z\int\int d\mathbf{R}_1$$
$$\times\exp[i\mathbf{K}\cdot(\mathbf{R}_0-\mathbf{R}_1)]G_k(\mathbf{R}_1,\mathfrak{R}_T)G_k(\mathfrak{R}_R,\mathbf{R}_0)$$
$$\times\exp\{-ik[(Z_T/W_T)\zeta(\mathbf{R}_1)+(Z_R/W_R)\zeta(\mathbf{R}_0)]\}. \quad (37)$$

The random character of p_b is concentrated in the last exponential. This assumes the value 1 if $\zeta=0$, in which case p_b reduces to the specular reflection.

As a consequence of the mathematical formulation in the frequency domain, p_b can be regarded as the response of the surface to a continuous signal of the form $\exp(-i\omega t)$. As the time dependency has been suppressed throughout the analysis, we conclude from Eq. 2 that

$$p_b(\mathfrak{R}_R)=H(\omega,t). \quad (38)$$

The dependency of p_b on frequency and time has, hence, to be incorporated. The frequency variable is

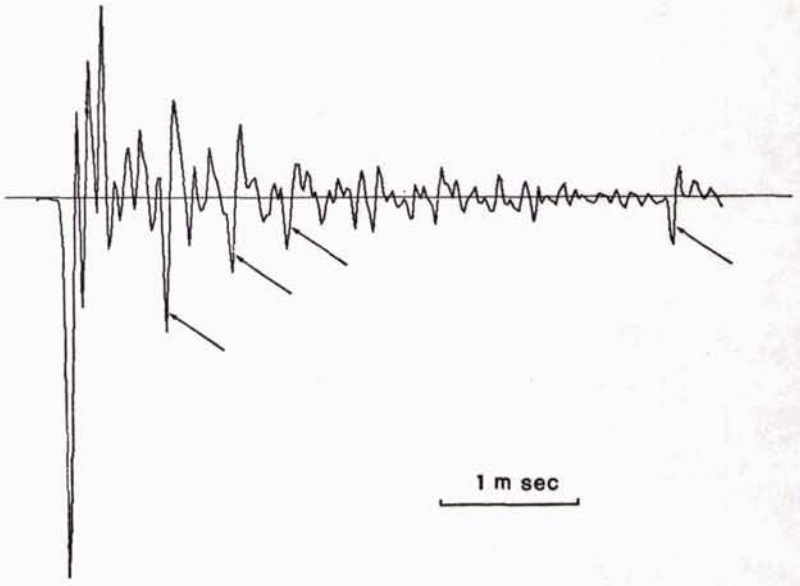


FIG. 7. Signal from an underwater explosion after reflection from the sea surface ($X_R=2200$ m, $Z_T=Z_R=100$ m, $v=12$ knots, sea state 2). The arrows indicate specular reflections from facets.

present via the wavenumber k in K_z, in the Green's functions, and in the phase of the random factor.

The time variable needs a bit more consideration. We want to observe the scattered field at time t. This field is built up by elementary waves, transmitted at the surface points $\mathbf{R}_0$. Each wave needs a time $t=W_R/c_0$ to reach the receiver. Consequently, $\zeta(\mathbf{R}_0)$ has to be evaluated at time $t_0=t-W_R/c_0$. In the same way a time $t_1=t_0-|\mathbf{R}_1-\mathbf{R}_0|/c_0$ can be assigned to $\zeta(\mathbf{R}_1)$. (If the effective scattering area is small with respect to W_T and W_R, we can take approximately $t_1=t_0$.) The complete formula for the transfer function of the sea surface then becomes

$$H(k,t)=\frac{i}{8\pi^3}\int\int d\mathbf{R}_0\int\int d\mathbf{K}K_z\int\int d\mathbf{R}_1 \times\exp[i\mathbf{K}\cdot(\mathbf{R}_0-\mathbf{R}_1)]G_k(\mathbf{R}_1,\mathfrak{R}_T)G_k(\mathfrak{R}_R,\mathbf{R}_0) \times\exp\{-ik[(Z_T/W_T)\zeta(\mathbf{R}_1,t_1) +(Z_R/W_R)\zeta(\mathbf{R}_0,t_0)]\}, \quad (39)$$

where

$$t_0=t-W_R/c_0, \qquad t_1=t_0-|\mathbf{R}_1-\mathbf{R}_0|/c_0. \quad (40)$$

W_T and W_R are defined by

$$W_T(\mathbf{R}_1)=(x_1^2+y_1^2+Z_T^2)^{\frac{1}{2}}, \qquad W_R(\mathbf{R}_0)=[(X_R-x_0)^2+y_0^2+Z_R^2]^{\frac{1}{2}}. \quad (41)$$

II. SOME PROPERTIES OF THE SCATTERED FIELD

Section I has produced a description of the scattered field that is not subject to strong restrictions on receiver–transmitter geometry, on sea state, or on incident sound frequency. The price for this general validity of Eq. 39 obviously is its great complexity. A detailed analysis is, therefore, a study in itself. However, some properties of $H(k,t)$ can be found relatively easily, if we consider sound frequencies so high that the integrals in Eq. 39 may be approximated via the *stationary-phase method.*

A. Multipath Effect

When k is sufficiently high, we enter the frequency domain where the ray theory is valid. The surface can then be considered as a combination of locally flat areas, or facets. It will act as a rough mirror, and each facet on the surface where the slope hsa the correct value will produce a local specular reflection. This effect occurs when the first few Fresnel zones are smaller than the facet. It has been observed at sea when impulsive underwater signals are reflected by the sea surface (Fig. 7). Mathematically, this multipath effect can be seen in Eq. 39 via a generalization of the method of *stationary phase.*[16] This generalization is straightforward from the one-dimensional to the six-dimensional case, but somewhat lengthy. It is hence omitted

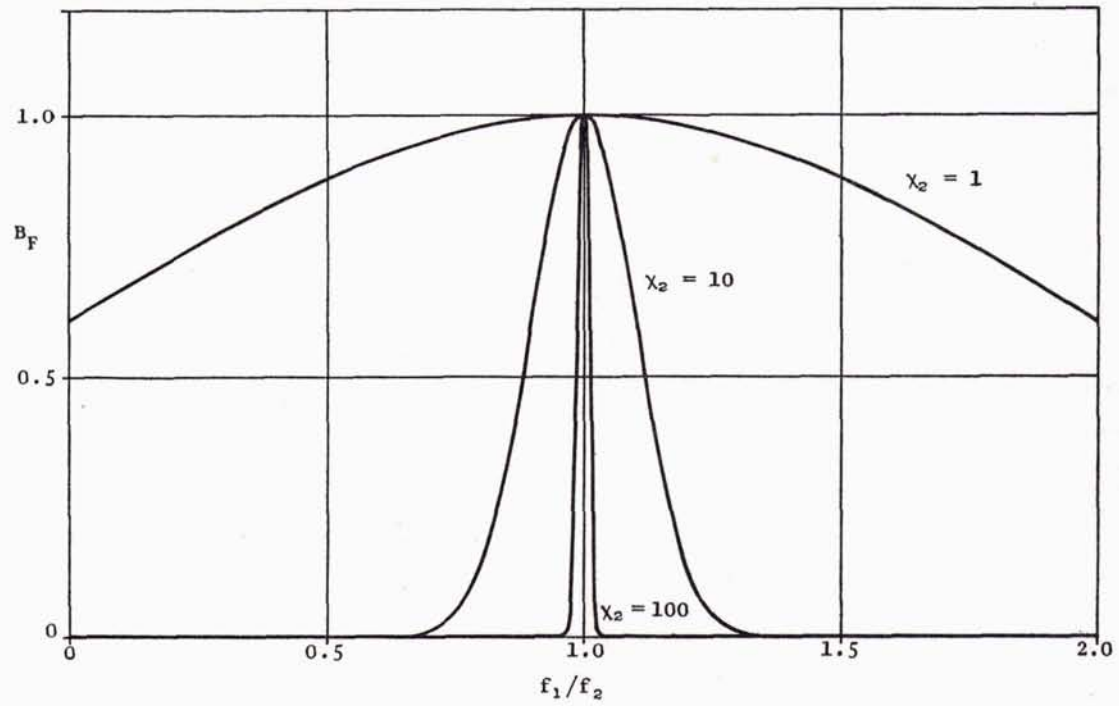


FIG. 8. The frequency correlation function B_F for constant f_2; $\chi=2\,kh\cos\theta_s$ is the roughness parameter.

here.[17] It indicates that each surface point where the slope has the geometrically correct value yields a contribution of the specular type $\exp(ikD)/D$.

B. Fraunhofer Diffraction

At lower frequencies or for a very smooth surface, the analysis in Sec. II-A indicates that there will be only one point of stationary phase: the point of specular reflection $\mathbf{R}_s=(X_s,Y_s)$, with $X_s=X_RZ_T/(Z_T+Z_R)$ and $Y_s=0$. The random factor in Eq. 39 then reduces to a constant that can be taken out of the integrals. The transfer function is then given by

$$H(k,t)\approx-\frac{\exp(ikD_0)}{D_0}\exp(-i\psi), \tag{42}$$

where

$$\psi=2k\cos\theta_s\zeta(\mathbf{R}_s,t_s). \tag{43}$$

Comparing this result with the transfer function of the perfectly flat surface, we conclude that the random boundary has introduced a phase fluctuation ψ, with zero mean value and with the same type of probability density function as the sea-surface elevation. For a Gaussian sea surface, the mean value of the scattered field and the correlation functions in frequency, time, and space can readily be calculated. An important role is played by roughness parameters of the type

$$\chi=2kh\cos\theta_s. \tag{44}$$

1. Mean Value

$$\langle H(k,t)\rangle=-\exp(ikD_0-\chi^2/2)/D_0. \tag{45}$$

This is the coherent part of the scattering. It is proportional with the specular reflection, and the proportionality factor decreases with growing roughness, either because the incident frequency increases, the incident angle decreases, or the variance of the surface elevation becomes greater. Note that the mean value does not depend on the surface correlation properties.

2. Frequency Correlation

For this type of correlation we consider coinciding receivers and equal observation times. Two frequencies are transmitted simultaneously: a variable f_1 and a fixed f_2. The normalized correlation function becomes

$$B_F(f_1,f_2=\text{const})=\exp[-\tfrac{1}{2}\chi_2^2(1-f_1/f_2)^2], \tag{46}$$

and on a f_1/f_2 scale we find curves with a Gaussian shape. Some are plotted in Fig. 8 for $\chi_2=1$, 10, and 100.

Coherent transmission is possible in a frequency band around f_2 in which B_F is close enough to unity. In this band all frequencies are affected by the rough surface in the same way, so that the shape of signals transmitted in this band remains unchanged. Then pulse elongation will not occur. If we accept the 3-dB points as the limits of the coherent band, we get $B_F\geq0.5$, so that the useful bandwidth equals $2\Delta f_1=2.36f_2/\chi_2$, a quantity independent of f_2, but dependent on wind speed and geometry.

The choice of f_1 and f_2 is not arbitrary, as the Fraunhofer approximation has to be valid. Adopting the usual assumption that the scattering is mainly coming from the first Fresnel zone and accepting relative path differences of up to 10%, we get the condition

$$f\geq(c_0X_R^2\times10^2)/4Z_T^2D_0 \quad \text{if} \quad Z_T=Z_R. \tag{47}$$

In order to illustrate the foregoing remarks we consider two examples: (a) $X_R=100$ m, (b) $X_R=1000$ m, both with $v=5$ m/sec or $h=9$ cm (Pierson–Moskowitz spectrum) and $Z_T=Z_R=100$ m.

Example (a): From Eq. 47 we obtain $f\geq168$ Hz, whereas $2\Delta f=3.54$ kHz.

Example (b): Now $f\geq3750$ Hz and $2\Delta f=15$ kHz.

Comparing these two examples, we see that at longer range the coherent bandwidth increases as the surface appears more smooth. However, the condition for the applicability of the Fraunhofer approximation shifts this coherent band to higher frequencies.

3. Time Correlation and Doppler Spread

When coinciding receivers and a single incident frequency are taken, the input signal to the random filter is of the type $\exp(-i\omega t)$, and its response equals $H(\omega,t)\exp(-i\omega t)$, as follows from Eq. 2. With Eq. 42 we see that this output signal is proportional with a harmonic oscillation that suffers from a random-phase fluctuation. This random-phase modulation broadens the frequency content of the signal: Instead of only the frequency ω, it also contains some energy in a band around ω. This effect is caused by the movement of the surface elements. It may hence be called "Doppler" spread.

Quantitative insight into this phenomenon can be gained via the time-correlation function of the filter

$$B_T(\tau)=\exp\{-\chi^2[1-\Phi(0,0,\tau)]\} \tag{48}$$

and its Fourier transform, the spectral density $S(\Omega)$. Strictly speaking, B_T has no Fourier transform because if $\tau\to\infty$, then $B_T=\exp(-\chi^2)\neq0$. However, we can substract this constant and transform it separately, the result being a delta pulse.

A useful simplification is possible when the surface is sufficiently smooth. For $\chi\leq0.625$ the spectral density is approximately[18]

$$S(\Omega)=2\pi\exp(-\chi^2)\times\left[\delta(\Omega)+\frac{\chi^2}{2\pi}\int_{-\infty}^{\infty}d\tau\exp(i\Omega\tau)\Phi(0,0,\tau)\right]. \tag{49}$$

The integral is recognized as the frequency spectrum

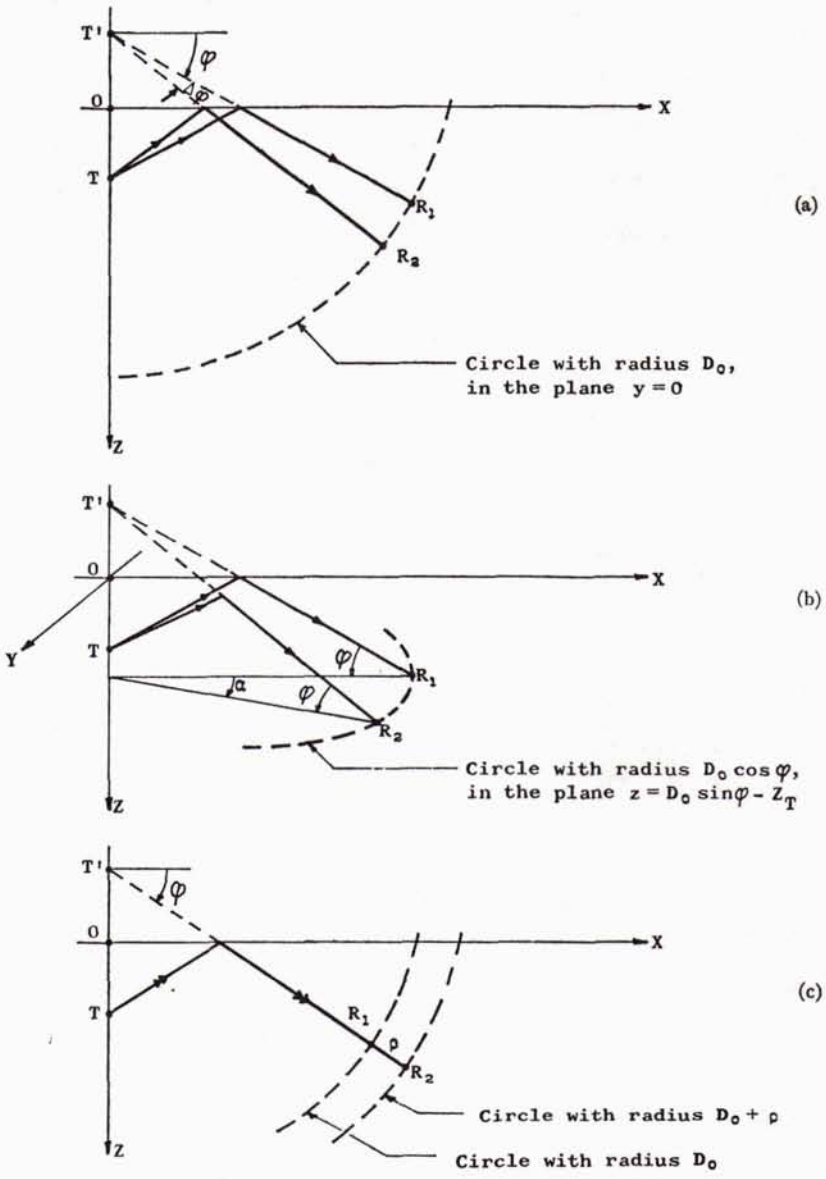


FIG. 9. Receiver positions for the spatial correlation of the scattered field: (a) receivers on an average wavefront in the plane $y=0$, (b) receivers on an average wavefront in the plane $z=$const, and (c) receivers in the direction of propagation.

of the surface waves $A^2(\omega_s)$,[19] so that

$$S(\Omega)=2\pi\exp(-\chi^2)[\delta(\Omega)+(\chi^2/4h^2)A^2(\Omega)]. \quad (50)$$

We are now ready to discuss the statistical properties of the output signal when a monochromatic signal of the type $\exp(-i\omega t)$ is applied to the input. The time-correlation function of such an output signal equals $B_T(\tau)\exp(-i\omega\tau)$. The spectral density function is hence obtained by a shift of $S(\Omega)$ over a frequency ω:

$$S_{\text{output}}(\Omega) = S_{\text{filter}}(\Omega-\omega) = 2\pi\exp(-\chi^2)[\delta(\Omega-\omega)+(\chi^2/4h^2)A^2(\Omega-\omega)]. \quad (51)$$

The delta pulse indicates the specular reflection: It is monochromatic and has the same frequency as the incident wave. Its importance decreases when the roughness is growing and at the same time the incoherent part becomes more pronounced. This incoherent part consists of two side bands. For a smooth surface they have the same shape as the surface-wave frequency spectrum. Experiments made by Roderick and Cron[20] confirm this. For a fully developed sea (Pierson–Moskowitz spectrum) the strongest surface-wave frequency equals $\omega_s=8.77\ g/v$, so that $f_D=14/v$ Hz is the most important Doppler frequency. Hence the Doppler spread amounts to only a few hertz, independent of ω.

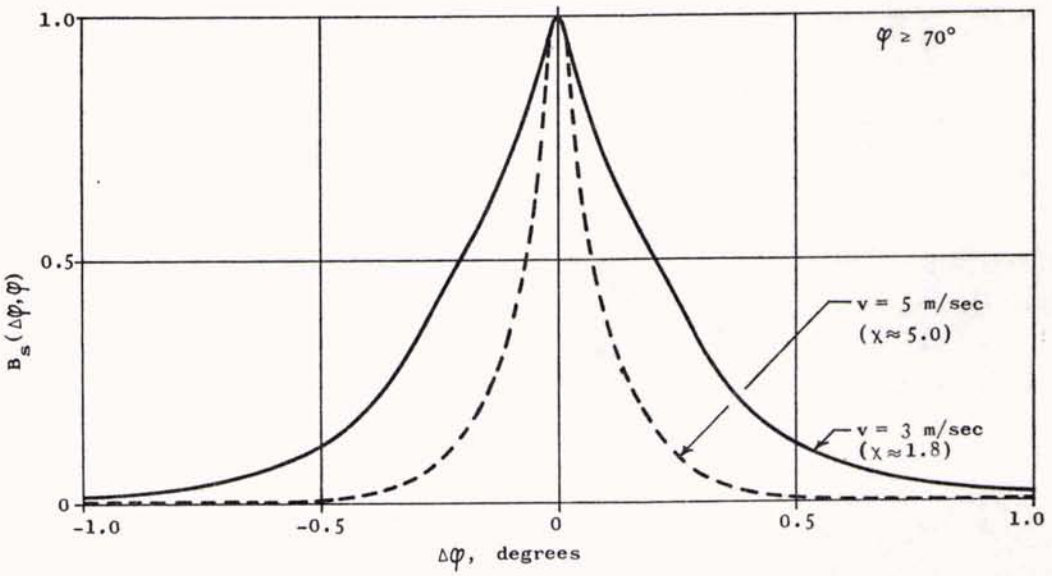


FIG. 10. The vertical transversal correlation function $B_S(\Delta\varphi,\varphi)$. The receivers are placed on an average wavefront, in the plane $y=0$, at positions given by the angles φ and $\varphi+\Delta\varphi$ [see Fig. 9(a)]; $Z_T=100$ m, $f=7.5$ kHz.

This makes the Doppler effect more important at lower incident frequencies.

4. *Spatial Correlation*

To study some aspects of the spatial correlation of the scattered field, we consider two receivers in three different relative positions: (a) on an average wavefront in the plane $Y=0$, (b) on an average wavefront in a plane $Z=$const, and (c) in the direction of propagation.

Figure 9 presents the three transmitter–receiver configurations and the pertinent parameters. Since the mean wind direction can be chosen arbitrarily, these geometries are perfectly general. They are, however, restricted by the Fraunhofer conditions.

Formulas for the spatial correlation functions are

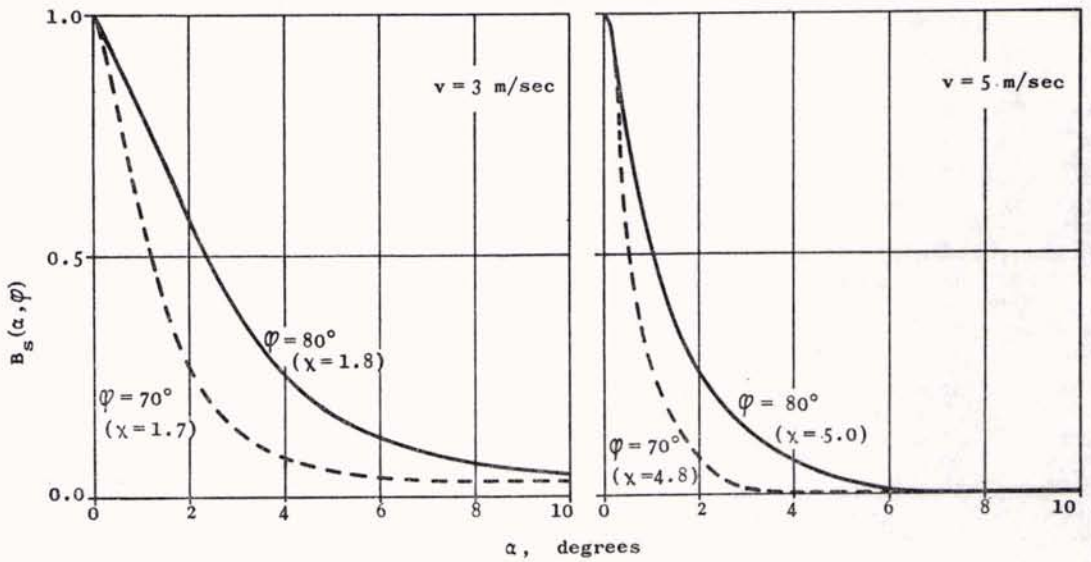


FIG. 11. The horizontal transversal correlation function $B_S(\alpha,\varphi)$. The receivers are placed on an average wavefront, in the plane $z=$const; their positions are determined by the angles φ and α [see Fig. 9(b)]; $Z_T=100$ m, $f=7.5$ kHz.

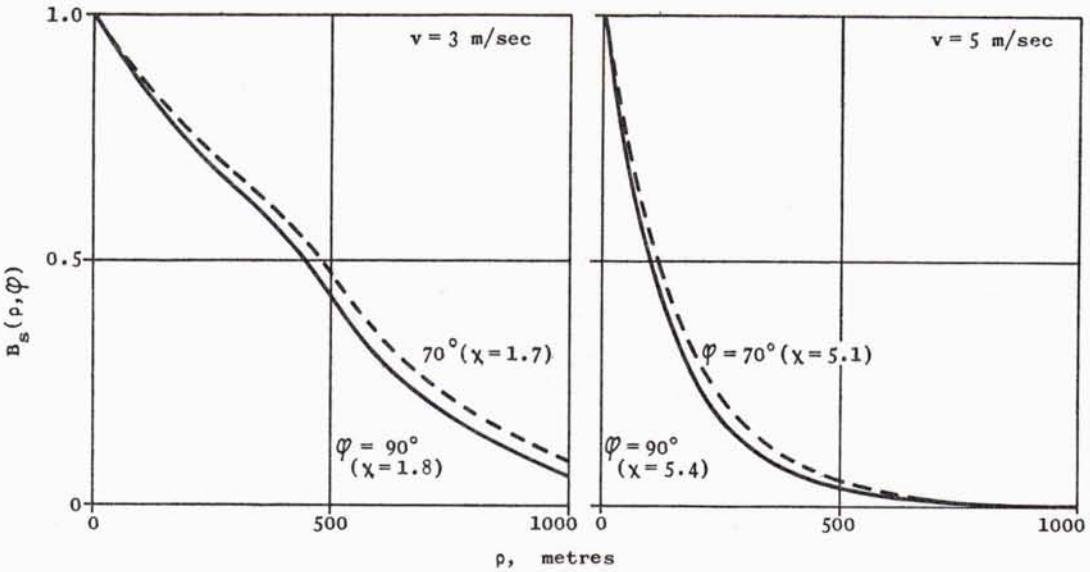


FIG. 12. The longitudinal correlation function $B_S(\rho,\varphi)$. The receivers are placed on a line in the direction of propagation; their positions are defined by φ and ρ [see Fig. 9(c)]; $Z_T=100$ m, $f=7.5$ kHz.

easily derived from Eq. 42. For a single incident frequency ω and equal observation times at both receivers, we get the following:

a. Vertical Transversal Correlation

$$B_S(\Delta\varphi,\varphi)=\exp\{-\tfrac{1}{2}\chi^2[1-2\gamma\Phi(\xi,0,0)+\gamma^2]\}, \quad (52)$$

where $\gamma=\sin(\varphi+\Delta\varphi)/\sin\varphi$ and $\xi=Z_T|\cot\varphi-\cot(\varphi+\Delta\varphi)|$, for small receiver spacings.

b. Horizontal Transversal Correlation

$$B_S(\alpha,\varphi)=\exp\{-\chi^2[1-\Phi(\xi,\eta,0)]\}, \quad (53)$$

with $\xi=Z_T|\cot\varphi\ (1-\cos\alpha)|$ and $\eta=Z_T|\cot\varphi\ \sin\alpha|$.

c. Longitudinal Correlation

$$B_S(\rho,\varphi)=\exp\{-\chi^2[1-\Phi(0,0,\tau)]\}, \quad (54)$$

where $\tau=\rho/c_0$.

For large values of $\Delta\varphi$, α, or ρ the influence of the surface correlation functions vanishes and the correlation functions tend to a constant. Only for small receiver spacings does Φ play a role.

Numerical examples are shown in Figs. 10–12, for an incident sound frequency of 7.5 kHz, a transmitter depth of 100 m, and wind speeds of 3 and 5 m/sec. The shape of the surface correlation function is hard to recognize in these results. In general, it can be said that an increasing roughness, either due to larger values of φ or of v, results in a decrease of the spatial correlation. However, in case b two effects are present when φ is growing: (1) the apparent roughness increases so that poorer correlation can be expected; (2) the specular points corresponding to a certain receiver spacing approach each other and the surface correlation function Φ therefore becomes more influential. Clearly in Fig. 11 the second effect is stronger than the first. In the limiting case $\varphi=90°$, the receivers coincide for any α, and $B_S=1$.

The longitudinal curves (Fig. 12) indicate that good correlation is maintained even at receiver distances of a few hundred meters, when $\chi<2$. This is due to the high sound speed.

III. SUMMARY

Underwater sound waves are randomly scattered and reflected by the sea surface. When the incident field is caused by a delta pulse, this boundary effect can be called the "impulse response of the sea surface." It is random and time variant.

An expression for the transfer function of the filter that can be thought to represent the sea surface has been derived using a generalized version of the Helmholtz diffraction integral. The normal derivative of the total field at the boundary—a random function required for the evaluation of the Helmholtz integral—has been approximated by means of a perturbation method. We have shown that for the upper boundary of the ocean it suffices to take the leading term of the perturbation series.

The resulting expression for the transfer function is rather complicated. It depends on the frequency of the incident wave, on the observation time, and on the geometry of source and receiver. Its validity is only

restricted by the assumptions that no subsurface layer of air bubbles is present, that source and receiver depth are large compared with the surface elevation, and that the bottom is infinitely far away.

For frequencies so high that the first few Fresnel zones are small compared with the surface facets, the formula indicates that specular reflection occurs at each surface point where the slope has the value required by geometrical optics.

For lower frequencies, in the domain of Fraunhofer diffraction, there exists only a virtual point of reflection: the specular point for the average surface. The effect of the random boundary is then a phase distortion of the specular reflection.

A detailed analysis of the statistical properties of the sea-surface transfer function is at present under way. Its results will be reported later. Some preliminary results are included, however, regarding mean value, and frequency, time and spatial correlation functions, for frequencies in the domain where the Fraunhofer approximation is valid.

ACKNOWLEDGMENT

Thanks are due to W. Wijmans for supplying Fig. 7.

[1] L. Fortuin, "A Survey of Literature on Reflection and Scattering of Sound Waves at the Sea Surface," SACLANT ASW Res. Centre, Tech. Rep. 138 (1969).

[2] L. Fortuin, "Survey of Literature on Reflection and Scattering of Sound Waves at the Sea Surface," J. Acoust. Soc. Amer. 47, 1209–1228 (1970).

[3] R. Laval *et al.*, "Coherence Problems in Underwater Acoustic Propagation," SACLANT ASW Res. Centre, Tech. Rep. 102 (1967).

[4] W. C. Meecham, "Fourier Transform Method for the Treatment of the Problem of the Reflection of Radiation from Irregular Surfaces," J. Acoust. Soc. Amer. 28, 370–377 (1956).

[5] T. Kailath, "Channel Characterization: Time-Variant Dispersive Channels," in *Lectures on Communication System Theory*, E. J. Baghdady, Ed. (McGraw-Hill, New York, 1961), Chap. 6, p. 100.

[6] P. M. Morse and H. Feshbach, *Methods of Theoretical Physics* (McGraw-Hill, New York, 1953), p. 806.

[7] B. B. Baker and E. T. Copson, *The Mathematical Theory of Huygen's Principle* (Clarendon, Oxford, England, 1953), Chap. 1, p. 23.

[8] For a perfectly flat surface we have $\partial p/\partial n = 2\partial p_0/\partial z$. In many studies this relation is also used for uneven surfaces; it is then known as the Kirchhoff approximation.

[9] It may be noted that P, not ϵ, is the perturbation parameter; ϵ is merely a label.

[10] Ref. 6, Chap. 7, pp. 820–823.

[11] L. M. Brekhovskikh, *Waves in Layered Media* (Academic, New York, 1960), Chap. 4, pp. 238–239.

[12] B. Kinsman, *Wind Waves, their Generation and Propagation on the Ocean Surface* (Prentice-Hall, Englewood Cliffs, N. J., 1965), p. 11.

[13] W. J. Pierson and L. Moskowitz, "A Proposed Spectral Form for Fully Developed Wind Seas Based on the Similarity Theory of S. A. Kitaigorodskii," J. Geophys. Res. 69, 5181–5190 (1964).

[14] J. G. De Boer, "On the Correlation Functions in Time and Space of Wind-Generated Ocean Waves," SACLANT ASW Res. Centre, Tech. Rep. 160 (1969).

[15] L. Fortuin and J. G. de Boer, "Spatial and Temporal Correlation of the Sea Surface," J. Acoust. Soc. Amer. 49, 1677–1679(L) (1971).

[16] Ref. 11, pp. 392–396.

[17] L. Fortuin, "Scattering and Reflection of Underwater Sound Waves from the Sea Surface. I. An Expression for the Scattered Field," SACLANT ASW Res. Centre, Tech. Rep. 181 (1970).

[18] B. E. Parkins, "Scattering from the Time-Varying Surface of the Ocean," J. Acoust. Soc. Amer. 42, 1262–1267 (1967).

[19] Ref. 12, pp. 340 and 376.

[20] W. I. Roderick and B. F. Cron, "Frequency Spectra of Forward-Scattered Sound from the Ocean Surface," J. Acoust. Soc. Amer. 48, 759–766 (1970).

5.3 Simplification of the formula for $H(\omega, t)$

5.3.1 The basic formula

We start our analysis with Section 5.2, Eq. (35). This equation gives an expression for the scattered field at the receiver that can be interpreted as the transfer function of the random filter we are studying. It may be written as:

$$H(\omega, t) = \iint \mathrm{d}\mathbf{R}_0 G_k(\mathscr{R}_R, \mathscr{R}_0^s) \Psi(\mathbf{R}_0), \tag{5.2}$$

where

$$\Psi(\mathbf{R}_0) = \frac{i}{8\pi^3} \iint \mathrm{d}\mathbf{K} K_z \exp(i\mathbf{K}\cdot\mathbf{R}_0) \iint \mathrm{d}\mathbf{R}_1 \exp(-i\mathbf{K}\cdot\mathbf{R}_1) G_k(\mathscr{R}_1^s, \mathscr{R}_T). \tag{5.3}$$

The first expression states that H can be obtained by a weighted summation of the effects of unit scatterers at the surface, the weighting function Ψ being given in (5.3). Physically, this weighting function is proportional to the normal derivative of the total field at the boundary. First we will concentrate our attention on this quantity.

5.3.2 The weighting function Ψ

In (5.3) appears the Green's function $G_k(\mathscr{R}_1^s, \mathscr{R}_T)$, which is the field that would be caused at the surface point $\mathscr{R}_1^s$, by a unit point source at $\mathscr{R}_T$ (i.e. by the transmitter), if the surface were absent. It represents a spherical wave and can be written as (see Section 5.2, Eq. (12)):

$$G_k(\mathscr{R}_1^s, \mathscr{R}_T) = \exp[ikw_T(\mathbf{R}_1)]/w_T(\mathbf{R}_1), \tag{5.4}$$

where

$$w_T(\mathbf{R}_1) = [R_1^2 + \{Z_T - \zeta(\mathbf{R}_1)\}^2]^{\frac{1}{2}}. \tag{5.5}$$

Substitution of (5.4) into (5.3), together with $\mathbf{R}_1 = \mathbf{R}_0 + \boldsymbol{\varrho}$ and $\mathbf{R}_0 = \mathbf{R}$, leads to

$$\Psi(\mathbf{R}) = \frac{i}{8\pi^3} \iint \mathrm{d}\mathbf{K} K_z \iint \mathrm{d}\boldsymbol{\varrho} \exp(-i\mathbf{K}\cdot\boldsymbol{\varrho} + ikw_T)/w_T. \tag{5.6}$$

It is impossible to continue the analysis without using approximate methods. We therefore apply a generalized version of the stationary phase method,[8] and find

$$\Psi(\mathbf{R}) = \frac{ik(Z_T - \zeta)\exp(ikw_T)}{2\pi w_T^2} \left\{1 + 2\frac{(x\zeta_x + y\zeta_y)}{Z_T - \zeta}\right\}^{\frac{1}{2}}, \tag{5.7}$$

with $w_T = w_T(\mathbf{R})$ being the distance between the transmitter and the surface point

[8] For the one-dimensional case this technique is described in [*5.4, pp. 752–753*]; the generalization to more dimensions is treated in [*5.5*].

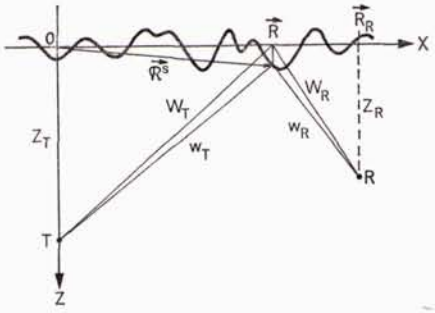


Fig. 5.1.
Distances from an arbitrary surface point to transmitter and receiver, and from its projection on the average surface $z = 0$.

$\mathscr{R}^s$ (see Fig. 5.1). Also ζ, ζ_x and ζ_y have to be evaluated at the point **R**. In the derivation of (5.7) we have used the inequalities $\zeta_x^2 \ll 1$ and $\zeta_y^2 \ll 1$, which follow from (3.23).

Details of the calculation can be found in Appendix B. There it is also shown that a better approximation, only subject to the condition

$$|\zeta(\mathbf{R})| \leqslant 0.01 Z_T, \tag{5.8}$$

can be obtained if in (5.7) the amplitude fluctuations outside the square root are neglected and only the phase fluctuations are retained. This simplifies the formula for Ψ into

$$\Psi(\mathbf{R}) = \frac{ikZ_T}{2\pi W_T^2} \exp(ikw_T) \sqrt{1+2\frac{(x\zeta_x + y\zeta_y)}{(Z_T - \zeta)}}, \tag{5.9}$$

where $W_T = (R^2 + Z_T^2)^{\frac{1}{2}}$.

The question of how good this approximation is, is difficult to answer because the exact solution is not known. The method of expanding Ψ in a series and estimating the error that is made when all the terms after the n^{th} are suppressed, offers no solution because of the complexity of the formula for Ψ. However, the analysis made in Appendix B indicates that (5.9) differs less than 20% from the exact solution for surface points inside an ellipse with semi-minor axis equal to 3.6 Z_T and semi-major axis 6.4 Z_T, the major axis of this ellipse being orientated perpendicular to the wind direction. It is also shown that Ψ is most significant inside this ellipse.

The condition (5.8) is easy to satisfy. For Z_T we will have a value of at least 100 m, so that $|\zeta|$ has to be smaller than 1 m. From (3.16) we see that for $v \leqslant 10$ m/s the standard deviation of ζ is given by $h \leqslant 0.368$ m, so that $3h \leqslant 1$ m. Since the probability that $|\zeta| \geqslant 3h$ is only 0.27%, the condition (5.8) cannot cause any problem.

5.3.3 The transfer function

With the foregoing results we return now to the transfer function. Using (5.9) in (5.2), and putting at the same time

$$G_k(\mathscr{R}_R, \mathscr{R}^s) = \exp(ikw_R)/w_R \tag{5.10}$$

with (see Fig. 5.1)

$$w_R = w_R(\mathbf{R}) = (|\mathbf{R}_R - \mathbf{R}|^2 + \{Z_R - \zeta(\mathbf{R})\}^2)^{\frac{1}{2}}, \tag{5.11}$$

the transfer function can be written as a surface integral:

$$H(\omega, t) = \frac{ikZ_T}{2\pi} \iint \mathrm{d}\mathbf{R} \frac{\exp[ik(w_T + w_R)]}{W_T^2 w_R} \left\{1 + 2\frac{(x\zeta_x + y\zeta_y)}{Z_T}\right\}^{\frac{1}{2}}. \tag{5.12}$$

The square root makes this somewhat difficult to handle. But for $R \leqslant 9\ Z_T$ this root can be expanded into a converging power series (see Appendix B). For H we have then

$$H = H_0 + H_1 + H_2 + \ldots \tag{5.13}$$

with

$$H_0(\omega, t) = \frac{ikZ_T}{2\pi} \iint \mathrm{d}\mathbf{R} \frac{\exp[ik(w_T + w_R)]}{W_T^2 w_R}, \tag{5.14}$$

$$H_1(\omega, t) = \frac{ik}{2\pi} \iint \mathrm{d}\mathbf{R} \frac{\exp[ik(w_T + w_R)]}{W_T^2 w_R} (x\zeta_x + y\zeta_y), \tag{5.15}$$

$$H_2(\omega, t) = -\frac{ik}{4\pi Z_T} \iint \mathrm{d}\mathbf{R} \frac{\exp[ik(w_T + w_R)]}{W_T^2 w_R} (x\zeta_x + y\zeta_y)^2, \tag{5.16}$$

etc.

The significant domain of integration lies inside the circle with radius $R \leqslant 9\ Z_T$. In that domain the power series expansion of $[1 + 2(x\zeta_x + y\zeta_y)/Z_T]^{\frac{1}{2}}$ is convergent. The function with which each term is multiplied, i.e. the integrand in (5.14), is smooth and has no singularities. Hence the series expansion of H is also convergent.

The physical interpretation of the expressions for H_0, H_1, H_2, etc. is very much the same as the one given in Section 5.2 for Eq. (7). Again we find that the transmitter induces elementary sources at the surface that reradiate the received energy omnidirectionally. For an arbitrary source on the boundary the distance to the transmitter equals w_T and the distance to the receiver is w_R, as is depicted in Fig. 5.1. Hence the phase delay at the surface amounts to kw_T and at the receiver it is $k(w_T + w_R)$. The weight of the sources for H_0 depends only on the surface elevation (via w_R), whereas for H_1, H_2, etc. the slopes are also involved.

5.4 Behaviour of H for high frequencies

5.4.1 Purpose of the analysis for high frequencies

For later use it will be convenient to have approximate versions of H_0, H_1 and H_2

that are valid when k is so large that the stationary phase method can be applied to solve the integrals in (5.14)–(5.16). As a side-issue that for the moment has only restricted value, we derive these approximations in this section, and discuss some of their properties.

5.4.2 The stationary phase method

Applying the stationary phase technique on the integrals for H_0, H_1 and H_2, we readily see that, for a surface with gentle slopes, there is only one point of stationary phase, namely the point of specular reflection. By "gentle slopes" we mean that ζ_x and ζ_y satisfy the following relations. For $X_R \approx 0$ their absolute values do not exceed the value α, for $X_R \geqslant 100$ m they are not larger than β and γ, where α, β, and γ are constants that depend on the geometry of transmitter and receiver:

$$\begin{aligned} \alpha &= 0.05(Z_T+Z_R)/Z_{T,R} \\ \beta &= 0.05\cos^2\theta_s X_R/Z_R \\ \gamma &= 0.15(Z_T+Z_R)^2/(X_R Z_{T,R}), \end{aligned} \tag{5.17}$$

and $Z_{T,R}$ being the larger of Z_T and Z_R. Details of the derivation of these conditions are collected in Appendix C. There it is also shown that the formulae for H_0, H_1, and H_2 reduce to

$$H_0(\omega, t) = -D_0^{-1}\exp(ikD_0 - i2k\cos\theta_s\zeta), \tag{5.18}$$

$$H_1(\omega, t) = \zeta_x \tan\theta_s H_0(\omega, t), \tag{5.19}$$

$$H_2(\omega, t) = -\tfrac{1}{2}\tan^2\theta_s\zeta_x^2 H_0(\omega, t), \tag{5.20}$$

when

$$2|\zeta_{x,y}|\tan\theta_s \leqslant 0.1 \tag{5.21}$$

and

$$|\zeta_{xx}|, |\zeta_{xy}|, |\zeta_{yy}| \ll \tfrac{1}{2}\cos^2\theta_s\left(\frac{1}{Z_T}+\frac{1}{Z_R}\right). \tag{5.22}$$

It should be remembered that in these equations the surface elevation and its derivatives have to be evaluated at the position $\mathbf{R}_s$ and at time t_s, as in Section 5.2, Eqs. (42) and (43). It is also worthwile noting that $H_0(\omega, t)$ is the same as $H(k, t)$ in those equations.

The foregoing results were derived under the condition that k is "sufficiently large". The frequency range in which (5.18)–(5.20) hold, could probably be established by an analysis of the stationary phase integration such as is described in [*5.6*]. But such an analysis will be very complicated, and since the formulae for H_0, H_1, and H_2 are only used here for comparison, we will not attempt such an investigation.

An indication about the degree of reliability of the stationary phase approximation can be obtained by letting $\zeta \to 0$ in (5.18)–(5.20): H_0 becomes

$$H_0(\omega, t) = -\exp(ikD_0)/D_0, \tag{5.23}$$

which is the *exact* solution for $\zeta = 0$, whereas all terms of higher order vanish.

5.4.2 *The convergence of the series expansion for H*

In Sub-Section 5.3.3 we found that the convergence of the series $H_0 + H_1 + H_2 + \ldots$ is guaranteed if $R \leqslant 9\ Z_T$. We can now give more significance to that statement because we have seen that the main contribution to H_0, H_1, H_2, etc. comes from the specular point. With that knowledge we can write that the convergence is guaranteed if $X_s \leqslant 9\ Z_T$, or $\tan\theta_s \leqslant 9$.

This result has only formal value. It states that the expansion (5.13) is convergent as long as $X_R \leqslant 9(Z_T + Z_R)$, but it does not indicate how many terms are needed to approximate H with a certain accuracy. However, the formulae for H_0, H_1, etc. are subject to condition (5.21), and if this condition is satisfied, we have automatically that

$$H_0 \gg H_1 \gg H_2 \gg \ldots \tag{5.24}$$

Hence H_0 is the leading term of a convergent series, and the higher order terms represent only corrections of relatively small importance, if $2|\zeta_{x,y}| \tan\theta_s \leqslant 0.1$.

5.4.3 *Significance of various conditions*

The results obtained in Section 5.4 are accompanied by four conditions on the slopes of the surface: in (5.17) the maximum acceptable values are given, and (5.21) requires the slope to be less than δ, where

$$\delta = 0.05/\tan\theta_s. \tag{5.25}$$

Furthermore, we have the condition on the slope quadrature ($\zeta_x^2 \ll 1$ and $\zeta_y^2 \ll 1$) that played a role in Section 5.2.

The slope of the sea surface is a random quantity with zero mean value and – for the Pierson-Moskowitz spectrum – with variances equal to 0.003 in down-wind and 0.001 in cross-wind direction. These values are three orders of magnitude smaller than one, so that the condition on the slope quadrature is amply satisfied.

The standard deviation of the slopes is at most about 0.05. In (5.17) we see that α is never smaller than 0.05, so that also the condition $|\zeta_{x,y}| \leqslant \alpha$ is observed.

The behaviour of β, γ and δ as functions of X_R and Z_R is more difficult to analyze. But we can easily see that

$$\gamma \geqslant 0.15/\tan\theta_s = 3\delta. \tag{5.26}$$

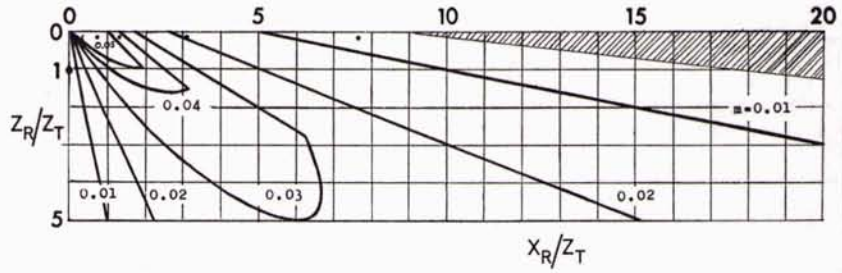


Fig. 5.2. Curves enclosing the areas in which both β and δ are larger than a given value m. (The dots indicate the receiver positions that are used in Tables 6.1 and 7.1).

Hence it is sufficient to require that the slopes are smaller than β and δ. Curves for constant β and δ can be plotted. For a certain value $\beta = \delta = m$, two curves are found that enclose a region where both β and δ are larger than m. In Fig. 5.2 such regions are indicated for several values of m. The curves in that picture can be used in two ways:

1. For a given geometry the value of m can be read; it is the smaller of β and δ, and our results are only valid if $|\zeta_{x,y}| \leqslant m$ for the chosen receiver position.
2. If the maximum value of the surface slopes is known, say equal to m_0, the area of receiver positions for which our formulae are valid can be found inside the curve for which $m = m_0$.

We note that in the second case the region of validity is decreasing when m goes up.

The condition (5.22) for the second derivatives of the surface elevation is less important than the one on the slopes, because it only affects the amplitude of H and not the convergence of the series expansion. From Appendix C it can be learned that H_0 will have a modulus

$$A' = A\left[1-2\left(\frac{Z_T Z_R}{Z_T+Z_R}\right)(\zeta_{xx}\cos^{-2}\theta_s+\zeta_{yy})+ \right.$$
$$\left. +4\left(\frac{Z_T Z_R}{Z_T+Z_R}\right)^2 \cos^{-2}\theta_s(\zeta_{xx}\zeta_{yy}-\zeta_{xy}^2)\right]^{-\frac{1}{4}}, \tag{5.27}$$

instead of $A = D_0^{-1}$, if (5.22) is not satisfied. Also the higher order terms have that factor, and so it does not influence our conclusions.

5.5 Justification of the use of the Helmholtz equation [9]

The wave equation in a medium with a time-dependent boundary

Leonard Fortuin
SACLANT ASW Research Centre, La Spezia, Italy
(Received 19 October 1972; revised 1 December 1972)

It is shown that the Helmholtz equation is not exactly correct for a medium with a time-dependent boundary. The equation can be used with very good approximation when the time-derivative of the surface elevation is much smaller than the speed of the waves through the medium. For underwater sound waves, reflected and scattered by an ocean surface that can be described by the Pierson–Moskowitz spectrum, this means that the wind speed has to be much less than the sound speed.

Subject Classification: 13.2, 13.4.

LIST OF SYMBOLS

A	amplitude
c_0	sound speed
h	standard deviation of surface elevation
i	$(-1)^{\frac{1}{2}}$
k	wavenumber of radiation
$\tilde{p}$	pressure (time dependent)
p	pressure (time independent)
p_b	pressure, due to the boundary
p_0	pressure in unbounded medium
$\mathbf{R}$	vector in horizontal plane
t	time
v	wind speed
γ_T, γ_R	direction cosines
ζ	surface profile
ρ_0	density
τ	time difference
Φ	correlation function of surface elevation
ω	angular frequency of incident wave
ω_s	frequency of surface wave

INTRODUCTION

The propagation of sound waves through the ocean is governed by a wave equation. In case of a monochromatic source this wave equation is usually written as[1]

$$(\nabla^2+k^2)p=0, \tag{1}$$

the so-called Helmholtz equation. This equation is exact when the boundaries of the medium in which the waves are propagating are independent of time. However, in case of a time-dependent boundary, such as the ocean surface, the Helmholtz equation can only be used when the boundary changes slowly enough. It is the purpose of this paper to derive a condition for the validity of Eq. 1 in that case. Also, the significance of the derived condition will be discussed.

I. THE CONDITION FOR THE VALIDITY OF THE HELMHOLTZ EQUATION

It is convenient to deal with the velocity potential $\tilde{U}$ rather than the sound pressure $\tilde{p}$. For sound waves of small amplitude these two quantities are related by the equation

$$\tilde{p}=\rho_0\partial\tilde{U}/\partial t. \tag{2}$$

The velocity potential satisfies the equation[2]

$$\nabla^2\tilde{U}=c_0^{-2}\partial^2\tilde{U}/\partial t^2. \tag{3}$$

Before treating the case of a time-dependent surface, we consider the "frozen" boundary for comparison.

A. The Time-Independent Surface

If the sound source is monochromatic, $\tilde{U}$ can be written as $\tilde{U}(t)=U\exp(i\omega t)$, where U is independent of time. We have then

$$\partial\tilde{U}/\partial t=i\omega\tilde{U}, \tag{4}$$

$$\partial^2\tilde{U}/\partial t^2=-\omega^2\tilde{U}, \tag{5}$$

and

$$\tilde{p}=i\omega\rho_0\tilde{U}, \tag{6}$$

so that Eq. 3 changes into

$$(\nabla^2+k^2)\tilde{U}=0. \tag{7}$$

Using Eq. 6 and dropping the time-factor $\exp(i\omega t)$, Eq. 1 is found without any approximation.

B. The Time-Variant Surface

The movement of the surface causes the sound field to depend on time in a more complicated way than in the foregoing case. To illustrate this we refer to the Doppler effect that is present in the scattered field, hence also in the total field $\tilde{p}$ and so in $\tilde{U}$. For this reason U is now a function of time.

[9] In the reprinted part it is wrongly stated that p represents a time-independent pressure. In reality, p is time-dependent, but does not include the harmonic factor $\exp(-i\omega t)$. Hence $\tilde{p}(t)=p(t)\exp(-i\omega t)$.

Consequently, instead of Eqs. 4 and 5 we find:

$$\partial\tilde{U}/\partial t=(i\omega U+\partial U/\partial t)\exp(i\omega t), \quad (8)$$

$$\partial^2\tilde{U}/\partial t^2=(-\omega^2U+i2\omega\partial U/\partial t+\partial^2U/\partial t^2)\exp(i\omega t), \quad (9)$$

and this result substituted into Eq. 3 does not produce Eq. 7. However, if the inequality

$$|\partial U/\partial t|\ll|\omega U| \quad (10)$$

is satisfied, Eqs. 8 and 9 may be replaced by Eqs. 4 and 5, and Eq. 7 does follow. So this is a sufficient condition for the validity of the Helmholtz equation in the case of a time-dependent boundary. In that case Eq. 6 also holds, so that the condition can be written as

$$|\partial p/\partial t|\ll|\omega p|. \quad (11)$$

It should be noted that p is the total sound field: $p=p_0+p_b$. As the incident field p_0 is independent of time, we get

$$|\partial p_b/\partial t|\ll\omega|p_0+p_b|, \quad (12)$$

where $\omega>0$.

If either $|p_0|\ll|p_b|$ or $|p_0|\gg|p_b|$, this condition is certainly satisfied when

$$|\partial p_b/\partial t|\ll\omega|p_b|. \quad (13)$$

But if $|p_0|$ and $|p_b|$ are of the same order of magnitude (as occurs close to the boundary), we have to observe the complete condition (Eq. 12) instead of the reduced condition (Eq. 13). The significance of both conditions is discussed in Sec. II.

II. SIGNIFICANCE OF THE CONDITIONS

A. The Reduced Condition

In Ref. 1 (Eq. 39) a formula is given for the scattered field that is derived from the Helmholtz equation. The time dependency is concentrated in the factor

$$F(t)\equiv\exp\{ik[\gamma_T\zeta(\mathbf{R}_1,t_1)+\gamma_R\zeta(\mathbf{R}_0,t_0)]\}, \quad (14)$$

where γ_T and γ_R are constants, smaller than or equal to 1. Replacing p_b by F in Eq. 13, we find the inequality

$$|\gamma_T\partial\zeta_1/\partial t_1+\gamma_R\partial\zeta_0/\partial t_0|\ll c_0. \quad (15)$$

This formula may be replaced by[3]

$$2|\partial\zeta/\partial t|\ll c_0, \quad (16)$$

as ζ is a stationary process and γ_T, $\gamma_R\leq1$. The left-hand side of this inequality is hard to deal with, because it is a random quantity. Therefore, we replace it by its mean value or its standard deviation. In both cases we find, for a sea-surface elevation that is Gaussian and that can be described by the Pierson–Moskowitz wave spectrum[4]

$$v\ll10c_0. \quad (17)$$

For realistic values of the windspeed, this condition is easily met. Details can be found in Appendix A.

B. The Complete Condition

For simplicity we take the Fraunhofer formula (Ref. 1, Eqs. 42 and 43) and find for a point close to the surface ($Z_R=\Delta z$):

$$p_b(t)=-\exp[ikD_0-i2k\cos\theta_s\zeta_s(t)]/D_0, \quad (18)$$

with $D_0=[X_R^2+(Z_T+\Delta z)^2]^{\frac{1}{2}}$. The direct wave for that same point is time-independent and given by

$$p_0=\exp(ikd)/d, \quad (19)$$

where $d=[X_R^2+(Z_T-\Delta z)^2]^{\frac{1}{2}}$. If now $\Delta z\ll Z_T$, we can put $D_0\approx d$ and

$$p_b(t)=-p_0\exp[-i2k\cos\theta_s\zeta_s(t)] \quad (20)$$

follows. This result into Eq. 12 yields

$$\sqrt{2}\cos\theta_s|\partial\zeta_s/\partial t|\ll c_0[1-\cos(2k\cos\theta_s\zeta_s)]^{\frac{1}{2}}. \quad (21)$$

Also this inequality has to be analyzed statistically. Using the mean-square criterium, plus some results of Appendix A, we obtain the condition

$$0.004v^2\ll c_0^2[1-\exp(-2k^2h^2\cos^2\theta_s)]. \quad (22)$$

Very low values of the windspeed (and consequently of h) need not be considered because the surface looses then its time dependency, and our problem disappears. Hence we assume that the quantity between square brackets in Eq. 22 has at least the value 10^{-5} (following from $k=1$, $v=1$ m/sec and $\cos\theta_s=0.6$). Then we find

$$v\ll0.05c_0\approx75\text{ m/sec}. \quad (23)$$

This condition is far more restrictive than the one found in the previous section, but still easy to satisfy.

III. SUMMARY

We have shown that for a medium with a time-dependent boundary the well-known Helmholtz equation holds only approximately. We have also derived a sufficient condition to which its use is subject: The time derivative of the surface elevation has to be much smaller than the speed at which the waves are propagating through the medium.

This condition has been analyzed statistically for the random sea surface. Using the Pierson–Moskowitz spectrum to describe the surface elevation, it is found that the wind speed has to be much smaller than the sound speed. This condition is very weak and easy to satisfy. Hence we conclude that it is permitted to use the Helmholtz equation in studies on sound scattering from the time-variant ocean surface.

ACKNOWLEDGMENT

Thanks are due to Prof. ir. E. W. Gröneveld (Technical University Twente, Enschede, The Netherlands) for pointing out the problem discussed in this paper.

APPENDIX A: MEAN VALUE AND VARIANCE OF $|\partial\zeta/\partial t|$

It is assumed that the sea-surface elevation ζ is a stationary process with Gaussian probability density. It can then be shown (Ref. 5, p. 147) that also the random process $\partial\zeta/\partial t$ is stationary and Gaussian. Its mean value equals zero, and its variance is given by

$$\sigma^2=\langle(\partial\zeta/\partial t)^2\rangle=-h^2\left[\frac{\partial^2}{\partial\tau^2}\Phi(0,0,\tau)\right]_{\tau\to 0}. \quad \text{(A1)}$$

The correlation function Φ can be expressed in terms of the surface-wave spectrum $A^2(\omega_s)$ (Ref. 6, p. 15):

$$\Phi(0,0,\tau)=(2h^2)^{-1}\int_0^\infty d\omega_s A^2(\omega_s)\cos(\omega_s\tau). \quad \text{(A2)}$$

Hence,

$$\sigma^2=\frac{1}{2}\int_0^\infty d\omega_s A^2(\omega_s)\omega_s^2. \quad \text{(A3)}$$

For A^2 we take the Pierson–Moskowitz spectrum (Ref. 4, p. 1679). The integral can then be solved analytically:

$$\sigma^2=0.002v^2. \quad \text{(A4)}$$

Next we turn to the random process $Q\equiv|\partial\zeta/\partial t|$. Its probability density follows from Ref. 7, pp. 130, 131:

$$f(Q)=2[\sigma(2\pi)^{\frac{1}{2}}]^{-1}\exp(-Q^2/2\sigma^2)U(Q), \quad \text{(A5)}$$

where U is the unit step function. Expected value and variance are readily obtained by integration:

$$\begin{aligned}E\{Q\}&=\sigma(2/\pi)^{\frac{1}{2}},\\ E\{Q^2\}&=\sigma^2.\end{aligned} \quad \text{(A6)}$$

Statistically, the condition $2Q\ll c_0$ means that we require

$$2\sigma\ll c_0. \quad \text{(A7)}$$

With Eq. A4 this yields

$$v\ll 5\sqrt{5}c_0\approx 10c_0. \quad \text{(A8)}$$

[1] L. Fortuin, "The Sea Surface as a Random Filter for Underwater Sound Waves," J. Acoust. Soc. Am. **52**, 302 (1972).

[2] B. B. Baker and E. T. Copson, *The Mathematical Theory of Huygen's Principle* (Clarendon, Oxford, England, 1953), p. 8.

[3] The same result follows if we substitute the Fraunhofer formula (Ref. 1, Eqs. 42 and 43) into Eq. 13.

[4] L. Fortuin and J. G. de Boer, "Spatial and Temporal Correlation of the Sea Surface," J. Acoust. Soc. Am. **49**, 1677 (1971).

[5] P. Beckmann, *Elements of Applied Probability Theory* (Harcourt, Brace, and World, New York, 1968).

[6] J. G. de Boer, "On the Correlation Functions in Time and Space of Wind-Generated Ocean Waves," Saclantcen Tech. Rep. 160 (15 Dec. 1969).

[7] A. Papoulis, *Probability, Random Variables, and Stochastic Processes* (McGraw-Hill, New York, 1965).

In the foregoing paper we have derived the condition under which the original differential equation

$$\nabla^2 \overline{U} = c_0^{-2} \partial^2 \overline{U} / \partial t^2 \tag{5.28}$$

is approximately equal to the Helmholtz equation

$$(\nabla^2 + k^2)\overline{U} = 0, \tag{5.29}$$

and we have stated that the use of (5.29) instead of (5.28) is justified if that condition is fulfilled. An important objection can be made against this reasoning: the fact that two differential equations are about equal does not at all mean that their solutions are very close. Indeed, a small perturbation in a differential equation may be integrated into a large disturbance of the original solution, so that the two solutions thus obtained are far apart.

A better justification has been found if we solve (5.29), and can show that this solution also satisfies (5.28). This will be done in the remaining part of this section.

In Section 5.2 we solved the Helmholtz equation for p, with the boundary condition $p = 0$. We found $p = p_0 + p_b$, where p_0 is the solution for a space without boundary:

$$p_0 = \exp(ikd)/d, \tag{5.30}$$

and p_b is the boundary effect:

$$p_b(\mathscr{R}_R, t) = \frac{i}{8\pi^3} \iint \mathrm{d}\mathbf{R}_0 \iint \mathrm{d}\mathbf{K} K_z \iint \mathrm{d}\mathbf{R}_1 \exp[i\mathbf{K}\cdot(\mathbf{R}_0 - \mathbf{R}_1)]$$
$$\times G_k(\mathscr{R}_1^s, \mathscr{R}_T) G_k(\mathscr{R}_R, \mathscr{R}_0^s). \tag{5.31}$$

In that analysis $\overline{U}$ and p were related via

$$\overline{U} = (i\omega\varrho_0)^{-1}(p_0 + p_b)\exp(-i\omega t). \tag{5.32}$$

Hence (5.29) is satisfied, if

$$\nabla^2 \bar{p}_0 = c_0^{-2} \partial^2 \bar{p}_0 / \partial t^2, \tag{5.33}$$

$$\nabla^2 \bar{p}_b = c_0^{-2} \partial^2 \bar{p}_b / \partial t^2. \tag{5.34}$$

The differential equation for $\bar{p}_0$ is easily checked: $\nabla^2 \bar{p}_0$ is equal to $-k^2 \bar{p}_0$, and the time dependency of $\bar{p}_0$ is only present in the factor $\exp(-i\omega t)$, so that $\partial^2 \bar{p}_0 / \partial t^2 = -\omega^2 \bar{p}_0$. This shows that for $\bar{p}_0$, (5.29) and (5.28) are identical.

For p_b the situation is more complicated. For $\nabla^2 \bar{p}_b$ we need to differentiate with

respect to X_R, Y_R and Z_R (because $\mathscr{R}_R$ is the point at which we check the solution) and this dependency is only present in $G_k(\mathscr{R}_R, \mathscr{R}_0^s)$. The time dependency of $\bar{p}_b$ is contained in both Green's functions:

$$G_k(\mathscr{R}_1^s, \mathscr{R}_T) G_k(\mathscr{R}_R, \mathscr{R}_0^s) \approx$$
$$\approx G_k(\mathbf{R}_1, \mathscr{R}_T) G_k(\mathscr{R}_R, \mathbf{R}_0) \exp\left[-ik \left\{ \frac{Z_T}{W_T} \zeta(\mathbf{R}_1, t_1) + \frac{Z_R}{W_R} \zeta(\mathbf{R}_0, t_0) \right\} \right], \quad (5.35)$$

with $t_0 = t - W_R/c_0$ and $t_1 = t_0 - |\mathbf{R}_1 - \mathbf{R}_0|/c_0$, and in the factor $\exp(-i\omega t)$. The approximation made in (5.35) is based on *Assumption 11*.

Turning now to the differential equation for $\bar{p}_b$ in (5.34) and assuming that in (5.31) the order of differentiation and integration can be exchanged, it is sufficient to demonstrate that

$$G_k(\mathscr{R}_1^s, \mathscr{R}_T) \exp(-i\omega t) \nabla^2 G_k(\mathscr{R}_R, \mathscr{R}_0^s) =$$
$$= c_0^{-2} \frac{\partial^2}{\partial t^2} \{ G_k(\mathscr{R}_1^s, \mathscr{R}_T) G_k(\mathscr{R}_R, \mathscr{R}_0) \exp(-i\omega t) \}. \quad (5.36)$$

The left hand side is easy to calculate: we find $-k^2 G_{k,T} G_{k,R} \exp(-i\omega t)$. For the right hand side we employ (5.35) and obtain

$$c_0^{-2} \frac{\partial^2}{\partial t^2} \{ G_{k,T} G_{k,R} \exp(-i\omega t) \} = -k^2 G_{k,T} G_{k,R} \exp(-i\omega t)$$
$$\times \left\{ \left[1 + c_0^{-1} \left(\frac{Z_T}{W_T} \zeta_{t1} + \frac{Z_R}{W_R} \zeta_{t0} \right) \right]^2 + \frac{i}{\omega c_0} \left(\frac{Z_T}{W_T} \zeta_{tt1} + \frac{Z_R}{W_R} \zeta_{tt0} \right) \right\}. \quad (5.37)$$

Therefore (5.36) is true if

$$\left| \frac{Z_T}{W_T} \zeta_{t1} + \frac{Z_R}{W_R} \zeta_{t0} \right| \ll c_0, \quad (5.38)$$

and

$$\left| \frac{Z_T}{W_T} \zeta_{tt1} + \frac{Z_R}{W_R} \zeta_{tt0} \right| \ll \omega c_0. \quad (5.39)$$

Condition (5.38) is the same as Eq. (15) of the first part of this section. It is true, for the Pierson-Moskowitz spectrum, if $v \ll 10\ c_0$. Hence (5.38) is always amply satisfied. Condition (5.39) can be replaced by

$$2|\zeta_{tt}| \ll \omega c_0. \quad (5.40)$$

In Chapter 3 we found $<\zeta_{tt}^2> = 0.4$ for the Pierson-Moskowitz spectrum. Therefore (5.39) is well fulfilled if $\omega \geqslant 0.1$ radian/sec.

Finally, collecting results, we arrive at the conclusion that the use of the Helmholtz equation is justified in studies that involve the time-variant sea surface, because such a boundary changes slowly enough with time.

5.6 Summary

Starting from the Helmholtz equation with boundary condition of zero total pressure, an expression for $H(\omega, t)$ has been derived. It is a six-fold integral that can be reduced to a convergent series of surface integrals, when the surface slopes are gentle enough ($|\zeta_{x,y}| \leqslant \frac{1}{2} \operatorname{cotan} \theta$). These surface integrals are examined for high frequencies. The first one is shown to be a good approximation for the whole series, if the first and second derivatives of the surface elevation do not exceed certain limits that depend on the geometry of transmitter and receiver. This approximation of zero order reduces to the exact solution when $\zeta \to 0$. For $\zeta \neq 0$, it can be improved by addition of the corrective terms H_1 and H_2. Further improvement is possible, at least in principle, by adding more terms, but the algebra will become quite formidable.

References

5.1 B. B. Baker and E. T. Copson, *The Mathematical Theory of Huygens' Principle* (Clarendon Press, Oxford, 1953).

5.2 L. Fortuin, "The Sea Surface as a Random Filter for Underwater Sound Waves", J. Acoust. Soc. Amer. **52**, 302–315 (1972).

5.3 L. Fortuin, "The wave equation in a medium with a time-dependent boundary", J. Acoust. Soc. Amer. **53**, 1683–1685 (1973).

5.4 M. Born and E. Wolf, *Principles of Optics* (Pergamon Press, Oxford, 1970).

5.5 L. Fortuin, "Scattering and Reflection of Underwater Sound Waves from the Sea Surface. I. An Expression for the Scattered Field", Saclant asw Research Centre, Tech. Rep. 181 (1970).

5.6 D. S. Jones and M. Kline, "Asymptotic Expansion of Multiple-Integrals and the Method of Stationary Phase", J. Math. & Phys. **37**, 1–28 (1958).

6

the deterministic part of the filter



CHAPTER 6

THE DETERMINISTIC PART OF THE FILTER

6.1 Introduction

After the derivation, in Chapter 5, of an expression for one of the system functions of the random filter, we are ready to embark on a statistical study. The first step, the determination of the filter's fixed part, will be made in this chapter.

This fixed part, also called *deterministic* or *coherent* part, is represented (see Section 4.4) by the mean value of a system function. We have chosen the transfer function H for this purpose. Its deterministic part is called H_d.

Further simplification of the formula for H is possible, starting from the one derived in Chapter 5. This is shown in Section 6.2. The calculation of H_d is treated in Section 6.3; some remarks about absorption are made in Section 6.4.

6.2 Further simplification of H

Starting point for the present analysis is the approximation

$$H \approx H_0 + H_1, \tag{6.1}$$

with H_0 and H_1 given as surface integrals, in (5.14) and (5.15). This truncation of the series for H is justified, at least in the upper part of the frequency domain, when (see (5.18)–(5.20))

$$|\zeta_x| \leqslant 0.5/\tan\theta_s. \tag{6.2}$$

For $|\zeta_x| \leqslant 0.05$ (Pierson-Moskowitz spectrum), this means $\tan\theta_s \leqslant 10$ or $\theta_s \leqslant 84°$. It allows for any geometry of transmitter and receiver, as long as the grazing angle is larger than 6°.

Examination of (5.15) reveals that the mean value of H_1 equals zero, since $<\zeta_x> = <\zeta_y> = 0$. Hence, as at present we are only interested in the mean value of H, we may write

$$H(\omega, t) = H_0(\omega, t)$$

$$= \frac{ikZ_T}{2\pi} \iint \mathrm{d}\mathbf{R} \frac{\exp\left[ik(w_T + w_R)\right]}{W_T^2 w_R}. \tag{6.3}$$

The distances w_T and w_R depend on the surface elevation $\zeta(\mathbf{R})$. This can be seen in (5.5) and (5.11). The dependency can be expressed more conveniently if we use the following approximations (see Fig. 5.1):

$$w_T = W_T - (Z_T/W_T)\zeta,$$
$$w_R = W_R - (Z_R/W_R)\zeta. \tag{6.4}$$

They are valid with an error less than 1%, because Z_T and Z_R are much larger than ζ (*Assumption 11*).

In the argument of the integrand it is important to conserve the random process ζ, but in the modulus we can go one step further and put $w_R \approx W_R$. Therefore $H(\omega, t)$ may be written as

$$H(\omega, t) = \frac{ikZ_T}{2\pi} \iint d\mathbf{R} \frac{\exp[ikD - ik\gamma\zeta(\mathbf{R}, t')]}{W_T^2 W_R}, \tag{6.5}$$

where

$$D = D(\mathbf{R}) = W_T + W_R,$$
$$\gamma = \gamma(\mathbf{R}) = Z_T/W_T + Z_R/W_R, \tag{6.6}$$
$$t' = t'(\mathbf{R}) = t - W_R/c_0.$$

The surface elevation has to be evaluated at time $t' < t$, in order to take into account the travel time required in going from the surface to the receiver.

6.3 Calculation H_d

In (6.5) the random character of H is represented by the phase term $-ik\gamma\zeta$. Consequently, H_d, the mean value of H, involves the characteristic function [*6.1, p. 153*] of $\zeta(\mathbf{R}, t')$. This process is stationary and Gaussian (*Assumptions 3 and 4*), with zero expectation and variance h^2, so that its characteristic function equals $\exp(-\frac{1}{2}k^2h^2\gamma^2)$. Thus we find from (6.5):

$$H_d(\omega) = \frac{ikZ_T}{2\pi} \iint d\mathbf{R} \frac{\exp(ikD - \frac{1}{2}k^2h^2\gamma^2)}{W_T^2 W_R}. \tag{6.7}$$

This integral will be evaluated numerically. But before doing so, it is useful to consider the outcome when the stationary phase method is applied. This technique produces a simple result:

$$H_d(\omega) = -\exp(ikD_0 - 2k^2h^2\cos^2\theta_s)/D_0, \tag{6.8}$$

which equals the mean of H_0 as given in (5.18). Formula (6.8) is interesting, but of little use – as long as it is unclear for which frequencies it holds.

The integrand in (6.7) is a complex function; this makes the integral less suitable for numerical calculations. For this reason we compute the Fourier transform of H_d,

that is the impulse response function $h_d(\tau)$. Using (4.2), together with [*6.2, Vol. 1, p. 15(11) and p. 73(19)*], we get

$$h_d(\tau) = -Z_T c_0^{-1} (2\pi)^{-\frac{1}{2}} \iint \mathrm{d}\mathbf{R} \frac{(\tau' - \tau)}{b^3 W_T^2 W_R} \exp\left[-\frac{(\tau' - \tau)^2}{2b^2}\right]. \tag{6.9}$$

Two new functions of **R** appear in this formula:

$$\begin{aligned} b(\mathbf{R}) &= h\gamma(\mathbf{R})/c_0, \\ \tau'(\mathbf{R}) &= D(\mathbf{R})/c_0. \end{aligned} \tag{6.10}$$

Table 6.1 Transmitter-receiver configurations and wind speeds, used for the numerical calculation of H_d.

	v in m/s			
X_R in m	1	2	5	10
0	case 01	case 02	case 03	case 04
100	11	12	13	14
200	21	22	23	24
500	31	32	33	34
1000	41	42	43	44
2000	51	52	53	54
5000	61	62	63	64

$Z_T = 650$ m, $Z_R = 100$ m.

The numerical calculation of h_d with (6.9) and (6.10) produces an interesting result: for all cases listed in Table 6.1 the numerical value of h_d does not differ significantly from the stationary phase approximation, i.e. from the Fourier transform of (6.8). This signifies that we have, with good approximation,

$$h_d(\tau) = -(b_s D_0 \sqrt{2\pi})^{-1} \exp\left[-\tfrac{1}{2}\left(\frac{\tau - \tau_s}{b_s}\right)^2\right], \tag{6.11}$$

where b_s and τ_s are the values of b and τ' at the specular point[10]:

$$\begin{aligned} b_s &= 2h \cos\theta_s / c_0, \\ \tau_s &= D_0 / c_0. \end{aligned} \tag{6.12}$$

An illustration is presented in Fig. 6.1, where we have plotted h_d, given by (6.11), together with the results of numerical integration for all cases, on normalized scales.

[10] Some authors (e.g. McDonald and Spindel [*6.3, p. 750*]) call b_s the "Rayleigh parameter". Usually this name is given to the quantity $\omega b_s = 2\,kh \cos\theta_s$ (Beckmann and Spizzichino [*6.4, p. 10*], Horton and Melton [6.5, *p. 300*], Venetsanopoulos and Tuteur [6.6, *p. 1102*]). Then it is identical to our *roughness* parameter χ.

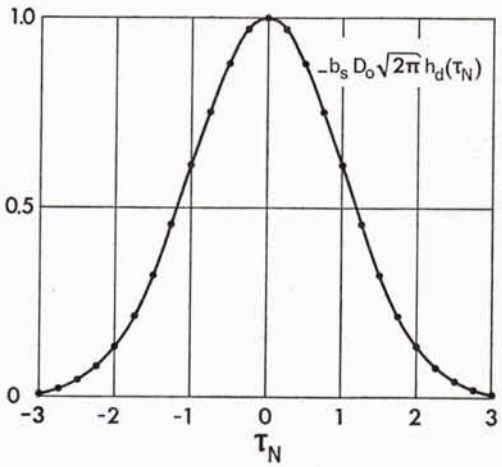


Fig. 6.1.
The impulse response function of the fixed part of the filter, on normalized scales: ——— stationary phase approximation (6.11), • numerical integration (6.9); $\tau_N = (\tau-\tau_s)/b_s$.

The foregoing results also mean that (6.8), although derived for high frequencies, can be used for all frequencies from 0 to ∞. Hence we arrive at an important and very useful conclusion: for the deterministic part of the filter, the stationary phase approximation can be used in the whole frequency domain, if we limit ourselves to moderate wind speeds ($v \leqslant 10$ m/s) and grazing angles ($\varphi \geqslant 8.5°$). In terms of the roughness parameter $\chi = 2kh \cos\theta_s$ (see Section 5.2, Eq. (44)) we have hence:

$$H_d(\omega) = -D_0^{-1} \exp(ikD_0 - \tfrac{1}{2}\chi^2). \tag{6.13}$$

It would be interesting to compare this result with an analysis of (6.7) by means of an extended stationary phase integration technique, for instance the one developed by JONES and KLINE [*6.7*]. The question whether discrepancies at low frequencies have been smeared out by the Fourier transformation could then also be answered. But as such an analysis is very complicated, it will not be attempted here.

Finally we elaborate on the meaning of (6.11): the deterministic part of the filter delays a unit delta pulse and changes it into a pulse with a Gaussian shape. The delay is proportional to the specular path length, the width of the pulse depends linearly on the cosine of the specular angle of incidence and on the variance of the surface elevation, whereas the pulse height is inversely proportional to that variance.

6.4 Absorption

Up to this point we have neglected the absorption in the medium. This phenomenon, which can become important enough to be taken into account in practice, can be built into our model by series connection of an absorption filter. This has been discussed in Chapter 1.

Such an absorption filter is time-independent and has the transfer function

$$H_a(\omega) = \exp(-\omega^2 L C_a), \tag{6.14}$$

with $C_a = 4.5 \times 10^{-13}$ dB/m (at a temperature of 20° C) and L the travelled distance, in meters. Thus by incorporating the absorption, the complete formula for H_d becomes:

$$H_d(\omega) = -D_0^{-1} \exp(ikD_0 - \tfrac{1}{2}\chi^2 - D_0 C_a \omega^2). \tag{6.15}$$

Its Fourier transform is easily obtained and differs from (6.11) only in one respect: b_s has to be replaced by b'_s, where

$$b'_s = (b_s^2 + 2D_0 C_a)^{\frac{1}{2}}. \tag{6.16}$$

Table 6.2 Values for b_s, b'_s and b'_s/b_s for the wind speeds and the transmitter-receiver configurations of Table 6.1.

	v in m/s			
X_R in m	1	2	5	10
0	$4.899_{10}-06$[1]	$1.960_{10}-05$	$1.225_{10}-04$	$4.899_{10}-04$
	$2.644_{10}-05$[2]	$3.254_{10}-05$	$1.252_{10}-04$	$4.906_{10}-04$
	$5.397_{10}+00$[3]	$1.661_{10}+00$	$1.022_{10}+00$	$1.001_{10}+00$
100	$4.856_{10}-06$	$1.942_{10}-05$	$1.214_{10}-04$	$4.856_{10}-04$
	$2.654_{10}-05$	$3.253_{10}-05$	$1.242_{10}-04$	$4.863_{10}-04$
	$5.466_{10}+00$	$1.675_{10}+00$	$1.023_{10}+00$	$1.001_{10}+00$
200	$4.734_{10}-06$	$1.893_{10}-05$	$1.183_{10}-04$	$4.734_{10}-04$
	$2.685_{10}-05$	$3.251_{10}-05$	$1.213_{10}-04$	$4.741_{10}-04$
	$5.673_{10}+00$	$1.717_{10}+00$	$1.025_{10}+00$	$1.002_{10}+00$
500	$4.076_{10}-06$	$1.630_{10}-05$	$1.019_{10}-04$	$4.076_{10}-04$
	$2.877_{10}-05$	$3.282_{10}-05$	$1.058_{10}-04$	$4.086_{10}-04$
	$7.059_{10}+00$	$2.013_{10}+00$	$1.038_{10}+00$	$1.002_{10}+00$
1000	$2.939_{10}-06$	$1.176_{10}-05$	$7.348_{10}-05$	$2.939_{10}-04$
	$3.367_{10}-05$	$3.554_{10}-05$	$8.078_{10}-05$	$2.958_{10}-04$
	$1.145_{10}+01$	$3.023_{10}+00$	$1.099_{10}+00$	$1.006_{10}+00$
2000	$1.720_{10}-06$	$6.881_{10}-06$	$4.300_{10}-05$	$1.720_{10}-04$
	$4.388_{10}-05$	$4.438_{10}-05$	$6.141_{10}-05$	$1.775_{10}-04$
	$2.551_{10}+01$	$6.450_{10}+00$	$1.428_{10}+00$	$1.032_{10}+00$
5000	$7.267_{10}-07$	$2.907_{10}-06$	$1.817_{10}-05$	$7.267_{10}-05$
	$6.746_{10}-05$	$6.752_{10}-05$	$6.986_{10}-05$	$9.915_{10}-05$
	$9.283_{10}+01$	$2.323_{10}+01$	$3.845_{10}+00$	$1.364_{10}+00$

[1] $b_s = 2h\cos\theta_s/c_0$; [2] $b'_s = (b_s^2 + 2D_0C_a)^{\frac{1}{2}}$; [3] b'_s/b_s.

Both b_s and b_s' are functions of wind speed and geometry. In Table 6.2 we have listed the values they assume for the cases of Table 6.1, and also their ratio b_s'/b_s. It can be seen that the absorption becomes influential for the longer ranges ($X_R \geqslant 1000$ m) and the lower windspeeds ($v \leqslant 2$ m/s).

6.5 Summary

The fixed part, or mean value, of the transfer function has been investigated in this chapter by considering the surface integrals derived in Chapter 5. The first one (H_0), integrated numerically after the mean value of the integrand has been calculated, produces the same result as the stationary phase integration, for wind speeds less than 10 m/sec and a grazing angle larger than 8.5°. The second one (H_1) is identically zero due to the statistical properties of the sea surface, the third and higher order terms produce results that are negligable compared with $< H_0 >$ for $\varphi \geqslant 6°$. Hence an important result is found: for many realistic combinations of geometry and wind speed, the deterministic part of the filter can be described with good approximation by the formula that follows from the stationary phase integration (i.e. the specular point formula).

References

6.1 A. PAPOULIS, *Probability, Random Variables and Stochastic Processes* (McGraw-Hill, New York, 1965).

6.2 A. ERDÉLYI, Ed., *Tables of Integral Transforms* (McGraw-Hill, New York, 1954).

6.3 J. F. MCDONALD and R. C. SPINDEL, "Implication of Fresnel Corrections in a Non-Gaussian Surface Scatter Channel", J. Acoust. Soc. Amer. **50**, 746–757 (1971).

6.4 P. BECKMANN and A. SPIZZICHINO, *The Scattering of Electromagnetic Waves from Rough Surfaces* (Macmillan, New York, 1963).

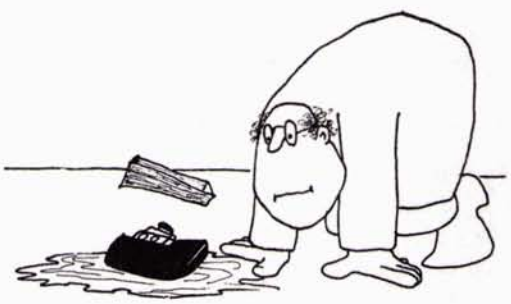
6.5 C. W. HORTON, Sr. and D. R. MELTON, "Importance of the Fresnel Correction in Scattering from a Rough Surface. II. Scattering Coefficient", J. Acoust. Soc. Amer. **47**, 299–303 (1970).

6.6 A. N. VENETSANOPOULOS and F. B. TUTEUR, "Stochastic Filter Modeling for the Sea-Surface Scattering Channel", J. Acoust. Soc. Amer. **49**, 1100–1107 (1971).

6.7 D. S. JONES and M. KLINE, "Asymptotic Expansion of Multiple-Integrals and the Method of Stationary Phase", J. Math. & Phys. **37**, 1–28 (1958).

7

the random part of the filter



CHAPTER 7

THE RANDOM PART OF THE FILTER

7.1 Introduction

The second step in the statistical analysis of the filter regards its random part. It is defined, as has been pointed out in Chapter 4, as that portion of the filter that remains after the fixed part has been removed. Again any system function could be used to describe it, and once more we have chosen the transfer function, that is H_r, in order to be consistent with the foregoing chapters.

A formula for H_r is derived in Section 7.2; its average value equals zero (as a consequence of the way in which H_r has been defined), its variance is considered in Section 7.3. For the evaluation of this variance, numerical integrations are required. Results are presented in Section 7.4. Conclusions about the best way to approximate H_r can then be drawn, which is the subject of Section 7.5.

7.2 Derivation of a formula for H_r

A definition of H_r follows readily from (4.17):

$$H_r(\omega, t) = H(\omega, t) - H_d(\omega, t). \tag{7.1}$$

In Chapter 5 it was found that in practical cases H_0 is a very good first approximation of H, whereas in Chapter 6 we have shown that H_d is time-independent. Thus we can write

$$H_r(\omega, t) = H_0(\omega, t) - H_d(\omega), \tag{7.2}$$

bearing in mind that improvement might be obtained by addition of H_1, H_2, etc. Expressions for H_0 and H_d have been derived in the previous chapter. Applying (6.5) and (6.8) to (7.2), we find

$$H_r(\omega, t) = \frac{ikZ_T}{2\pi} \iint \mathrm{d}\mathbf{R} \frac{\exp\left[ikD - ik\gamma\zeta(\mathbf{R}, t')\right]}{W_T^2 W_R} + \exp\left(ikD_0 - 2k^2h^2\cos^2\theta_s\right)/D_0. \tag{7.3}$$

If the stationary phase approximation is used, this simplifies into

$$H_r(\omega, t) = -\frac{\exp(ikD_0)}{D_0}\left\{\exp\left[-i2k\cos\theta_s\zeta(\mathbf{R}_s, t_s)\right] - \exp\left(-2k^2h^2\cos^2\theta_s\right)\right\}, \tag{7.4}$$

with $t_s = t - Z_R\tau_s/(Z_T + Z_R)$ and $\tau_s = D_0/c_0$.

7.3 The variance of H_r

Using the fact that $\zeta(\mathbf{R}, t')$ is Gaussian and stationary (*Assumptions 3 and 4*), we derive easily from (7.3)

$$< |H_r(\omega,t)|^2 > = \left(\frac{kZ_T}{2\pi}\right)^2 \iint \frac{d\mathbf{R}_1}{(W_T^2 W_R)_1} \iint \frac{d\mathbf{R}_2}{(W_T^2 W_R)_2} \exp[ik(D_1 - D_2)] \times$$
$$\times \exp[-\tfrac{1}{2}k^2h^2\{\gamma_1^2 - 2\gamma_1\gamma_2\Phi(\mathbf{R}_2 - \mathbf{R}_1, t_2' - t_1') + \gamma_2^2\}] +$$
$$- \exp(-4k^2h^2\cos^2\theta_s)/D_0^2, \tag{7.5}$$

where the subscripts 1 and 2 refer to $\mathbf{R}_1$ and $\mathbf{R}_2$, respectively.

The integrations over $\mathbf{R}_1$ and $\mathbf{R}_2$ are coupled via the surface correlation function Φ. If Φ were equal to zero, the coupling would disappear and the double surface integral would be cancelled by the second term; the variance would then vanish. This property can be used to simplify the expression for the variance.

If we use the indentity

$$\exp(k^2h^2\gamma_1\gamma_2\Phi_{12}) \equiv 1 + [\exp(k^2h^2\gamma_1\gamma_2\Phi_{12}) - 1] \tag{7.6}$$

in (7.5), we get

$$< |H_r(\omega,t)|^2 > = \left(\frac{kZ_T}{2\pi}\right)^2 \iint \frac{d\mathbf{R}_1}{(W_T^2 W_R)_1} \iint \frac{d\mathbf{R}_2}{(W_T^2 W_R)_2} \exp[ik(D_1 - D_2)] \times$$
$$\times \{\exp[-\tfrac{1}{2}k^2h^2(\gamma_1^2 - 2\gamma_1\gamma_2\Phi_{12} + \gamma_2^2)] - \exp[-\tfrac{1}{2}k^2h^2(\gamma_1^2 + \gamma_2^2)]\}. \tag{7.7}$$

In this expression it is easy to see that the integrand tends to zero, when $\mathbf{R}_1$ and $\mathbf{R}_2$ are so far apart that Φ vanishes. Hence, if we introduce centre-of-mass-coordinates and relative coordinates:

$$\begin{array}{l|l} \mathbf{R}_1 = \mathbf{R} - \tfrac{1}{2}\boldsymbol{\varrho} & \mathbf{R} = \tfrac{1}{2}(\mathbf{R}_1 + \mathbf{R}_2) \\ \mathbf{R}_2 = \mathbf{R} + \tfrac{1}{2}\boldsymbol{\varrho} & \boldsymbol{\varrho} = \mathbf{R}_2 - \mathbf{R}_1 \end{array} \tag{7.8}$$

we find an integral over $\boldsymbol{\varrho}$ that has as integration domain the area S_ϱ around the origin in which $\Phi \neq 0$. We now suppose S_ϱ to be so small that: (1) $t_2' - t_1' \sim 0$ for any $\boldsymbol{\varrho}$ inside this area, (2) D_1 and D_2 may be replaced by a Taylor expansion up to the first order term, around the point $\mathbf{R}$, as follows,

$$\begin{aligned} D_1 &\approx D - \tfrac{1}{2}(\xi D_x + \eta D_y) \\ D_2 &\approx D + \tfrac{1}{2}(\xi D_x + \eta D_y), \end{aligned} \tag{7.9}$$

and (3) W_T and W_R can be replaced by their values at **R**. These approximations are correct with an error not larger than 2%, if

$$\begin{aligned} &|x\xi_{\max}+y\eta_{\max}| \leqslant 0.2W_T^2(\mathbf{R}), \\ &|(X_R-x)\xi_{\max}-y\eta_{\max}| \leqslant 0.2W_R^2(\mathbf{R}). \end{aligned} \tag{7.10}$$

Replacing $\xi_{\max}$ and $\eta_{\max}$ by the effective correlation distances, this yields for the most representative surface point $\mathbf{R}=\mathbf{R}_s$,

$$L_{dw}, L_{cw} \leqslant 0.4Z_{T,R}, \tag{7.11}$$

in which $Z_{T,R}$ is the smaller of Z_T and Z_R.

In (3.21) and (3.22) we have the effective correlation distances for the Pierson-Moskowitz spectrum. Using those values in (7.11), together with a minimum of 100 m for $Z_{T,R}$, the condition turns out to be equivalent to $v^2 \leqslant 160$ m^2/s^2, or $v \leqslant 12.6$ m/s. This condition is always observed, because v will be at most 10 m/s.

Returning now to (7.7) we see that the time-dependency disappears, and we get

$$\begin{aligned} <|H_r(\omega,t)|^2> = \left(\frac{kZ_T}{2\pi}\right)^2 \iint \frac{d\mathbf{R}}{(W_T^2W_R)^2} \iint_{S_\varrho} d\varrho \exp[ik(D_x\xi+D_y\eta)] \times \\ \times (\exp[-k^2h^2\gamma^2\{1-\Phi(\varrho,0)\}]-\exp(-k^2h^2\gamma^2)). \end{aligned} \tag{7.12}$$

In this formula we need to substitute $\Phi(\varrho, 0)$, the spatial correlation function of the surface elevation. The results of Chapter 3 could be used in full detail, but both surface integrals would then have to be evaluated numerically. Rather then undertaking this formidable task (for a rigorous examination the geometry, the sound frequency, the wind speed and its direction would have to be varied, and for each combination of these parameters a four-fold integration would have to be performed), we seek to do the integration over ϱ analytically. To this end we approximate $\Phi(\varrho, 0)$ in the following way:

$$\begin{aligned} \Phi(\xi,\eta,0) &= 1 \quad \text{for} \quad |\xi| \leqslant L_{dw} \quad \text{and} \quad |\eta| \leqslant L_{cw}, \\ &= 0 \quad \text{otherwise}, \end{aligned} \tag{7.13}$$

the effective correlation distances L_{dw} and L_{cw} being given in (3.21) and (3.22). It may seem from (7.13) that we are restricting ourselves to a wind blowing along the X-axis, but the cross-wind case follows by exchanging L_{dw} and L_{cw}. Next integrating over ϱ, we obtain a relatively simple answer:

$$\begin{aligned} <|H_r(\omega,t)|^2> = \left(\frac{kZ_T}{\pi}\right)^2 L_{dw}L_{cw} \iint \frac{d\mathbf{R}}{W_T^4W_R^2} \times \\ \times \{1-\exp(-k^2h^2\gamma^2)\} \operatorname{sinc}(kD_xL_{dw}) \operatorname{sinc}(kD_yL_{cw}). \end{aligned} \tag{7.14}$$

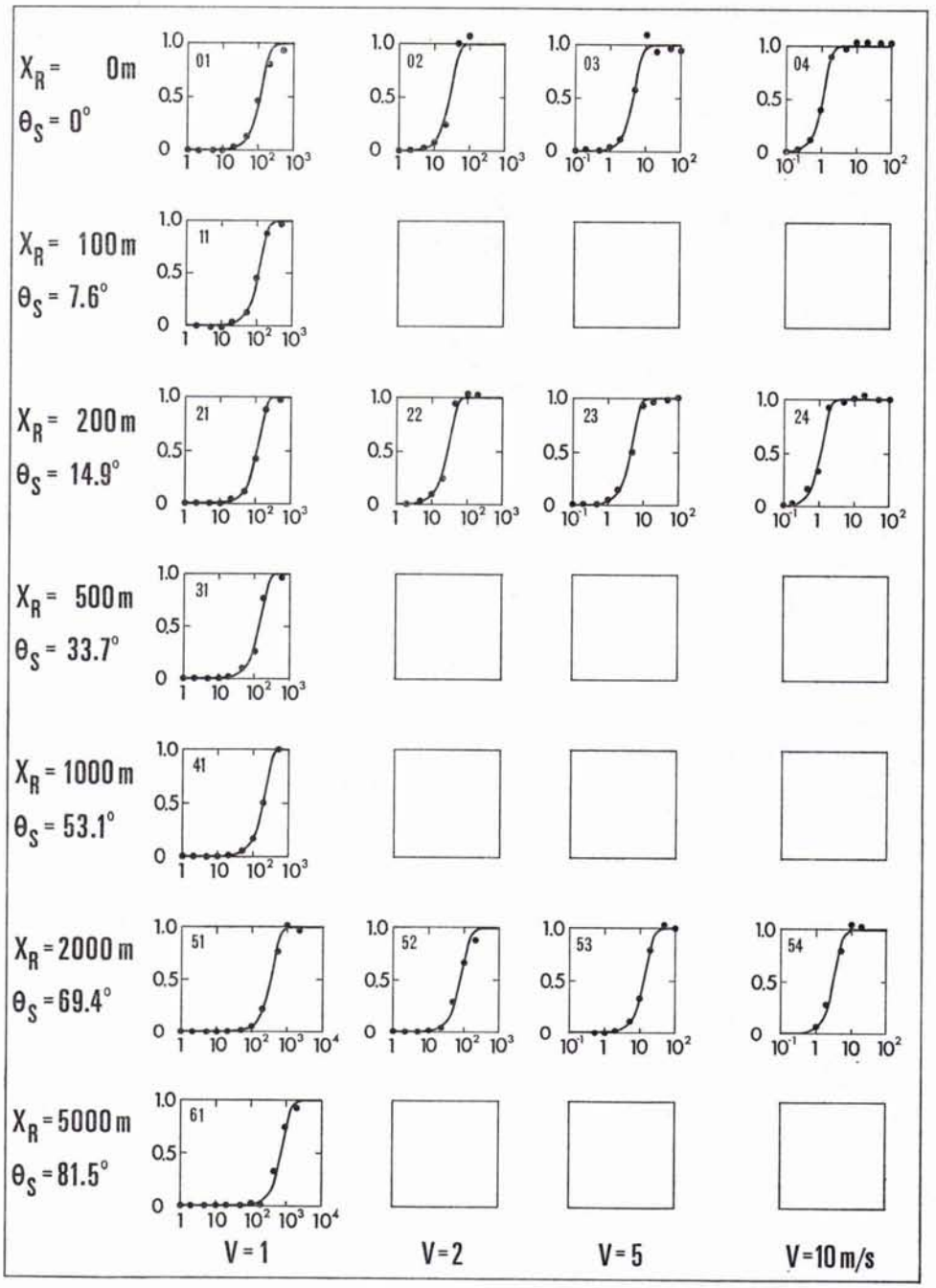


Fig. 7.1. The variance of H_r (normalized) versus k, for 16 combinations of wind speed and geometry of transmitter and receiver; ——— stationary phase approximation (7.15), • numerical integration (7.14); $Z_T = 650$ m, $Z_R = 100$ m.

In this formula sinc (x) is a shorthand notation for $\sin(x)/x$ [*7.1, p. 23*].

The corresponding stationary phase approximation follows from (7.4):

$$< |H_r(\omega, t)|^2 > = D_0^{-2}\{1 - \exp(-4k^2h^2\cos^2\theta_s)\}. \tag{7.15}$$

With the roughness parameter $\chi = 2kh\cos\theta_s$ (see Section 5.2, Eq. (44)), this can be written as

$$< |H_r(\omega, t)|^2 > = D_0^{-2}\{1 - \exp(-\chi^2)\}. \tag{7.16}$$

7.4 Numerical results

In (7.14) we see that the variance of H_r is not only a function of frequency, but it depends also on wind speed (via h, L_{dw} and L_{cw}) and on the geometry (via Z_T, Z_R and X_R). For a numerical integration, actual values have to be chosen for these parameters. Several combinations have been analyzed, namely the cases of Table 7.1. The computer results are plotted in Fig. 7.1, together with the pertinent stationary phase curves, derived from (7.15). The vertical scale has been normalized by multiplication with D_0^2.

Table 7.1 Transmitter-receiver configurations and wind speeds, used for the numerical calculation of the variance of H_r.

	v in m/s			
X_R in m	1	2	5	10
0	case 01	case 02	case 03	case 04
100	11			
200	21	22	23	24
500	31			
1000	41			
2000	51	52	53	54
5000	61			

$Z_T = 650$ m, $Z_R = 100$ m.

Another way of presenting these results is shown in Fig. 7.2. There the roughness parameter χ is used as the independent variable, and the curve is described by (7.16). Both figures show an important property of the variance of H_r: in practical cases it can be represented satisfactorily by the stationary phase approximation (7.15), over the whole frequency range from 0 to ∞.

The physical meaning of Fig. 7.2 is interesting and simple to see:

1. For $\chi < 0.1$ the variance of H_r is practically zero, and as also its average equals zero, the random part has no influence on the characteristics of the filter. In other words: the filter is entirely *coherent*, with a transfer function given by (6.13), and there is only specular reflection.

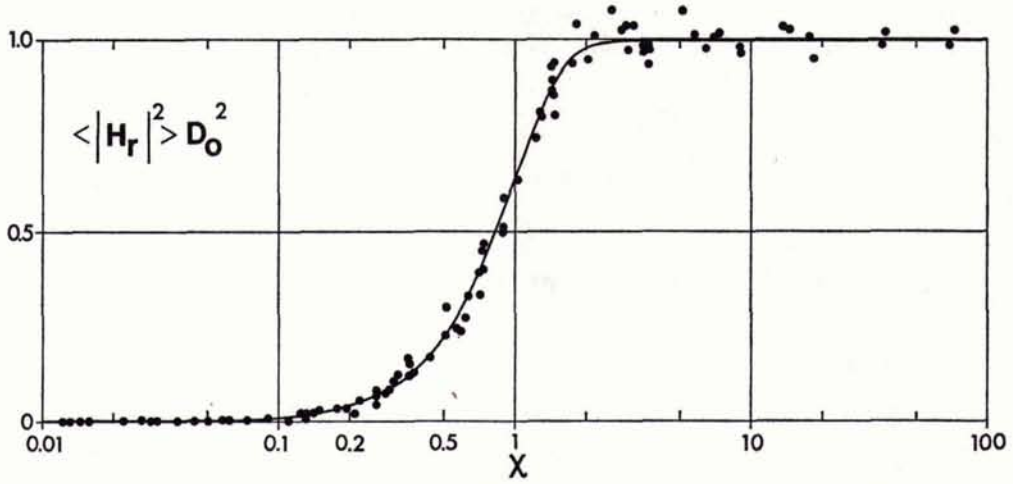


Fig. 7.2. The variance of H_r (normalized) as function of the roughness parameter $\chi = 2kh \cos \theta_s$.

2. For $\chi > 2$ the deterministic part has vanished (see (6.13)) and the filter is totally *incoherent*. No specular reflection occurs, there is only random scattering.
3. In the intermediate region $0.1 < \chi < 2$, both the deterministic and the random part play a role, and there is specular reflection as well as random scattering.

7.5 Approximation of H_r and H

In the preceding section we reached the conclusion that the stationary phase approximation is useful to describe the variance of H_r, over the whole frequency range from 0 to ∞. Compared with the correlation functions of H_r in time, frequency and space, this variance is merely a special case: it is the value of the correlation functions for equal frequencies, equal times, coinciding receivers and coinciding transmitters.

It seems reasonable to suppose that the stationary phase approximation maintains its validity when correlation in frequency, time and space is considered (*Assumption 12*). Accepting this supposition, we can take (7.4) as the starting point for the calculation of the correlation functions of H_r and consequently of H. As for the latter one, with the foregoing supposition the formula for the transfer function of the random filter as a whole becomes very simple. Taking (7.4) and adding H_d as given in (6.13), we get

$$H(\omega, t) = -D_0^{-1} \exp\left[ikD_0 - i2k \cos \theta_s \zeta(\mathbf{R}_s, t_s)\right]. \tag{7.17}$$

As this approximation depends only on the random surface at the specular point, we call it the *specular point approximation*. Formula (7.17) will be used for the analysis of time, frequency, and space correlation of the scattered field, in the following

chapters. When necessary, we will multiply H by H_a as given in (1.1) to take the absorption of the medium into account. The incorporation of the absorption has an important consequence: it guarantees the existence of the Fourier transform with respect to ω. During the analysis in the ω-domain, however, we will often meet cases in which $\omega^2 D_0 C_a$ is very small, because C_a has such a low value ($\sim 4.5 \times 10^{-13}$ dB/m). We can then simply use (7.17).

7.6 Summary

In this chapter the variance of the transfer function, describing the random part of the filter, has been examined. Numerical integration produced a result similar to that found for the mean value: for many practical combinations of wind speed and geometry, the variance of H can be presented satisfactorily by the specular point formula.

These results for mean value and variance have been generalized into the assumption that also the correlation functions of H in time, frequency, and space can be described by a specular point formula (*Assumption 12*). In this way a simple expression has been obtained as the starting point for the calculation of these functions.

References

7.1 P. Beckmann and A. Spizzichino, *The Scattering of Electromagnetic Waves from Rough Surfaces* (Macmillan, New York, 1963).

8

time and frequency correlation



CHAPTER 8

TIME AND FREQUENCY CORRELATION

8.1 Introduction

As a result of the foregoing chapters, we have found that in practical cases the filter can – with good approximation – be described by:

$$H(\omega, t) = -D_0^{-1} \exp\left[ikD_0 - i2k\cos\theta_s \zeta(\mathbf{R}_s, t_s)\right],$$
$$t_s = t - \left(\frac{Z_R}{Z_T + Z_R}\right)\frac{D_0}{c_0}. \tag{8.1}$$

This represents a random function of time and frequency. The random character is contained in the function ζ; the statistical properties of this Gaussian process were discussed in Chapter 3. For very large distances H has to be multiplied by H_a, the absorption function (see Sub-Section 1.2.2); H_a can also be invoked at high frequencies to guarantee the existence of Fourier transforms (see Section 7.5).

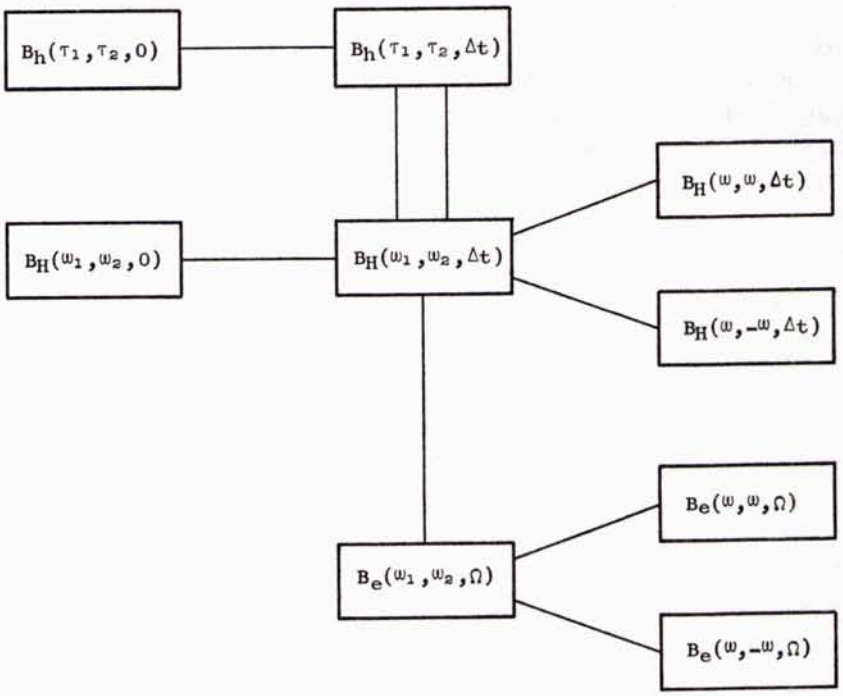


Fig. 8.1. Some system correlation functions and their special versions.

As ζ is stationary in time, the time correlation of H depends only on the time difference Δt and not on the actual times. Hence the diagram of Fig. 4.6 is applicable for the calculation of the various system correlation functions.

In the analysis of output signals (Chapter 10) not all correlation functions are needed: it turns out that B_H, B_e and B_h are sufficient. These are treated successively in Sections 8.2, 8.3 and 8.4.

Often, in practical cases, we consider either the correlation in time or the correlation in frequency, at the same time keeping the other variables constant or even equal. The correlation functions reduce then to special versions. Figure 8.1 gives a summary of the functions that will be examined; their formula can be found in the corresponding sections.

8.2 Correlation of the transfer function

8.2.1 A general expression for B_H

In its most general form the correlation function of H is given by

$$B_H(\omega_1, \omega_2, \Delta t) = < H(\omega_1, t-\Delta t)H^*(\omega_2, t) > \\ = D_0^{-2} \exp\left[-\tfrac{1}{2}\{\chi_1^2 - 2\chi_1\chi_2\Phi(0, \Delta t) + \chi_2^2\} + i(\omega_1 - \omega_2)\tau_s\right]. \quad (8.2)$$

The argument of this complex function depends linearly on the frequency difference, the modulus can be characterized as a Gaussian "hat". The maximum value, equal to D_0^{-2}, is reached at the origin of the $\chi_1\chi_2$-coordinate system; the contours are concentric ellipses orientated along the diagonal $\chi_1 = \chi_2$. Their properties depend strongly on Φ: for $\Phi = 1$ the semi-major axes tend to infinity, for $\Phi = 0$ the ellipses reduce to circles. A few examples are drawn in Fig. 8.2. For $\Phi = 1$ the correlation function depends apparently only on the frequency difference. This is further discussed in Sub-Section 8.2.4.

8.2.2 Equal frequencies

By taking equal frequencies in (8.2) we find that the time-correlation function of H can be written as[11]

$$B_H(\omega, \omega, \Delta t_N) = D_0^{-2} \exp\left[-\chi^2\{1 - \Phi(0, \Delta t_N)\}\right]. \quad (8.3)$$

This is a function of χ that tends to the value D_0^{-2} for $\chi \leqslant 0.1$. For $\Delta t_N \to \infty$ it reaches the value $D_0^{-2} \exp(-\chi^2)$, a constant that represents the fixed part of the filter.

---

[11] The time difference has been normalized, in accordance with Chapter 3; thus: $\Delta t_N = (g/v)\Delta t$.

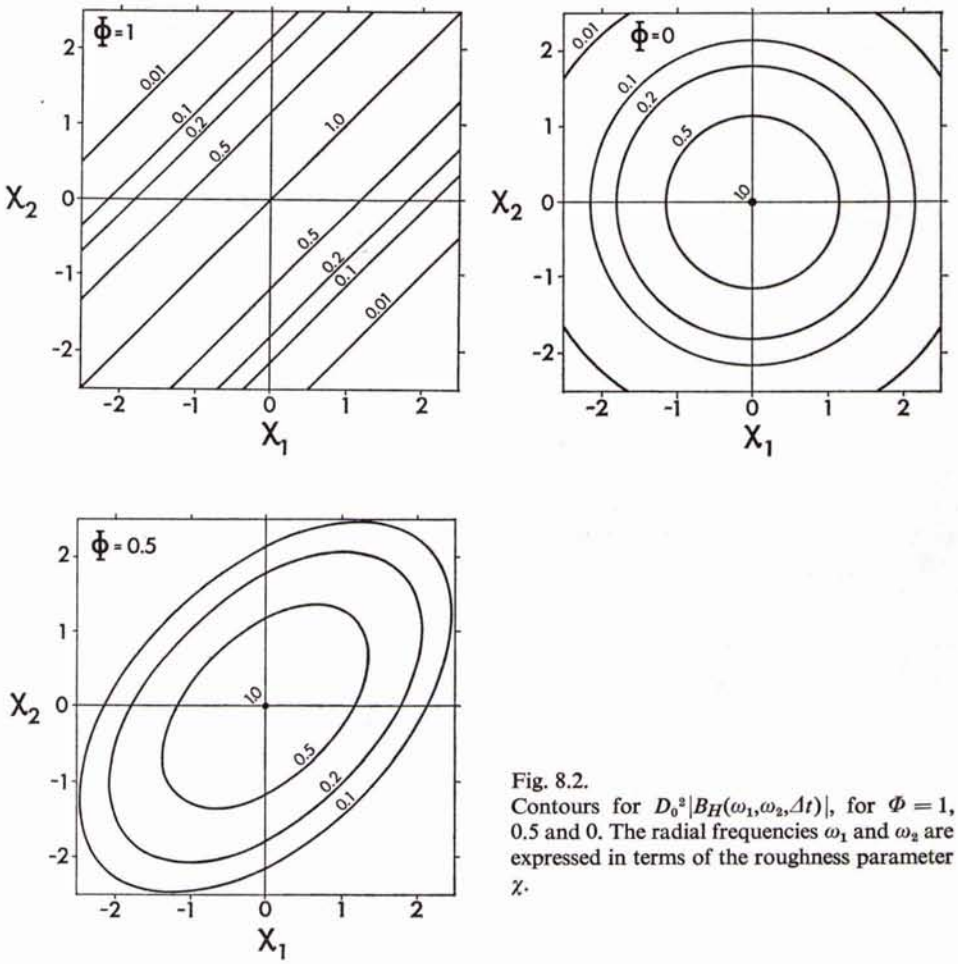


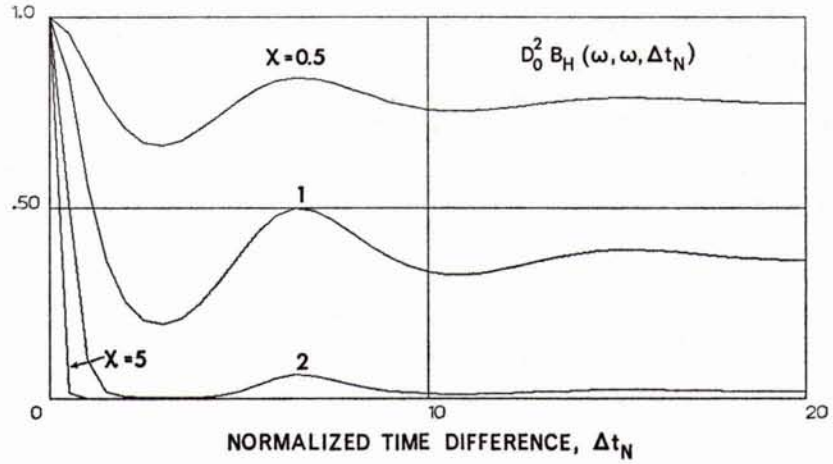
Fig. 8.2.
Contours for $D_0^{-2}|B_H(\omega_1,\omega_2,\Delta t)|$, for $\Phi = 1$, 0.5 and 0. The radial frequencies ω_1 and ω_2 are expressed in terms of the roughness parameter χ.

When χ is small enough, a useful simplification of (8.3) can be obtained by power series expansion of the exponential function; we get

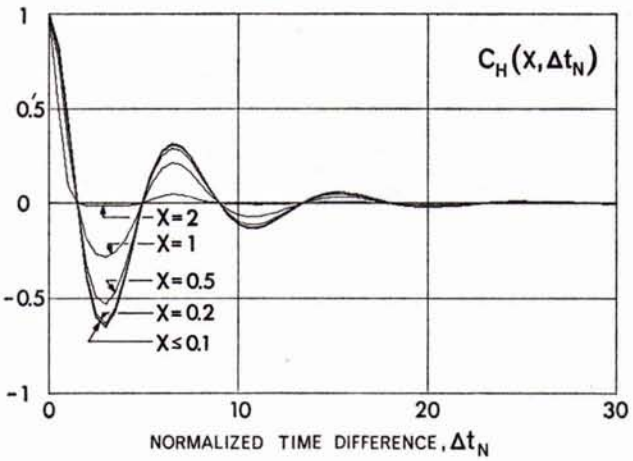
$$B_H(\omega, \omega, \Delta t_N) = D_0^{-2}[1+\chi^2\Phi(0, \Delta t_N)], \quad \text{if} \quad \chi \leqslant 0.2. \tag{8.4}$$

The first term inside the square brackets represents the fixed part of the filter, the second stands for the random part. The time-correlation function of H_r is apparently proportional to the time-correlation function of the surface elevation, for χ less than 0.2.

In Fig. 8.3-A the function $B_H(\omega, \omega, \Delta t_N)$ is plotted for some values of χ, after multiplication by D_0^2. The constant value to which B_H tends for large Δt_N reflects the influence of the fixed part of the filter. The true time correlation can be observed



(A)



(B)

Fig. 8.3. (A) The time-correlation function of $H(\omega,t)$ for equal frequencies on a normalized time scale ($\Delta t_N = g\Delta t/v$) with χ as parameter; (B) the normalized time-correlation function of $H_r(\omega,t)$, with the inverse of the variance of H_r as normalizing factor.

better if we subtract this effect and normalize the curves. This is done by defining a new correlation function:

$$C_H(\chi, \Delta t_N) = \frac{D_0^2 B_H(\omega, \omega, \Delta t_N) - \exp(-\chi^2)}{1 - \exp(-\chi^2)}. \tag{8.5}$$

This is the normalized correlation function of H_r, and it assumes the value 1 for $\Delta t_N = 0$ and any value of χ. Curves for various values of χ are drawn in Fig. 8.3-B.

The normalizing factor is the inverse of the variance of H_r. Its value can be obtained from Fig. 7.2. An interesting result follows for small χ:

$$C_H(\chi, \Delta t_N) = \Phi(0, \Delta t_N), \quad \text{if} \quad \chi \leqslant 0.2. \tag{8.6}$$

8.2.3 Zero time difference

In (8.2) we put $\Delta t = 0$, i.e. $\Phi = 1$, and get

$$B_H(\omega_1, \omega_2, 0) = D_0^{-2} \exp\left[-\tfrac{1}{2}(\chi_1 - \chi_2)^2 + i(\omega_1 - \omega_2)\tau_s\right]. \tag{8.7}$$

This depends only on the *difference* between ω_1 and ω_2, so that the contours of $|B_H|$ in a $\chi_1\chi_2$-plane are straight lines (see Fig. 8.2).

The dependency on the frequency difference only has an important consequence: $B_h(\tau_1, \tau_2, 0)$, the double Fourier transform of $B_H(\omega_1, \omega_2, 0)$, will contain a delta function (see Sub-Section 8.4).

8.3 The function $B_e(\omega, \omega, \Omega)$

According to Fig. 4.6, we can find $B_e(\omega, \omega, \Omega)$ by taking the Fourier transform of (8.3) or (8.4) with respect to Δt_N. In general, this cannot be done analytically, but using the Fast Fourier Transform technique on the numerical values of Fig. 8.3-A we readily obtain a digital representation of $B_e(\omega, \omega, \Omega_N)$. This function, depicted[12] in Fig. 8.4, together with the normalized version $C_e(\chi, \Omega_N)$, characterizes the frequency spread in the channel. The normalizing factor is again the inverse of the variance of H_r.

The special case $\chi \leqslant 0.2$ is interesting, because an analytic expression for B_e can then be found by application of some results of Chapter 3. First we write the Fourier transform of (8.4) as a cosine transform; this is possible because $\Phi(0, \Delta t_N)$ is even. Using then (3.10) we find

$$B_e(\omega, \omega, \Omega_N) = D_0^{-2}[\delta(\Omega_N) + \chi^2 h^{-2} A^2(\Omega_N)] \qquad (\chi \leqslant 0.2), \tag{8.8}$$

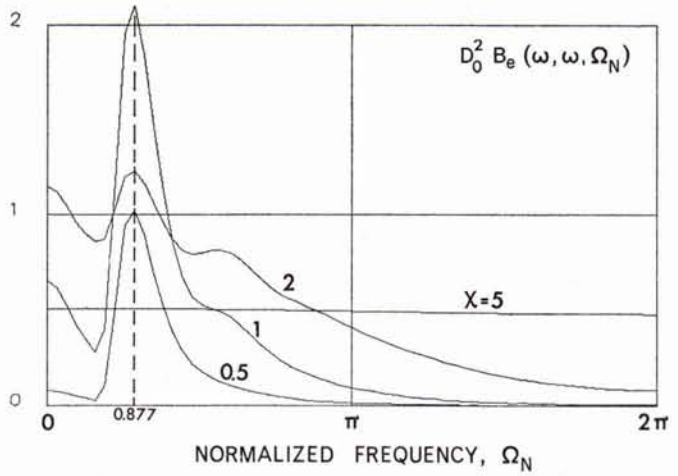
with $\Omega_N = v\Omega/g$. The second term between brackets is caused by the random part of the filter; it is proportional to the sea surface wave spectrum. The normalized version of B_e is easily found:

$$C_e(\chi, \Omega_N) = h^{-2} A^2(\Omega_N), \qquad \text{if} \quad \chi \leqslant 0.2; \tag{8.9}$$

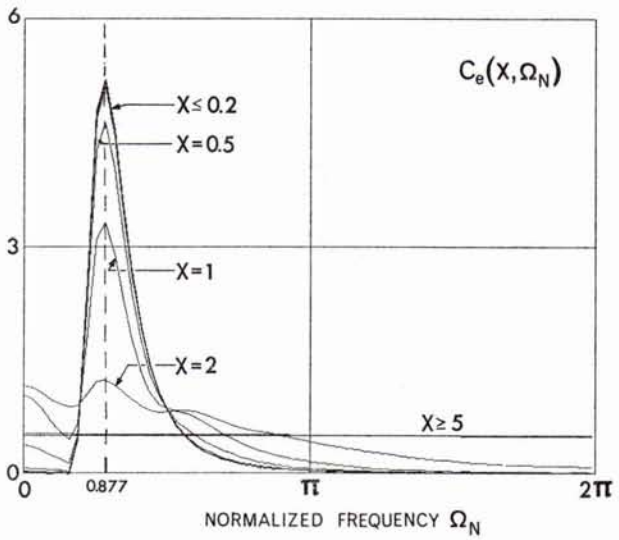
this result is confirmed by comparison of Figs. 8.4 and 3.1.

---

[12] We have suppressed the delta function at $\Omega_N = 0$. It represents the fixed part of the filter and is irrelevant here.



(A)



(B)

Fig. 8.4. (A) The frequency-correlation function $B_e(\omega,\omega,\Omega_N)$ on a normalized scale ($\Omega_N = v\Omega/g$) with χ as parameter; (B) the normalized correlation function, with the inverse of the variance of H_r as normalizing factor.

8.4 Correlation of the impulse response function

Examination of Fig. 8.1 reveals that the correlation function of $h(\tau, t)$ can be found as the inverse double Fourier transform of $B_H(\omega_1, \omega_2, \Delta t)$, with ω_1 and ω_2 as the independent variables. B_H is a two-dimensional Gaussian function. The Fourier transform can hence be found analytically (with $\Delta t = 0$ as a special case) and will have Gaussian properties too.

We apply the operator described by (4.4) on (8.2) and take into account the nomenclature of Fig. 8.1. Also using the parameter b_s, defined in (6.12), we obtain for $\Delta t \neq 0$ (i.e. $\Phi = \Phi(0, \Delta t) < 1$):

$$B_h(\tau_1, \tau_2, \Delta t) = (2\pi D_0^2 b_s^2 \sqrt{1-\Phi^2})^{-1} \exp\left[-\frac{(T_1^2 - 2\Phi T_1 T_2 + T_2^2)}{2(1-\Phi^2)} \right], \tag{8.10}$$

where $T_n = (\tau_n - \tau_s)/b_s$, and $n = 1, 2$. This changes into

$$B_h(\tau_1, \tau_2, 0) = (\sqrt{2\pi}\, D_0^2 b_s^2)^{-1} \delta(T_1 - T_2) \exp\left[-\tfrac{1}{8}(T_1 + T_2)^2\right] \tag{8.11}$$

when $\Delta t = 0$ and consequently $\Phi = 1$.

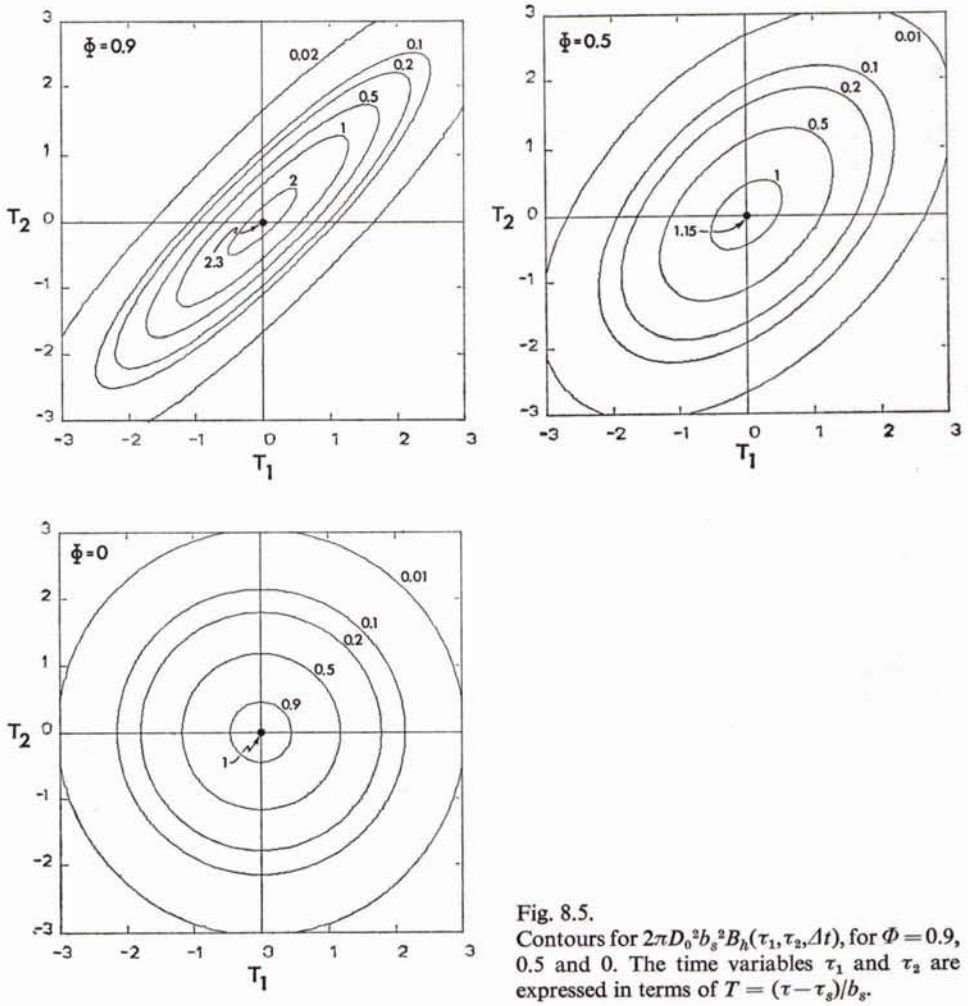


Fig. 8.5.
Contours for $2\pi D_0^2 b_s^2 B_h(\tau_1, \tau_2, \Delta t)$, for $\Phi = 0.9$, 0.5 and 0. The time variables τ_1 and τ_2 are expressed in terms of $T = (\tau - \tau_s)/b_s$.

The Gaussian character of B_h is clearly visible. The maximum value is reached for $T_1 = T_2 = 0$; it depends on Φ as $(1-\Phi^2)^{-\frac{1}{4}}$ for $\Phi < 1$. The contours are again concentric ellipses with major axes along the diagonal $T_1 = T_2$. Examples are plotted in Fig. 8.5.

A remarkable property of B_h is that for $\Delta t = 0$ it is only non-zero if $\tau_1 = \tau_2$. This is caused by the fact that $B_H(\omega_1, \omega_2, 0)$ depends only on the *difference* between ω_1 and ω_2.

If B_H is multiplied with the absorption factor $\exp[-(\omega_1^2+\omega_2^2)D_0C_a]$, the case $\Delta t = 0$ needs no special treatment any more. For B_h we then get a slightly modified version of (8.10): b_s has to be replaced by b_s', defined in (6.16), and Φ by $\Phi' = (b_s/b_s')^2\Phi$. Since $b_s' > b_s$ we have $\Phi' < 1$ which explains why $\Phi = 1$ is no longer a special case.

8.5 Summary

The specular point formula for the transfer function, taken as the starting point for the statistical description of the filter, contains the random surface elevation linearly in the exponent. As this random process is Gaussian (*Assumption 4*), any kind of correlation function can be calculated easily. Time and frequency correlation have been considered in this chapter. The results depend strongly on the roughness parameter χ. For $\chi \leqslant 0.2$ there is a distinct correspondence between the surface statistics and the filter properties *(coherent scattering)*, which property is gradually lost for χ increasing beyond the value 1 *(incoherent scattering)*.

9

space correlation



CHAPTER 9

SPACE CORRELATION

9.1 *Introduction*

In Chapter 4 it was mentioned in passing that a third variable can be distinguished when the surface channel is considered as a random filter, namely the geometry of transmitter and receiver. The influence of this third variable will be investigated in this chapter, by looking at the spatial correlation of the scattered field. A brief analysis of this type of correlation has been made in Section 5.2. The material presented in this chapter is an extension thereof.

A wide variety of possibilities could be considered, because now the filter functions depend on eight independent variables: the three coordinates of the transmitter, the three coordinates of the receiver, and the two variables dealt with in the foregoing chapter. We will not attempt to analyze the influence of all these variables; we restrict ourselves (see Fig. 9.1) to a fixed transmitter, radiating a constant frequency ω, and we observe the scattered field at two receiver positions and at equal instants of time. This signifies that the number of independent variables on which the filter functions now depend has been reduced to three: the coordinates of the receiver, while ω, t and the transmitter coordinates are merely parameters.

Since the input signal is monochromatic, the output signal will be proportional to $H(\omega, t)$, according to (4.9). Hence the spatial correlation as taken here is best examined by means of the frequency transfer function.

A general formula for the spatial correlation function is easily derived from (8.1). Calling the two receivers R_1 and R_2, placing R_1 in the plane $y = 0$ and R_2 in its vicinity, labeling all quantities that distinguish the two receivers from each other with 1 and 2

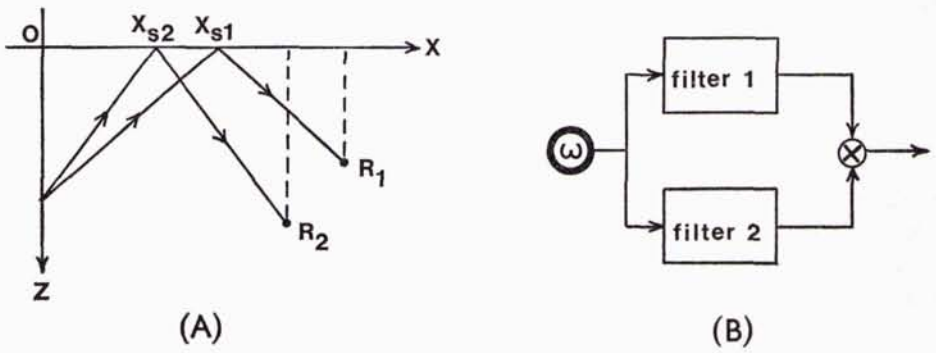


Fig. 9.1. Spatial correlation of the scattered sound field; (A) geometry of transmitter and receivers (for simplicity both receivers are drawn in the plane $y = 0$, but R_2 can have a non-zero y-component), (B) blockdiagram.

respectively, and assuming the average wind direction to make an angle α_w with the positive X-axis ($0 \leqslant \alpha_w \leqslant \pi/2$), we obtain:

$$< H_1(\omega,t)H_2^*(\omega,t) > = (D_{01}D_{02})^{-1} \exp[ik(D_{01}-D_{02})] \times \exp[-\tfrac{1}{2}\{\chi_1^2 - 2\Phi(\xi,\eta,\tau)\chi_1\chi_2 + \chi_2^2\}], \tag{9.1}$$

where $\chi_n = 2kh \cos\theta_{sn}$,

$$\begin{aligned} \xi &= Y_{s2}\sin(\alpha_w) + (X_{s2}-X_{s1})\cos(\alpha_w), \\ \eta &= Y_{s2}\cos(\alpha_w) - (X_{s2}-X_{s1})\sin(\alpha_w), \\ \tau &= |t_{s1}-t_{s2}|, \end{aligned} \tag{9.2}$$

and

$$\begin{aligned} X_{sn} &= \left(\frac{Z_T}{Z_T+Z_{Rn}}\right) X_{Rn}, \\ Y_{sn} &= \left(\frac{Z_T}{Z_T+Z_{Rn}}\right) Y_{Rn}, \\ t_{sn} &= t - \left(\frac{Z_{Rn}}{Z_T+Z_{Rn}}\right)\frac{D_{0n}}{c_0}, \end{aligned} \tag{9.3}$$

with $n = 1, 2$.

An important property of (9.1) can be noted immediately: if ξ, η, and/or τ are so large that Φ equals zero, the spatial correlation function reaches a constant value that is in general non-zero. This value is due to the deterministic part of the filter. For the analysis of the spatial correlation this constant level is irrelevant. Hence we subtract it, which means that we will examine the spatial correlation of H_r instead of H. Furthermore, in (9.1) only the second exponential function is important for the spatial correlation, because the other elements merely describe an amplitude and a phase shift. Therefore we drop them and so we are concerned with the *reduced* space-correlation function, defined by

$$C(\mathscr{R}_{R1}, \mathscr{R}_{R2}) = \exp[-\tfrac{1}{2}\{\chi_1^2 - 2\Phi(\xi,\eta,\tau)\chi_1\chi_2 + \chi_2^2\}] - \exp[-\tfrac{1}{2}(\chi_1^2+\chi_2^2)]. \tag{9.4}$$

This function will be analyzed in two steps: in Section 9.2 we consider the spatial correlation on and across an average wave front (c.f. Section 5.2), and after that we investigate the correlation in X, Y, and Z-direction, in Section 9.3. To distinguish the various correlation functions that appear in this way, they will carry a descriptive label.

For sufficiently high frequencies the concept of *wave fronts* is often used. They are surfaces of constant phase. For a perfectly flat boundary these surfaces are spheres with the image T' of the transmitter T as centre. When the boundary is random these spheres will be distorted, in a stochastic manner. The extent of this distortion is analyzed statistically in Section 9.4.

9.2 Correlation on and across an average wave front

In this section we are concerned with the receiver positions that are already discussed in Section 5.2 (page 312–Fig. 9). This time, however, we assume the wind direction to be arbitrary: whereas in Section 5.2 the average wind was blowing along the X-axis, it now makes an angle α_w (with values between 0 and $\pi/2$) with that axis.

9.2.1 Vertical transversal correlation

The receivers are placed on an average wave front, in the plane $y=0$. Their positions are conveniently expressed in terms of the angles φ and $\Delta\varphi$ (see Section 5.2, Fig. 9a). Then (9.4) can be written as

$$C_{VT}(\Delta\varphi,\varphi)=\exp\left[-\tfrac{1}{2}\{\chi_1^2-2\Phi(\xi,\eta,0)\chi_1\chi_2+\chi_2^2\}\right]-\exp\left[-\tfrac{1}{2}(\chi_1^2+\chi_2^2)\right] \quad (9.5)$$

where $\chi_1=2kh\sin(\varphi)$, $\chi_2=2kh\sin(\varphi+\Delta\varphi)$ and

$$\begin{aligned}\xi &= Z_T[\cot(\varphi+\Delta\varphi)-\cot(\varphi)]\cos(\alpha_w),\\ \eta &= -Z_T[\cot(\varphi+\Delta\varphi)-\cot(\varphi)]\sin(\alpha_w).\end{aligned} \quad (9.6)$$

We have put $\tau=0$, because the difference in travel time between R_1 and R_2 is only depending on the surface elevation at the specular points, whereas ξ and η depend on the coordinates of these points. This makes the influence of τ an effect of second order.

Examination of (9.5) reveals that C_{VT} is not even in $\Delta\varphi$. This is caused by the fact that the transfer function (see (8.1)) is not stationary in φ.

In order to investigate C_{VT} as a function of $\Delta\varphi$ and φ, we have to chose the parameters Z_T, k, v, and α_w. Some results[13] are shown in Fig. 9.2. The following conclusions can be drawn:

1. When the surface roughness increases either because v or k is augmented, or both, the $\Delta\varphi$-range in which some correlation can be expected, becomes narrower.
2. The correlation range for the cross-wind case is about twice as large as the $\Delta\varphi$-range for the down-wind case. This corresponds to the property of the sea surface that $L_{cw}\sim 2L_{dw}$ (see (3.21) and (3.22)).
3. For $\chi<1$, the spatial correlation function C_{VT} has the same shape as the spatial correlation function of the surface elevation (c.f. Fig. 3.5). This is confirmed by (9.5), which reduces for $\chi_1,\ \chi_2\leqslant 0.2$ to $C_{VT}(\Delta\varphi,\varphi)\sim\chi_1\chi_2\Phi(\xi,\eta,0)$. Especially for low values of φ this effect can be noted.

---

[13] We have restricted ourselves to negative values of $\Delta\varphi$. This causes no loss of generality because when $\Delta\varphi>0$, we simply exchange the receivers R_1 and R_2.

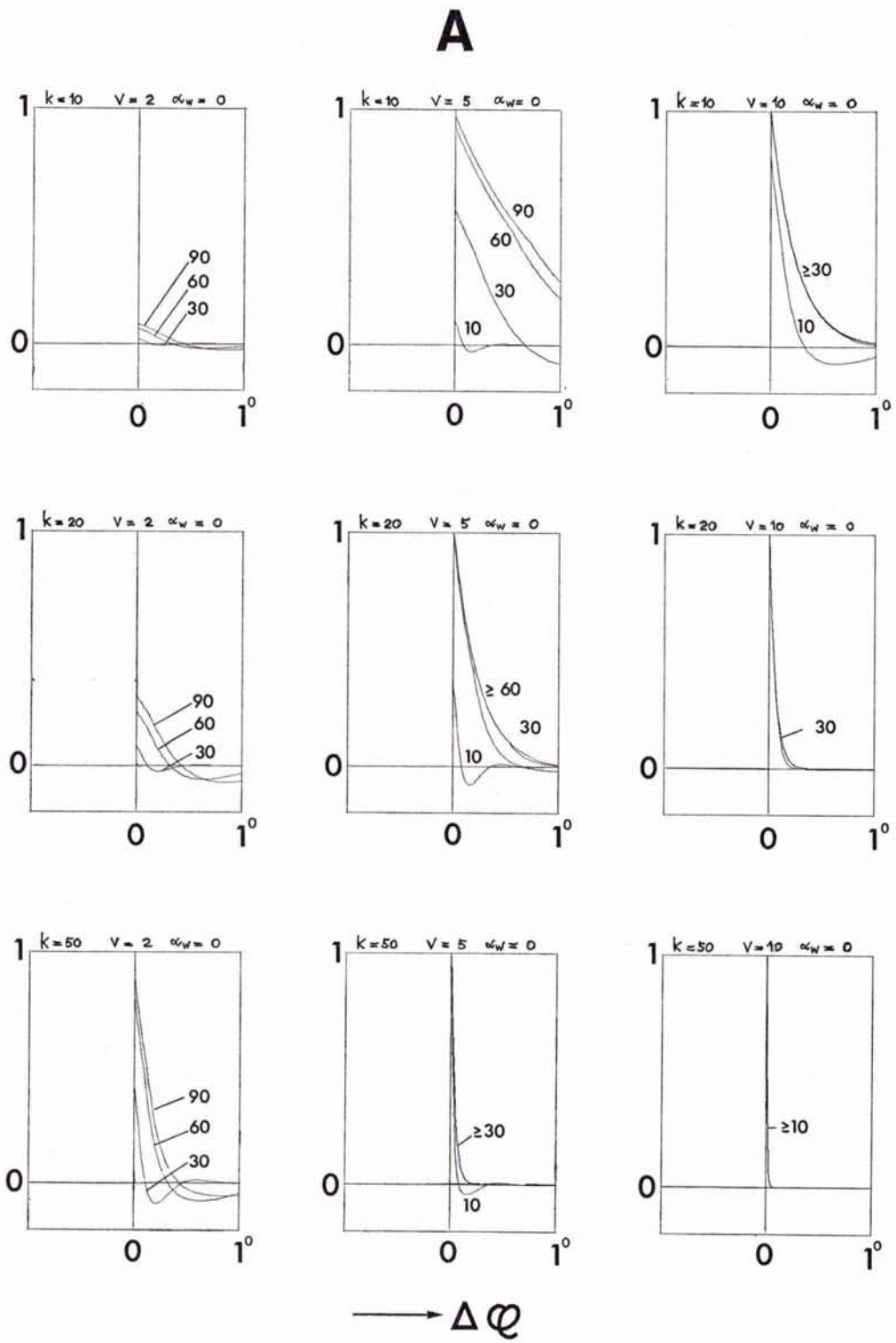
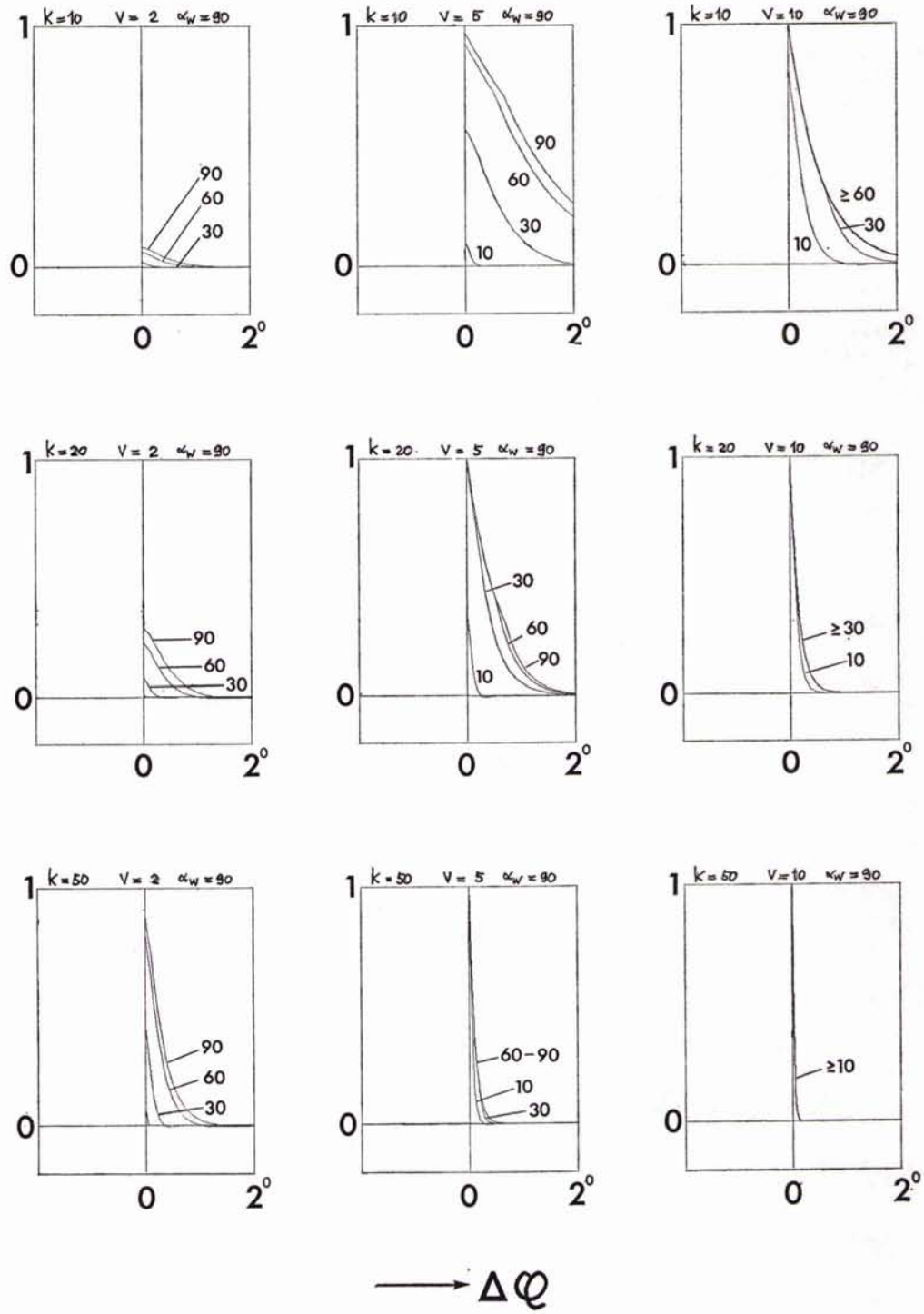


Fig. 9.2. The vertical transversal correlation function $C_{VT}(\Delta\varphi,\varphi)$, with φ as parameter, (A) in down-wind direction, (B) in cross-wind direction ($Z_T = 100$ m).

B


k=10 V=2 αw=90
90
60
30
k=10 V=5 αw=90
90
60
30
10
k=10 V=10 αw=90
≥60
30
10
k=20 V=2 αw=90
90
60
30
k=20 V=5 αw=90
30
60
90
10
k=20 V=10 αw=90
≥30
10
k=50 V=2 αw=90
90
60
30
k=50 V=5 αw=90
60-90
10
30
k=50 V=10 αw=90
≥10
1
0
0
2°
Δφ

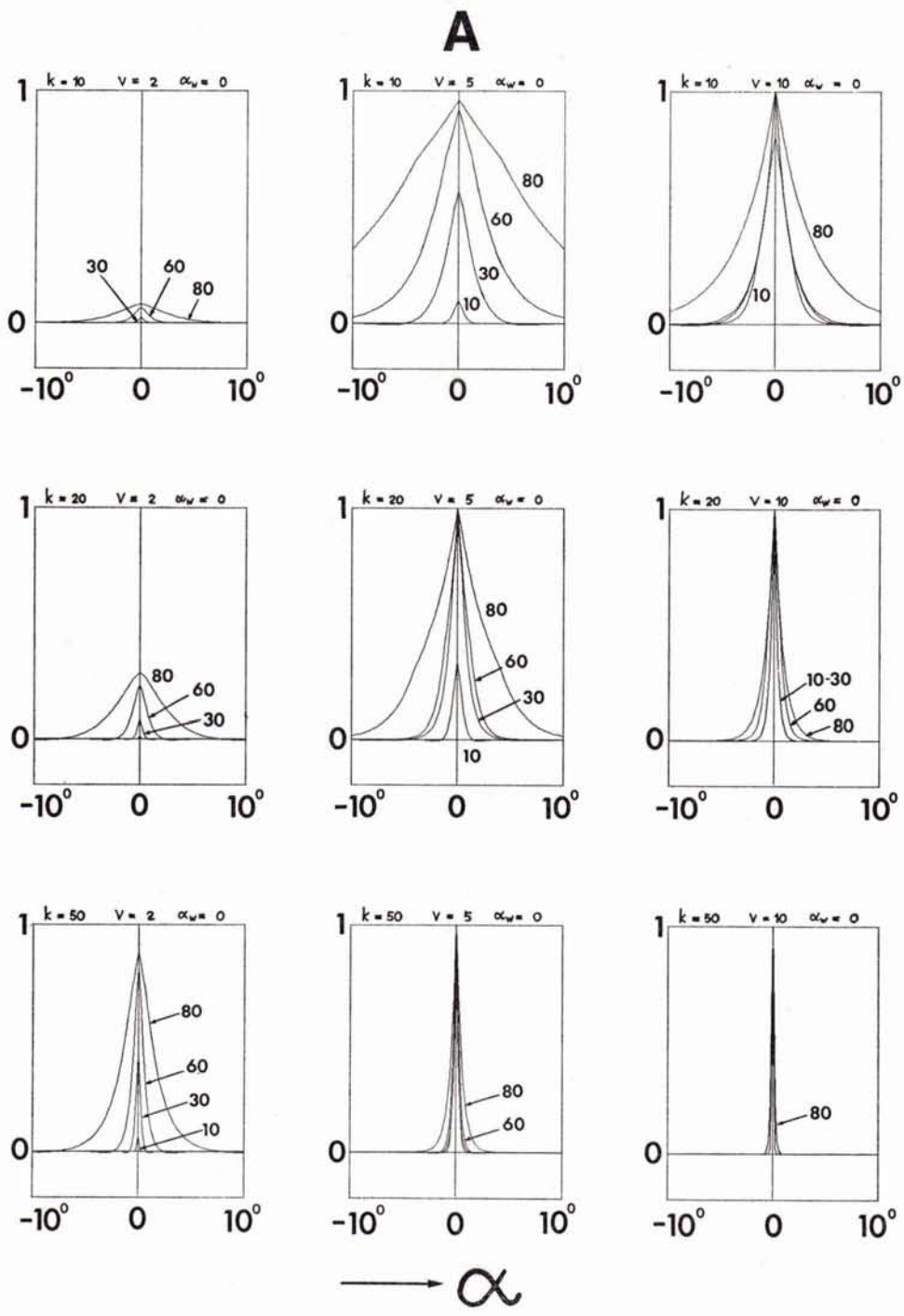
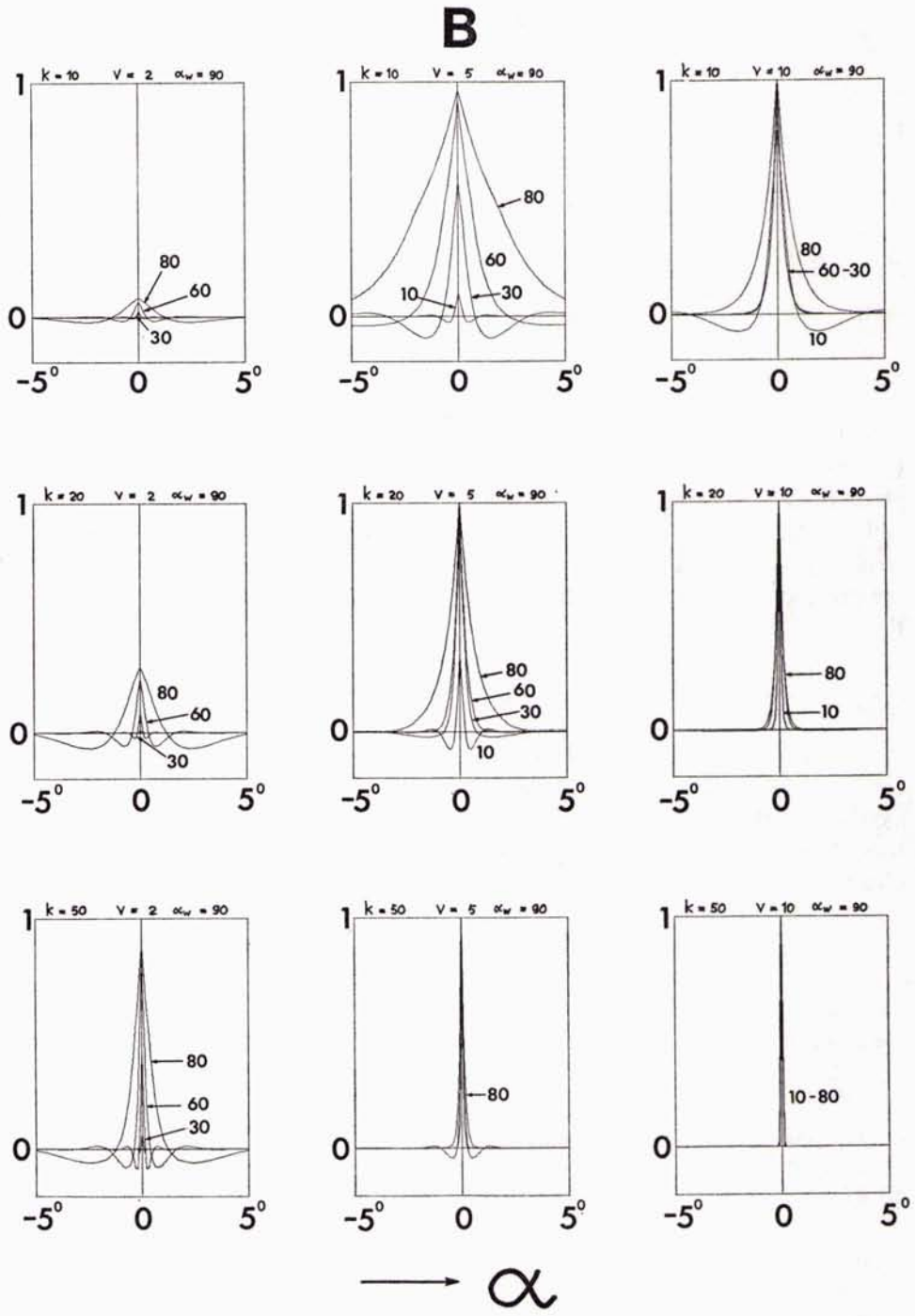


Fig. 9.3. The horizontal transversal correlation function $C_{HT}(\alpha,\varphi)$, with φ as parameter, (A) in down-wind direction, (B) in cross-wind direction ($Z_T = 100$ m).


B
k = 10 V = 2 α_w = 90
k = 10 V = 5 α_w = 90
k = 10 V = 10 α_w = 90
k = 20 V = 2 α_w = 90
k = 20 V = 5 α_w = 90
k = 20 V = 10 α_w = 90
k = 50 V = 2 α_w = 90
k = 50 V = 5 α_w = 90
k = 50 V = 10 α_w = 90
1
0
-5°
0
5°
80
60
30
10
60-30
10-80
α

9.2.2 *Horizontal transversal correlation*

The receivers are placed on an average wave front in a horizontal plane. Their positions are given by the angles φ and α (see Section 5.2, Fig. 9b) and the correlation function becomes

$$C_{HT}(\alpha, \varphi) = \exp\left[-\chi^2\{1-\Phi(\xi, \eta, 0)\}\right] - \exp\left[-\chi^2\right] \tag{9.7}$$

with $\chi = 2kh \sin(\varphi)$ and

$$\begin{aligned} \xi &= Z_T \cot(\varphi)\left[\cos(\alpha_w - \alpha) - \cos(\alpha_w)\right], \\ \eta &= -Z_T \cot(\varphi)\left[\sin(\alpha_w - \alpha) - \sin(\alpha_w)\right]. \end{aligned} \tag{9.8}$$

With the same justification as in the previous sub-section we have put $\tau \approx 0$. Results can be found in Fig. 9.3. The conclusions that can be drawn from the curves there are about the same as in the preceding sub-section. The main difference is that the down-wind and cross-wind cases have exchanged their role, due to the passage from vertical to horizontal transversal correlation (see Section 5.2 – Fig. 9). The curves for $\varphi = 90°$ are not plotted, because C_{HT} degenerates into a constant ($C_{HT} = 1 - \exp(-\chi^2)$) for that value of φ. This follows from (9.7) and (9.8) in a straightforward way.

9.2.3 *Longitudinal correlation*

The receivers are placed in the mean direction of propagation: R_1 on a sphere with radius D_0, R_2 on a sphere with radius $D_0 + \varrho$. Their position is further determined by the grazing angle φ (see Section 5.2, Fig. 9c). The specular points coincide, so that $\xi = \eta = 0$. The time difference is not negligible any more, because now it is directly coupled to the receiver positions. For the correlation function we find

$$C_L(\varrho, \varphi) = \exp\left[-\chi^2\{1-\Phi(0, 0, \tau)\}\right] - \exp\left[-\chi^2\right], \tag{9.9}$$

where $\tau = \varrho/c_0$ and $\chi = 2kh \sin(\varphi)$. This formula is illustrated by Fig. 9.4. There we see that:

1. The correlation function becomes more peaked when the roughness increases (when k, v, or φ is augmented).
2. The shape of the time-correlation function of the sea surface elevation can be recognized, especially for small values of χ ($\chi < 1$).
3. The distances over which there is some correlation are large, due to the fact that we are considering the propagation in the mean direction of propagation, and the propagation speed is high.

An interesting case arises when the observation times are not taken equal but differ by exactly the amount τ, i.e. at R_1 the scattered field is observed at time t, at

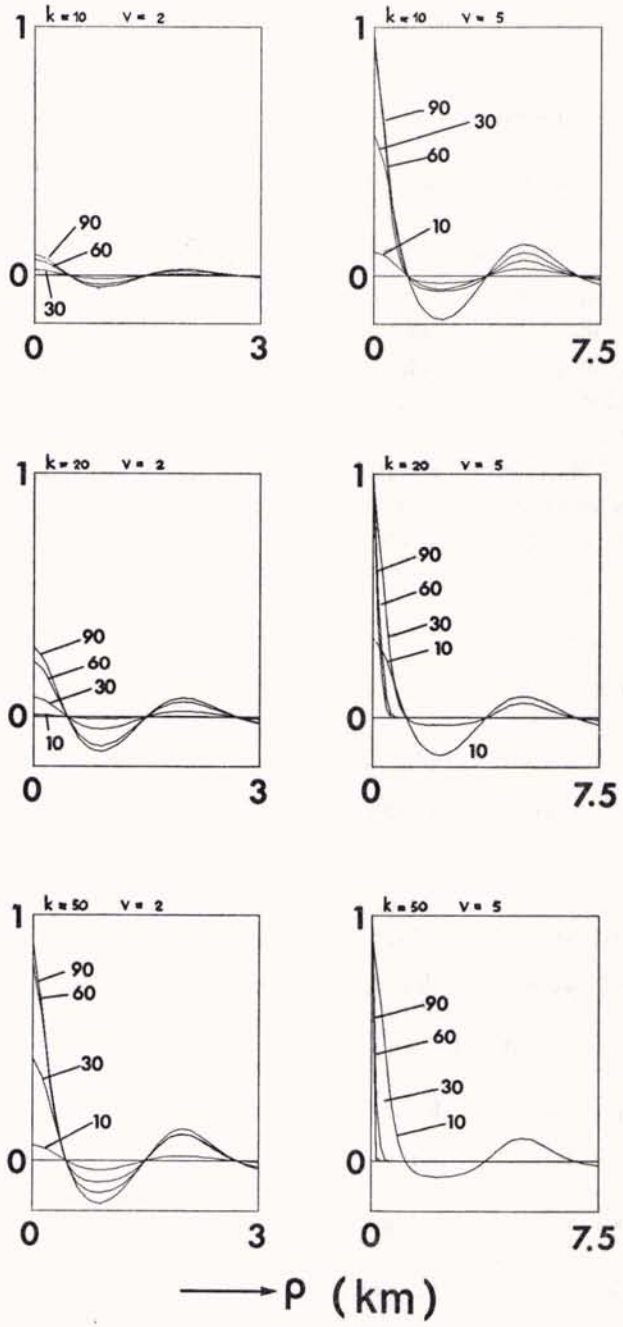


Fig. 9.4. The longitudinal correlation function $C_L(\varrho,\varphi)$, with φ as parameter, for $Z_T = 100$ m.

R_2 the observation takes place at time $t+\tau$. The observer travels then with the wave, and the propagation delay from R_1 to R_2 is compensated. Hence we get

$$C_L(\varrho, \varphi) = 1-\exp(-\chi^2), \tag{9.10}$$

which is independent of ϱ, and equals the variance of $H_r(\omega, t)$.

9.2.4 *Correlation between two arbitrarily placed receivers*

Up to this point we have been discussing the correlation of the scattered field in the three orthogonal directions that were suggested by the concept of average wave fronts. These average wave fronts are spheres; hence we have been working in a polar coordinate system $(\varrho, \varphi, \alpha)$, and we have considered successively the correlation in the direction of φ, α, and ϱ.

The question arises whether the spatial correlation between two arbitrarily placed receivers can be expressed in terms of the correlation functions C_{VT}, C_{HT}, and C_L. In order to find an answer, we assume that the first receiver has the coordinates $(\varrho_R, \varphi, 0)$ and the second one $(\varrho_R+\varrho, \varphi+\Delta\varphi, \alpha)$. The specular points are then given by

$$\begin{aligned} X_{s1} &= Z_T \cot(\varphi), \\ Y_{s1} &= 0, \end{aligned} \tag{9.11}$$

and

$$\begin{aligned} X_{s2} &= Z_T \cot(\varphi+\Delta\varphi)\cos(\alpha), \\ Y_{s2} &= Z_T \cot(\varphi+\Delta\varphi)\sin(\alpha), \end{aligned} \tag{9.12}$$

so that (c.f. (9.6) when $\alpha = 0$ and (9.8) when $\Delta\varphi = 0$):

$$\begin{aligned} \xi &= Z_T[\cot(\varphi+\Delta\varphi)\cos(\alpha_w-\alpha)-\cot(\varphi)\cos(\alpha_w)], \\ \eta &= -Z_T[\cot(\varphi+\Delta\varphi)\sin(\alpha_w-\alpha)-\cot(\varphi)\sin(\alpha_w)]. \end{aligned} \tag{9.13}$$

Next we return to (9.4) and write

$$\begin{aligned} C(\mathscr{R}_{R1}, \mathscr{R}_{R2}) &\equiv C_0(\varrho, \Delta\varphi, \alpha) \\ &= \exp[-\tfrac{1}{2}\{\chi_1^2-2\Phi(\xi, \eta, \tau)\chi_1\chi_2+\chi_2^2\}]-\exp[-\tfrac{1}{2}(\chi_1^2+\chi_2^2)]. \end{aligned} \tag{9.14}$$

The relative coordinates ξ and η are given by (9.13), and $\tau = \varrho/c_0$. For sufficiently small values of ϱ, $\Delta\varphi$ and α, we can expand C_0 in a Taylor series around the point for which $\varrho = \Delta\varphi = \alpha = 0$, i.e. the position of the first receiver. This expansion yields (in *symbolic* notation):

$$C_0(\varrho, \Delta\varphi, \alpha) = C_0(0,0,0) + \sum_{n=1}^{\infty} \frac{1}{n!}\left(\frac{\partial C_0}{\partial \varrho}\varrho + \frac{\partial C_0}{\partial \Delta\varphi}\Delta\varphi + \frac{\partial C_0}{\partial \alpha}\alpha\right)^n. \tag{9.15}$$

The derivatives of C_0 have to be evaluated at the point (0, 0, 0). Therefore we can write:

$$C_0(\varrho, \Delta\varphi, \alpha) = 1 - \exp(-\chi^2) + \\ + \sum_{n=1}^{\infty} \frac{1}{n!} \left(\frac{\partial C_L}{\partial \varrho} \Big|_{\varrho=0} \cdot \varrho + \frac{\partial C_{VT}}{\partial \Delta\varphi} \Big|_{\Delta\varphi=0} \cdot \Delta\varphi + \frac{\partial C_{HT}}{\partial \alpha} \Big|_{\alpha=0} \cdot \alpha \right)^n. \tag{9.16}$$

This result indicates that the spatial correlation between two arbitrarily placed receivers can indeed be expressed in terms of C_{VT}, C_{HT} and C_L, when small displacements are considered. Unfortunately, it is mainly of formal value only and does not enhance our insight in the spatial correlation of the scattered field, unless a special case is considered. To illustrate this point, we examine the first two terms of the series. The calculation of the coefficients is a matter of straightforward, but tedious algebra. The results are collected in Table 9.1. We note that the coefficient of $\Delta\varphi$ is not zero; this shows that C_{VT} is not even in $\Delta\varphi$.

Table 9.1 First and second derivatives of C_L, C_{VT} and C_{HT}, for $\varrho = \Delta\varphi = \alpha = 0$.

function	first derivative	second derivative
C_L	0	$\chi^2 c_0^{-2} \Phi_{tt}$
C_{VT}	$\chi^2 \exp(-\chi^2) \tan\theta_s$	$\chi^2 Z_T^2 \cos^{-4}\theta_s [\Phi_{xx} \cos^2(\alpha_w) + \Phi_{yy} \sin^2(\alpha_w)] +$ $-\chi^2 \tan^2\theta_s - \chi^2 \exp(-\chi^2) [1 + (\chi^2 - 1) \tan^2\theta_s]$
C_{HT}	0	$\chi^2 Z_T^2 \tan^2\theta_s [\Phi_{xx} \sin^2(\alpha_w) + \Phi_{yy} \cos^2(\alpha_w)]$

For $\Delta\varphi = 0$, we have only second order terms, so that

$$C_0(\varrho, 0, \alpha) \approx 1 - \exp(-\chi^2) + m_\varrho \varrho^2 + m_\alpha \alpha^2; \tag{9.17}$$

the contours of constant correlation in the (ϱ, α)-plane are consequently ellipses, for small ϱ and α The coefficients m_ϱ and m_α follow from Table 9.1 and Chapter 3. For the Pierson-Moskowitz spectrum we obtain:

$$m_\varrho = -\frac{\chi^2}{h^2} \left(\frac{v}{c_0} \right)^2 \cdot 10^{-3}, \\ m_\alpha = -\frac{\chi^2}{2h^2} Z_T^2 \tan^2\theta_s [3 \sin^2(\alpha_w) + \cos^2(\alpha_w)] \cdot 10^{-3}. \tag{9.18}$$

It is easy to see that $|m_\varrho| \ll |m_\alpha|$. The aforementioned contours are consequently very long and narrow ellipses, with major axes in the ϱ-direction.

9.3 Correlation in cartesian coordinates

9.3.1 The general formula

In experiments it often happens that an array of hydrophones is hanging vertically from a ship, or that the array is towed in more or less a horizontal position. The data so obtained produce information about the spatial coherence of the scattered field in X, Y, or Z-direction. Some formulae are derived in this section, and some curves are plotted, to facilitate the comparison with such experiments.

In general the coordinates of the two receivers differ by an amount ϱ. If ϱ is small compared to the other distances that determine the geometry of R_1 and R_2, we can base the formulae for the correlation functions on the geometry of R_1 (the receiver in the plane $y = 0$), with $\varrho = (\Delta x, \Delta y, \Delta z)$ as a (small) deviation. R_1 is further determined by Z_R and X_R. For simplicity we take $Z_R = Z_T$, and investigate the range dependency of the spatial correlation.

The specular points are again very close together; hence we neglect the time difference τ. From (9.4) we derive

$$C_{XYZ}(\Delta x, \Delta y, \Delta z, X_R) = \\ = \exp\left[-\tfrac{1}{2}\chi^2\{1-2\Phi(\xi,\eta,0)\gamma+\gamma^2\}\right]-\exp\left[-\tfrac{1}{2}\chi^2(1+\gamma^2)\right], \tag{9.19}$$

where ξ and η are defined in (9.2) and

$$\chi = 2kh\left[1+\left(\frac{X_R}{2Z_T}\right)^2\right]^{-\frac{1}{2}}. \tag{9.20}$$

The quantity γ is the ratio between the roughness parameters as "seen" by the receivers. Its complete formula is

$$\gamma(\Delta x, \Delta y, \Delta z) = \sqrt{\frac{1+\left(\frac{X_R}{2Z_T}\right)^2}{1+\left(\frac{X_R+\Delta x}{2Z_T+\Delta z}\right)^2+\left(\frac{\Delta y}{2Z_T+\Delta z}\right)^2}}. \tag{9.21}$$

Simplification of γ, and also of ξ and η, results when the correlation in X, Y, or Z-direction is considered.

9.3.2 Horizontal correlation in X-direction

The correlation function $C(\Delta x, 0, 0, X_R) \equiv C_x(\Delta x, X_R)$ follows from (9.19) with $\gamma = \gamma(\Delta x, 0, 0)$ and

$$\xi = \tfrac{1}{2}|\Delta x|\cos(\alpha_w), \\ \eta = \tfrac{1}{2}|\Delta x|\sin(\alpha_w). \tag{9.22}$$

Fig. 9.5 shows some graphs for C_x, with acoustic wave number, wind speed, and range as parameters. They indicate that:

1. The correlation function of the sea surface elevation can be distinguished clearly, especially for values of χ less than 1. This also results from (9.19) by series expansion of the exponential functions, for $\chi \leqslant 0.2$.
2. The correlation in case of cross-wind is stronger than for a wind blowing along the X-axis. This can be understood by realizing that the sea surface is approximately a "wash board" with the waves extending in the direction of the mean wind.
3. When the *apparent* surface roughness χ is increased by growth of k or decrease of range, the correlation functions become more peaked. This indicates loss of coherence.
4. When the *true* surface roughness increases as a consequence of higher wind speed, the correlation functions become less peaked. This is caused by the changing character of the sea surface.

9.3.3 *Horizontal correlation in Y-direction*

Putting $\Delta x = \Delta z = 0$, the correlation function $C(0, \Delta y, 0, X_R) \equiv C_y(\Delta y, X_R)$ is found. Its formula is given by (9.19), this time with $\gamma = \gamma(0, \Delta y, 0)$ and

$$\begin{aligned} \xi &= \tfrac{1}{2}|\Delta y| \sin(\alpha_w), \\ \eta &= \tfrac{1}{2}|\Delta y| \cos(\alpha_w). \end{aligned} \tag{9.23}$$

Some curves are presented in Fig. 9.6. They show the same tendencies as Fig. 9.5, with only one exception: the correlation is stronger for a wind blowing in the direction of the X-axis than for a wind blowing in the direction in which the spatial correlation is observed, i.e. the Y-axis.

9.3.4 *Vertical correlation (in Z-direction)*

Finally we examine $C(0, 0, \Delta z, X_R) \equiv C_z(\Delta z, X_R)$. This function is described by (9.19) with $\gamma = \gamma(0, 0, \Delta z)$ and

$$\begin{aligned} \xi &= \tfrac{1}{2}|\Delta z| \left(\frac{X_R}{2Z_T}\right) \cos(\alpha_w), \\ \eta &= \tfrac{1}{2}|\Delta z| \left(\frac{X_R}{2Z_T}\right) \sin(\alpha_w). \end{aligned} \tag{9.24}$$

An impression about the behaviour of C_z can be obtained from Fig. 9.7. Again we see that with increasing χ the curves become more peaked. The shape of the sea surface correlation function is less easy to detect. The correlation for $\alpha_w = 90°$ is better than for $\alpha_w = 0°$.

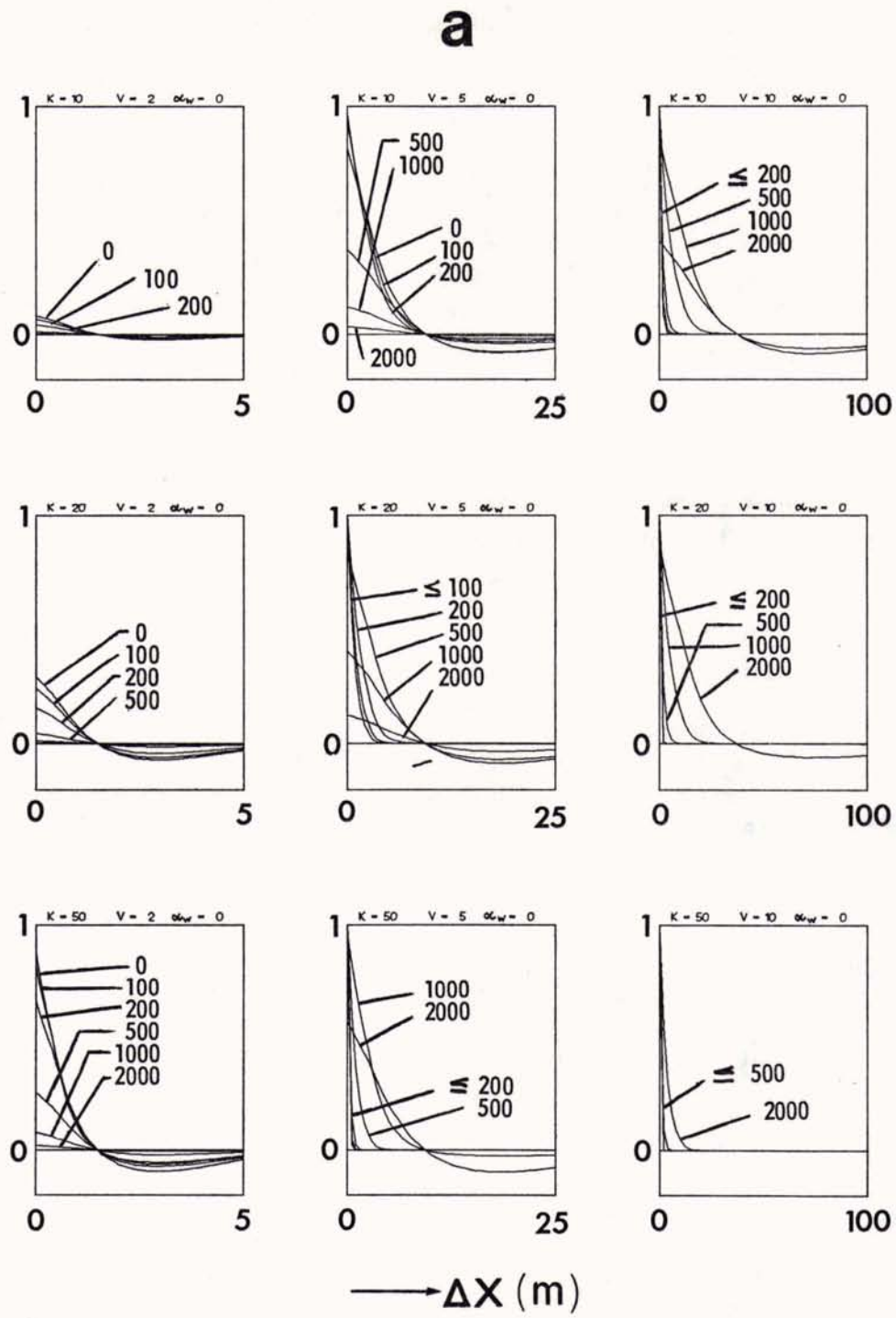
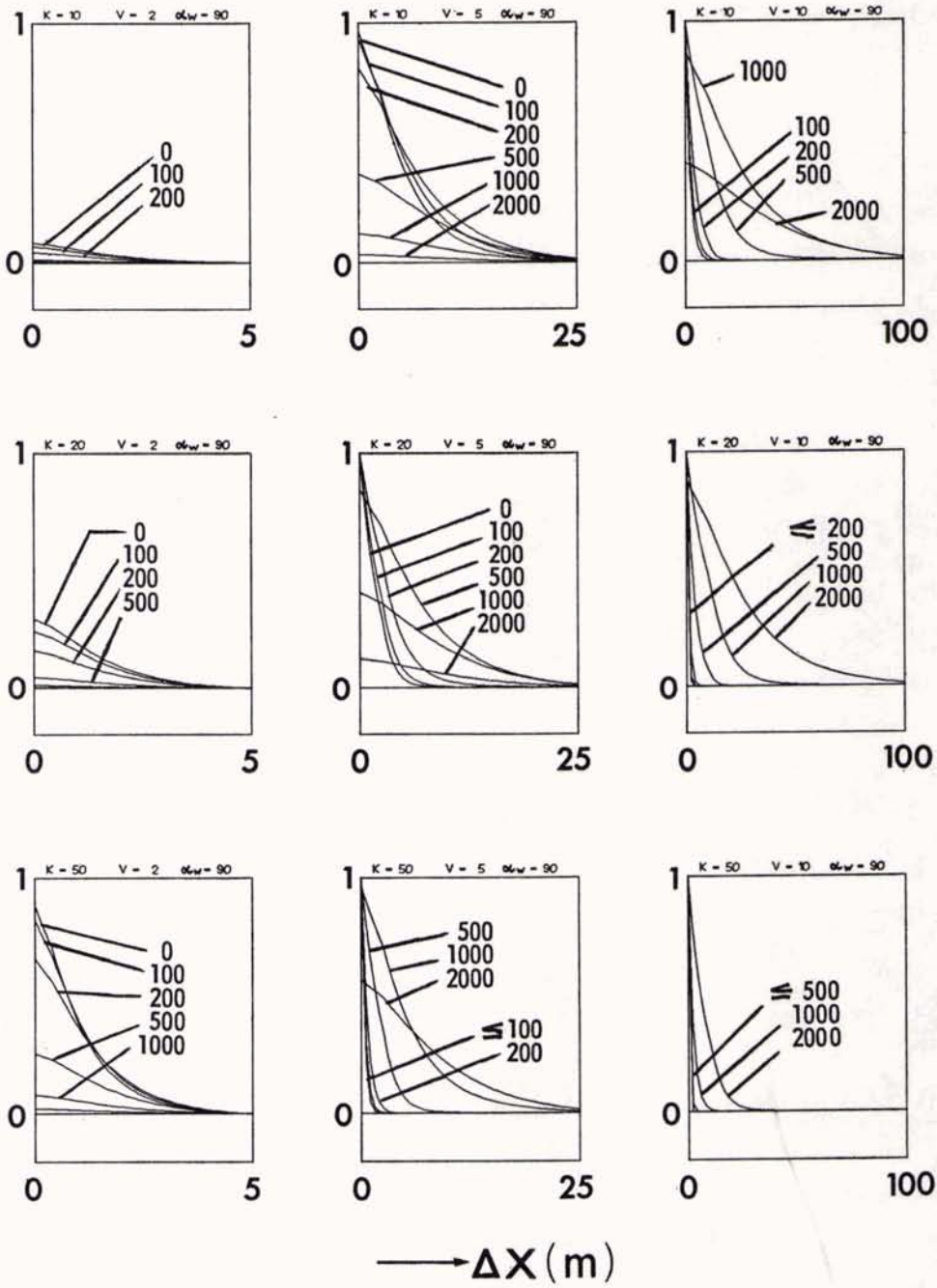


Fig. 9.5. The correlation function $C_x(\Delta x, X_R)$, with X_R as parameter, (A) in down-wind direction, (B) in cross-wind direction ($Z_T = Z_R = 100$ m).

b


K = 10 V = 2 αw = 90
0
100
200
K = 10 V = 5 αw = 90
0
100
200
500
1000
2000
K = 10 V = 10 αw = 90
1000
100
200
500
2000
K = 20 V = 2 αw = 90
0
100
200
500
K = 20 V = 5 αw = 90
0
100
200
500
1000
2000
K = 20 V = 10 αw = 90
200
500
1000
2000
K = 50 V = 2 αw = 90
0
100
200
500
1000
K = 50 V = 5 αw = 90
500
1000
2000
100
200
K = 50 V = 10 αw = 90
500
1000
2000
1
0
5
25
100
ΔX (m)

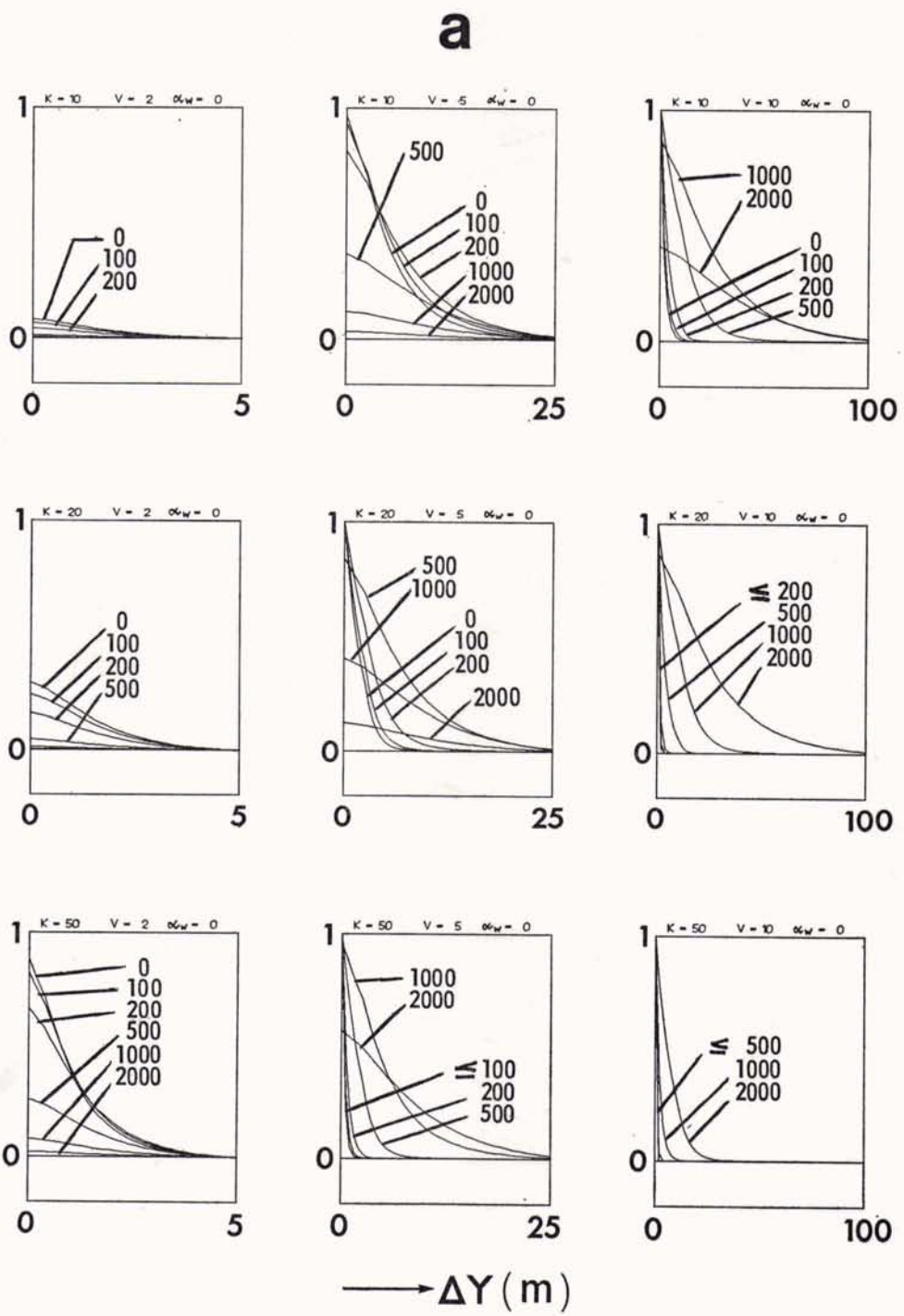
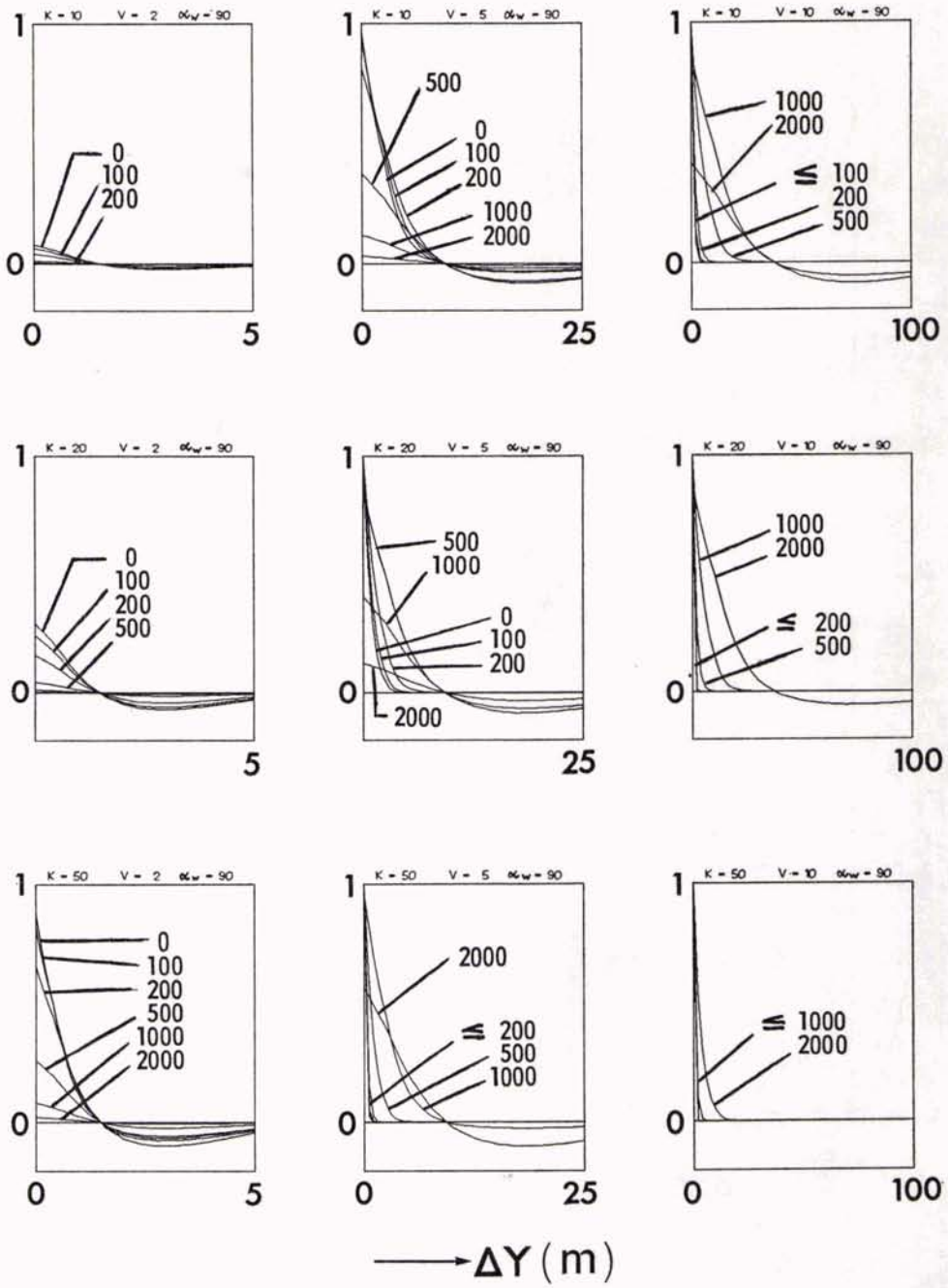


Fig. 9.6. The correlation function $C_y(\Delta y, X_R)$, with X_R as parameter, (A) in down-wind direction, (B) in cross-wind direction ($Z_T = Z_R = 100$ m).

b


K = 10 V = 2 α_w = 90
0
100
200
K = 10 V = 5 α_w = 90
500
0
100
200
1000
2000
K = 10 V = 10 α_w = 90
1000
2000
≦ 100
200
500
K = 20 V = 2 α_w = 90
0
100
200
500
K = 20 V = 5 α_w = 90
500
1000
0
100
200
2000
K = 20 V = 10 α_w = 90
1000
2000
≦ 200
500
K = 50 V = 2 α_w = 90
0
100
200
500
1000
2000
K = 50 V = 5 α_w = 90
2000
≦ 200
500
1000
K = 50 V = 10 α_w = 90
≦ 1000
2000
1
0
0
5
25
100
ΔY (m)

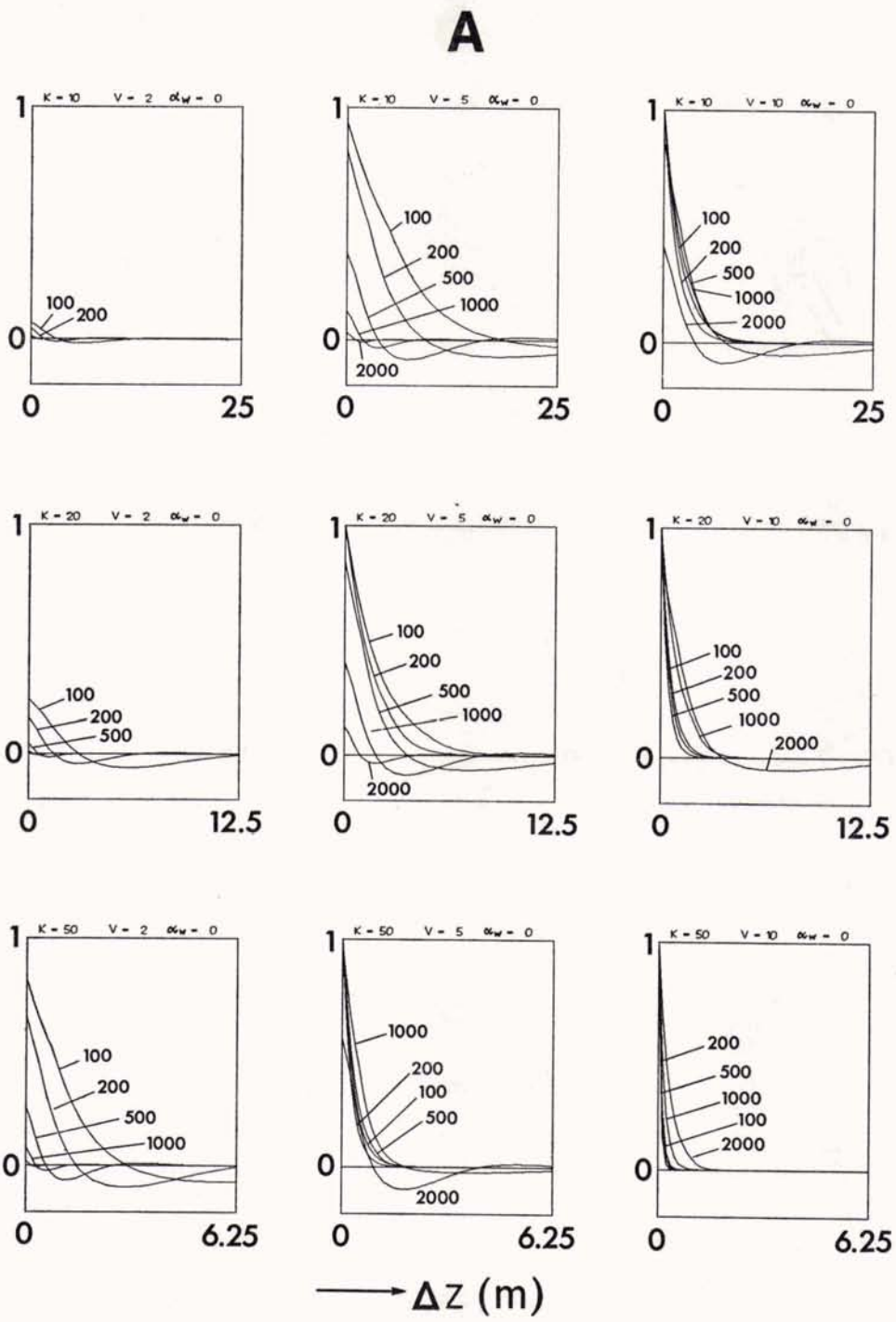
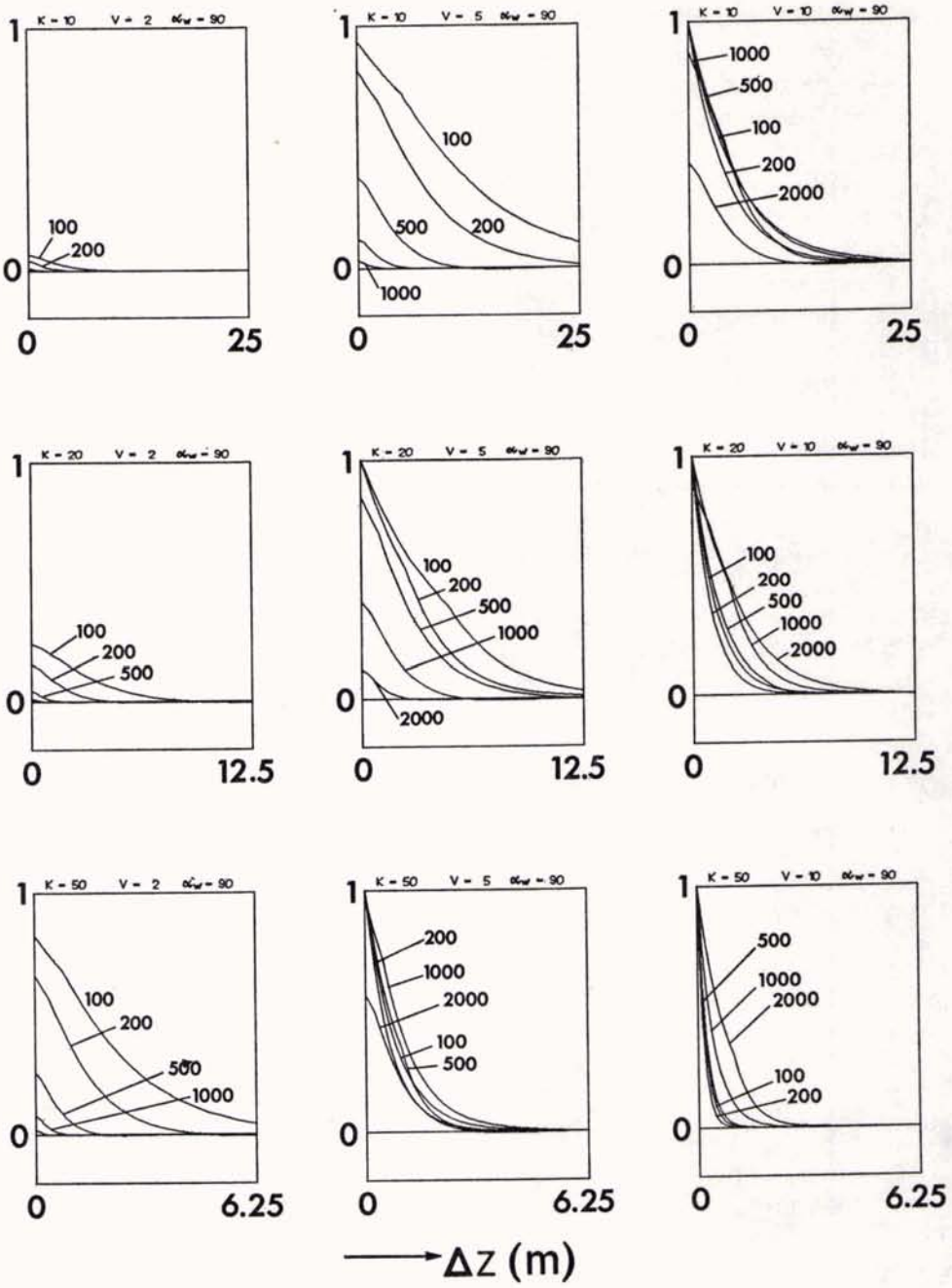


Fig. 9.7. The correlation function $C_z(\Delta z, X_R)$, with X_R as parameter, (A) in down-wind direction, (B) in cross-wind direction ($Z_T = Z_R = 100$ m).

B


K = 10 V = 2 α_w = 90
100
200
1
0
0
25
K = 10 V = 5 α_w = 90
100
500
200
1000
1
0
0
25
K = 10 V = 10 α_w = 90
1000
500
100
200
2000
1
0
0
25
K = 20 V = 2 α_w = 90
100
200
500
1
0
0
12.5
K = 20 V = 5 α_w = 90
100
200
500
1000
2000
1
0
0
12.5
K = 20 V = 10 α_w = 90
100
200
500
1000
2000
1
0
0
12.5
K = 50 V = 2 α_w = 90
100
200
500
1000
1
0
0
6.25
K = 50 V = 5 α_w = 90
200
1000
2000
100
500
1
0
0
6.25
K = 50 V = 10 α_w = 90
500
1000
2000
100
200
1
0
0
6.25
ΔZ (m)

9.4 Wave front distortion

With a perfectly flat surface the reflected waves have spherical wave fronts that are concentric around the point T', the image of the transmitter T, with radius D_0. This follows from (8.1) by putting $\zeta = 0$.

When the reflecting surface is random, the surfaces with constant phase are corrugated spheres, according to (8.1) with $\zeta \neq 0$ (see Fig. 9.8). For not too extreme values of ζ, they may still be considered as originating from the centre T', but the distance r_{WF} from T' to a point P on the wave front is now a random function of the direction $T'P$. As (in statistical sense) there is rotation symmetry with respect to the Z-axis, it is sufficient to study the random wave fronts in the plane $y = 0$.

Along a wave front the phase is constant, say equal to kC. Mathematically, the surface can therefore be described (for $y = 0$) by the equation

$$r_{WF}(\varphi) = C + 2\sin(\varphi)\zeta(\mathbf{R}_s, t_s). \tag{9.25}$$

The average wave fronts are spheres, with radius C, as for the flat boundary. The standard deviation depends on φ:

$$\sigma_{WF}(\varphi) = 2h\sin(\varphi), \tag{9.26}$$

as it should, because for larger grazing angles the surface appears rougher. It may also be noted that σ_{WF} is independent of r_{WF}. This means that after the spherical incident wave front has been distorted by the random boundary, its randomness remains untouched by the spherical spreading. Only the scale over the sphere is expanded as time goes on, but each "trough" and "crest" retains its depth or height, in accordance with the assumption of an ideal medium. But it should be emphasized that this result

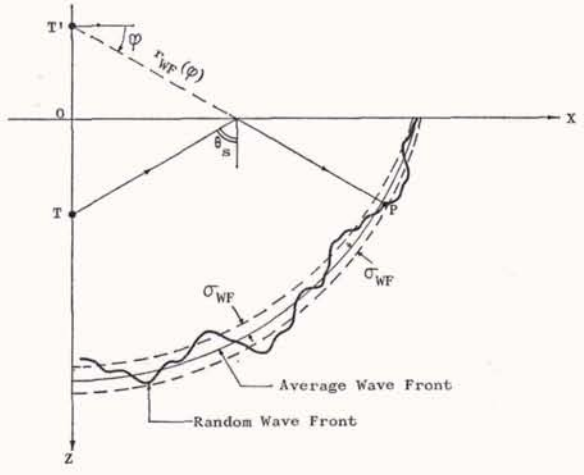


Fig. 9.8.
Corrugation of wave front. The average wave front is a sphere with centre at T', the distorted wave front has a variance that increases with φ.

can only be true locally and temporarily. A physical reasoning, based on Huygens' principle, quickly shows the limitation of this "frozen" wave front: each point on the wave front acts as a secondary source, and each "ray" is propagating in a direction perpendicular to the wave front, so that the shape of this equi-phase surface is continuously changing.

In (9.25) the second term on the right hand side represents the corrugation of the wave front. Its correlation properties are easily found. Considering, as in Section 9.2, the correlation on and across the average wave front, we get:

Vertical Transversal Correlation

$$c_{vt}(\Delta\varphi, \varphi) = 4h^2 \sin(\varphi + \Delta\varphi) \sin(\varphi) \Phi(\xi, \eta, 0), \tag{9.27}$$

with ξ and η given in (9.6);

Horizontal Transversal Correlation

$$c_{ht}(\alpha, \varphi) = 4h^2 \sin^2(\varphi) \Phi(\xi, \eta, 0), \tag{9.28}$$

with ξ and η defined in (9.8);

Longitudinal Correlation

$$c_l(\varrho, \varphi) = 4h^2 \sin^2(\varphi) \Phi(0, 0, \tau), \tag{9.29}$$

with $\tau = \varrho / c_0$.

The most remarkable property of these correlation functions is their linear dependency on the correlation function of the sea surface elevation. For small values of $\Delta\varphi$ and α, ξ and η are proportional to $\Delta\varphi$ and α. This can be seen in (9.6) and (9.8). The properties of the wave front corrugations are therefore closely related to the properties of the sea surface. These were discussed in Chapter 3. Finally we note that the correlation functions of the wave fronts are frequency-independent.

9.5 Summary

The spatial correlation of the scattered field is studied in this chapter, for a fixed transmitter that radiates a harmonic signal with frequency ω. Various possibilities, as for the receiver positions, are considered: vertical transversal correlation (two receivers on an average wave front, in a vertical plane), horizontal transversal correlation (two receivers on an average wave front, in a horizontal plane), longitudinal correlation (two receivers in the mean direction of propagation), and correlation in X-, Y-, and Z-direction. It is found that the space-correlation functions reflect the shape of the surface correlation function, for small values of χ ($\chi \leqslant 1$). For larger values this effect is lost, and the correlation becomes very poor (incoherent scattering).

10

statistical properties of output signals



CHAPTER 10

STATISTICAL PROPERTIES OF OUTPUT SIGNALS

10.1 Introduction

After the analysis of the statistical properties of the various system functions, the questions arise what characteristics the output signals of the random filter have in time and frequency and how they are related to those of the filter. The answers to these questions, which may be of interest for the experimentalist who uses the underwater sound channel for communication purposes,[14] will be given in this chapter, for three different types of input signals. First, in Section 10.2, we will give our attention to monochromatic input signals. After that, in Section 10.3, the input signals will be delta pulses. Finally, arbitrary input signals will be considered briefly, in Section 10.4.

Mainly the first and second order statistical moments will be investigated, but in some occasions it will also be possible to say something about probability density functions.

An important restriction is caused by the stationarity (in time) of our filter: only two system functions are defined, namely $H(\omega, t)$ and $h(\tau, t)$. This means that for the second moments the scheme of Fig. 4.6 has to be applied.

10.2 Monochromatic input signals

10.2.1 Random expressions

We recall some results of Chapter 4 (Table 4.1) and write them in a more complete form, expressing the fact that a monochromatic signal not only depends on time, but also on the input frequency ω_0. So we have at the input

$$\begin{cases} x(t, \omega_0) = \exp(-i\omega_0 t), \\ X(\omega, \omega_0) = 2\pi\delta(\omega - \omega_0), \end{cases} \tag{10.1}$$

and at the output

$$y(t, \omega_0) = H(\omega_0, t)\exp(-i\omega_0 t). \tag{10.2}$$

The time function $y(t, \omega_0)$ is, according to (8.1) and (10.2), a time-shifted and phase-modulated version of $x(t, \omega_0)$:

---

[14] Similar questions can be posed about the characteristics in space.

$$y(t, \omega_0) = -D_0^{-1} \exp\left[-i\omega_0(t-\tau_s) - i2k_0 \cos\theta_s \zeta_s(t_s)\right]. \tag{10.3}$$

It is stationary in time, due to the stationarity of ζ. Its spectrum is hence not defined.

10.2.2 Mean values

Using the results of Chapter 6 we get from (10.2):

$$< y(t, \omega_0) > = H_d(\omega_0) \exp(-i\omega_0 t). \tag{10.4}$$

Comparing this result with the input signal, we see that the filter has introduced the factor $H_d(\omega_0)$. From (6.13) it follows that this factor, apart from the spherical spreading represented by D_0^{-1}, describes a frequency-dependent attenuation with a Gaussian shape, and a time delay $\tau_s = D_0/c_0$.

10.2.3 Second order moments in general

In the most general case we have at the input a number of monochromatic signals of the type $x(t, \omega_n) = \exp(-i\omega_n + \varphi_n)$ with $n = 1, 2, \ldots$, and observe the output signal, that is the combined effect of the input signals, at two different instants of time (t and t'). It can be shown easily that no loss of generality occurs when only two frequencies (ω_1 and ω_2) are assumed to be applied at the input. The block diagram for this situation is sketched in Fig. 10.1.

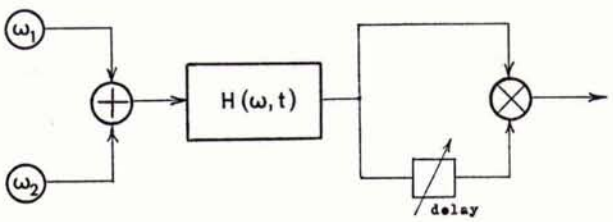


Fig. 10.1.
Time and frequency correlation of the output signal, for purely harmonic input signals with angular frequencies ω_1 and ω_2.

The output of the random filter, before the delay and multiplication, is equal to $f(t) = y(t, \omega_1) + y(t, \omega_2)$, so that the second moment consists out of four correlation functions of the type $< y(t, \omega_1) y^*(t', \omega_2) >$. An expression for such a correlation function can be obtained from (10.2). It can be evaluated by using the results of Chapter 8. We have

$$< y(t, \omega_1) y^*(t', \omega_2) > = B_H(\omega_1, \omega_2, t-t') \exp\left[-i(\omega_1 t - \omega_2 t')\right], \tag{10.5}$$

of which special cases can be derived rapidly.

10.2.4 *Time correlation*

When only one frequency is presented at the input ($\omega_1 = \omega_2 = \omega_0$) and when the output signal is sampled at two instants of time, Δt units apart, we can construct (see Fig. 10.2) the time-correlation function of y. In formula we have

$$< y(t, \omega_0) y^*(t-\Delta t, \omega_0) > = B_H(\omega_0, \omega_0, \Delta t) \exp(-i\omega_0 \Delta t) \tag{10.6}$$

which is a phase-shifted version of B_H for constant ω. Fig. 8.3 gives a qualitative description of the time correlation of the random part of the output signal. For $\chi \leqslant 0.2$ the time correlation of the surface elevation is linearly present in the output of the filter; for $\chi > 2$ the output signal is almost uncorrelated, unless Δt is very small.

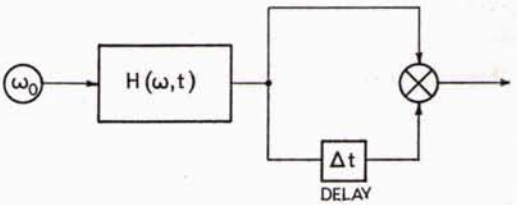


Fig. 10.2.
Time correlation of the output signal, for a purely harmonic input; the output signal is sampled at two times, Δt units apart.

10.2.5 *Frequency correlation*

For coinciding instants of time, the second moment of the output signal in Fig. 10.1 involves correlation functions of the type $< y(t, \omega_1) y^*(t, \omega_2) >$. A formula follows from (10.5) by putting $t' = t$:

$$\begin{aligned} < y(t, \omega_1) y^*(t, \omega_2) > &= B_H(\omega_1, \omega_2, 0) \exp[-i(\omega_1 - \omega_2)t] \\ &= |B_H(\omega_1, \omega_2, 0)| \exp[-i(\omega_1 - \omega_2)(t - \tau_s)]. \end{aligned} \tag{10.7}$$

The argument is linear in ω_1 and ω_2 and is therefore not very relevant. The modulus is plotted in Fig. 8.2 ($\Phi = 1$).

As in Section 5.2, we can investigate the "coherent bandwidth". To this end we put $\omega_2 = \text{constant} = \omega$ (the "center frequency") and $\omega_1 = \omega + \Delta\omega$ into (10.7) with the following result

$$< y(t, \omega + \Delta\omega) y^*(t, \omega) > = B_H(\omega + \Delta\omega, \omega, 0) \exp(-i\Delta\omega t). \tag{10.8}$$

With (8.7) this becomes

$$< y(t, \omega + \Delta\omega) y^*(t, \omega) > = D_0^{-2} \exp[-\tfrac{1}{2}\chi^2 (\Delta\omega/\omega)^2 - i\Delta\omega(t - \tau_s)]. \tag{10.9}$$

The modulus is drawn in Fig. 10.3 with $\Delta\omega/\omega$ as variable and χ as parameter. The Gaussian curves of Section 5.2 are found once more.

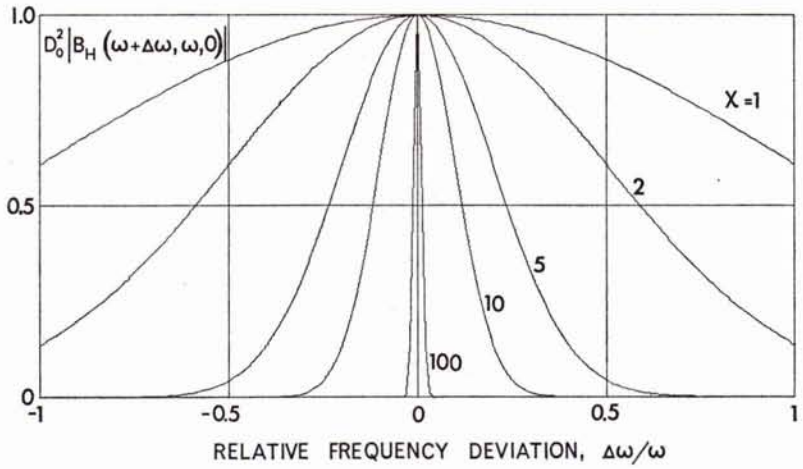


Fig. 10.3. Curves for the "coherent bandwidth" of the output, for monochromatic input signals.

Quantitative insight into the "coherent bandwidth" can easily be gained by considering the 3-dB points, i.e. the values of $\Delta\omega$ for which the curves of Fig. 10.3 have decreased to the level 0.5. A bandwidth equal to $2\Delta f = 0.188\ c_0(h\cos\theta_s)^{-1}$ follows. This is only dependent on wind speed and transmitter-receiver geometry. Taking the same combinations as in Table 6.1, we can compute the value of $2\Delta f$. Results are collected in Table 10.1. They indicate that at longer range the coherent bandwidth increases, whereas an augmenting wind speed causes this bandwidth to decrease. This can be understood by looking at the apparent surface roughness, expressed in the parameter χ: the roughness decreases with range and increases with wind speed. As an example we take $v = 5$ m/s, $X_R = 1000$ m, and $f = 7.5$ kHz. A coherent bandwidth of 5.1 kHz is found, which means that signals with a frequency content ranging from 5 to 10 kHz are received without too much loss of coherence.

Table 10.1 Some values of the coherent bandwidth ($2\Delta f = 0.188\ c_0(h\cos\theta_s)^{-1}$) as function of wind speed and transmitter-receiver configuration (all frequencies in kHz.).

	v in m/s			
X_R in m	1	2	5	10
0	76	19	3.0	0.8
100	77	19	3.1	0.8
200	78	20	3.1	0.8
500	91	23	3.7	0.9
1000	127	32	5.1	1.3
2000	217	54	8.7	2.2
5000	500	127	20.0	5.1

These values hold for $Z_T = 650$ m and $Z_R = 100$ m.

10.2.6 The variance spectrum of y

In (10.6) we have a formula for the time-correlation function of $y(t, \omega_0)$, when a single frequency ω_0 is applied at the input. The Fourier transform of this time-correlation function is equal to $B_e(\omega_0, \omega_0, \omega-\omega_0)$, as can be seen from (10.6) with (4.1) and Fig. 4.6. It is the *variance* spectrum of the output signal.

For the evaluation of $B_e(\omega_0, \omega_0, \omega-\omega_0)$ we have – in general – to employ Fig. 8.4-A: the variance spectrum of y is simply obtained by shifting the origin of the curves to the angular frequency ω_0. However, when $\chi_0 \leqslant 0.2$, we can apply (8.8), getting

$$B_e(\omega_0, \omega_0, \omega-\omega_0) = D_0^{-2}[\delta(\omega-\omega_0)+\chi_0^2 h^{-2} A^2(\omega-\omega_0)]. \tag{10.10}$$

This last result indicates clearly that, in the coherent[15] frequency domain ($\chi \leqslant 0.2$), the Doppler spread in the channel is simply related to the surface movements: a single input frequency ω_0 causes an output signal with a variance spectrum that is composed of two side-bands with the shape of the surface wave spectrum, centered at ω_0. For increasing roughness, though, this property is gradually lost, and the spread in the channel increases. A qualitative illustration of this statement is presented in Fig. 10.4.

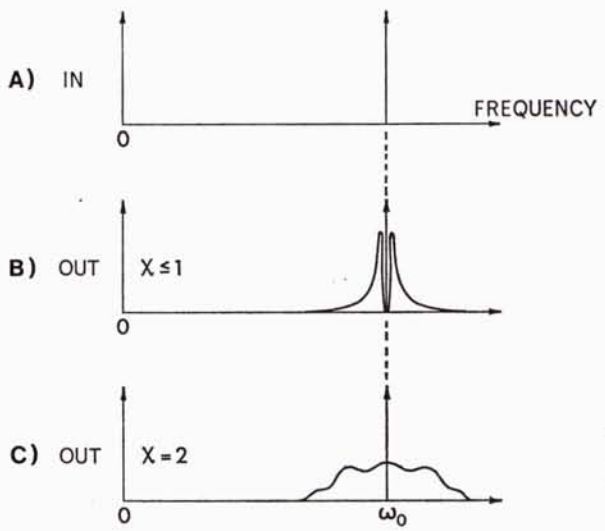


Fig. 10.4.
The variance spectrum of the output for a harmonic input signal with radial frequency ω_0.

The dominant surface wave frequency occurs, according to Fig. 3.1, at $\omega_s = 8.77/v$ radians. This gives the side-bands in Fig. 10.4-B a frequency off-set of about $1.4/v$ Hz. Table 10.2 lists some values.

[15] The word *coherent* has more than one significance. In general it means that the random filter part is negligable ($\chi < 0.1$). Here it indicates that the correlation function can be simplified by series expansion ot the exponential function ($\chi < 0.2$). When used in connection with bandwidth, it merely refers to the fact that the signal distortion remains within acceptable limits.

Table 10.2 Values of the frequency off-set of the side-bands generated by the movement of the surface ($\chi < 0.2$).

wind speed (m/s)	frequency off-set (Hz)
1	1.40
2	0.70
5	0.28
10	0.14
20	0.07

10.2.7 The variance of y

The variance of a complex quantity z is defined as [*10.1, p. 241*]

$$v = E\{|z - E\{z\}|^2\}. \tag{10.11}$$

For y this gives

$$v(\omega_0) = D_0^{-2}[1 - \exp(-\chi_0^2)]. \tag{10.12}$$

This result follows from (10.3), (10.4), and (10.6) with $\Delta t = 0$.

10.2.8 Probability density functions

We return to (10.3), the formula for $y(t, \omega_0)$. Dropping the factor $-D_0^{-1}$, which represents the phase inversion caused by the surface and the spherical spreading and which is of no importance in the present analysis, we are dealing with a vector of unit length and with a phase that fluctuates randomly (see Fig. 10.5) about the mean value $\varphi = \omega_0(t - \tau_s)$. The phase fluctuation is described by

$$\Delta\varphi = 2k_0 \cos\theta_s \zeta_s(t_s); \tag{10.13}$$

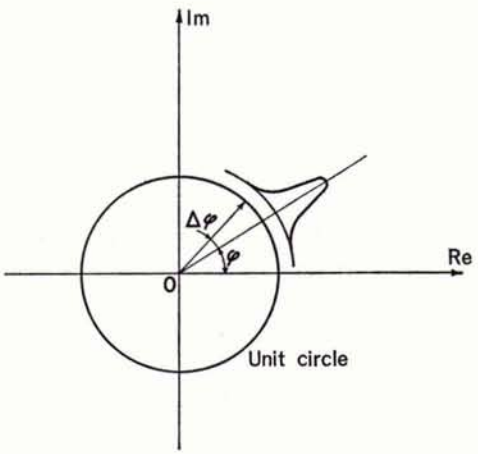


Fig. 10.5.
The random vector y (after normalization), representing the output signal caused by a harmonic input signal (see (10.3)).

it has a Gaussian probability density function:

$$f_{\Delta\varphi}(\Delta\varphi) = (\chi_0\sqrt{2\pi})^{-1} \exp\left[-\frac{(\Delta\varphi)^2}{2\chi_0^2}\right]. \tag{10.14}$$

This expression is correct and useful when the phase fluctuations are small ($\chi_0 \ll \pi$), but when $|\Delta\varphi| > \pi$ radians (which is likely to happen when $\chi_0 \geqslant \pi$) the probabilities in the intervals ..., $(-5\pi, -3\pi)$, $(-3\pi, -\pi)$, $(\pi, 3\pi)$, $(3\pi, 5\pi)$, ... have to be added to the probability in $(-\pi, \pi)$ because a $\Delta\varphi$ in one of these intervals is not distinct from $\Delta\varphi$ in the central interval. It is easy to see that in this way $\Delta\varphi$ tends to be distributed uniformly:

$$\left.\begin{aligned} f_{\Delta\varphi}(\Delta\varphi) &= \frac{1}{2\pi} \quad \text{if} \quad -\pi \leqslant \Delta\varphi \leqslant \pi \\ &= 0 \quad \text{otherwise} \end{aligned}\right\} \quad \text{for} \quad \chi_0 \gg \pi. \tag{10.15}$$

An illustration is given in Fig. 10.6.

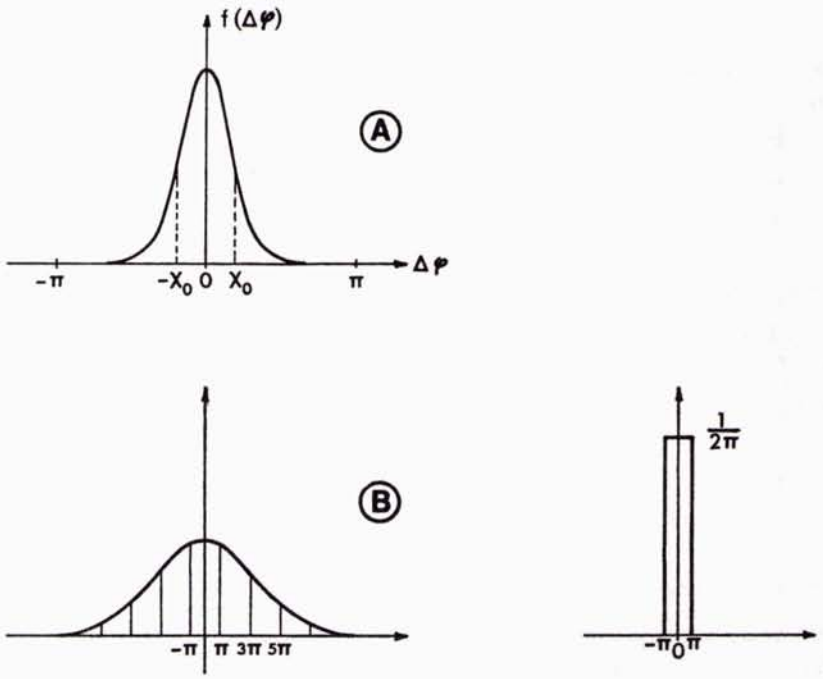


Fig. 10.6. The probability density function of $\Delta\varphi$, (A) for $\chi_0 \ll \pi$, (B) for $\chi_0 \gg \pi$; $\Delta\varphi$ is expressed in radians.

10.3 Delta pulses at the input

10.3.1 Random formulae

At time $t = t_0$ a unit delta pulse is applied at the input. From Table 4.1 we have then

$$\begin{cases} x(t, t_0) = \delta(t - t_0), \\ X(\omega, t_0) = \exp(i\omega t_0), \end{cases} \tag{10.16}$$

and at the output

$$\begin{cases} y(t, t_0) = h(t - t_0, t), \\ Y(\omega, t_0) = \int_{-\infty}^{\infty} \mathrm{d}t\, h(t - t_0, t) \exp(i\omega t). \end{cases} \tag{10.17}$$

The random output signal $y(t, t_0)$ is a delta pulse, as follows from Fourier transformation of (8.1) with (4.7):

$$y(t, t_0) = -D_0^{-1} \delta[t - t_0 - \tau_s + 2 \cos\theta_s \zeta(t_s)/c_0]. \tag{10.18}$$

The average arrival time equals $t_0 + \tau_s$, the actual time fluctuates around that instant in a random fashion with Gaussian distribution (zero mean value, and standard deviation b_s).

10.3.2 Mean values

It follows from (10.17) that

$$\begin{cases} < y(t, t_0) > = h_d(t - t_0), \\ < Y(\omega, t_0) > = H_d(\omega) \exp(i\omega t_0). \end{cases} \tag{10.19}$$

So in the mean we have a Gaussian pulse at the output, centered at $t = t_0 + \tau_s$ (see (6.11)). This Gaussian shape is caused by the Gaussian distribution of the random arrival time of the output delta pulse. The average output spectrum is identical to the transfer function of the deterministic part of the filter, with a phase shift of ωt_0.

10.3.3 Second order moments in general

Two delta functions are applied at the input, one at time t_1 and the other at time t_2. The output signals are measured at the instants of time t and t', the spectra are observed for the frequencies ω and ω'. In this way we can study $< y(t, t_1) y(t', t_2) >$ and $< Y(\omega, t) Y^*(\omega', t_2) >$. First we derive their formulae

$$< y(t,t_1)y(t',t_2) > = B_h(t-t_1, t'-t_2, t'-t),$$
$$< Y(\omega,t_1)Y^*(\omega',t_2) > = \exp[i(\omega t_1 - \omega' t_2)] \tag{10.20}$$
$$\times \int_{-\infty}^{\infty} d\tau_1 \int_{-\infty}^{\infty} d\tau_2 B_h(\tau_1, \tau_2, \tau_2-\tau_1+t_2-t_1)\exp[i(\omega\tau_1+\omega'\tau_2)].$$

The integral for $< YY^* >$ cannot be written in terms of B_H, because the third variable of B_h contains the integration variables τ_1 and τ_2. For this reason we shall concentrate our attention on the time-correlation function.

10.3.4 Time correlation

When $t_1 = t_2 = t_0$ we can study the time correlation of the output signal from

$$< y(t,t_0)y(t',t_0) > = B_h(t-t_0, t'-t_0, t'-t) \tag{10.21}$$

with (8.10) and Fig. 8.5. The observation times t and t' have to be taken close to $t_0+\tau_s$ to find some correlation.

Two input delta pulses, observed at the output at time t, give a correlation function

$$< y(t,t_1)y(t,t_2) > = B_h(t-t_1, t-t_2, 0). \tag{10.22}$$

This function is zero, unless $t_1 = t_2 = t_0$ (see (8.11)), in which case it assumes the value infinity. In practice this correlation function is therefore of little interest.

10.4 Arbitrary input signals

For an arbitrary input signal $x(t)$, with spectrum $X(\omega)$, the output signal and its spectrum can only be described by using the input-output relations of Chapter 4:

$$y(t) = \int_{-\infty}^{\infty} d\tau\, x(t-\tau)h(\tau,t)$$
$$= \frac{1}{2\pi}\int_{-\infty}^{\infty} d\omega\, X(\omega)H(\omega,t)\exp(-i\omega t) \tag{10.23}$$

and

$$Y(\omega) = \int_{-\infty}^{\infty} dt \int_{-\infty}^{\infty} d\tau\, x(t-\tau)h(\tau,t)\exp(i\omega t). \tag{10.24}$$

Average values result from these expressions when the system functions are replaced by their mean values. For the second order moments we can derive complicated integrals that involve the system correlation functions B_H, B_h and B_e. They can only be evaluated when x or X is specified.

10.5 Summary

The question of what statistical properties the output signals have, has been answered in this chapter for

- harmonic input signals,
- delta pulses at the input.

The results can be summarized as follows.

10.5.1 Harmonic input signals

A harmonic or monochromatic input signal $x(t, \omega) = \exp(-i\omega t)$ produces an output signal that differs from the input only in one respect: it has a phase that fluctuates randomly. In the domain of coherent scattering ($\chi \leqslant 0.2$) it is quasi-harmonic. The distribution of the phase fluctuations is Gaussian, but in the domain of incoherent scattering ($\chi > 2$) it is practically uniform.

The mean value of the output signal shows a decrease in amplitude that is frequency-dependent:

$$< y(t, \omega) > = -D_0^{-1} \exp(-\tfrac{1}{2}\chi^2) x(t-\tau_s, \omega). \tag{10.25}$$

The standard deviation of the complex amplitude is given by

$$\sigma(\omega) = D_0^{-1}\{1-\exp(-\chi^2)\}^{\frac{1}{2}}. \tag{10.26}$$

For $\chi \leqslant 0.2$ the time correlation of the surface elevation is directly present in the output signal, whereas the surface wave spectrum can be distinguished in the output variance spectrum. These properties are lost with increasing roughness. Loss of coherence with increasing roughness is also indicated by the fact that the "coherent bandwidth" becomes narrower as χ gets larger.

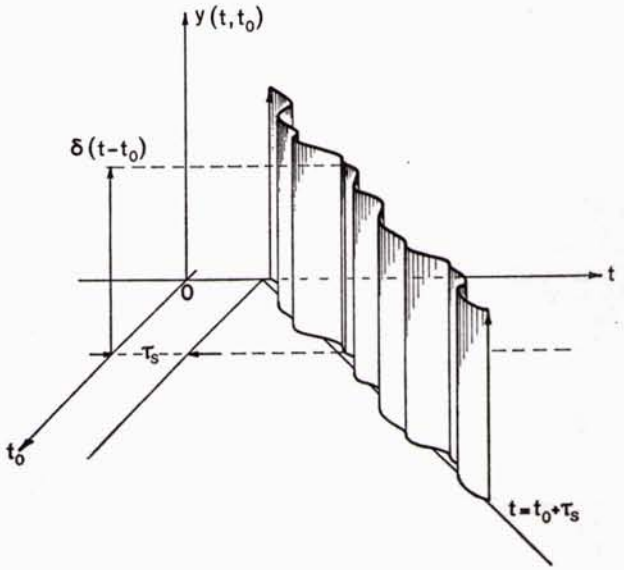
10.5.2 Delta functions

An input signal $x(t, t_0) = \delta(t-t_0)$ gives at the output a delta pulse with an arrival time that fluctuates around the value $t_0+\tau_s$, with Gaussian distribution (see Fig. 10.7). The average of this fluctuating delta pulse is a Gaussian pulse:

$$< y(t, t_0) > = -(b_s D_0 \sqrt{2\pi})^{-1} \exp\left[-\tfrac{1}{2}\left(\frac{t-t_0-\tau_s}{b_s}\right)^2\right]. \tag{10.27}$$

Also the correlation function has a Gaussian character. Its significance is lost when one delta pulse is transmitted and the output signal is observed at one instant of time only.

Fig. 10.7.
The output signal $y(t,t_0)$ when the input signal is a delta function: $x(t,t_0) = \delta(t-t_0)$.



References

10.1 A. PAPOULIS, *Probability, Random Variables and Stochastic Processes* (McGraw-Hill, New York, 1965).

11

discussion of the results



CHAPTER 11

DISCUSSION OF THE RESULTS

11.1 Introduction

The foregoing chapters have produced theoretical results that can be divided into two parts. First of all, we have found that the stationary phase approximation (also called specular point approximation), although basically developed for high frequencies, can be used over a broad frequency range when practical cases are considered. This conclusion is based on an analysis of mean value and variance of the transfer function of the surface channel. In the second place the correlation in frequency, time, and space of the scattered field has been examined for many combinations of transmitter-receiver geometry, wind speed, and wind direction. A rather large number of drawings and tables has been the result. Two types of sound source have been used in that examination: the monochromatic and the broadband (impulsive) transmitter, both radiating omni-directionally. Also the receivers have been assumed to possess equal sensitivity in all directions.

In order to be able to express a judgement about the validity and usefulness of the above mentioned theoretical results, experimental data are required for comparison. Several reasons, however, make it difficult to find material that is suitable for comparison:

1. *Ensembles* of data would be required for the computation of statistical averages. But at sea these ensembles are hard to collect, because fixation of the geometry (stable platforms) is almost impossible. As a consequence, this fact puts a limitation on the confidence level of experimental data.[16]
2. Unless explosives are employed, the sound sources are not usually omni-directionally radiating.
3. At sea the geometry can be held approximately constant when backscattering is measured. But then we are limited to the mono-static case ($X_R = 0$).
4. Another way to fix the geometry, and – in addition – to control all other parameters involved, consists in model tank experiments. However, for this kind of experiment only directional sources and receivers are available. For the purpose of comparison with our model, we have to select the data dealing with specular scattering and reflection. Moreover, there is the basic question about the usefulness of model studies for the prediction of surface scattering and reflection in the true ocean.
5. Our model employs the Pierson-Moskowitz spectrum and its derivatives to

[16] The validation of data, necessary before reliable statistical conclusions can be drawn, has only recently been taken into account [*11.1*]. This could be done because it concerns a study of a lake surface where the transmitter and receiver could be rigidly fixed.

characterize the sea surface. That spectrum applies to a fully developed sea, and needs the wind speed as an input parameter. In many experiments at sea the environment is described very poorly, e.g. by sea state or wind speed, without indication about the state of development of the surface waves.

These remarks suffice to explain why the amount of experimental data available to check our theoretical work is small and incomplete, notwithstanding the fact that many experiments have been reported (see Chapter 2). Summarizing the difficulties, it can be said that of the existing literature on field work only those papers may be useful that deal with

a. Explosive sources;
b. Directional sources, together with the measurement of *specular* scattering;
c. Directional sources, together with the measurement of *backscattering* in a monostatic geometry. (This is a special case of specular scattering, namely with $\theta_s = 0$).

Another possibility for comparison is offered by the theoretical results of other workers. But again we have to search for theoretical models that involve omnidirectional sources, or directional transmitters in combination with the specular case. Moreover, agreement with the results of other theories does not necessarily signify agreement with reality; it only enhances the confidence that one can have in our theory as a tool for the prediction of the scattering phenomenon.

In this chapter both experimental and theoretical material will be employed to back up our theoretical results. This verification will take place in three steps: First of all the validity of the specular point approximation will be checked (Section 11.2), then the mean value of some system functions will be discussed (Section 11.3), and finally the correlation functions in time, frequency and space are examined (Section 11.4). Also a few other subjects deserve some comments; these can be found in Section 11.5. Finally, in Section 11.6, we will try to answer the question of which of our results can be verified best by experiment.

11.2 The validity of the specular point formula

The analysis of mean value (Chapter 6) and variance (Chapter 7) of the transfer function $H(\omega, t)$ of the sea surface leads to the conclusion that (a) numerical integration over the whole surface (this is basically the Helmholtz integral, in which the scattered field is expressed as a weighted summation of the contributions of omnidirectionally radiating point sources induced at the surface) and (b) approximation of the surface integral by means of the stationary phase method, yield about the same results. This is somewhat surprising given the complexity of the underlying theory, although we have to admit that at one stage of the analysis the stationary phase technique has been used, namely in the approximation of Ψ, the weighting function.

As a consequence of the foregoing conclusion, the first and second order statistical moments of H can be described, in many practical cases, by relatively simple formulae:

Mean value

$$H_d(\omega) = -D_0^{-1} \exp(ikD_0 - \tfrac{1}{2}\chi^2); \tag{11.1}$$

Variance

$$< |H_r(\omega, t)|^2 > = D_0^{-2}[1 - \exp(-\chi^2)]. \tag{11.2}$$

Confirmation of (11.1) can be found in the theoretical work of many authors:

BECKMANN and SPIZZICHINO [*11.2, p. 81*] gave a formula for the average normalized specular reflection that is equal to (11.1) when the factor $D_0^{-1} \exp(ikD_0)$ is dropped. They also derived a formula for the mean coherently scattered power [*11.2, p. 88*] that is – apart from a normalizing factor – equal to $|H_d|^2$.

CLARKE [*11.3*] computed the coherent acoustic intensity at the receiver after acoustic energy is radiated by a transmitter with arbitrary directivity and reflected by a rough random surface. His results [*11.3, p. 290*] reduce to

$$q_r \Big|_{\text{coh}} = D_0^{-2} \exp(-\chi^2) \tag{11.3}$$

for an omni-directional source that radiates unit total power. This is equal to $|H_d|^2$.

VENETSANOPOULOS and TUTEUR [*11.4, p. 1102*] found an expression proportional to (11.1) when considering the first-order statistics of the surface channel.

BOYD and DEAVENPORT [*11.5, p. 794*] assumed a directional source and found a formula for the mean scattered pressure that is proportional to (11.1).

The theoretical models used by these authors are all based on the Kirchhoff approximation, or on the variant developed by Eckart (see Section 2.2-IIIB.1). So we arrive at the conclusion that the theory here presented leads, in first approximation (i.e. using only H_0), to the same result as the Eckart theory. This agrees with the statement of SPINDEL and SCHULTHEISS [*11.6, p. 1817*] that Eckart's scattering model gives

$$E\{H(\omega, t)\} = \exp(-2k^2h^2 \cos^2\theta_s). \tag{11.4}$$

Two points of difference can be noted, however:

1. The validity of our results is not restricted to high frequencies, but includes in practice the frequency range from 0 to ∞. This is important, because only then is Fourier transformation of $H(\omega, t)$ allowed.
2. The way in which these results have been derived is entirely different: instead of making an a priori assumption about the derivative of the total field at the boundary ($\partial p/\partial n = 2\partial p_0/\partial n$, the Kirchhoff approximation), we have maintained so much rigour in our analysis that we obtained the Eckart results only as a first approximation. Improvement is possible by adding more terms of the series for H, or by studying H from (5.12), without series expansion. This last possibility may prove difficult in practice, because the statistical moments require integration over the joint probability density function of ζ, ζ_x and ζ_y.

The variance, as given in (11.2), can be regarded as the intensity of the incoherently scattered field. Addition of (11.2) and the square of (11.1) shows that the total amount of scattered power is proportional to D_0^{-2}, and independent of time and frequency, and of the surface statistics. This result can be derived in a more straightforward way by looking at H, the sum of H_d and H_r. Within the present approximation its formula is given by (8.1):

$$H(\omega, t) = -D_0^{-1} \exp\left[ikD_0 - i2k\cos\theta_s \zeta(\mathbf{R}_s, t_s)\right]. \tag{11.5}$$

Formula (11.5) describes a spherical wave that suffers from phase distortions. Its average intensity at a point on a sphere with radius D_0 equals

$$< |H(\omega, t)|^2 > = D_0^{-2}; \tag{11.6}$$

this is the same as the intensity on such a sphere in the case of a perfectly flat boundary, which signifies that our theory does respect the law of energy conservation. It also says that the surface focussing has no preferred direction. Experimental work performed at the SACLANT ASW Research Centre by WIJMANS [*11.7*] confirms this, at least for not too large values of h, and also ADLINGTON [*11.8*] reported that the scattered energy is independent of grazing angle and wind speed.

Specular reflection has been measured by WELTON *et al.* [*11.9*]. Their results show that there is no dependence on grazing angle and hardly on frequency. They do find, on the other hand, that the surface statistics (i.e. h) have some influence. A possible explanation of the discrepancy between this last result and our model may be found in the fact that the surface slopes are not included in H_0, the approximation of H on which our simplified model is based.

WELTON and his co-workers [*11.9*] also investigated the influence of the geometry. They found a $(1/D_0)$ – law (geometrical acoustics) rather than a $(w_T w_R)^{-1}$ – dependency. This proves the validity of what they call the "image solution" and what we have named "specular point approximation".

From the foregoing discussion our approximation emerges as a valid and useful way to describe the first and second order statistical moments of the scattered field. Nevertheless, physical arguments can be found that suggest its breakdown under certain circumstances:

1. When the frequency of the incident sound is high and the slopes of the surface are steep enough, there can be more than one surface point that produces specular reflection. This so called "multipath effect" has been found experimentally (also for slopes that are allowed in our model) and is discussed in Section 5.2.
   It is not predicted by (11.1) and (11.2), but it could be included to a certain extent in our theory via H_1, H_2 etc., the terms in the expansion of H that were discarded in Section 5.4 and that involve the surface slope.

2. In Section 9.4 it was indicated that the specular point formula predicts "frozen" wave fronts. But this comes in conflict with the well-known physical fact that the sound rays are propagating along paths that are perpendicular to the wave fronts. Hence it can only be true locally, and during a short time.

11.3 Mean values of system functions

The expectation of system functions is not a quantity often encountered in experimental studies: only one paper has been found that deals with this subject, namely the one by SPINDEL and SCHULTHEISS [*11.6*]. It describes a model tank experiment with a wind-driven surface, and the measurements were concentrated on the impulse response of the surface channel. Typical results for the average impulse response function are copied in Fig. 11.1. They indicate a Gaussian pulse, as predicted by the

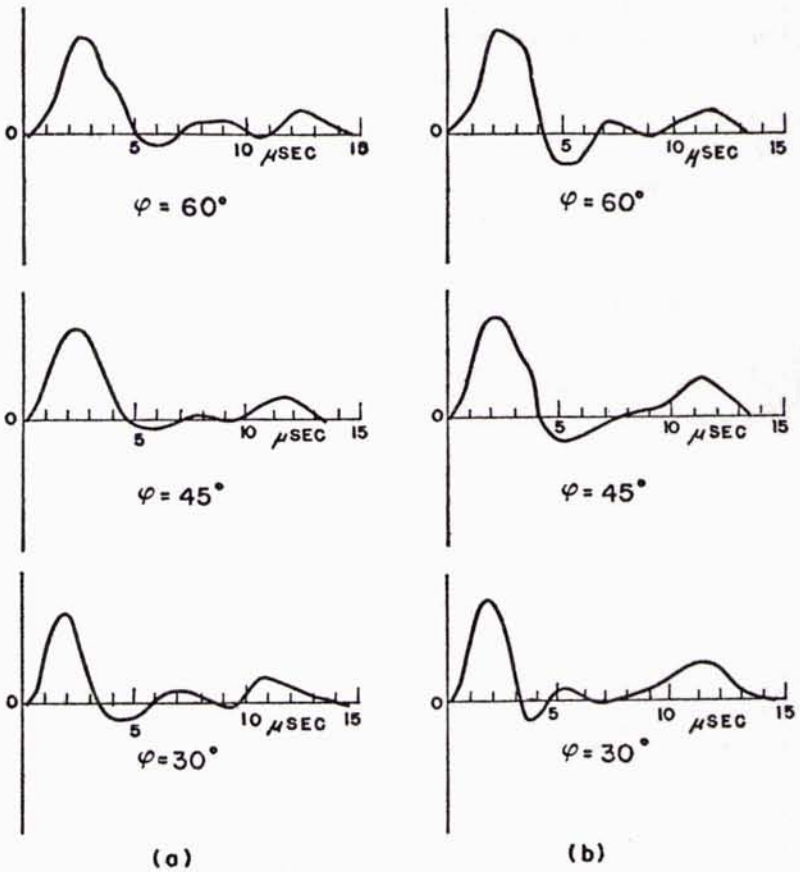


Fig. 11.1. Ensemble averages of the impulse response, found experimentally by SPINDEL and SCHULTHEISS [*11.6*]; (a) cross-wind, (b) down-wind direction.

Fourier transform of H_d (c.f. (6.11)), followed by one or two smaller peaks. This tail shows that our model is not complete. This point is also brought out in the analysis of H_d, where the agreement between (11.1) and the data is reasonably good but not perfect. It should be noted, however, that the experimental surface had a wave spectrum with a peak at ~ 6 Hz. This is much higher than at sea (see Table 10.2), so that perhaps the experiment falls outside the validity domain of our model.

As for the leading Gaussian pulse, (10.27) gives us an estimate for the width. The turning points of the curve for $< y >$ occur at $T = \pm 1$, where $T = (t - t_0 - \tau_s)/b_s$. If we define the width as the time that elapses between these two points, we get a pulse width in real time equal to $2b_s$. Looking in Table 6.2 we see that for low wind speeds, values of the order of a few μseconds follow. This agrees pretty well with Fig. 11.1.

11.4 Examination of correlation functions

11.4.1 Time correlation and frequency spread

In this sub-section we are dealing with the results that were derived in Chapter 10 for harmonic input signals. Their essence is described in Sub-Section 10.5.1, together with Figs. 8.3 and 8.4.

In the case of a monochromatic input signal, our theory predicts an output signal with a time-correlation function in which the time correlation of the surface elevation

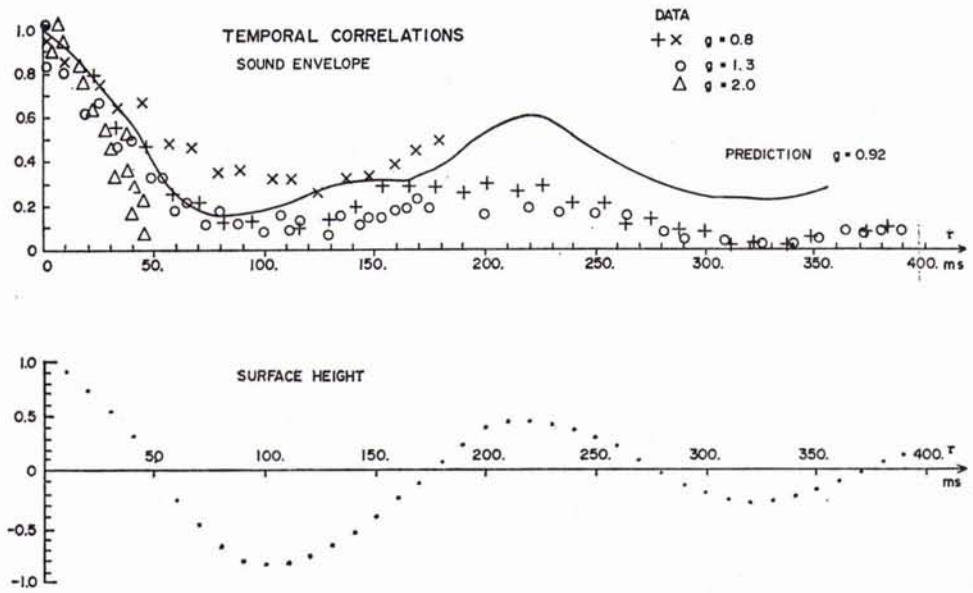


Fig. 11.2. Comparison between the measured time-correlation functions of the scattered sound field and the surface elevation (from MEDWIN and CLAY [*11.11*]; their parameter g equals 2χ).

can be distinguished clearly (see Fig. 8.3). The similarity between both correlation functions is better the lower the value of χ. This theoretical result is completely confirmed by the experimental work of GULIN and MALYSHEV [*11.10*] for $\chi = 0.52$, 0.74 and 1.4 and a sea surface with swell, and by that of MEDWIN and CLAY [*11.11*] for $\chi = 0.9$, 1.1 and 1.4 and a large laboratory "sea". Fig. 11.2 gives an illustration.

The frequency spread of the output signal is represented by the side-bands around the transmitted frequency. According to our theory these side-bands have the same shape as the surface wave spectrum when χ is less than 0.2, and the peak frequency differs from the centre frequency by an amount Δf equal to the peak frequency of the surface wave spectrum. With increasing roughness, the side-bands broaden and gradually lose their resemblance to the surface wave spectrum. Experimental confirmation of these predictions can be found in the work of KINGSBURY [*11.12*] for $0.4 < \chi < 4$ and in that of RODERICK and CRON [*11.13*] for $\chi = 0.4$ and 0.8.

SPINDEL and SCHULTHEISS [*11.6*] studied the bi-frequency function $e(\omega, \Omega)$. Its correlation function shows a peak that coincides with the peak in the spectrum of the surface waves, which agrees with our Fig. 8.4.

11.4.2 Frequency correlation and time spread

Next we consider the results of Chapter 10 that were obtained for delta pulses at the input. They are summarized in Sub-Section 10.5.2. Agreement on the basis of mean values of the predicted time spread (amounting to a few μseconds) with experimental data collected by SPINDEL and SCHULTHEISS [*11.6*] has been mentioned already in Section 11.3. For the second order statistical moments dealing with frequency correlation and time spread, no data have been found, which is not surprising in view of the remark at the end of Sub.-Section 10.5.2.

11.4.3 Spatial correlation

GULIN and MALISHEV [*11.14*] have studied the correlation in X-, Y-, and Z-direction. They used CW-pulses ($f = 4$, 7, and 15 kHz, or $k \cong 16$, 20, and 60 m^{-1}), the sea surface had a standard deviation h with values between 0 and 40 cm, $Z_T = 80$ m, $Z_R = 30$–60 m, and $X_R = 600$–700 m. They concluded [*11.14, p. 368*] that:[17]

1. "The signal amplitude spatial correlation coefficient in the case of small values of the Rayleigh parameter usually takes the form of damped-oscillation functions. (...) The oscillation period is related to the average wavelength of the water waves on the sea surface.
2. In the case $kh > 1$ a more abrupt drop in the correlation coefficient is observed, and the quasi-periodic behaviour disappears.
3. The vertical spatial correlation for amplitude fluctuations, at small grazing angles of incidence, decays much more rapidly than the horizontal correlation."

---

[17] The Rayleigh parameter is identical with χ, the roughness parameter.

This is in qualitative agreement with Figs. 9.5, 9.6 and 9.7.

The vertical transversal correlation has been analyzed by MEDWIN and CLAY [*11.11*]. Their results, for $\chi = 0.15$, 0.4 and 1.0, show the same tendencies as Fig. 9.2.

11.5 Various comments

11.5.1 Coherence functions

When the statistical characteristics of an acoustic field scattered by a randomly rough surface are studied, one of the quantities of interest is often the coherence of the scattered field. Usually, for stationary processes, a measure of the coherence in the scattered field is defined by [*11.15, p. 501*]:

$$\gamma_{12}(\Delta) = B_{12}(\Delta)[B_{11}(0)B_{22}(0)]^{-\frac{1}{2}}, \tag{11.7}$$

where the subscripts 1 and 2 refer to two observations of the scattered field, and Δ is some quantity that separates the two observations. If, for instance, $\Delta = \varrho$, we are dealing with *spatial* coherence; *temporal* coherence follows from $\Delta = \Delta t$, whereas *frequency* coherence can be studied by taking $\Delta = \Delta\omega$.

It is also possible that the subscripts indicate input and output signal, or spectrum, of a filter. This is the interpretation of WIJMANS [*11.7*]. Still another definition that produces useful results is presented by NOVARINI and CARUTHERS [*11.16*]. They compare the scattered field with the field coming from a perfectly plane surface.

With the material presented in Chapters 8–10, any kind of coherence function can easily be computed. The results will not differ essentially from ours, because (11.7) provides merely a normalization of the correlation functions we have analyzed.

11.5.2 Amplitude fluctuations

In experiments at sea that have long CW-pulses as input signals, both amplitude and phase fluctuations can be observed. Only the latter are predicted by our theory (see (8.1)). A possible explanation of the experimental amplitude fluctuations may be found in the instability of the transmitter-receiver configuration.

11.5.3 The joint probability density of the surface elevation

The statistical description of the sea surface employed in this study, is based on the assumption that the surface elevation is a Gaussian process in space and time (*Assumption 4*). But "measurements of the two-dimensional wave height probability distribution of wind-driven waves in a model tank", performed by SPINDEL and SCHULTHEISS, "suggest that the use of bi-variate Gaussian statistics in acoustic scattering computational approximation may be less realistic than assuming Gaussian behaviour in only one dimension" [*11.17, p. 1065 – abstract*].

11.6 Suggested experiments

The main problem for the experimentalist who wants to study the scattering of underwater sound waves from the sea surface, is caused by the necessity of fixing the geometry of transmitter and receiver. This is so because when measuring fluctuations, he wants to be sure that these are indeed introduced by the surface, and not by the swinging of transducer and/or receiver(s) down below a ship, at the far end of a cable. Reduction of this basic problem is possible, to a limited extent, by mounting transmitter and receiver on the same cable so that T and R are equally effected by the ship movements. The possibility to study the influence of the geometry is lost in this way, because now $\theta_s = 0$.

One way to solve the foregoing problem is offered by model tank experiments, but they have the disadvantage that one has to determine how representative they are for the true ocean.

Another possibility could be found in sources and receivers that are bottom mounted, for instance on the continental shelf, or mounted on cables anchored at the bottom and kept vertical by a buoy floating on the surface.

The simplest way to use such an arrangement is by driving it with CW-pulses of variable frequency, and generating ensembles of output signals by taking sets of, say, 30 pulses for each experiment. In this way the time- and frequency-correlation functions can be established as functions of the roughness parameter. Especially for low values of χ this would be interesting, if concurrently the temporal correlation function of the surface is measured (or its Fourier transform, the surface wave spectrum).

If more than one transmitter signal is available in the foregoing fixed set-up, the coherent bandwidth can easily be measured. This is done by transmitting simultaneously two CW-pulses, one with frequency ω, the other with frequency $\omega+\Delta\omega$, and varying $\Delta\omega$ after every set of pulses.

The space-correlation functions can be mesaured by providing an array of hydrophones on the receiver side. A problem is caused, however, by the requirement that the orientation of such an array with respect to the transmitter is known.

11.7 Summary

The theoretical results derived in the preceding chapters have been commented on and compared with material found in the literature, both of experimental and theoretical nature. It turned out that our specular point formula is in essence equivalent to the Kirchhoff-Eckart approximation, albeit that the derivation is entirely different.

Little experimental data is available for comparison, mainly due to the fact that generation of ensembles of output signals that allow for a statistical treatment is almost impossible. Nevertheless, for the essential results of our theoretical work, confirmation could be found, especially in the domain of coherent scattering.

Suggestions for further experimental work have been given. A crucial point in this respect is the availability of a fixed geometry so that *ensembles* of data can be generated.

References

11.1 T. D. PLEMONS, J. A. SHOOTER and D. MIDDLETON, "Underwater Acoustic Scattering from Lake Surfaces. I. Theory, Experiment, and Validation of the Data", J. Acoust. Soc. Amer. **52**, 1487–1502 (1972).

11.2 P. BECKMANN and A. SPIZZICHINO, *The Scattering of Electromagnetic Waves from Rough Surfaces* (Macmillan, New York, 1963).

11.3 R. H. CLARKE, "Coherent Reflection by the Rough Sea Surface of the Acoustic Field from a Source of Arbitrary Directivity", J. Acoust. Soc. Amer. **52**, 287–293 (1972).

11.4 A. N. VENETSANOPOULOS and F. B. TUTEUR, "Stochastic Filter Modeling for the Sea-Surface Scattering Channel", J. Acoust. Soc. Amer. **49**, 1100–1107 (1971).

11.5 M. L. BOYD and R. L. DEAVENPORT, "Forward and specular scattering from a rough surface: theory and experiment", J. Acoust. Soc. Amer. **53**, 791–801 (1973).

11.6 R. C. SPINDEL and P. M. SCHULTHEISS, "Acoustic Surface-Reflection Channel Characterization through Impulse Response Measurements", J. Acoust. Soc. Amer. **51**, 1812–1824 (1972).

11.7 W. WIJMANS, "An Experimental Study of Forward Scattering and Reflection of Underwater Sound Waves from the Rough Sea Surface", SACLANT ASW Research Centre, Tech. Rep. (to be published).

11.8 R. H. ADLINGTON, "Acoustic-Reflection Losses at the Sea Surface, Measured with Explosive Sources", J. Acoust. Soc. Amer. **35**, 1834–1835 (L) (1963).

11.9 P. J. WELTON, H. G. FREY and P. MOORE, "Experimental Measurements of the Scattering of Acoustic Waves by Rough Surfaces", J. Acoust. Soc. Amer. **52**, 1553–1563 (1972).

11.10 É. P. GULIN and K. I. MALYSHEV, "Statistical Characteristics of Sound Signals Reflected from the Undulating Sea Surface", Sov. Phys.-Acoust. **8**, 228–234 (1963).

11.11 H. MEDWIN and C. S. CLAY, "Dependence of Spatial and Temporal Correlation of Forward-Scattered Underwater Sound on the Surface Statistics. II. Experiment", J. Acoust. Soc. Amer. **47**, 1419–1429 (1970).

11.12 F. J. KINGSBURY, "An Experimental Model Study of Underwater Acoustic Scattering from a Wind-Driven Surface", Naval Underwater Systems Centre, Rep. No. NL-3021 (1970).

11.13 W. I. RODERICK and B. F. CRON, "Frequency Spectra of Forward-Scattered Sound from the Ocean Surface", J. Acoust. Soc. Amer. **48**, 759–766 (1970).

11.14 É. P. GULIN and K. I. MALYSHEV, "Experiments in the Spatial Correlation of the Amplitude and Phase Fluctuations of Acoustic Signals Reflected from a Rough Ocean Surface", Sov. Phys.-Acoust. **10**, 365–368 (1965).

11.15 M. BORN and E. WOLF, *Principles of Optics* (Pergamon, Oxford, 1970).

11.16 J. C. NOVARINI and J. W. CARUTHERS, "The Degree of Coherence of Acoustic Signals Scattered at Randomly Rough Surfaces", J. Acoust. Soc. Amer. **51**, 417–418 (1972) (L).

11.17 R. C. SPINDEL and P. M. SCHULTHEISS, "Two-Dimensional Probability Structure of Wind-Driven Waves", J. Acoust. Soc. Amer. **52**, 1065–1068 (1972) (L).

12

conclusions



CHAPTER 12

CONCLUSIONS

The following conclusions can be drawn from the study presented in this thesis. They are subject, where such applies, to the validity of the assumptions listed on page 13.

1. The phenomenon of scattering and reflection of underwater sound waves from the randomly rough sea surface can be successfully studied by considering the surface channel as a random, linear, time-dependent filter.

2. This filter can be divided into a *deterministic* part and a purely *random* part. These two sections are connected in parallel.

3. *Meecham's* perturbation method is a useful technique to solve the wave equation with the *Dirichlet* condition of zero total pressure on the boundary.

4. Its result is complicated. But for wind speeds not exceeding 10 m/s and specular grazing angles larger than 6°, the formula for the transfer function of the filter reduces to the same simple expression as the one that follows from the *Kirchhoff-Eckart theory.*

5. This *Kirchhoff-Eckart formula* can be applied – under the foregoing conditions – over the whole frequency domain of interest (0–20 kHz). It indicates that specular and omni-directional scattering and reflection produce identical results: only the specular point is important; the contribution from surrounding points cancel each other.

6. The statistical properties of the sea surface can be distinguished in the output of the random filter, if a harmonic input signal is used and χ is less than 1: the time-correlation function of the output *signal* reflects the time-correlation function of the surface elevation, the output variance *spectrum* shows the surface wave spectrum.

7. Narrowband signals are transmitted without distortion if their relative bandwith $2\Delta f/f$ is smaller than $2.3/\chi$.

8. A delta pulse propagating through the channel suffers only from fluctuations in the arrival time. These fluctuations have a Gaussian probability density with zero mean value and standard deviation equal to $2h \cos \theta_s/c_0$.

9. Also the space-correlation functions of the scattered field reflect the statistical properties of the surface when $\chi \leqslant 1$: the transversal and the horizontal correlation functions have the same shape as the spatial correlation function, the longitudinal correlation function resembles the time-correlation function of the surface elevation.

10. The sea surface has no preferred direction for scattering and reflection of underwater sound waves, when it is insonified by an omni-directional source.

11. Available experimental data confirm the conclusions 4, 5, 6, 9 and 10.

12. For the collection of ensembles of experimental data to check further the theoretical work here presented, it is essential to employ an arrangement of transmitter and receiver(s) that is rigidly fixed. Such an installation does not seem to be available at present.

acknowledgements

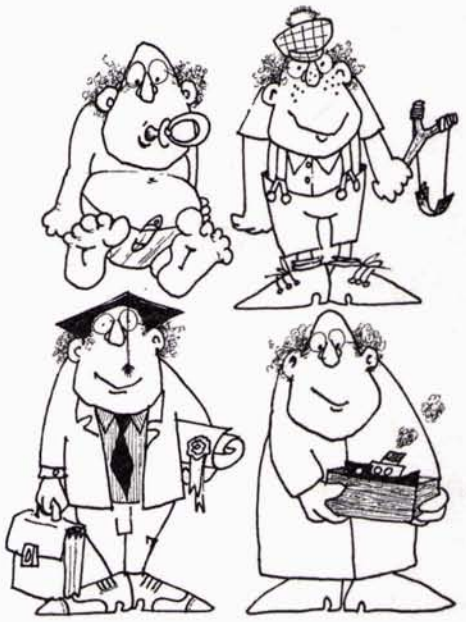


ACKNOWLEDGEMENTS

The author is very grateful to Prof. B. W. CONOLLY, Dr. R. H. CLARKE and Ir. H. R. KROL for the scientific discussions he had with them and the help he received from them during the preparation of this report, to Mr. F. FAGGIONI for the care and the talent with which he produced most of the scientific drawings and diagrams, to Mr. E. CAPRIULO for the assistance he gave in writing and running the necessary computer programs, and to Mr. J. P. BETHEL for editing the manuscript and turning "translated Dutch" into correct English.

Also the financial support for the printing of this thesis, received from the SACLANT ASW Research Centre, is highly appreciated and therefore gratefully acknowledged.

curriculum vitae



CURRICULUM VITAE

LEONARD FORTUIN was born in Meppel (The Netherlands) on April 7, 1937. After having obtained the *HBS-B diploma* from the *Openbaar Lyceum* in his home town, he started his studies at the Technical University of Delft, in September 1955. From the department of electrotechnical engineering he received the master-of-science degree (*elektrotechnisch ingenieur*) in October 1961.

As a warrant officer (*vaandrig*) he fulfilled his military duty from March 1962 until September 1963 with the Royal Dutch Army Artillery Experimental Board (*Commissie van Proefneming*) in The Hague. He was in charge of a mobile Doppler radar installation.

From October 1963 until October 1973 he was employed by the SACLANT ASW Research Centre at La Spezia (Italy) as a research scientist. At present he is with Corporate I.S.A., a division of the *N.V. Philips' Gloeilampenfabrieken*, at Eindhoven (The Netherlands).

He is married and has two daughters.

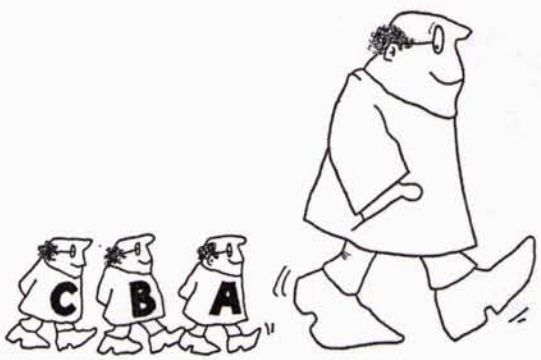
LEONARD FORTUIN werd geboren te Meppel op 7 april 1937. Nadat hij aan het Openbaar Lyceum in zijn geboorteplaats het diploma HBS-B had behaald, begon hij zijn studie aan de Technische Hogeschool te Delft, in september 1955. Van de afdeling Elektrotechniek ontving hij het ingenieursdiploma in oktober 1961.

Zijn militaire dienstplicht vervulde hij als vaandrig bij de Commissie van Proefneming in Den Haag. Daar was hij belast met de zorg voor een mobiele Doppler radar installatie.

Van oktober 1963 tot oktober 1973 werkte hij bij het SACLANT ASW Research Centre in La Spezia (Italië) als *research scientist*. Thans is hij werkzaam bij Corporate I.S.A., een onderdeel van de N.V. Philips' Gloeilampenfabrieken, te Eindhoven.

Hij is gehuwd en heeft twee dochters.

appendices



APPENDIX A

Some derivatives of ζ

Formulae for the variances of the first and second order derivatives of the surface elevation follow from (3.3), (3.4) and (3.5) as limits:

$$\begin{aligned} <\zeta_x^2> &= -h^2 \lim_{\xi \to 0} \partial^2 \Phi(\xi,0,0)/\partial \xi^2, \\ <\zeta_y^2> &= -h^2 \lim_{\eta \to 0} \partial^2 \Phi(0,\eta,0)/\partial \eta^2, \end{aligned} \tag{A.1}$$

$$\begin{aligned} <\zeta_{xx}^2> &= h^2 \lim_{\xi \to 0} \partial^4 \Phi(\xi,0,0)/\partial \xi^4, \\ <\zeta_{yy}^2> &= h^2 \lim_{\eta \to 0} \partial^4 \Phi(0,\eta,0)/\partial \eta^4, \end{aligned} \tag{A.2}$$

$$\begin{aligned} <\zeta_t^2> &= -h^2 \lim_{\tau \to 0} \partial^2 \Phi(0,0,\tau)/\partial \tau^2, \\ <\zeta_{tt}^2> &= h^2 \lim_{\tau \to 0} \partial^4 \Phi(0,0,\tau)/\partial \tau^4. \end{aligned} \tag{A.3}$$

Before we can actually use these relations, we have to compute the spatial correlation function Φ for small values of ξ and η. To this end we consider (3.12) and note that

$$\begin{aligned} \Phi(\xi,0,0) &= I_1(\xi) - I_2(\xi) \\ \Phi(0,\eta,0) &= I_2(\eta), \end{aligned} \tag{A.4}$$

with I_1 and I_2 defined by (3.13) and (3.14).

Fig. 3.1 indicates that the spectral function $A^2(\omega_s)$ is practically zero, when $\omega_s \geqslant \omega_{sm} = 3g/v$. Therefore we can make the arguments of the Bessel functions in (3.13) and (3.14) as small as we want, by taking values of ξ and η close to zero. Hence J_0 and J_1 can be replaced by the first three terms of their power series expansion, that is [*A.1, p. 360*]

$$\begin{aligned} J_0(z) &= 1 - \tfrac{1}{4}z^2 + \tfrac{1}{64}z^4, \\ \frac{J_1(z)}{z} &= \tfrac{1}{2} - \tfrac{1}{16}z^2 + \tfrac{1}{384}z^4. \end{aligned} \tag{A.5}$$

The first terms of these expansions, substituted into (3.13) and (3.14), yield the value 2 respectively 1 (see (3.11)), so that l_1 and l_2 may be approximated as follows:

$$\begin{aligned} l_1(\varrho) &= 2-4\frac{\varrho^2}{h^2}I_2+6\frac{\varrho^4}{h^2}I_4, \\ l_2(\varrho) &= 1-\frac{\varrho^2}{h^2}I_2+\frac{\varrho^4}{h^2}I_4, \end{aligned} \tag{A.6}$$

in which expressions the constants I_2 and I_4 are defined by

$$\begin{aligned} I_2 &\equiv \frac{1}{16g^2}\int_0^\infty \mathrm{d}\omega_s A^2(\omega_s)\omega_s^4, \\ I_4 &\equiv \frac{1}{384g^4}\int_0^\infty \mathrm{d}\omega_s A^2(\omega_s)\omega_s^8. \end{aligned} \tag{A.7}$$

Using now (A.4), we find

$$\begin{aligned} \Phi(\xi,0,0) &= 1-3\frac{\xi^2}{h^2}I_2+5\frac{\xi^4}{h^2}I_4, \\ \Phi(0,\eta,0) &= 1-\frac{\eta^2}{h^2}I_2+\frac{\eta^4}{h^2}I_4. \end{aligned} \tag{A.8}$$

Then we are ready to perform the operations required in (A.1) and (A.2); they yield

$$\begin{aligned} <\zeta_x^2> &= 6I_2, \\ <\zeta_y^2> &= 2I_2, \end{aligned} \tag{A.9}$$

$$\begin{aligned} <\zeta_{xx}^2> &= 120I_4, \\ <\zeta_{yy}^2> &= 24I_4. \end{aligned} \tag{A.10}$$

The calculation of I_2 and I_4 has to be done by substitution of (3.15) into (A.7), bearing in mind that the upper limit of integration equals ω_{sm}. We obtain

$$I_2 = \frac{C}{16}\int_0^{\omega_{sm}} \mathrm{d}\omega_s \omega_s^{-1}\exp(-0.74g^4/\omega_s^4 v^4), \tag{A.11}$$

$$I_4 = \frac{C}{384g^2}\int_0^{\omega_{sm}} \mathrm{d}\omega_s \omega_s^3\exp(-0.74g^4/\omega_s^4 v^4). \tag{A.12}$$

These integrals can be brought in a tabulated form [*A.1, pp. 228–229*] by using the substitution $t = (\omega_{sm}/\omega_s)^4$. Putting at the same time, for convenience,

$$z = 0.74(g/v\omega_{sm})^4 = 0.009, \tag{A.13}$$

we find

$$\begin{aligned} I_2 &= 0.0005, \\ I_4 &= 0.04v^{-4}. \end{aligned} \tag{A.14}$$

Substitution of these values into (A.9) and (A.10) gives the desired results for the spatial derivatives:

$$\begin{aligned} &<\zeta_x^2> = 0.003, \\ &<\zeta_y^2> = 0.001, \end{aligned} \tag{A.15}$$

$$\begin{aligned} &<\zeta_{xx}^2> = 5v^{-4} \quad (\mathrm{m}^{-2}), \\ &<\zeta_{yy}^2> = v^{-4} \quad (\mathrm{m}^{-2}). \end{aligned} \tag{A.16}$$

The time derivatives follow from (3.9) by performing the operations described in (A.3):

$$<\zeta_t^2> = -\tfrac{1}{2}\int_0^\infty \mathrm{d}\omega_s A^2(\omega_s)\omega_s^2, \tag{A.17}$$

$$<\zeta_{tt}^2> = \tfrac{1}{2}\int_0^\infty \mathrm{d}\omega_s A^2(\omega_s)\omega_s^4. \tag{A.18}$$

The second one is equivalent with $8g^2 I_2$ (see (A.7)). From (A.14) we get therefore:

$$<\zeta_{tt}^2> = 0.4. \tag{A.19}$$

For the calculation of $<\zeta_t^2>$ we substitute (3.15) into (A.17) and get

$$<\zeta_t^2> = -\tfrac{1}{2}Cg^2\int_0^\infty \mathrm{d}\omega_s \omega_s^{-3}\exp(-0.74g^4/\omega_s^4 v^4), \tag{A.20}$$

which becomes

$$<\zeta_t^2> = Cv^2(4\sqrt{0.74})^{-1}\int_0^\infty \mathrm{d}t \exp(-t^2) \tag{A.21}$$

after we have put $t = g^2\sqrt{0.74}/(\omega_s^2 v^2)$. This yields with $C = 8\times 10^{-3}$:

$$<\zeta_t^2> = 0.002v^2. \tag{A.22}$$

References

A.1 M. Abramowitz and I. A. Stegun, *Handbook of Mathematical Functions* (National Bureau of Standards, Washington-DC, 1965).

APPENDIX B

Approximation of Ψ starting from the stationary phase method

We rewrite (5.6) in the following way

$$\Psi(\mathbf{R}) = \frac{i}{8\pi^3}\iint \mathrm{d}\mathbf{K}\iint \mathrm{d}\boldsymbol{\varrho}(K_z/w_T)\exp\left[i\psi(\mathbf{K},\boldsymbol{\varrho})\right] \tag{B.1}$$

where

$$\psi(\mathbf{K},\boldsymbol{\varrho}) = -\mathbf{K}\cdot\boldsymbol{\varrho} + kw_T. \tag{B.2}$$

This phase depends on 4 variables:

$$\psi = \psi(K_x, K_y, \xi, \eta) = -K_x\xi - K_y\eta + kw_T(\xi,\eta); \tag{B.3}$$

w_T is given in (5.5). When k is such that ψ varies rapidly with $\boldsymbol{\varrho}$ and $\mathbf{K}$, the integral will be small because the components of the integrand with different (K_x, K_y, ξ, η) will cancel. However, this cancellation will be minimum at values of $(\mathbf{K}, \boldsymbol{\varrho})$ for which the derivatives of ψ with respect to $\mathbf{K}$ and $\boldsymbol{\varrho}$ are zero. At these points, the points of stationary phase, the mutual cancellation of the sinusoidal waves in the integrand will be least. Consequently, for a given value of k, these points will be dominant [*B.1, p. 392*].

Differentiation of ψ in (B.3) reveals that it is only stationary at the "point" $P(K_x, K_y, \xi, \eta)_s$ for which

$$\begin{aligned} \xi_s &= \eta_s = 0, \\ K_{xs} &= k[x-(Z_T-\zeta)\zeta_x]/w_T, \\ K_{ys} &= k[y-(Z_T-\zeta)\zeta_y]/w_T, \end{aligned} \tag{B.4}$$

where now w_T, ζ and ζ_x, ζ_y have to be evaluated for $\boldsymbol{\varrho} = 0$. According to the stationary phase method, ψ is developed in a Taylor series around the point $P(K_{xs}, K_{ys}, 0, 0)$:

$$\begin{aligned} \psi(K_x, K_y, \xi, \eta) &= \psi(K_{xs}+u, K_{ys}+v, \xi, \eta) \\ &= \psi(K_{xs}, K_{ys}, 0, 0) + \tfrac{1}{2}(\psi_{xx}\xi^2 + 2\psi_{xy}\xi\eta + \psi_{yy}\eta^2 + \ldots). \end{aligned} \tag{B.5}$$

The constants ψ_{xx}, ψ_{xy}, ... etc. are the 16 second derivatives of ψ with respect to two

of the four variables. Investigation of these derivatives shows that more than half of them equal zero; (B.5) reduces to

$$\psi = kw_T + \tfrac{1}{2}(\psi_{xx}\xi^2 + 2\psi_{xy}\xi\eta + \psi_{yy}\eta^2) - u\xi - v\eta. \tag{B.6}$$

With this expansion the integral for Ψ is then approximated in the following way:

$$\Psi(\mathbf{R}) = \frac{i}{8\pi^3}\left(\frac{K_z}{w_T}\right)_s \exp(i\psi_s) \times \int d\xi \int d\eta \int du \int dv \exp\left[\frac{i}{2}(\psi_{xx}\xi^2 + 2\psi_{xy}\xi\eta + \psi_{yy}\eta^2) - iu\xi - iv\eta\right]. \tag{B.7}$$

Only small values of u, v, ξ, and η, both positive and negative, will be significant in the integral. The integration can therefore be taken between the limits $-\infty$ to $+\infty$ [*B.1, p. 396*]. Integration over u and v yields then $4\pi^2\delta(\xi)\delta(\eta)$, which makes the integration over ξ and η very simple. The result is, after evaluation of K_z and ψ at the stationary point:

$$\Psi(\mathbf{R}) = \frac{ik\exp(ikw_T)}{2\pi w_T^2}\sqrt{(Z_T-\zeta)^2(1-\zeta_x^2-\zeta_y^2) + 2(Z_T-\zeta)(x\zeta_x + y\zeta_y)}. \tag{B.8}$$

The square root can be simplified somewhat, because $\zeta_x^2, \zeta_y^2 \ll 1$. Using these inequalities we finally obtain

$$\Psi(\mathbf{R}) = \frac{ik(Z_T-\zeta)\exp(ikw_T)}{2\pi w_T^2}\sqrt{1 + 2\frac{(x\zeta_x + y\zeta_y)}{(Z_T-\zeta)}}. \tag{B.9}$$

For $\zeta = 0$, this reduces to

$$\Psi(\mathbf{R}) = \frac{ikZ_T\exp(ikW_T)}{2\pi W_T^2} \tag{B.10}$$

with $W_T = (R^2 + Z_T^2)^{\frac{1}{2}}$, whereas Ψ_0, the exact solution for the perfectly plane surface, is given by (see [*B.2, p. 28*])

$$\Psi_0(\mathbf{R}) = \Psi(\mathbf{R})\Big|_{\zeta=0} = \frac{Z_T(ikW_T - 1)}{2\pi W_T^3}\exp(ikW_T). \tag{B.11}$$

This reduces to (B.10) if $kW_T \gg 1$, which seems to indicate that our approximation is good in the far field.

The question arises now how good the foregoing approximation (B.9) is, or – in other words – what conditions have to be satisfied for its application. In order to

give an answer to this question we will try to find an upper and a lower limit for Ψ, and require that the approximate solution falls between these two limits. The error is then at most equal to the difference between these bounds. By chosing the parameters involved so that these bounds ly close together, we can keep the error within reasonable limits.

We assume that $kW_T \gg 1$, or $k \geqslant 10/Z_T$. For $Z_T \geqslant 100$ m, this means $k \geqslant 0.1$ m^{-1} or $f \geqslant 25$ Hz. In practice this will always be true. Therefore we can write Ψ_0 as

$$\Psi_0(\mathbf{R}) = \frac{ikZ_T}{2\pi W_T^2} \exp(ikW_T). \tag{B.12}$$

In order to gain some insight in the behaviour of Ψ, we return to (5.6) and expand the factor $\exp(ikw_T)/w_T$ in plane waves. So we get as the starting point of our analysis

$$\Psi(\mathbf{R}) = -\frac{1}{16\pi^4} \iint \frac{\mathrm{d}\mathbf{M}}{M_z} \exp[i\mathbf{M}\cdot\mathbf{R} + iM_z Z_T] \iint \mathrm{d}\mathbf{K} K_z \times \iint \mathrm{d}\boldsymbol{\varrho} \exp[i\boldsymbol{\varrho}\cdot(\mathbf{M}-\mathbf{K}) - iM_z\zeta(\mathbf{R}+\boldsymbol{\varrho})]. \tag{B.13}$$

The dependence of ζ on $\boldsymbol{\varrho}$ makes that the integrals cannot be solved analytically. Therefore we concentrate our attention on the factor $F \equiv \exp[-iM_z\zeta(\mathbf{R}+\boldsymbol{\varrho})]$. We note that two domains of M have to be distinguished: 1) $M \leqslant k$, for which $M_z = (k^2 - M^2)^{\frac{1}{2}}$ is real and F is a unit vector in the complex plane with random phase equal to $M_z\zeta(\mathbf{R}+\boldsymbol{\varrho})$; and 2) $M > k$, for which M_z becomes purely imaginary and F is real and equal to $\exp[\zeta(\mathbf{R}+\boldsymbol{\varrho})\sqrt{M^2-k^2}]$.

In the latter case, when $M > k$, it is easy to see that the following inequality holds:

$$L_1 \leqslant \iint \mathrm{d}\boldsymbol{\varrho} \exp[i\boldsymbol{\varrho}\cdot(\mathbf{M}-\mathbf{K}) - iM_z\zeta(\mathbf{R}+\boldsymbol{\varrho})] \leqslant L_2 \tag{B.14}$$

where

$$\begin{aligned} L_1 &= \exp[-|\zeta(\mathbf{R})|\sqrt{M^2-k^2}] \iint \mathrm{d}\boldsymbol{\varrho} \exp[i\boldsymbol{\varrho}\cdot(\mathbf{M}-\mathbf{K})], \\ L_2 &= \exp[+|\zeta(\mathbf{R})|\sqrt{M^2-k^2}] \iint \mathrm{d}\boldsymbol{\varrho} \exp[i\boldsymbol{\varrho}\cdot(\mathbf{M}-\mathbf{K})]. \end{aligned} \tag{B.15}$$

Clearly the equality signs in (B.14) hold for $\zeta = 0$.

For $M \leqslant k$, the situation is less simple, because now L_1 and L_2 are each others complex conjugate:

$$\begin{aligned} L_1 &= \exp[+iM_z|\zeta(\mathbf{R})|] \iint \mathrm{d}\boldsymbol{\varrho} \exp[i\boldsymbol{\varrho}\cdot(\mathbf{M}-\mathbf{K})], \\ L_2 &= \exp[-iM_z|\zeta(\mathbf{R})|] \iint \mathrm{d}\boldsymbol{\varrho} \exp[i\boldsymbol{\varrho}\cdot(\mathbf{M}-\mathbf{K})]. \end{aligned} \tag{B.16}$$

Nevertheless, L_1 and L_2 must indicate limiting values, since the random phase fluctuations around zero in F have been replaced by fixed values (compare coherent

addition of unit vectors versus random or incoherent addition). This idea is confirmed if L_1 and L_2 are substituted in (B.13): Ψ_1, obtained with L_1, depends now on $(Z_T+|\zeta|)$, whereas Ψ_2 is a function of $(Z_T-|\zeta|)$.

In (B.16) the integration over ϱ yields $4\pi^2\delta(\mathbf{M}-\mathbf{K})$. The quantities Ψ_1 and Ψ_2 can therefore be calculated explicitly. Substitution of L_1 and L_2 into (B.13) and integration over $\mathbf{K}$, which is easy because of the selective properties of the delta function, produces

$$\Psi_1(\mathbf{R}) = -\frac{1}{4\pi^2}\iint \mathrm{d}\mathbf{M} \exp\left[i\mathbf{M}\cdot\mathbf{R} + iM_z\{Z_T+|\zeta(\mathbf{R})|\}\right],$$
$$\Psi_2(\mathbf{R}) = -\frac{1}{4\pi^2}\iint \mathrm{d}\mathbf{M} \exp\left[i\mathbf{M}\cdot\mathbf{R} + iM_z\{Z_T-|\zeta(\mathbf{R})|\}\right]. \tag{B.17}$$

Integrals of this type can be calculated by using polar coordinates (M, θ) instead of $\mathbf{M} = (M_x, M_y)$. The general expression for Ψ_1 and Ψ_2 is then

$$\begin{aligned}\Psi_j(\mathbf{R}) &= \Psi_j(x, y)\\ &= -\frac{1}{4\pi^2}\int_0^\infty \mathrm{d}M\, M \exp\left(iZ_j\sqrt{k^2-M^2}\right)\int_0^{2\pi} \mathrm{d}\theta \exp\left[iM(x\cos\theta + y\sin\theta)\right],\end{aligned} \tag{B.18}$$

or, after integration over θ and substitution of $\beta = \varepsilon - ik$ with $\varepsilon \to 0$,

$$\Psi_j(\mathbf{R}) = -\frac{1}{2\pi}\int_0^\infty \mathrm{d}M\, M J_0(MR) \exp\left(-Z_j\sqrt{M^2+\beta^2}\right). \tag{B.19}$$

This last integral is a Hankel transform. The solution is found in [*B.3, Vol. 2, p. 9(23)*]:

$$\Psi_j(\mathbf{R}) = -\frac{Z_j(1+\beta\sqrt{R^2+Z_j^2})}{2\pi(R^2+Z_j^2)^{\frac{3}{2}}} \exp\left(-\beta\sqrt{R^2+Z_j^2}\right); \tag{B.20}$$

for $\varepsilon \to 0$ it reduces to

$$\Psi_j(\mathbf{R}) = -\frac{Z_j(1-ik\sqrt{R^2+Z_j^2})}{2\pi(R^2+Z_j^2)^{\frac{3}{2}}} \exp\left(ik\sqrt{R^2+Z_j^2}\right). \tag{B.21}$$

This is the general solution. For Ψ_1 we have $Z_1 = Z_T+|\zeta(\mathbf{R})|$, and $Z_2 = Z_T-|\zeta(\mathbf{R})|$ for Ψ_2. Defining now two distances, w_1 and w_2:

$$\begin{aligned} w_1 &= \left[R^2+\{Z_T+|\zeta(\mathbf{R})|\}^2\right]^{\frac{1}{2}},\\ w_2 &= \left[R^2+\{Z_T-|\zeta(\mathbf{R})|\}^2\right]^{\frac{1}{2}},\end{aligned} \tag{B.22}$$

and remembering the assumption $kw \gg 1$, we have

$$\Psi_1(\mathbf{R}) = \frac{ik(Z_T+|\zeta|)}{2\pi w_1^2}\exp(ikw_1),$$

$$\Psi_2(\mathbf{R}) = \frac{ik(Z_T-|\zeta|)}{2\pi w_2^2}\exp(ikw_2). \tag{B.23}$$

Next, as $|\zeta| < 0.1\ Z_T$ (*Assumption 11*), we have $Z_T|\zeta| \leqslant 0.1\ W_T^2$, where $W_T = (R^2 + Z_T^2)^{\frac{1}{2}}$, so that (with an error less than 1%) we can write

$$\begin{aligned} w_1 &= W_T + Z_T|\zeta|/W_T, \\ w_2 &= W_T - Z_T|\zeta|/W_T. \end{aligned} \tag{B.24}$$

Hence

$$\begin{aligned} \Psi_1 &= \Psi_0\left\{1 - \frac{|\zeta|(Z_T^2-R^2)}{Z_T(Z_T^2+R^2)}\right\}\exp(+ikZ_T|\zeta|/W_T), \\ \Psi_2 &= \Psi_0\left\{1 + \frac{|\zeta|(Z_T^2-R^2)}{Z_T(Z_T^2+R^2)}\right\}\exp(-ikZ_T|\zeta|/W_T) \end{aligned} \tag{B.25}$$

follows from (B.23). Again we note that for $\zeta \to 0$ both Ψ_1 and Ψ_2 reduce to Ψ_0.

With these results we are ready to judge the approximate solution given in (B.9). Using the same approximations as for Ψ_1 and Ψ_2, we have

$$\Psi = \Psi_0\left\{1 - \frac{\zeta(3Z_T^2+R^2)}{Z_T(Z_T^2+R^2)}\right\}\exp(-ikZ_T\zeta/W_T)\sqrt{1+2\frac{x\zeta_x+y\zeta_y}{Z_T-\zeta}}. \tag{B.26}$$

The phase of Ψ is lying between those of Ψ_1 and Ψ_2, for any value of k and R. The mean phase is about equal to kW_T, the fluctuations are at most $kZ_T|\zeta|/W_T$. These phase excursions will be 1% or less, if the condition

$$|\zeta| \leqslant 0.01 Z_T \tag{B.27}$$

is satisfied.

Turning now to the moduli of Ψ_1 and Ψ_2, we see that their relative behaviour is governed by the expressions between curled brackets. The mean values of these quantities are sketched in Fig. B.1, together with their standard deviations. This produces the shaded areas. Corresponding curves for Ψ are drawn as dotted lines. Fig. B.1 leads to the conclusion that Ψ is likely to fall outside the limits Ψ_1 and Ψ_2. But it also suggests a possible improvement of the formula for Ψ: if we take

$$\Psi = \Psi_0\exp(ikZ_T\zeta/W_T)\sqrt{1+2\frac{x\zeta_x+y\zeta_y}{Z_T-\zeta}} \tag{B.28}$$

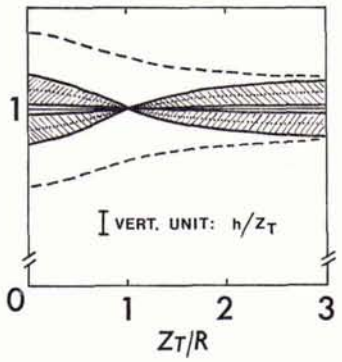


Fig. B.1.
Relative behaviour of the moduli of Ψ_1, Ψ_2 and Ψ.

instead of (B.26), we have an approximation of which the mean value can be brought between the bounds Ψ_1 and Ψ_2, if we see to it that the square root in (B.28) is close to 1.

This last statement needs a qualitative investigation. First we require that

$$2\left|\frac{x\zeta_x + y\zeta_y}{Z_T - \zeta}\right| < 1 \tag{B.29}$$

in the x, y-range where $|\Psi_0|$ is not negligible, because the square root can then be expanded in a converging series, which will be useful later on. The useful x, y-range can be found from (B.12): the modulus $|\Psi_0|$ has a maximum equal to $k(2\pi Z_T)^{-1}$ at $R = 0$, and at $R = 10\ Z_T$ it has decreased to 1% of that maximum. So the most important surface part is the area for which $R \leqslant 10\ Z_T$, and in that area (B.29) has to hold. This condition is certainly satisfied if

$$|x|\,|\zeta_x| + |y|\,|\zeta_y| < \tfrac{1}{2} Z_T. \tag{B.30}$$

Considering the mean value of the random quantities involved, together with the numbers derived in Chapter 3, this yields:

$$|y| + 1.76\,|x| < 20 Z_T, \tag{B.31}$$

whereas the mean square criterium produces

$$0.003x^2 + 0.001y^2 < 0.25 Z_T^2. \tag{B.32}$$

Equation (B.31) indicates a rhombic area with $-20\ Z_T \leqslant y \leqslant 20\ Z_T$ and $-12\ Z_T \leqslant x \leqslant 12\ Z_T$, (B.32) an ellipse with semi-axes equal to $9\ Z_T$ and $16\ Z_T$. Most of the area inside the circle $R = 10\ Z_T$ falls inside the rombic and the ellipse, so we conclude that for $R \leqslant 9\ Z_T$, the series expansion of $\sqrt{1 + 2(x\zeta_x + y\zeta_y)/Z_T}$ is convergent.

As a result of the foregoing analysis we see that for

$$-0.2 \leqslant (x\zeta_x + y\zeta_y)/Z_T \leqslant 0.2 \tag{B.33}$$

we have

$$\sqrt{1+2\frac{x\zeta_x+y\zeta_y}{Z_T}} \sim 1 + \frac{x\zeta_x+y\zeta_y}{Z_T} \leqslant 1.2 \tag{B.34}$$

with an error less than 2%. The mean value of this expression is equal to one, for any (x, y), as was required in the discussion of (B.28). The variance increases with x^2 and y^2, as can be seen from (B.33). Taking the mean square of this expression, we have the condition

$$0.003x^2 + 0.001y^2 \leqslant 0.04Z_T^2. \tag{B.35}$$

This condition is of course much more demanding than (B.32). The corresponding limiting ellipse is consequently smaller: now the semi-axes are 3.6 Z_T and 6.4 Z_T. Inside this ellipse (B.28) is an acceptable approximation of Ψ.

Finally we note that these results indicate limiting values. In most of the cases the errors are less. The complete formula for Ψ, as it emerges from this discussion, is found by substitution of Ψ_0 into (B.28):

$$\Psi(R) = \frac{ikZ_T}{2\pi W_T^2} \exp(ikw_T) \sqrt{1+2\frac{x\zeta_x+y\zeta_y}{Z_T}}, \tag{B.36}$$

with $W_T = (R^2 + Z_T^2)^{\frac{1}{2}}$ and $w_T = [R^2 + (Z_T - \zeta)^2]^{\frac{1}{2}}$.

References

B.1 L. M. Brekhovskikh, *Waves in Layered Media* (Academic Press, New York, 1960).

B.2 L. Fortuin, "Scattering and Reflection of Underwater Sound Waves from the Sea Surface. I. An Expression for the Scattered Field", Saclant ASW Research Centre, Tech. Rep. 181 (1970).

B.3 A. Erdélyi, Ed., *Tables of Integral Transforms* (McGraw-Hill, New York, 1954).

Behaviour of H for high frequencies

In (5.12) we have the complete formula for H. It can be written as

$$H(\omega, t) = \frac{ikZ_T}{2\pi} \iint \mathrm{d}\mathbf{R} (W_T^2 w_R)^{-1} \sqrt{1 + 2\frac{x\zeta_x + y\zeta_y}{Z_T}} \exp[i\psi(x, y)], \tag{C.1}$$

with

$$\begin{aligned} \psi(x, y) &= k(w_T + w_R) \\ &\approx k\left\{W_T + W_R - \left(\frac{Z_T}{W_T} + \frac{Z_R}{W_R}\right)\zeta(x, y)\right\}, \end{aligned} \tag{C.2}$$

and $W_T = (R^2 + Z_T^2)^{\frac{1}{2}}$, $W_R = (|\mathbf{R}_R - \mathbf{R}|^2 + Z_R^2)^{\frac{1}{2}}$. The approximation in (C.2) is based on $|\zeta| \leqslant 0.01\ Z_T, Z_R$ (*Assumption 11*).

The points of stationary phase follow by differentiation of (C.2) with respect to x and y, i.e. from the equations

$$\begin{aligned} \frac{x}{W_T} - \frac{(X_R - x)}{W_R} &= \zeta_x \left(\frac{Z_T}{W_T} + \frac{Z_R}{W_R}\right), \\ y\left(\frac{1}{W_T} + \frac{1}{W_R}\right) &= \zeta_y \left(\frac{Z_T}{W_T} + \frac{Z_R}{W_R}\right). \end{aligned} \tag{C.3}$$

Exact solutions are difficult to obtain, except when $\zeta = \zeta_x = \zeta_y = 0$. Then $x = X_s = Z_T X_R/(Z_T + Z_R)$ and $y = Y_s = 0$ follows; X_s and Y_s are the coordinates of the specular point.

In order to derive a condition for which the solution of (C.3) is sufficiently close to $x = X_s$ and $y = 0$, we suppose that $x = X_s + \Delta x$ and $y = \Delta y$ satisfy (C.3), and require that Δx and Δy are small compared with the geometry of transmitter and receiver. Two cases have now to be distinguished: A) $X_R \geqslant 100$ m, and B) $X_R \approx 0$.

A. For $X_R \geqslant 100$ m, we can write

$$\begin{aligned} W_T &\approx W_{Ts}[1 + \Delta x X_s / W_{Ts}^2] \\ W_R &\approx W_{Rs}[1 - \Delta x (X_R - X_s)/W_{Rs}^2]. \end{aligned} \tag{C.4}$$

These approximations will hold with an error less than 3% if in (C.4) the deviations are smaller than 0.3.

With (C.4) we can rewrite (C.3), and find as first order approximations:

$$\begin{aligned} \Delta x &= 2\zeta_x Z_T Z_R D_0^2/(Z_T+Z_R)^3, \\ \Delta y &= 2\zeta_y Z_T Z_R/(Z_T+Z_R). \end{aligned} \tag{C.5}$$

Requiring next that Δx and Δy are at most 10% of X_s, we obtain the following conditions for the slopes:

$$\begin{aligned} |\zeta_x| &\leqslant 0.05\cos^2\theta_s X_R/Z_R, \\ |\zeta_y| &\leqslant 0.05 X_R/Z_R. \end{aligned} \tag{C.6}$$

Since ζ_x and ζ_y are exchangeable, and $\cos^2\theta_s \leqslant 1$, this means that

$$|\zeta_{x,y}| \leqslant 0.05\cos^2\theta_s X_R/Z_R. \tag{C.7}$$

This result is subject to the conditions

$$\begin{aligned} |\Delta x| X_s/W_{Ts}^2 &\leqslant 0.3, \\ |\Delta x|(X_R-X_s)/W_{Rs}^2 &\leqslant 0.3, \end{aligned} \tag{C.8}$$

to make (C.4) valid. Using (C.5) this leads to

$$|\zeta_{x,y}| \leqslant 0.15(Z_T+Z_R)^2/(X_R Z_{T,R}). \tag{C.9}$$

In the denominator the larger of Z_T and Z_R has to be taken.

B. For $X_R \approx 0$ we have

$$\begin{aligned} W_T &\approx Z_T\left(1+\frac{\Delta x^2+\Delta y^2}{Z_T^2}\right), \\ W_R &\approx Z_R\left(1+\frac{\Delta x^2+\Delta y^2}{Z_R^2}\right), \end{aligned} \tag{C.10}$$

with the condition

$$\begin{aligned} (\Delta x^2+\Delta y^2) &\leqslant 0.3 Z_R^2 \quad \text{if} \quad Z_T > Z_R, \\ &\leqslant 0.3 Z_T^2 \quad \text{if} \quad Z_T < Z_R. \end{aligned} \tag{C.11}$$

With (C.10) substituted into (C.3), Δx and Δy are easily found. In first approximation we get

$$\Delta x = 2\zeta_x Z_T Z_R/(Z_T+Z_R),$$
$$\Delta y = 2\zeta_y Z_T Z_R/(Z_T+Z_R). \tag{C.12}$$

These have to be small compared with Z_T and Z_R. Therefore

$$|\zeta_{x,y}| \leqslant 0.05(Z_T+Z_R)/Z_{T,R} \tag{C.13}$$

has to be true.

Turning finally to the condition (C.11), we derive with (C.12):

$$\zeta_x^2+\zeta_y^2 \leqslant 0.3(Z_T+Z_R)^2/(4Z_{T,R}^2). \tag{C.14}$$

The quantity on the right hand side is not smaller than 0.075. So (C.14) is certainly satisfied, if

$$\zeta_x^2+\zeta_y^2 \leqslant 0.075. \tag{C.15}$$

According to KINSMAN [*C.1, p. 11*] the slopes cannot be larger than 1/7. Thus the maximum value of $\zeta_x^2+\zeta_y^2$ equals 0.04, so that condition (C.11) is always observed.

Summarizing the results of A. and B. we find that the phase ψ in (C.2) has approximately one stationary point – namely $P(X_s, Y_s)$, the point of specular reflection – if the slopes of the surface elevation satisfy the following relations: For $X_R \approx 0$ their absolute values have to be less than or equal to α, for $X_R \geqslant 100$ m they cannot exceed the values β and γ, where α, β, and γ are constants that depend on the geometry of transmitter and receiver in the following way:

$$\alpha = 0.05\,(Z_T+Z_R)/Z_{T,R},$$
$$\beta = 0.05\cos^2\theta_s X_R/Z_R, \tag{C.16}$$
$$\gamma = 0.15\,(Z_T+Z_R)^2/(X_R Z_{T,R}).$$

In the expressions for α and γ the larger of Z_T and Z_R has to be taken.

Returning to (C.1) and (C.2), we expand the phase in a Taylor series around the stationary point:

$$\psi(x, y) = \psi(X_s+\xi, Y_s+\eta)$$
$$= \psi(X_s, Y_s)+\tfrac{1}{2}(\psi_{xx}\xi^2+2\psi_{xy}\xi\eta+\psi_{yy}\eta^2), \tag{C.17}$$

and get from (C.1):

$$H(\omega,t) \approx \frac{ikZ_T}{2\pi}(W_{Ts}^2 w_{Rs})^{-1}(1+2\zeta_x X_s/Z_T)^{\frac{1}{2}} \times$$
$$\times \exp[i\psi(X_s, Y_s)] \int_{-\infty}^{\infty} d\xi \int_{-\infty}^{\infty} d\eta \exp\left[\frac{i}{2}(\psi_{xx}\xi^2 + 2\psi_{xy}\xi\eta + \psi_{yy}\eta^2)\right]. \tag{C.18}$$

After evaluation of the double integral (see [*C.2, p. 86*]) and substitution of X_s and Y_s, this gives

$$H(\omega,t) = -k\frac{(Z_T+Z_R)^3}{Z_T Z_R D_0^3}\frac{\sqrt{1+2\zeta_x\tan\theta_s}}{\sqrt{\psi_{xx}\psi_{yy}-\psi_{xy}^2}}\exp[ik(D_0-2\zeta\cos\theta_s)]. \tag{C.19}$$

The constants ψ_{xx}, ψ_{xy}, and ψ_{yy} are the second derivatives of ψ at the stationary point. Their complete formulae are rather complicated:

$$\psi_{xx} = k\cos\theta_s\left\{\cos^2\theta_s\left(\frac{1}{Z_T}+\frac{1}{Z_R}\right)(1-\zeta_x^2) - 2\zeta_{xx} + 2\zeta_x\sin\theta_s\cos\theta_s\left(\frac{1}{Z_T}-\frac{1}{Z_R}\right)\right\},$$
$$\psi_{xy} = k\cos\theta_s\left\{-\zeta_x\zeta_y\cos^2\theta_s\left(\frac{1}{Z_T}+\frac{1}{Z_R}\right) - 2\zeta_{xy} + \zeta_x\sin\theta_s\cos\theta_s\left(\frac{1}{Z_T}-\frac{1}{Z_R}\right)\right\},$$
$$\psi_{yy} = k\cos\theta_s\left\{\left(\frac{1}{Z_T}+\frac{1}{Z_R}\right)(1-\zeta_y^2\cos^2\theta_s) - 2\zeta_{yy}\right\}, \tag{C.20}$$

but ζ_x^2, $\zeta_x\zeta_y$, ζ_y^2 are much smaller than 1, so that some simplification is possible. If moreover

$$2|\zeta_{x,y}|\tan\theta_s \leqslant 0.1 \tag{C.21}$$

and

$$|\zeta_{xx}|, |\zeta_{xy}|, |\zeta_{yy}| \ll \tfrac{1}{2}\cos^2\theta_s\left(\frac{1}{Z_T}+\frac{1}{Z_R}\right), \tag{C.22}$$

we can write

$$\psi_{xx}\psi_{yy} - \psi_{xy}^2 \approx k^2\cos^4\theta_s\left(\frac{1}{Z_T}+\frac{1}{Z_R}\right)^2. \tag{C.23}$$

Then (C.19) becomes

$$H(\omega,t) = -D_0^{-1}\exp[ik(D_0-2\zeta\cos\theta_s)]\sqrt{1+2\zeta_x\tan\theta_s}. \tag{C.24}$$

Series expansion of the square root, which is permitted in view of (C.21), leads to the formulae for H_0, H_1, etc. given in (5.18)–(5.20).

References

C.1 B. KINSMAN, *Wind Waves, Their Generation and Propagation on the Ocean Surface* (Prentice Hall, Englewood Cliffs, N.J., 1965).

C.2 L. FORTUIN, "Scattering and Reflection of Underwater Sound Waves from the Sea Surface. I. An Expression for the Scattered Field", SACLANT ASW Research Centre, Techn. Rep. 181 (1970).

theses/stellingen



THESES

1

The Kirchhoff-Eckart theory is better than it seems.

2

The Doppler spread in the surface sound channel is mainly determined by the vertical surface movements.

3

The Pierson-Moskowitz spectrum is *physically* unrealistic because a fully developed sea occurs seldom, and *mathematically* because of the behaviour for $v \rightarrow 0$ of functions that can be derived from it.

4

The application of a fast digital computer is a useful way to advance a theory for the description of a physical phenomenon.

5

It is possible to measure the velocity as function of time or position of a projectile inside the barrel of a gun by means of Doppler radar, if the caliber of the gun is at least 75% of the free space wavelength of the radiated radar signal.

6

A function is sufficiently sampled if it can be reconstructed by drawing a smooth curve through the sample points.

7

In many research projects the recording and reporting of results and methods are wrongly treated as a requirement that can wait until the project is finished. Proper reporting and recording form an essential aspect of a research project: they can help to clarify vague ideas and detect errors in an early stage.

8

The informal contacts between scientists working in international organizations – for the total scientific output as important as the organizational relations – are usually established in three steps: first with persons of the same nationality, next with colleagues from nations with a cultural pattern similar to the own, and finally with others. Often the last step is not made at all.

9

In Holland, but strangely enough also in other parts of The Netherlands, the teaching of both national history and local geography fail to create sufficient insight into and understanding of the difference between "Holland" and "The Netherlands".

10

Persons in directorial positions always leave a chaos behind at the moment of their departure – in the eyes of their successors.

11

Italian labourers that work in The Netherlands are not representative of their countrymen. Opinions about the Italian people should therefore not be based on the behaviour and appearance of these labourers.

12

It is an illusion to believe that the world can be improved by means of theses added to a dissertation.

13

It is most remarkable that bathroom mirrors do exchange left and right, but not up and down.

Januari 1974

LEONARD FORTUIN

ISBN 90 212 4007 6

INITIAL DISTRIBUTION

MINISTRIES OF DEFENCE	Copies
MOD Belgium	1
DND Canada	10
CHOD Denmark	8
MOD France	8
MOD Germany	15
MOD Greece	11
MOD Italy	10
MOD Netherlands	12
CHOD Norway	10
MOD Portugal	5
MOD Turkey	5
MOD U.K.	20
SECDEF U.S.	71

NATO AUTHORITIES	
Defence Planning Committee	3
NAMILCOM	2
SACLANT	10
SACLANTREPEUR	1
CINCWESTLANT	1
COMIBERLANT	1
CINCEASTLANT	1
COMSUBACLANT	1
COMOCEANLANT	1
COMCANLANT	1
COMMAIREASTLANT	1
COMNORLANT	1
COMSUBEASTLANT	1
SACEUR	2
CINCNORTH	1
CINCSOUTH	1
COMNAVSOUTH	1
COMSTRIKFORSOUTH	1
COMEDCENT	1
COMSUBMED	1
COMMARAIRMED	1
CINCHAN	1

SCNR FOR SACLANT	
SCNR Belgium	1
SCNR Canada	1
SCNR Denmark	1
SCNR Germany	1
SCNR Greece	1
SCNR Italy	1
SCNR Netherlands	1
SCNR Norway	1
SCNR Portugal	1
SCNR Turkey	1
SCNR U.K.	1
SCNR U.S.	2

NATIONAL LIAISON OFFICERS	
NLO Italy	1
NLO U.K.	1
NLO U.S.	1

NLR TO SACLANT	
NLR Belgium	1
NLR Canada	1
NLR Denmark	1
NLR Germany	1
NLR Greece	1
NLR Italy	1
NLR Norway	1
NLR Portugal	1
NLR Turkey	1
ESRO/ELDO Doc. Service	1
Total initial distribution	247
SACLANTCEN Library	10
Stock	43
Total number of copies	300